

# **Modeling and Interpretation of Galaxy Spectra: the Stellar Populations of Nearby Galaxies**

Dissertation der Fakultät für Physik  
der  
Ludwig-Maximilians-Universität München

vorgelegt von Anna Gallazzi  
aus Busto Arsizio, Italien

München, den 3. April 2006

Erstgutachter: Prof. Dr. Simon D. M. White

Zweitgutachter: Prof. Dr. Ralf Bender

Tag der mündlichen Prüfung: 29. June 2006

*A mia mamma Aurora*



# Contents

<b>Zusammenfassung (Summary in German)</b>	<b>3</b>
<b>Summary</b>	<b>7</b>
<b>1 Introduction</b>	<b>9</b>
1.1 The theory of structure growth . . . . .	9
1.2 The physics of galaxy formation . . . . .	14
1.2.1 Models . . . . .	14
1.2.2 Observations . . . . .	17
1.3 The stellar populations in galaxies . . . . .	25
1.3.1 Star formation and chemical evolution . . . . .	26
1.3.2 Population synthesis models . . . . .	31
1.4 Extragalactic surveys . . . . .	35
1.4.1 The Sloan Digital Sky Survey . . . . .	35
1.4.2 Multiwavelength high-redshift surveys . . . . .	39
1.5 The thesis . . . . .	41
<b>2 The Ages and Metallicities of Galaxies in the Local Universe</b>	<b>49</b>
2.1 Introduction . . . . .	50
2.2 The approach . . . . .	52
2.2.1 Observed and model spectra . . . . .	52
2.2.2 Stellar absorption diagnostics of age and metallicity . .	53
2.2.3 Statistical estimates of age and metallicity . . . . .	56
2.2.4 Accuracy of the estimates . . . . .	59
2.3 The ages and metallicities of nearby galaxies . . . . .	65
2.3.1 Age, metallicity and mass distributions . . . . .	67
2.3.2 Relations between age, stellar metallicity, stellar mass and gas-phase metallicity . . . . .	69
2.3.3 Age versus metallicity . . . . .	77
2.3.4 Aperture bias . . . . .	83
2.4 Summary and conclusions . . . . .	86

## Contents

---

<b>3</b>	<b>Physical origin of the colour-magnitude and the <math>Mg_2-\sigma_V</math> relations for early-type galaxies</b>	<b>97</b>
3.1	Introduction . . . . .	98
3.2	Observational sample . . . . .	100
3.3	Physical origin of observed relations for early-type galaxies . . . . .	106
3.3.1	The colour-magnitude relation . . . . .	106
3.3.2	The $Mg_2-\sigma_V$ relation . . . . .	114
3.3.3	Environmental dependence . . . . .	120
3.3.4	Correlations between physical parameters . . . . .	123
3.4	Summary and conclusions . . . . .	136
<b>4</b>	<b>The stellar metallicity distribution in the local Universe</b>	<b>147</b>
4.1	Introduction . . . . .	148
4.2	The approach . . . . .	151
4.2.1	The sample . . . . .	151
4.2.2	The stacking technique . . . . .	153
4.3	The distribution of metals in the local Universe . . . . .	155
4.3.1	The total stellar metallicity in the local Universe . . . . .	156
4.3.2	An inventory of the stellar metallicity and stellar mass . . . . .	161
4.4	Summary and conclusions . . . . .	165
<b>5</b>	<b>Conclusions and outlook</b>	<b>175</b>
5.1	Motivations . . . . .	175
5.2	Main results . . . . .	177
5.3	Outlook . . . . .	182
	<b>Acknowledgements</b>	<b>185</b>
	<b>Curriculum Vitae</b>	<b>187</b>

# Zusammenfassung

Unser derzeitiges Verständnis der Strukturentstehung im Universum scheint durch ein hierarchisches Szenario gut beschrieben werden zu können, in dem kleine Einheiten sich zuerst zusammenfügen um größere Systeme zu bilden. In den letzten Jahren haben sich allerdings die Hinweise verdichtet, daß die Sternentstehung im Gegensatz dazu eine anti-hierarchische Entwicklung durchgemacht hat. Um Aufschluß über diese anscheinende Dichotomie zwischen Massenaggregation und Sternentstehungsaktivität zu erhalten, ist es wünschenswert, das Alter und die chemische Zusammensetzung von Sternpopulationen in Galaxien möglichst genau eingrenzen zu können.

Die integrierten Spektren von Galaxien enthalten wertvolle Hinweise auf Alter und Metallizität der Sterne, die dieses Licht erzeugen. Allerdings manifestieren sich beide Eigenschaften, Alter und Metallizität, auf sehr ähnliche Weise im Spektrum, weshalb es notwendig ist, verfeinerte Diagnosemethoden, wie etwa individuelle stellare Absorptionsmerkmale, anzuwenden, um diese Parameter besser eingrenzen zu können. Diese Methode war bisher auf eine kleine Auswahl von elliptischen Galaxien beschränkt, zudem unter Verwendung von "Population Synthesis" Modellen beschränkter Auflösung und für einen eingeschränkten Bereich effektiver Sterntemperaturen.

Diese Doktorarbeit widmet sich der Interpretation optischer Spektren einer großen Anzahl von nahen Galaxien, um Informationen über helligkeitsgewichtete Metallizität, Alter und Masse ihrer Sternpopulationen zu gewinnen. Ich habe eine neue Methode entwickelt, die es ermöglicht, für jeden physikalischen Parameter gleichzeitig eine Median-Likelihood-Schätzung sowie die zugehörigen Konfidenzintervalle zu erhalten. Basierend auf einem aktuellen "Population Synthesis" Modell mit hoher Auflösung, welches alle Sterntemperaturbereiche abdeckt, vergleicht diese Methode jedes beobachtete Spektrum mit einer umfassenden Bibliothek von möglichen Sternentstehungsverläufen. Der Grad der Übereinstimmung hängt davon ab, wie gut eine Anzahl optimal ausgewählter Absorptionsmerkmale im Spektrum wiedergegeben werden.

Ich habe diese Methode auf  $\sim 200.000$  Galaxien im Sloan Digital Sky Survey Katalog angewendet, der, was die Vorgeschichte der Sternentstehung in den Galaxien betrifft, praktisch das gesamte Spektrum abdeckt, von seit langem passiven elliptischen Galaxien bis hin zu denen, die nach wie vor aktiv

## Zusammenfassung

---

Sterne bilden. Dank der beispiellosen statistischen Güte der Daten, konnte ich die Verteilung im gesamten physikalischen Parameterraum genau beschreiben. Die Beziehungen zwischen Metallizität, Alter und stellarer Masse zeigt einen sprunghaften Übergang von massearmen, jungen und metallarmen Galaxien hin zu massereichen, alten Galaxien hoher Metallizität. Die Trennlinie kann bei etwa  $3 \times 10^{10} M_{\odot}$  stellarer Masse angesetzt werden, was auch für andere beobachtete Bimodalitäten von Galaxieneigenschaften eine charakteristische Größe darstellt. Der Zusammenhang zwischen stellarer Metallizität und Masse wird als Auswirkung galaktischer Winde interpretiert, welche desto effizienter Metalle wegtragen können, je flacher die Potentialtöpfe sind, also je masseärmer die Galaxien.

Als nächstes habe ich die Implikationen der beschriebenen Zusammenhänge untersucht, um den physikalischen Ursprung der beobachteten Skalierungsabhängigkeiten für elliptische Galaxien neu zu beurteilen, wobei die leuchtende und dynamische Masse der Galaxien zu den Eigenschaften ihrer stellaren Populationen in Beziehung gesetzt wurden. Die Relationen werden bestimmt von einem Ansteigen von Metallizität, Alter und Elementhäufigkeit mit der Galaxienmasse. Die Streuung wird zu gleichen Teilen von Alter und Metallizität beigetragen. Der Anstieg der Schwankungsbreite in Richtung niedrigeres Alter und kleine stellare Masse weist darauf hin, daß massearme elliptische Galaxien ihre Sterne entweder erst später gebildet haben, oder ihre Sternentstehungsgeschichte länger angedauert hat. Das ist ein Zeichen für eine allgemeine Verschiebung der Sternentstehungsaktivität hin zu weniger massereichen Galaxien in den vorangegangenen Epochen bis heute.

Aufgrund des enormen Umfanges der beobachtbaren und physikalischen Parameter die der SDSS abdeckt, stellt er eine repräsentative Stichprobe des lokalen Universums dar. Daher konnte ich die absolute Massendichte von baryonischer Materie und Metallen, welche gegenwärtig in den Sternen enthalten sind, ableiten. Ich habe ebenfalls die Verteilung von Metallen und stellarer Materie als Funktion unterschiedlicher Galaxieneigenschaften untersucht. Die Galaxien, welche den Großteil der Sternmasse enthalten (massive, elliptische Galaxien mit alten Sternpopulationen), tragen auch das meiste zur gesamten Masse an Metallen bei, wie man aufgrund der Massen-Metallizitäts Relation erwarten konnte. Diese Größen stellen die fundamentalen zeitlichen Randbedingungen dar, die das Modell bestimmen, welches die Geschichte der kosmischen Sternentstehung und der chemischen Elementanreicherung beschreiben kann.

Die detailliertere Kenntnis der Zusammenhänge zwischen den einzelnen physikalischen Parametern erlaubt einen direkteren Vergleich mit den Voraussagen semi-analytischer Modelle der Entstehung und Entwicklung von Galaxien. Des Weiteren stellt die genauere Bestimmung der Eigenschaften bei Rotver-

schiebung Null eine wichtige Kalibrierung für ähnliche Studien bei höheren Rotverschiebungen dar.

## Zusammenfassung

---

# Summary

Our current understanding of structure formation in the Universe seems to be well described by a hierarchical scenario, in which small units assemble first to produce more massive systems. In recent years, much observational evidence has been accumulated, indicating that star formation proceeded instead in an antihierarchical fashion. Constraining the age and chemical composition of the stellar populations in galaxies should help shed light on this apparent dichotomy between mass assembly and star formation activity.

The integrated spectra of galaxies contain valuable clues about the ages and metallicities of the stars producing the light. However, at first order, they are affected in a similar way by age and metallicity. Studies of more refined spectral diagnostics, such as individual stellar absorption features, are thus needed to provide more stringent constraints on these parameters. This method has been limited so far to small samples of elliptical galaxies, using population synthesis models with limited spectral resolution and restricted coverage in stellar effective temperatures.

The objective of this thesis is the interpretation of the optical spectra of large samples of nearby galaxies in terms of the light-weighted metallicity, age and mass of their stellar populations. I have developed a new method to simultaneously derive median-likelihood estimates of each physical parameter and the associated confidence intervals. The method, based on a recent high-resolution population synthesis code with full temperature coverage, consists in comparing each observed spectrum with a comprehensive library of star formation histories. The constraints are set by the simultaneous fit of an optimally selected set of spectral absorption features.

I have applied this method to a sample of  $\sim 200,000$  galaxies from the Sloan Digital Sky Survey, including galaxies with any star formation history, from quiescent early-type to actively star forming galaxies. Thanks to the unprecedented statistics, I could give an accurate description of the galaxy distribution in the full physical parameters space. The relation between stellar metallicity, age and stellar mass shows a rapid transition from low-mass, young, metal-poor to high-mass, old, metal-rich galaxies at a stellar mass of  $3 \times 10^{10} M_{\odot}$ , the same characteristic scale of several observed bi-modalities in galaxy properties. The stellar metallicity-mass relation is interpreted as a manifestation of

## Summary

---

galactic winds, which are more efficient in removing metals from the shallow potential well of low-mass galaxies.

I then explored the implications of the above relations to re-assess the physical origin of observed scaling relations of elliptical galaxies, linking their luminous and dynamical mass to the properties of their stellar populations. The relations are driven by an increase in metallicity, age and element abundance ratios with galaxy mass. The scatter is contributed by a similar amount by both age and metallicity. The increasing spread towards younger ages at low stellar masses indicates that low-mass ellipticals either formed their stars later or have a more extended star formation history. This hints at a shift in stellar growth towards less massive galaxies in recent epochs.

The large ranges in observational and physical properties covered by SDSS galaxies make it a representative sample of the local Universe. I could thus derive the total mass density of metals and baryons locked up in stars today. I have also studied how metals and stellar mass are distributed as a function of various galaxy properties. The galaxies containing the bulk of the total stellar mass (massive, bulge-dominated galaxies with old stellar populations) are also those that contribute the largest fraction of metals, as expected from the mass-metallicity relation. These quantities set the fundamental constraints at the present epoch of the cosmic star formation and chemical enrichment histories.

The more detailed knowledge of the relations between galaxy physical parameters allows a more direct comparison with predictions from semi-analytic models of galaxy formation and evolution. Moreover, the more robust constraints represent an important calibration at redshift zero for similar studies at higher redshifts.

*Quis potis est dignum pollenti pectore carmen  
condere pro rerum maiestate hisque repertis? qui-  
sve valet verbis tantum, qui fingere laudes pro me-  
ritis eius possit, qui talia nobis pectore parta suo  
quaesitaque praemia liquit? nemo, ut opinor, erit  
mortali corpore cretus.*

Lucrezio, De Rerum Natura

# 1

## Introduction

### Abstract

In this chapter I outline the theoretical basis and the most significant results of observational cosmology, which constitutes the framework in which the present thesis is developed. I will briefly introduce the favoured cosmological model and the theory of structure formation in the Universe, on which current galaxy formation models are based. Of particular relevance is the baryonic content of the Universe and the physical mechanisms related to the conversion of gas into stars and thus the formation and evolution of galaxies as they appear today. I will give an overview of the fundamental properties and relations obeyed by galaxies, with particular emphasis on the stellar populations of nearby galaxies. I will give the basic theoretical background to study star formation and metal production in galaxies, needed to construct models of chemical evolution. I will then introduce evolutionary population synthesis models, as the principal tool to interpret the spectro-photometric properties of galaxies in terms of the physical parameters of their stellar populations, and the classical spectral diagnostics used. Finally I will give a broad overview on galaxy redshift surveys, focusing on optical, low-redshift surveys on which this work is based.

### 1.1 The theory of structure growth

When looking at the night sky we recognise an enormous richness of systems and structures spanning several orders of magnitude in size: from the myriads of stars in the disk of our own Galaxy to a large variety of complex ‘stellar

## 1 Introduction

---

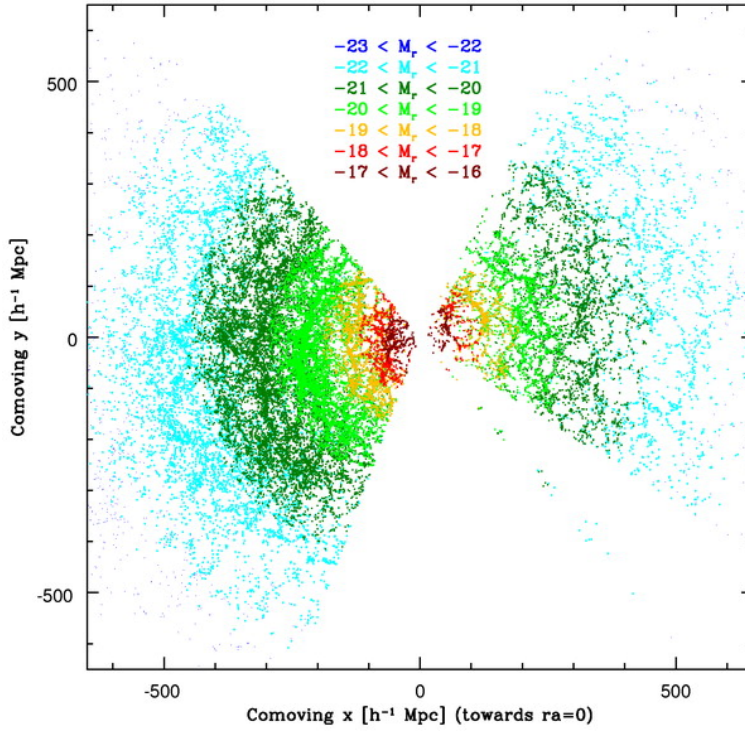


**Figure 1.1:** The pie diagram shows the distribution on the sky of  $\sim 70,000$  galaxies from the Sloan Digital Sky Survey within 5 arcmin of the equatorial plane. It is possible to appreciate that galaxies are not uniformly distributed, but they organize in clusters, walls and filamentary structures. These surround regions of ‘voids’, with a much lower density of galaxies. Small voids can also be nested within larger ones. The colour-code reflects the luminosity of the galaxies. This shows that, in a magnitude-limited survey, brighter galaxies (blue) are visible to larger distances, while fainter galaxies (red) are progressively missed at large distances and are visible only locally. (from Tegmark et al. 2004)

systems’, the galaxies, ranging from dwarf galaxies of only few  $\text{kpc}^1$  in size and  $10^6 - 10^8 M_\odot^2$  in mass, to giant ellipticals with size of the order of ten  $\text{kpc}$  and masses of about  $10^{12} M_\odot$ . Moving out to larger distances, galaxies are further organised in clusters of galaxies, extending some  $\text{Mpc}$ , up to large super-clusters and filamentary structures, surrounding regions of space almost totally devoided of galaxies (see Fig. 1.1).

Despite the complexity of structures and their highly correlated spatial

---

<sup>1</sup> $1\text{pc} = 3.086 \times 10^{18}\text{cm}$

<sup>2</sup> $1M_\odot = 1.989 \times 10^{33}\text{g}$

## 1.1 The theory of structure growth

---

distribution, on large enough scales (several hundreds of Mpc) our Universe is remarkably simple and approaches homogeneity and isotropy: no preferred position and no preferred direction can be identified in it. This homogeneity is still reflected in the Cosmic Microwave Background (CMB), the relic of the primordial black-body radiation observed now with a temperature of  $T_{\text{CMB}} = 2.725 \pm 0.002\text{K}$  (Mather et al. 1999). This radiation was first predicted by George Gamow, together with Alpher and Bethe in 1948, but had to wait until 1965 to be almost accidentally discovered by Penzias and Wilson. Tiny temperature fluctuations have been measured in the microwave background. These witness the primordial density fluctuations that are the seeds of the structure formation in the early Universe.

According to the standard model (the Hot Big Bang), the Universe we see today developed from an original state of extremely high temperature and density about 13.7 billion years ago. The Universe keeps on expanding, in the sense that the relative distance between two points increases at a rate proportional to the distance itself

$$\frac{dl}{dt} = H_0 l \quad (1.1)$$

where  $H_0$ , the *Hubble constant*, is the present value of the time-dependent constant of proportionality. The Wilkinson Microwave Anisotropy Probe (WMAP, Bennett et al. 2003) data have provided a very accurate estimate of the Hubble constant of  $H_0 = 72 \pm 5 \text{ km s}^{-1} \text{ Mpc}^{-1}$ . Despite the accuracy reached by the latest estimate, it is still common to express the Hubble constant as  $H_0 = 100 h \text{ km s}^{-1} \text{ Mpc}^{-1}$ , condensing into the dimensionless parameter  $h$  the uncertainty on  $H_0$ .

The dynamics of the expanding Universe is governed by the Einstein's general relativity theory. For a homogeneous and isotropic Universe, the space-time can be described by the Robertson-Walker metric in the spherical coordinates  $r, \theta, \phi$  (Peacock 1999):

$$dl^2 = c^2 dt^2 - a^2(t) \left( \frac{dr^2}{1 - kr^2} + r^2(d\theta^2 + \sin^2\theta d\phi^2) \right) \quad (1.2)$$

where  $k$  is the curvature which defines the Universe as flat ( $k = 0$ ), open ( $k < 0$ ) or closed ( $k > 0$ ), and  $a(t)$  is the scale factor of the Universe which is related to the Hubble parameter (i.e. the expansion rate of the Universe) by  $H = \dot{a}/a$ . With this metric, Einstein's field equations can be simply written as:

$$\frac{\ddot{a}}{a} = -\frac{4\pi G}{3} \left( \rho + \frac{3p}{c^2} \right) + \frac{\Lambda c^2}{3} \quad (1.3)$$

## 1 Introduction

---

$$\left(\frac{\dot{a}}{a}\right)^2 = \frac{8\pi G}{3}\rho - \frac{kc^2}{a^2} + \frac{\Lambda c^2}{3} \quad (1.4)$$

here  $\rho$  represents the matter density,  $p$  the pressure and  $\Lambda$  is the cosmological parameter that acts as an energy density of the vacuum  $\rho_\Lambda c^2 = c^4\Lambda/8\pi G$ .

It is useful to introduce some density parameters, defined at the present time:

$$\Omega_M = \frac{\rho}{\rho_c}, \quad \Omega_\Lambda = \frac{\Lambda c^2}{3H_0^2}, \quad \Omega_c = -\frac{kc^2}{a_0^2 H_0^2} \quad (1.5)$$

where  $\rho_c = 3H_0^2/8\pi G$  is the critical density that represents the matter content of the Universe.

Several methods can be adopted to measure these cosmological parameters. Clusters of galaxies are powerful tools to constrain the matter density of the Universe,  $\Omega_M$ , while the observation to high redshift of Supernovae of type Ia (SNIa) can provide information about the geometry of the Universe. Fundamental constraints can also be obtained by measuring the temperature fluctuations in the microwave background radiation. All these observational data seem to converge toward a *concordance* cosmological picture of a low-density ( $\Omega_M = 0.3$ ), vacuum-dominated ( $\Omega_\Lambda = 0.7$ ) Universe, whose rate of expansion is accelerating.

A fundamental concept to introduce is that of cosmological redshift. The light emitted by an object at cosmological distance is shifted to longer wavelength by an amount  $z = (\lambda_{obs} - \lambda_{em})/\lambda_{em}$ , where the subscripts ‘obs’ and ‘em’ stand for ‘observed’ and ‘emitted’. Neglecting peculiar motions, the redshift can be expressed as

$$1 + z = \frac{a(t_0)}{a(t_{em})} \quad (1.6)$$

which, for small distances  $d$ , simplifies into

$$z = \frac{v}{c} = \frac{d}{D_H} \quad (1.7)$$

where  $v$  is the radial velocity of the object and  $D_H = c/H_0 = 3000 h^{-1}\text{Mpc}$  is the Hubble distance. This redshift arises because the Universe itself is expanding. It is of fundamental importance and usefulness because it is directly and easily measured from the spectrum of the objects and characterises both the distance of the objects and the epoch of the emission of their light.

It is worth noting that, although much more complex physics needs to be included to understand the evolution of galaxies (see section 1.2), the dominant interaction that governs the dynamics of the Universe is gravitation. Therefore, as long as we describe large enough scales, only the laws of gravity are relevant. This simplification is supported by the evidence that our

## 1.1 The theory of structure growth

---

Universe is dominated by a non-baryonic form of matter which interacts only gravitationally and so far escaped detection through effects other than gravity. The idea of the existence of this form of ‘dark matter’ originated in the 30’s when Zwicky realized that the dynamical mass inferred from the velocities of galaxies in rich clusters would have to be 100 times larger than the mass contained in galaxies (the baryonic mass) to keep the systems bound (Zwicky 1937). Further evidence of its existence came in the 70’s when it was demonstrated that the rotation curve of spiral galaxies is flat or rising at the optical edge of the galaxy, contrary to the expected Keplerian fall-off. At present, observational studies seem to favour a dark matter in the form of cold<sup>3</sup>, collisionless, Weakly Interacting Massive Particles (WIMPs).

It is assumed that dark matter behaves as a collisionless fluid for most of the history of the Universe, and, since the number of particles is expected to be large, the system can be described by a distribution function in the phase-space. The current favoured models of structure formation assume that structures grow out of primordial quantum fluctuations in the dark matter density field due to gravitational instability. These primordial quantum fluctuations get amplified during a short period ( $\Delta t \sim 10^{-33}\text{s}$ ) of fast expansion, called *inflation*. As long as these perturbations are small they can be treated with the *linear theory*, that means that the equations of motion can be linearised by expanding around the homogeneous solution. The equations are usually expressed in terms of the density contrast  $\delta(\mathbf{x}, t)$ . The primordial perturbations start to grow at the epoch of decoupling, when the Universe transitions from a radiation-dominated phase to a matter-dominated phase. After the epoch of recombination (when the Universe is cool enough for protons to capture electrons), these seeds accrete baryonic matter and they keep on growing in size, sweeping up more and more material. The overdense regions ( $\delta > 0$ ), under the action of their own gravity, will slow down their expansion and eventually detach from the Hubble flow and collapse (*turn-around*). The formation of bound systems is already in a non-linear regime. Under the assumption of the spherical symmetry and homogeneous density, it can be shown that the collapse occurs when the density contrast has a value of  $\delta = 5.55$ . Once the perturbation has turned-around, it keeps on collapsing over a free-fall timescale ( $\sim (G\rho)^{1/2}$ ), in a process called *violent relaxation*. A virialized structure will eventually form when the density is 178 times higher than the background Universe density.

It has to be noted that in the context of galaxy formation, where the mean density can be  $10^7$  times higher than the background, linear theory is com-

---

<sup>3</sup>Dark matter candidates have been classified as ‘hot’ or ‘cold’ depending on their kinematical state at the time of decoupling between radiation and matter in the early Universe.

## 1 Introduction

---

pletely useless. However only few analytic solutions of the non-linear collapse of structures have been investigated. An indispensable tool in cosmology is thus represented by numerical N-body simulations, which describe the dynamics of a collection of N particles (stars in a galaxy, galaxies in a cluster) under their mutual gravity (see Fig 1.2).

In the Cold Dark Matter scenario, smaller systems are formed first: galaxy-size objects are made through gravitational coalescence of subunits, larger systems up to galaxy clusters are formed via hierarchical merging of smaller structures in a ‘bottom-up’ fashion. It is important to realize that this hierarchical process of structure formation involves dark matter ‘haloes’. The process of evolution of the baryonic matter, in particular the star formation in galaxies, is governed by a much more complex physics. It could be that baryonic matter follows a different evolutionary path and that the transformation of baryons into stars occurs in an antihierarchical fashion.

### 1.2 The physics of galaxy formation

As discussed above, most of the material in the Universe is in the form of non-baryonic dark matter which interacts only gravitationally and whose dynamical evolution seems to be well understood. Nevertheless, there is clearly a contribution to the matter density from ordinary baryonic matter: this is indeed the constituent of the luminous components in the Universe that we can directly observe. Baryons sink to the cores of dark matter haloes; the subsequent cooling, fragmentation and collapse of the gas lead to formation of stars and thus give rise to the galaxies we see today. Then, it is clear that, in order to understand how the structures we see today formed and evolved, we have to understand the baryonic matter and the physical processes related to the conversion of gas into stars. This has largely become the fundamental target of cosmological investigations in the last decade. It has to be tackled from both theoretical and observational point of view. I will sketch the main aspects and results of the two approaches in what follows, with particular attention to the observational constraints against which models have to be confronted.

#### 1.2.1 Models

From the theoretical point of view, cosmological simulations need to explicitly include the evolution of the baryonic component in order to make a close link between theoretical predictions and observations. This is however not an easy task, especially considering that the actual process of star formation is not understood in detail. Condensation of gas represents the initial step that leads

## 1.2 The physics of galaxy formation

---

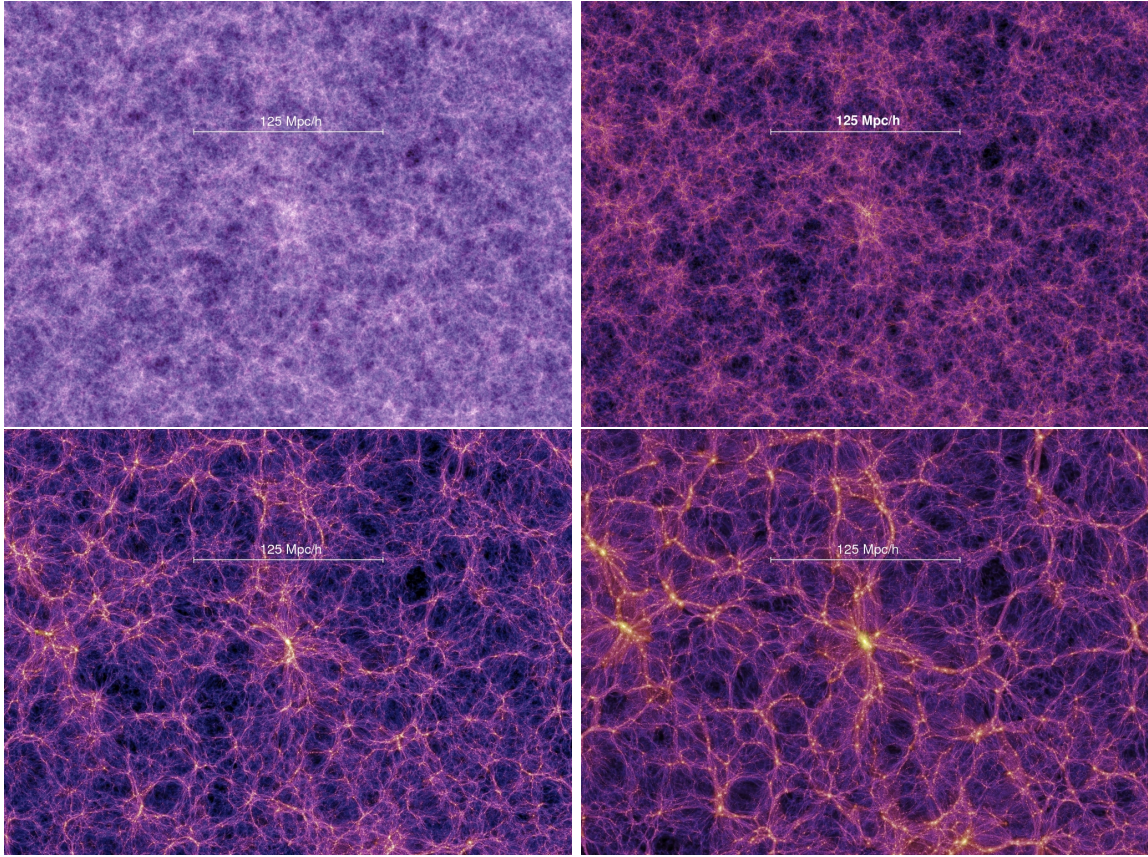


**Figure 1.2:** Cold dark matter N-body simulation, based on the *Millennium Simulation* (Springel 2005), showing the evolution of dark matter structures under the mutual gravitational interaction. Four redshift slices are shown, from  $z = 18.3$  when the Universe was only 0.2 Gyr old (top-left panel), to  $z = 5.7, 1.4,$  and  $0$ , i.e. today (bottom-right panel). At early times small density perturbations are visible. They evolve with time by growing in amplitude, by accreting more and more material which flows into filamentary structures towards the density peaks. Regions of overdensity, under the action of their own gravity, slow down their expansion and detach from the Hubble flow, eventually leading to the formation of bound structures. Baryonic particles (not included in the simulation shown here) follow dark matter particles, bringing to the formation of galaxies and galaxy clusters in correspondence of dark matter overdensities. Cold dark matter simulations in the concordance cosmological framework can reproduce well the observed distribution of galaxies on large scales (see Fig. 1.1).

## 1 Introduction

---

to the formation of a complex multi-phase interstellar medium (ISM), where giant molecular clouds form. The cores of these molecular clouds can then undergo further collapse to densities that allow the onset of thermonuclear reactions. The stars formed interact with the ISM, by ionizing the surrounding gas with UV radiation, by powerful winds and eventually by supernovae explosions at the death of massive stars. Both the processes that trigger star formation and the processes with which energy is deposited back into the ISM (referred to as *feedback*) are not well known. All these processes need however to be modelled. On one side, radiative heating and cooling are necessary for the onset of star formation. On the other side, feedback provides an important regulation mechanism for star formation.

The inclusion of all these processes can be done through hydrodynamical simulations, following directly the gas dynamics. In the Smoothed Particle Hydrodynamics (SPH) technique gas particles are gravitationally bound to dark matter particles but also feel hydrodynamical forces arising from thermal pressure. Full cosmological hydrodynamical simulations have been carried out with some success (Springel & Hernquist 2003), however they are numerically very costly, given the high resolution required. In this respect, an alternative and more efficient method is provided by semi-analytic models, pioneered by White & Rees (1978) and developed by several groups (Kauffmann et al. 1993; Baugh et al. 1996; Somerville & Primack 1999; Cole et al. 2000), in which the gas-dynamical equations are replaced with simple, yet physically and observationally motivated prescriptions for star formation and feedback.

There is an increasing evidence that the inclusion of feedback in hydrodynamical simulations and semi-analytic models can solve many of the problems encountered in reproducing observational constraints. Among these are the overcooling problem, i.e. the fact that without feedback too much gas cools and forms knots of cold, dense gas; the shape of the galaxy luminosity function both at the faint- and bright-end; the abundance of metals in the intergalactic medium (IGM); the properties of the stellar populations in nearby elliptical galaxies. Several sources of feedback have been proposed (supernovae, active galactic nuclei, UV ionizing background, cosmic ray pressure), yet it is not clear what is their relative contribution.

Semi-analytic models in the context of hierarchical clustering scenario can be coupled to population synthesis models (see section 1.3.2) to predict the luminosities, colours, the luminosity function and other observed relation of nearby galaxies. The treatment of metal enrichment and the enrichment of individual elements is fundamental to compare model predictions with the observed properties of the stellar populations in galaxies, in particular of elliptical galaxies (Kauffmann & Charlot 1998; Thomas 1999; De Lucia et al. 2004). Still, as I will explain in section 1.2.2 below, the properties of the stel-

lar populations in these galaxies represent a major challenge for these models. Several observational evidences, among which the colour-magnitude relation and the relation between the galaxy velocity dispersion and the strength of some spectral absorption features, hint at old mean ages and short star formation timescales for massive ellipticals. This appears contrary to the expectation of hierarchical clustering, in which more massive systems form later, and the relatively long star formation timescales predicted in semianalytic models. Again, some sort of feedback that can rapidly quench gas cooling and hence star formation in massive systems is required.

### 1.2.2 Observations

To understand the origin and evolution of the observed structures in the Universe requires understanding the link between the luminous and baryonic matter and compare the assembly processes that govern the two. Observationally this can be done studying the stellar content of the Universe, through the radiation over the spectral energy distribution of galaxies, that brings records of the processes and timescales of the transformation of gas into stars. There are basically two approaches to achieve this. Perhaps the most obvious but also the most observationally challenging is to directly trace back galaxy evolution through observations at different redshift and reconstruct how the activity of star formation in galaxies varied over cosmic time. The other approach is the so-called ‘fossil cosmology’, which can be essentially described as a demographic investigation of the star formation rates in nearby galaxies and of the ages and chemical abundances of their stellar populations.

#### 1.2.2.1 The low-redshift Universe

Galaxies in the local Universe ( $z \sim 0.1$ ) appear in a large variety of shapes, sizes, luminosities and colours at different wavelengths. This variety reflects differences in the present star formation activity, gas and dust content, and the past activity of star formation and possibly interactions with the surrounding environment that led galaxies to look like they are today. Galaxies have been classified according to their morphology into the so-called Hubble sequence, from elliptical to irregular galaxies, passing through systems with varying fractions of a bulge and a disk component, the latter showing different degree of spiral structures. This sequence reflects a sequence in star formation activity, from quiescent systems to actively star forming galaxies. The galaxy star formation rate as a function of time is often modelled by a simple, smooth function such as an exponential or a delayed exponential model, which has a peak at time  $\tau$  followed by an exponential tail with a

## 1 Introduction

---

characteristic timescale  $\tau$ . Models with small  $\tau$  resemble an early burst of star formation, while large  $\tau$  describe constant or presently increasing SFR (see Fig 1.3). This is only a simplified description of the actual star formation history (SFH) in galaxies, which can be often characterized by subsequent bursts of star formation. These can be triggered by internal mechanisms, such as density waves and secular instabilities, or by external mechanisms, such as tidal interactions or mergers with other galaxies, or *ram-pressure* (i.e. the pressure of the intra-cluster medium on the inter-stellar gas for galaxies infalling into galaxy clusters).

A simple but interesting feature of galaxies is that they show a bi-modal distribution in several quantities and they can be separated into two broad classes at a characteristic stellar mass of  $M_{crit} \sim 3 \times 10^{10} M_{\odot}$  (e.g. Kauffmann et al. 2003; Baldry et al. 2004; Kannappan 2004). Above this scale, which corresponds to a mass of the hosting dark matter halo of  $\sim 10^{12} M_{\odot}$ , galaxies are predominantly red, bulge-dominated, with old stellar populations and low gas fractions. They lie preferentially in high-density environments, such as galaxy clusters. Below the critical mass, galaxies are blue, disk-dominated, with a high gas fraction which supplies the on-going star formation. Moreover, this characteristic mass represents a ‘knee’ in various relations of galaxy properties against stellar mass: while there is a rapid variation of galaxy properties with the mass of the system below  $M_{crit}$ , above this regime the relations flatten and galaxies form a more homogeneous class. At this scale the total mass-to-light ratio has a minimum, indicating a maximum efficiency of conversion of baryons into stars. It has been proposed that the observed bimodalities reflect a scale-dependent efficiency of the feedback processes that regulate star formation: while supernovae and radiative feedback regulates star formation below the critical scale, feedback from energetic sources such as active galactic nuclei keeps the gas hot and prevents further star formation and disk growth (Dekel & Birnboim 2004).

### 1.2.2.2 Elliptical galaxies

While there is predominance of star forming systems below the transition mass, elliptical galaxies, which have basically completed their star formation, dominate at high masses, in the regime where galaxy properties display a small scatter. Indeed, elliptical galaxies seem to form a very homogeneous class of objects, obeying several tight scaling relations. Among these, it is worth mentioning the Fundamental Plane, that describes the relation between the central velocity dispersion, the effective radius and the surface brightness inside the effective radius (e.g., Bender et al. 1992). Other fundamental relationships are those linking the mass of early-type galaxies with the physical parameters

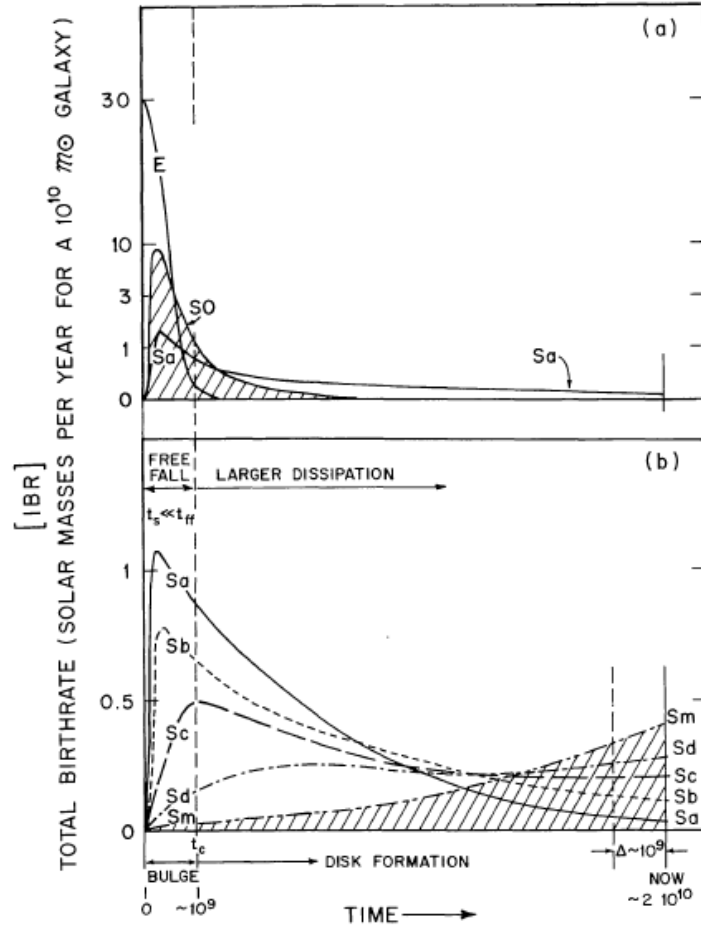


**Figure 1.3:** Schematic representation of the star formation history (‘integrated birthrate’ in units of  $M_{\odot}\text{yr}^{-1}$  as a function of time) for different types of galaxies. Galaxies are classified into the ‘Hubble sequence’ from ellipticals (‘E’), S0-Sa, dominated by a bulge, to spiral galaxies (Sb to Sm), with increasing contribution from a disk. The star formation history is peaked at early times for bulge-dominated galaxies. The peak shifts at later times and the star formation history gets broader for disk-dominated galaxies. It is still rising at present (‘now’) for the latest types (Sm), which have today the highest star formation rates. The vertical dashed line on the left marks the time of dissipative collapse: the ratio of this time and the time needed to complete star formation determines whether a disk forms and what the bulge-to-disk ratio is. (from Sandage 1986)

# 1 Introduction

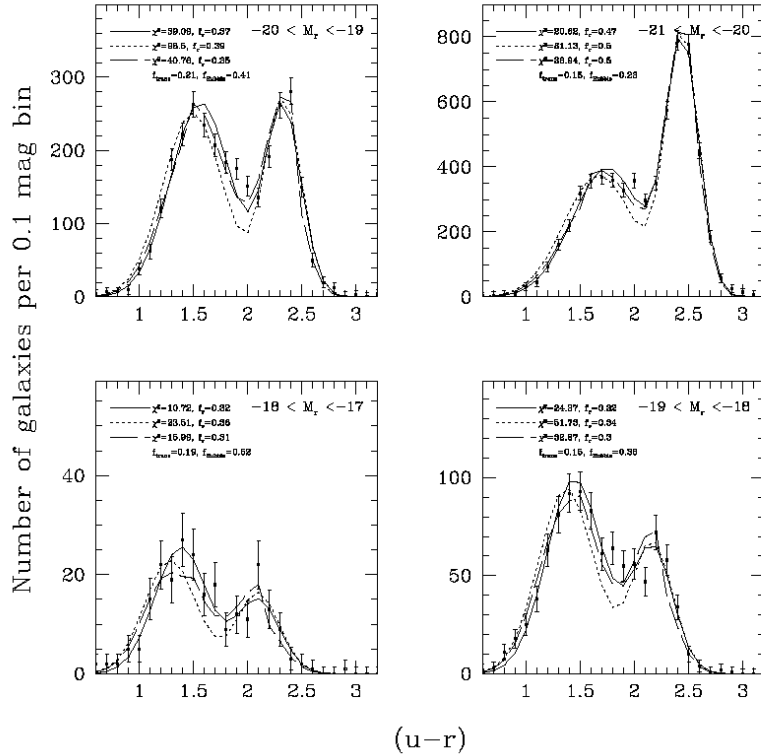


**Figure 1.4:** Distribution in the optical  $u - r$  colour for a sample of  $\sim 70,000$  galaxies from the Sloan Digital Sky Survey. The sample is divided in four luminosity bins, from faint (bottom-left panel) to bright galaxies (top-right panel). Each distribution is double-peaked (bi-modality) and there is a clear distinction between blue (i.e. with more flux in the shorter-wavelength  $u$  band) and red galaxies. The relative weight of the blue and the red population varies systematically from the faint to the bright galaxies bin: red galaxies dominate at the bright end. (from Baldry et al. 2004)

of their stellar populations, such as the colour-magnitude relation and the relation between the Mg absorption strength and the velocity dispersion (e.g., Baum 1959; Faber 1973; Bender et al. 1993; Worthey 1994). Such relations indicate that:

1. Elliptical galaxies are on average metal-rich and they form a sequence of increasing stellar metallicity with increasing mass;
2. The abundance ratio of  $\alpha$ -elements over Fe-peak elements is enhanced in massive ellipticals with respect to the average value in the solar neigh-

## 1.2 The physics of galaxy formation

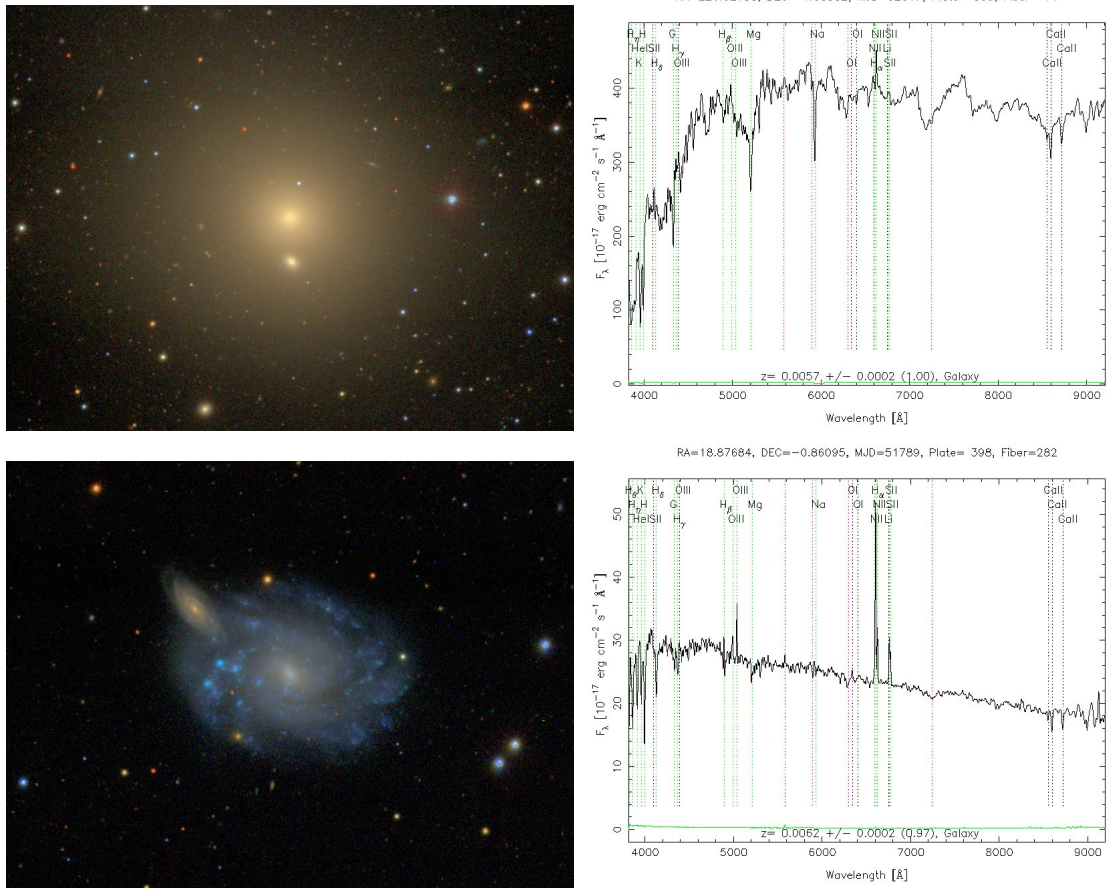


**Figure 1.5:** Comparison of the photometric and spectral properties of an elliptical and a spiral galaxy. The images on the left are obtained as mosaics of the images in three optical bands ( $g, r, i$ ) of the Sloan Digital Sky Survey (SDSS). On the right it is shown the corresponding optical spectrum from 3800 to 9200  $\text{\AA}$  as obtained from the SDSS with a 3-arcsec diameter fibre. The redshift of the galaxy is indicated at the bottom of the spectrum. Several absorption and emission lines are also marked. The elliptical galaxy (NGC 5446, top row) displays red colours indicative of old stellar populations. This is reflected in the spectrum which has a sharp decline of the flux around 4000  $\text{\AA}$  and is characterised by prominent absorption lines whose strength is an indicator of the age and metallicity of the galaxy (see section 1.3). The galaxy on the bottom row (NGC 450) displays instead a much bluer colour, indicative of younger stellar populations. The structure is not as homogeneous as for the elliptical galaxy, and spiral patterns are visible with compact regions of higher surface brightness where star formation is occurring. Contrary to the elliptical galaxy, the spectrum is characterised by a stellar continuum rising at short wavelengths and with weak absorption lines. The strong emission lines (in particular H $\alpha$  at 6563  $\text{\AA}$ ) come from the ionized gas surrounding young massive stars: their strength is thus an indicator of the present star formation rate.

## 1 Introduction

---

bourhood;

3. The scatter in the observed relations, although small, seems to reflect a scatter in the mean stellar age. Evidence is accumulating that this scatter increases with decreasing mass and that low-mass early-type galaxies are on average younger than more massive ones.

The first constraint requires a high degree of chemical processing in massive ellipticals, meaning that a large fraction of gas has to be converted into stars, but does not necessarily involve any constraint on the timescale of star formation. The high  $\alpha$ -elements-to-Fe abundance ratios in massive ellipticals hint at shorter star formation timescales.<sup>4</sup> Items 2 and 3 together indicate that the most massive ellipticals formed their stars early and fast. Lower-mass galaxies, instead, either have a more extended SFH or started to form their stars at later epochs (this shift in star formation activity to later epochs in less massive systems is often called ‘downsizing’).

In a classical model early-type galaxies formed through the dissipation-less collapse of a single gas cloud with star formation taking place on short timescales at the beginning of the collapse (‘monolithic collapse’, Eggen et al. 1962; Larson 1974). Such a model can easily predict timescales short enough to produce the degree of  $\alpha$ -enhancement observed in massive ellipticals. Moreover, the onset of galactic winds (in the form of supernova-driven winds) is able to expel metal-loaded gas from the shallow potential wells of low-mass galaxies, reproducing the observed mass-metallicity relation.

Beside the observational evidence of the occurrence of galaxy mergers and their role in altering galaxy properties, the main disadvantage of this scenario is that it does not consider galaxy formation in a cosmological framework. Models of hierarchical galaxy formation are naturally based on the theory of structure growth from primordial density fluctuations (see section 1.1). In such models an elliptical galaxy is formed through subsequent merging of smaller units and eventually by the merger of two galaxies of similar size (‘major merger’). Renditions of such models that include chemical evolution and strong feedback, together with metallicity-dependent population synthesis models (see section 1.3.2), can reproduce the observed relations in terms of a mass-metallicity relation. The main challenge for these models is represented by the observed values of  $\alpha$ /Fe ratio and the increase of this ratio with galaxy mass, which require shorter star formation timescales in more massive ellipticals. This calls for a feedback mechanism able to quench star

---

<sup>4</sup>Note that generally both observational constraints are more easily met if variations in the initial mass function (IMF, see below) are allowed, e.g. by invoking for massive ellipticals an IMF that gives more weight to high-mass stars (i.e. in a burst of star formation more massive stars are produced with respect to the standard IMF).

formation on short timescale and that is more efficient in doing so in more massive galaxies. Such source of feedback may be represented by active galactic nuclei. It has to be noticed that the range of observed  $\alpha/\text{Fe}$  ratios is reproduced also in hierarchical models of galaxy formation that impose a flatter IMF (i.e. more skewed toward high masses) during the starburst ignited by the major merger that produced the elliptical. To reproduce the increase of  $\alpha/\text{Fe}$  with mass, however, it would require an IMF systematically flatter in more massive systems, which is not observationally justified. Finally, the old mean ages of the most massive ellipticals and the ‘downsizing’ trend appear in contradiction with the expectation of hierarchical galaxy formation, where small systems form first to produce at later epochs larger systems through mergers. However, this hierarchy refers to the *assembly* history of galaxies and not necessarily to the history of star formation: the stars in a present-day massive elliptical may have formed much before the bulk of the galaxy we see today assembled. Mergers between gas-poor systems, such as elliptical galaxies, could occur without triggering a star formation event (‘dry mergers’)

### 1.2.2.3 The star formation history of the Universe

Understanding the history of conversion of baryons into stars requires measurements of star formation rates, chemical abundances and stellar masses of galaxies at various redshifts. While star formation rates directly tell us how the activity of star formation varied with cosmic time, the degree of chemical enrichment and the amount of mass in stars at various epochs are the result of the fuel consumption and of the nucleosynthesis by all stars ever produced up to then. This kind of studies aim at understanding, among others, whether there is a characteristic epoch of stars and elements formation in galaxies, when early-type galaxies formed, what is the origin of disk galaxies.

A successful technique for the identification of high-redshift star-forming galaxies makes use of a particular signature in galaxy spectra, the Lyman-continuum break at  $912\text{\AA}$ . This feature arises from an intrinsic discontinuity in the spectra of hot stars and the effect of atomic hydrogen absorption in the intergalactic medium along the galaxy line of sight. This reduces significantly the emission at wavelength shorter than  $912\text{\AA}$ . At  $z \sim 3$  the Lyman-break is shifted to  $\sim 4000\text{\AA}$  and can be easily identified by comparing the fluxes measured short-ward and long-ward of this wavelength. Those galaxies having UV flux significantly smaller than the optical flux (i.e. red UV-optical colours) are likely to be star-forming galaxies at  $z \sim 3$ . This technique is also known as ‘UV drop-out’. Similarly, ‘drop-outs’ at longer wavelength are able to select star-forming galaxies at higher redshifts ( $z \sim 4$ ). The rest-frame UV radiation (between  $3000\text{\AA}$  and the Lyman-break) of star-forming galaxies is a

## 1 Introduction

---

direct tracer of the instantaneous star formation rate and metal ejection rate, because they are both related to the number of young, hot, massive stars in the galaxy. From the UV emission density it is then possible to derive, with appropriate conversion factors, the density of star formation rate or metal ejection rate for samples of star-forming galaxies at various redshifts.

Several studies in this field have converged into a picture of cosmic star formation history rapidly declining from  $z = 1$  to the present. The redshift range  $1 < z < 2$  appears as a critical epoch when most of the star formation activity occurred (e.g. Lilly et al. 1996; Madau et al. 1996, 1998). Whether the star formation rate density of the Universe decreases again at higher redshift or it stays almost constant is more controversial, the main uncertainty arising from the poorly known (yet presumably high) correction for dust attenuation affecting SFR estimates of high-redshift starburst galaxies. The behaviour of the cosmic star formation history is also reproduced by models of cosmic chemical evolution (Pei & Fall 1995, see also section 1.3.1): the predictions of such models about the total amount of metals produced at different epochs have to be compared with observations, to discriminate different scenarios.

A parallel and complementary effort toward the understanding of the history of star formation in the Universe is the measurement of chemical abundances at various redshifts. Large progresses have been achieved in this sense in the last decade, allowing to trace the stellar nucleosynthesis over most of the age of the Universe. Emission lines in the spectra of star forming galaxies have been widely used to derive abundances in galaxies up to  $z \sim 1$  (e.g. Pagel et al. 1979; Kobulnicky & Zaritsky 1999; Ellison et al. 2005). However, some discrepancies persist between the different indicators adopted and different calibrations of the same indicator. Resonance absorption lines in the rest-frame UV are another important tool for determining the abundances in the interstellar gas. These have been used in high-redshift absorption systems seen in the spectra of QSO. Such absorption systems can probe different hydrogen column densities. Perhaps the most studied are the Damped Ly- $\alpha$  Absorbers (DLA)<sup>5</sup>, which have the largest column densities of neutral gas and show readily measurable spectral features (e.g. Pettini et al. 1997). These systems are particularly interesting in that they have column densities comparable to those of the disks of present-day spiral galaxies, of which they may be precursors. The comparison between absorption-lines and emission-lines measured abundances can provide information about abundance gradients in galaxies (the former probing the outer regions with a larger cross-section for absorption against a background source, the latter probing the high surface density

---

<sup>5</sup>They are called in this way because the density is sufficiently high ( $N_{\text{HI}} > 10^{20} \text{ cm}^{-2}$ ) to produce detectable damping wings in the Ly- $\alpha$  absorption profile.

### 1.3 The stellar populations in galaxies

---

star forming regions of a galaxy), or of the existence of extended envelopes of unprocessed gas in galaxy outskirts. An interesting result from these studies is the detection of bright star-forming galaxies which have gained near-solar metallicity at  $z = 2-3$ , indicating an intense activity already at these redshifts and before.

Additional and complementary insight can also be gained from the galaxy stellar mass, which provides the link between structure growth and assembly and star formation in galaxies. The global stellar mass density as a function of redshift has been derived by Dickinson et al. (2003). The result is consistent with other derivations of the cosmic SFH, showing a rapid rise in the stellar mass density down to  $z = 1$  and then only a mild change to the present. This indicates that the intermediate-redshift range between 1 and 2 is a critical epoch of rapid growth. Furthermore, studying the cosmic SFH in combination with stellar mass measurements can provide information about the contribution from different galaxies at different epoch. It seems clear that the most massive galaxies were dominated by star formation at high redshift and they almost completed their star formation by  $z = 1$ . On the contrary, low-mass systems dominate the SFR density at the present epoch. This is another manifestation of the so-called ‘downsizing’. These results are supported by several observational evidences of the fact that massive galaxies with very high SFR were already in place at  $z = 2 - 3$  (e.g. Smail et al. 2002). These may be the precursors of present-day massive ellipticals.

It is clear that all these studies at high redshifts, for which the measurements are more difficult, should agree with those derived by low-redshift studies that allow a detailed analysis of the ages and chemical abundances of the stellar populations in massive galaxies. Moreover, the total amount of mass in stars and metals at the present epoch represents a fundamental zero-point constraints on the cosmic star formation history.

### 1.3 The stellar populations in galaxies

The properties of the stellar populations in the galaxies we see today are the result of their past history of star formation and chemical evolution. To set constraints on the formation mechanisms of the stellar populations in galaxies models of chemical evolution have to be studied. These describe the fundamental equations governing the cycle of metal production and ejection, as a result of the galaxy star formation history and the physics of stellar evolution (section 1.3.1). The integrated spectra of galaxies carry information about the ages and chemical abundances of the stars in galaxies, and thus on the star formation and chemical enrichment history of the Universe. Population

## 1 Introduction

---

synthesis models are the major tool to interpret integrated colours and spectra of galaxies in terms of the physical parameters of their stellar populations (section 1.3.2). I will give here a basic overview of chemical evolution and population synthesis models.

### 1.3.1 Star formation and chemical evolution

During primordial nucleosynthesis, in the first few minutes after the Big Bang, only hydrogen and helium, and a small amount of lithium, are synthesized. In the early Universe, temperature and density are not high enough for further nucleosynthesis to take place, and thus heavier elements are not produced. Thermonuclear reactions that produce metals<sup>6</sup> can instead take place in the core of stars, depending on the initial mass of the star. Elements up to carbon and nitrogen are synthesized in the cores of intermediate-mass stars ( $\lesssim 8M_{\odot}$ ), while heavier elements are produced in stars more massive than  $8M_{\odot}$ . In order to enter the cycle of chemical evolution in a galaxies, the newly produced elements need to be ejected into the interstellar medium (ISM).

Some fraction of synthesized elements can be ejected into the ISM during the life of the star, through mass-loaded stellar winds. These bring into the ISM mainly the elements out of which the star was formed and some newly produced elements that have been dredged up to the surface. A major source of enrichment with heavy elements comes from the supernova explosions at the end of the stellar evolution. Supernovae can be classified into two main classes, having different origin, different timescales and yielding different amounts of heavy elements:

- Supernovae of type II (SN II) are the final evolutionary stage of short-lived (10 Myr), massive stars. During the explosion, the envelope containing the elements produced in hydrostatic nuclear burning is ejected. Further nucleosynthesis takes place during the explosion, in which iron and heavier elements are produced. Note that the iron supplied by SN II to the ISM is only the one synthesized during the explosion, while the iron core at the centre of the star at the time of explosion forms the stellar remnant and will evolve into a neutron star or a black hole. SN II contribute primarily to the enrichment of the so-called  $\alpha$ -elements (N, O, Mg, Ca, Na, Ne, S, Si, Ti) and the total metallicity.
- According to the most favoured models, supernovae of type Ia (SN Ia) are produced in close binary systems, consisting of long-lived (0.1-1

---

<sup>6</sup>In astrophysics, it is conventional to call ‘metals’ all the elements heavier than helium, and metallicity is the mass fraction of all elements heavier than helium over the total mass of all elements.

### 1.3 The stellar populations in galaxies

---

Gyr), intermediate- and low-mass stars. The primary star, evolved into a degenerate white dwarf, accretes material from the evolved secondary star until it fills its Roche lobe and a carbon-deflagration occurs, probably completely disrupting the system. SN Ia contribute a substantial fraction to the enrichment of iron.

The different timescale of the two types of supernovae and their different heavy elements yields have a great impact in the use of metallicity and elements abundances to gain insight into the galaxy star formation history. In particular, the longer timescales of SN Ia imply that the production of Fe is delayed with respect to  $\alpha$ -elements. Therefore, the  $\alpha$ /Fe abundance ratio carries information about the timescale of chemical enrichment and hence star formation. The total metallicity, on the other hand, does not depend directly on the timescale of star formation, but rather on the total fraction of gas that has been converted into stars.

Both total metallicity and elements abundance ratios are also affected by the initial mass function (IMF), which describes the distribution in mass of a freshly formed stellar population<sup>7</sup>. It is clear that an IMF that is more heavily weighted toward high-mass stars would result in the production of more metals per mass of a stellar generation, so the total metallicity would be higher. Moreover, an IMF that contains more massive stars produce more  $\alpha$ -elements per stellar generation and thus it would lead to higher  $\alpha$ /Fe abundance ratios.

It is usually assumed that  $\phi(m)$  can be described by a simple function, commonly a power law. This is justified by the argument that star formation is a chaotic process, with densities and temperatures varying by orders of magnitudes. As such it is unlikely to bear the imprint of any particular scale, so the IMF should be rather featureless. In a classical work Salpeter (1955) concluded that the IMF should scale as  $\phi(m) \propto m^{-\alpha}$  with  $\alpha = 2.35$ . More recent works imply an exponent  $\alpha > 2$  at low masses and  $\alpha < 2$  at high masses, avoiding divergence of the total mass involved in a starburst (Salpeter 1955; Scalo 1998; Kroupa 2001; Chabrier 2003). Whether the shape of the IMF is universal and constant in time, or whether it varies with redshift and with galaxy properties is not clear. Several observations of the chemical abundances in elliptical galaxies seem to require variable IMF, either from galaxy to galaxy (in the sense that more massive galaxies have flatter IMF) or along the galaxy star formation history (a flatter IMF could be required in merger-induced bursts of star formation). However, no direct observational evidence supports a variable IMF.

---

<sup>7</sup>The initial mass function  $\phi(m)$  is normalized over the total mass of new-born stars rather than on their total number, so that  $\phi(m)dm$  is the number of stars born with mass between  $m$  and  $m + dm$ .

## 1 Introduction

---

Together with the star formation rate (SFR) and star formation history (SFH), the IMF represents one of the necessary input parameters in chemical evolution models. I briefly describe here the fundamental equations of such models.

The formation of stars and the re-ejection of processed gas in galaxies can be described by the following phenomenological equations (Tinsley 1980; Pagel 1997, 2002):

$$\dot{M}_{tot} = f \quad (1.8)$$

$$\dot{M}_* = \psi - E \quad (1.9)$$

$$\dot{M}_g = -\psi + E + f \quad (1.10)$$

Equation 1.8 tells us that the total mass  $M_{tot} = M_g + M_*$ , given by the mass in gas and the mass in stars, varies with time only according to the infall or outflow  $f$  of primordial or enriched gas. Equation 1.9 shows that the stellar mass increases at a rate given by the star formation rate  $\psi$  and decreases due to the ejection of gas  $E$ . The mass of gas behaves contrary to the mass of stars, with the additional component of the infalling or outflowing gas (equation 1.10).

The gas ejection rate  $E$  is obtained by integrating the ejected mass fraction  $(m - w_m)$ , where  $w_m$  is the mass of the remnant at the end of the evolution of a star of mass  $m$ , convolved with the IMF and the star formation rate at time  $(t - \tau_m)$ , where  $\tau_m$  is the lifetime of a star of mass  $m$ , from the turn-off mass  $m_t$  to infinity:

$$E(t) = \int_{m_t}^{\infty} (m - w_m) \psi(t - \tau_m) \phi(m) dm \quad (1.11)$$

For the products of SN II (hence  $\alpha$ -elements and total metallicity) that occur on short timescales ( $10^8$  yr), over which the star formation rate should keep almost constant, the lifetime  $\tau_m$  can be neglected. This is equivalent to assume instantaneous recycling of the produced elements. Note that this is different from the instantaneous mixing approximation (i.e. the ejected metals are instantaneously mixed into the ISM), which is assumed in most chemical evolution models. The instantaneous recycling may be not a good approximation for the products of SN Ia, which occur on much longer timescales (few Gyr). This can affect in particular galaxies in which the star formation history is not smooth but characterized by episodes of intense activity.

At this point it is useful to introduce two quantities, the returned mass fraction  $R$ , which is the mass of gas returned to the ISM by evolved stars, and the stellar yield  $y$ , which is the mass of produced metals per remnant mass.

### 1.3 The stellar populations in galaxies

---

Their expression, under the instantaneous recycling approximation, is given by:

$$R = \int_{m_1}^{\infty} (m - w_m)\phi(m)dm \quad (1.12)$$

$$y = \frac{1}{1 - R} \int_{m_1}^{\infty} mp_Z\phi(m)dm \quad (1.13)$$

where  $p_Z$  is the mass fraction of new metals produced by a star of mass  $m$ . Using these quantities, equation 1.11 simplifies into  $E(t) = R\psi(t)$ . Inserting this in equations 1.9 and 1.10, it is easy to obtain:

$$\dot{M}_* = (1 - R)\psi(t) \quad (1.14)$$

$$\dot{M}_g = -(1 - R)\psi(t) + f \quad (1.15)$$

The evolution of the metal mass fraction  $Z$  can be obtained combining

$$\frac{d(ZM_g)}{dt} = -Z(t)\psi(t) + RZ\psi(t) + (1 - R)y(t)\psi(t) + Z_f f \quad (1.16)$$

where  $Z_f$  is the abundance of the infalling or outflowing gas, with equation 1.15. This gives:

$$M_g \frac{dZ}{dt} = (1 - R)y(t)\psi(t) + (Z_f - Z)f \quad (1.17)$$

Equations 1.14, 1.15 and 1.17 govern chemical evolution under the assumption of instantaneous recycling approximation.

I note passing that this set of equations can be extended to study the global chemical evolution of the Universe. Models of cosmic chemical evolution have been developed e.g. by Pei & Fall (1995). These models are governed by very similar equations as those given above expressed in terms of mean co-moving densities of stars and gas, measured in units of the present-day critical density. The predictions of such models can be compared with observational measurements of the densities of mass and of metals at various epochs to get constraints on the global evolution of star formation rate and metal production rate with look-back time.

The simplest evolution model is one in which the galaxy is assumed to be a ‘closed-box’, in the sense that there is no exchange of mass with the surrounding environment and the total mass is conserved (i.e., the rhs of equation 1.8 is zero). Assuming that initially the mass is only in the gaseous component with zero metallicity, equations 1.15 and 1.17 can be combined to give:

$$\frac{1}{M_g} \frac{dM_g}{dZ} = -\frac{1}{y} \quad (1.18)$$

## 1 Introduction

---

We can now express the metallicity of the gas as:

$$Z(t) = \bar{y} \ln \frac{M_{tot}}{M_g(t)} \quad (1.19)$$

We can ask as well which is the metallicity of the stars. In a closed-box model the stars and the gas must contain all the elements ever produced, which translates into the equation:

$$Z_* M_* + Z M_g = (1 - R) \bar{y} \bar{\psi} t \quad (1.20)$$

where the barred letters refer to averages over the star formation history. Approximating the stellar mass with  $(1 - R) \bar{\psi} t$ , this gives:

$$Z_* M_* = \bar{y} M_* - Z M_g \quad (1.21)$$

It is interesting to note some implications of equations 1.19 and 1.21. The metallicity of the gas is not an explicit function of time, but it depends only on the yield and the gas mass fraction  $\mu_{gas} = M_g/M_{tot}$ . If a measure of the gas metallicity and of  $\mu_{gas}$  of a galaxy is available it is possible to derive an ‘effective yield’ by inverting equation 1.19. If the simple model holds, this should be equal to the true yield. This test has been done by Garnett (2002) on a small sample of nearby spirals and irregular galaxies and repeated by Tremonti et al. (2004) on a much larger sample of star forming galaxies drawn from the SDSS (see section 1.4.1). There is a clear indication that the effective yield is not constant, but decreases with mass below a total (gas+stars) mass of about  $10^{9.5} M_\odot$ . Equation 1.21 tells us that, when there is almost no gas supply anymore (i.e.  $M_g \ll M_*$ ), the stellar metallicity should approach the yield and be independent of any other galaxy property. As I will show in this work (Chapter 2), this is not observed: even considering galaxies which have terminated their star formation, the stellar metallicity is not constant but decreases with stellar mass. This is true for low-mass galaxies ( $\lesssim 10^{10} M_\odot$ ). Such relation is significant only for elliptical galaxies, with no ongoing star formation. For star forming galaxies, instead, the stellar metallicity is not simply determined by the stellar mass but can vary significantly between galaxies with similar stellar mass depending on the gas mass fraction. This is reflected in the much larger scatter in the  $M_* - Z_*$  relation for star forming galaxies.

Exploring models with outflows of gas or infall of unenriched gas, Edmunds (1990) has shown that the simple closed-box model is ‘maximal’, in the sense that it provides an upper bound on the gas metallicity when a given gas mass fraction is reached, and on the (mass-weighted) stellar metallicity. Either inflow of unenriched gas or outflows can thus explain the results mentioned

above. It is likely that both mechanisms are at play during galaxy evolution, however other independent observational evidence favours gas outflows in the form of supernova-driven galactic winds as the origin of the mass-metallicity relation: the gas can be heated to the escape velocity more easily in low-mass systems, with shallow potential wells, thus carrying out metals from the galaxy.

#### 1.3.2 Population synthesis models

Here I introduce the basic concepts of evolutionary population synthesis models. They represent the fundamental tool for the interpretation of galaxy spectra in terms of the physical parameters of their underlying stellar populations.

Distant galaxies cannot be resolved in their stellar populations, rather what we can observe is their integrated light, which is the result of the superposition of different stellar populations of various age and metallicity. In the 70's attempts were made to interpret the integrated spectra of galaxies by reproducing the spectrum with a linear combination of individual spectra of stars of different types. This idea was soon abandoned because it involved too many free parameters, and replaced in the 80's by evolutionary population synthesis technique (Tinsley 1978; Arimoto & Yoshii 1987; Guiderdoni & Rocca-Volmerange 1987; Bruzual A. & Charlot 1993; Fioc & Rocca-Volmerange 1997; Maraston 1998; Vazdekis 1999; Bruzual & Charlot 2003). The only free parameters involved here are the star formation rate, the initial mass function and, in some cases, the chemical enrichment rate. The technique is based on the idea that a stellar population with any star formation history can be decomposed into a series of instantaneous starbursts, or 'Simple Stellar Populations' (SSP, i.e. a coeval population of stars formed instantaneously). The goal of population synthesis models is to describe the time-dependent distribution of stars in the colour-magnitude diagram and derive the integrated spectral evolution of the stellar population.

The spectral energy distribution of a stellar population characterized by star formation rate  $\psi(t)$  and metallicity  $Z(t)$  can be written as:

$$F_{\lambda}(t) = \int_0^t \psi(t-t') S_{\lambda}(t', Z(t-t')) dt \quad (1.22)$$

where  $S_{\lambda}(t', Z(t-t'))$  is the spectral energy distribution of the *isochrone*<sup>8</sup> of an SSP of age  $t$  and metallicity  $Z(t-t')$ . Stars are distributed along the

---

<sup>8</sup>An isochrone describes an SSP of given age and metallicity, by specifying the stellar parameters bolometric luminosity, effective temperature and surface gravity of the individual stellar masses.

## 1 Introduction

---

isochrone according to the IMF.

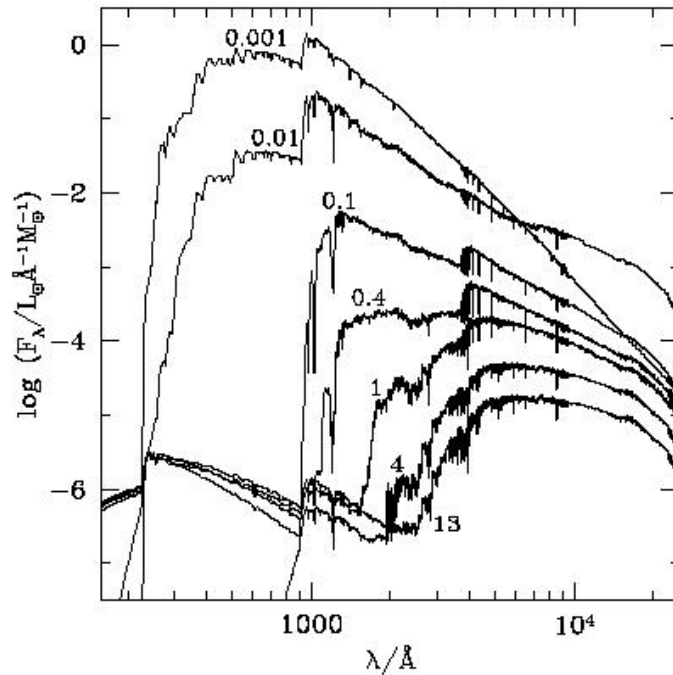
The two main ingredients necessary for the calculation of  $S_\lambda$  are the stellar evolution prescription, which gives the theoretical stellar evolutionary tracks of single stars of mass  $m$ , and the stellar spectral libraries. Both theoretical stellar atmosphere libraries and observed stellar spectra can be used. Observational stellar libraries are limited to spectra of stars in the Milky Way and in the Magellanic Clouds (and thus they have scaled-solar elements abundance ratios). The libraries of individual stellar spectra are necessary to assign spectra to stars in the various evolutionary stages of the isochrone. Finally, the spectral energy distribution of the SSP is obtained by summing the spectra of individual stars along the isochrone.

Figure 1.6 illustrates the spectral evolution of an SSP of solar metallicity from  $10^6$  yr to 13 Gyr. When the population is young, the spectrum is dominated by short-lived, massive stars that produce a strong emission in the ultraviolet (UV), below  $2000\text{\AA}$ . As time goes by the most massive stars leave the main sequence and evolve into red giant stars, causing a decrease in the UV light and an increase in the near-infrared (IR) light. After a few Gyrs, red giant stars account for most of the near-IR emission. The UV emission starts again to rise until 13 Gyr because of the accumulation of low-mass, post Asymptotic Giant Branch stars. From 4 to 13 Gyr the shape of the spectrum from the optical to the near-IR is almost unevolving, because low-mass stars cover a narrow temperature range during their entire evolution. The spectral evolution can be appreciated also in the strength of stellar absorption lines. In particular, between 0.1 and 1 Gyr there is a marked strengthening of all the Balmer lines (from  $H\alpha$  at  $6563\text{\AA}$  to the continuum limit at  $3646\text{\AA}$ ). The strength of the Balmer lines represent a powerful diagnostic tool of recent burst of star formation. Another important spectral feature is the so-called  $4000\text{\AA}$ -break which arises from the prominence in cool stars of many metallic lines blueward of  $4000\text{\AA}$ . This feature is widely used as age indicator, but it shows also a dependence on metallicity at old ages. All these spectral lines, plus other metallic lines associated to Ca, Mg, Fe, continue to evolve even between 4 and 13 Gyr when the shape of the continuum is almost constant.

The interpretation of observed galaxy spectra in terms of physical parameters relies often on the comparison of their broad-band colours with the predictions from population synthesis models<sup>9</sup>. The main problem in this respect is the similar effect that age and metallicity have on the integrated light of a stellar population. The ages and metallicities derived from integrated galaxy

---

<sup>9</sup>The stellar ages and metallicities derived from galaxy spectra have to be interpreted as the light-weighted mean ages and metallicities of all the stellar population in a galaxy.



**Figure 1.6:** Spectral evolution from the ultraviolet to the infrared of a Simple Stellar Population of solar metallicity, obtained from the Bruzual & Charlot (2003) population synthesis code. At young ages (indicated on each spectrum in units of Gyr) the light is dominated by the UV emission of young, short-lived, massive stars. These stars soon leave the main sequence and evolve into Red Giants, causing a drop of the UV emission and a rise in the infrared. Between 1 and 13 Gyr the shape of the continuum does not change significantly, because it is dominated by long-lived, low-mass stars, which cover a small temperature range. Over this time interval, it can be appreciated the strengthening of several absorption lines and the characteristic break at  $4000\text{\AA}$ . These are important diagnostics of the ages and metallicities of stars in galaxies.

spectra are therefore highly degenerate. This problem is further complicated in galaxies with a significant content of dust, which produces a reddening of the optical spectrum similar to that caused by increasing age or metallicity.

A well-established method to try and solve this degeneracy is to use spectral diagnostics which involve single spectral absorption features that have different sensitivities to age and metallicity. The most successful combinations of absorption features are those involving a hydrogen Balmer line, as a diagnostic of age, and ‘metallic’ features sensitive to the abundance of elements

## 1 Introduction

---

such as Fe or Mg. Moreover, these spectral absorption features are defined on narrower wavelength ranges than colours, and so they are believed to be almost insensitive to the reddening of the continuum due to dust absorption.

In order to allow a universal analysis of galaxy spectra Burstein et al. (1984) and Faber et al. (1985) introduced a set of absorption line indices in the optical, known as the *Lick system*, which has become the most widely used set of absorption indices. It includes 25 features over the wavelength range from 4000 to 6400Å. In the Lick system, an index is defined by a central ‘feature bandpass’, bracketed by two ‘pseudo-continuum bandpasses’ (Worthey 1994; Worthey & Ottaviani 1997). Atomic indices are conventionally expressed in Å of equivalent width, while molecular indices in magnitudes. The strength of these features were originally parametrized as a function of stellar parameters, such as effective temperature  $T_{eff}$  and surface gravity  $g$ , using a sample of 460 Galactic stars. These *fitting functions* are purely empirical and were used to measure index strengths of theoretical SSPs. There are several problems, however, related to the use of the fitting functions. The stellar library used to define the Lick system is sparse at supra-solar metallicities. Therefore, the fitting functions are well defined only around solar metallicity and are mostly extrapolated at higher metallicities. Moreover, the Lick stellar library lacks of hot stars, necessary for the interpretation of young populations, so this kind of studies were usually limited to old stellar populations. Moreover, the Lick spectra were not flux-calibrated and had low resolution ( $\Delta\lambda \sim 8\text{Å}$ , almost three times lower than the resolution of modern spectroscopic surveys). The calibration of the index strengths onto the Lick system requires therefore to degrade observed galaxy spectra to the lower resolution of the Lick spectrograph. Since the Lick standards are not flux-calibrated, the shape of the continuum has to be corrected, introducing another source of uncertainty.

All these limits associated with the use of the fitting functions and the calibration onto the Lick system have now been overcome with population synthesis models based on higher-resolution stellar spectra that cover the entire temperature range (Bruzual & Charlot 2003). The 3Å resolution matches the resolution of the spectra gathered by modern spectroscopic surveys, and allows to measure the indices on the model spectra using directly the bandpass definitions, in the same way as in observed spectra. There is no need to degrade the observed spectra to lower resolution. Moreover, the full temperature coverage allows to extend the use of the Lick indices to star-forming galaxies with younger stellar populations. As explained in Chapter 2 I will use these models in this work.

## 1.4 Extragalactic surveys

A significant step forward in our understanding of structure formation and galaxy evolution has been represented by the advent of large galaxy redshift surveys. The large amount of data, with information about the redshift, the photometric and spectroscopic properties of galaxies have allowed to gain a deep insight into the large scale structure of the Universe, the distribution and the properties of high-redshift objects, the detailed structural and physical properties of nearby galaxies.

The first redshift surveys, started in the 80's and 90's, such as the CfA (Huchra et al. 1983), the Las Campanas (Lin 1995), and the Canada-France Redshift Survey (CFRS, Lilly et al. 1995) have provided redshift measurements for tens of thousands of galaxies. An impressive progress in this respect has occurred with the advent of multi-fibre technology, which allows to measure redshifts for several hundreds galaxies in a single exposure. Such large samples have been collected by spectroscopic surveys in the optical such as the 2dF Galaxy Redshift Survey (2dFGRS, Colless et al. 2001) and the Sloan Digital Sky Survey (SDSS, York et al. 2000).

In this work I will make use exclusively of SDSS data, therefore I here give an overview of the relevant features of this survey (section 1.4.1). However, it is also worth mentioning other surveys at higher redshifts and over wavelength domains other than optical. These are relevant as they open the possibilities to extensions and new applications of the work presented in this Thesis. I will briefly introduce them below (section 1.4.2).

### 1.4.1 The Sloan Digital Sky Survey

It is not overstated to say that the Sloan Digital Sky Survey is one of the most ambitious large-scale optical surveys of the sky ever undertaken. Started in 2000, the SDSS has by now covered almost one quarter of the sky with five-band imaging and medium-resolution spectroscopy. The area surveyed is centred on the north Galactic cap and includes three stripes in the southern Galactic hemisphere (one of those has been devoted to study variable objects and obtain deeper observations). With the fourth data release the survey has provided images of hundred millions of objects and  $\sim 70$  millions of galaxies with  $r$ -band magnitude brighter than 22.2, and spectra for 849,920 objects (including 565,715 galaxies).

The principal science objective of the survey is to produce a complete three-dimensional map of the Universe out to redshift 0.4. The amount of data and spectro-photometric information it provides, however, has had and still will have in the near future a significant impact in several astronomical branches,

## 1 Introduction

---

including properties and distribution of high-redshift quasars, properties of galaxies and galaxy clusters, detailed investigation of the stellar populations in galaxies, the stellar structure of our own Galaxy, stars, and asteroids in the Solar System.

### 1.4.1.1 Photometry

The imaging survey covers  $\pi$  steradians of the northern sky and provides images in five pass-band filters ( $u, g, r, i, z$ ) that span the entire optical spectral range, from the atmospheric ultra-violet cut-off to the near-infrared. The imaging data are acquired at the dedicated 2.5m f/5 modified Ritchey-Chretien altitude-azimuth telescope located at Apache Point Observatory (APO) in south-east New Mexico. The 3 degree field of view is covered with 30  $2048 \times 2048$  CCDs arranged in six columns of five CCDs each. The camera operates in a drift-scan mode and produces five images of a given object with an effective exposure time of 54 seconds.

Automated pipelines have been developed to reduce the imaging data, performing the standard reduction and calibration procedures. These include sky subtraction, deblending of overlapping sources, extraction of the catalogue of objects and measurement of their photometric properties (Lupton et al. 2001).

It is worth mentioning some of the photometric quantities provided for each object by the SDSS, in particular the magnitude of galaxies. Contrary to stars, galaxies do not have sharp edges and have different surface brightness profiles. Different types of magnitudes can thus be measured. The SDSS pipeline calculates model magnitudes and Petrosian magnitudes.

The *model* magnitudes are calculated by fitting to the two-dimensional image in the  $r$ -band a de Vaucouleurs and an exponential surface brightness profile<sup>10</sup>. Total magnitudes are then calculated from the better fit of the two models. The same model is fitted to the images in the other bands and the corresponding flux is obtained from the normalization constant relative to the  $r$ -band. In this way, the flux is measured at the same effective aperture in all bands. These models are also corrected for the point spread function<sup>11</sup>. Another version of the model magnitude is the *cmodel* magnitude. This is obtained from the best-fit de Vaucouleurs and exponential model and combining them into the best-fit linear combination. The flux of the composite model is obtained by summing the fluxes of the two models, weighted by the

---

<sup>10</sup>The surface brightness  $I(r)$  is proportional to  $\exp(-r^{1/4})$  for a de Vaucouleurs profile and to  $\exp(-r)$  for an exponential profile.

<sup>11</sup>The point spread function (PSF) measures the typical size of a point source, due to finite resolution and atmospheric distortions.

corresponding coefficient in the linear combination. The coefficients are also stored and they can be useful quantities to separate different galaxy types (e.g. elliptical galaxies can be selected according to the criterion that they prefer a de Vaucouleurs rather than an exponential profile).

The *Petrosian* magnitudes have the advantage of measuring a constant fraction of the total galaxy light, independent of the distance of the object. The idea is to measure fluxes in an aperture of radius defined by the shape of the azimuthally averaged light profile. First, the Petrosian radius  $r_P$  is defined as the radius at which the local surface brightness in an annulus at  $r_P$  is 20 percent of the mean surface brightness within  $r_P$ . The Petrosian flux is obtained integrating the surface brightness profile out to  $2r_P$ . The aperture in all bands is set by the profile in the  $r$  band. This ensures that the colours, measured by comparing the Petrosian fluxes in different bands, are measured through a consistent aperture. For a de Vaucouleurs profile, the Petrosian flux is about 98 percent of the total flux, and about 80 percent for an exponential profile.

Finally, *fibre* magnitudes are also estimated. These are obtained from the flux contained within an aperture of 3 arcsec diameter, which corresponds to the aperture of the spectroscopic fibre (see below). These magnitudes can be useful when combining spectroscopic and photometric measurements.

Galaxy sizes are often given in terms of Petrosian radii, defined as the radius that contains a given fraction of the Petrosian flux. Particularly used are the Petrosian  $R_{50}$  and  $R_{90}$  radii (containing respectively 50 and 90 percent of the total flux). Their ratio defines the concentration parameter of a galaxy, which is the fundamental tool for the morphological classification in the SDSS.

### 1.4.1.2 Spectroscopy

The spectroscopic survey provides complete samples of three categories of objects:

- Bright galaxies, which constitute the ‘main’ sample, selected to have Petrosian  $r$ -band magnitude brighter than 17.77;
- Luminous Red Galaxies, selected on the basis of their colour and magnitude to yield a sample of luminous intrinsically red galaxies extending to higher redshift than the main sample ( $z \sim 0.45$ );
- Quasars, selected by their distinct colours in the SDSS photometric system, and by radio detection in the FIRST survey catalog.

The spectra are taken with two fibre-fed spectrographs, mounted on the image rotator of the APO telescope. In the spectroscopic mode the camera is

## 1 Introduction

---

substituted with a fibre plug plate, which is drilled according to the astrometric coordinates obtained from the imaging data to accommodate 640 fibres. The fibres have a fixed aperture diameter of 3 arcsec. The light collected by the fibre is thus only a limited fraction of the total light emitted by a galaxy, depending on the apparent size of the galaxy on the sky, hence on the distance of the galaxy and the concentration of its light profile. On average this fraction is 30 percent and this means that the spectra represent more properly the light coming from the inner region or bulge of the galaxies.

The spectra cover the wavelength range from 3800 to 9200Å and have an average spectral resolution of  $\lambda/\Delta\lambda = 2000$ . The spectra are reduced with automated devoted pipelines, which perform the flux and wavelength calibration of the spectra and the sky subtraction. The redshift of each spectrum is obtained using emission and absorption lines independently. Emission lines are identified by positive peaks in the spectrum and are compared to known emission lines of galaxies and quasars. For the absorption, the observed spectrum is cross-correlated to a high signal-to-noise template spectrum. The most reliable redshift estimate is given as fiducial redshift of the object. Finally, sources are classified into different classes (star, galaxy, QSO, high-redshift QSO) by comparison with template spectra of different astronomical sources.

Several other quantities are measured from the spectra of galaxies, in particular velocity dispersion, emission lines and absorption features. Velocity dispersions are measured by comparing the observed galaxy spectrum whose velocity dispersion is to be determined with a fiducial template spectrum, which can be the spectrum of a star or of a high signal-to-noise galaxy with known velocity dispersion. The template spectra are convolved to a maximum velocity dispersion of  $420 \text{ km s}^{-1}$ , so velocity dispersions higher than this are not reliable. Likewise, velocity dispersions below  $70 \text{ km s}^{-1}$ , which is the instrumental resolution of the SDSS, are not accurate.

The emission lines and absorption features are estimated from the spectra using the procedure developed and outlined by Tremonti et al. (2004), which is optimised for use on SDSS galaxy spectra. This consists in performing first a non-negative least-squares fit of the emission-line-free regions of the observed spectrum, using a set of model template spectra broadened to the observed velocity dispersion (the template spectra correspond to 30 instantaneous-burst models of different ages and metallicities computed using the Bruzual&Charlot 2003 code). Once the fitted spectrum is subtracted from the observed spectrum, the residuals can be fitted to Gaussian-broadened emission-line templates. The method assumes a single broadening width for all the Balmer lines, and another (independent) width for all the forbidden lines. The strength of each line is fitted independently.

The accurate measurement of the emission lines, obtained with this procedure

and thanks to the high resolution of the model template spectra, is useful not just in itself but is fundamental in order to obtain an accurate measure of absorption lines from the spectra of star-forming galaxies. In order to measure spectral absorption features, the fitted emission lines are subtracted from the original observed spectrum to produce a ‘pure’ absorption-line spectrum suited to our analysis. The measured absorption features relevant for this work are the indices define in the Lick system. A calibration onto the Lick system is not possible, because spectra of Lick stars are not available in the SDSS. Moreover it would require to broaden the observed spectra to the lower resolution of the Lick system. Instead, the absorption features are measured directly from the spectrum adopting the band-pass definition of Worthey (1994) and Worthey & Ottaviani (1997).

### 1.4.2 Multiwavelength high-redshift surveys

The SDSS provides the largest optical photometric and spectroscopic dataset of galaxies in the local Universe, which is fundamental to put constraints on the end products of the processes of galaxy evolution. A consistent picture of galaxy formation and evolution can be reached by combining complementary information in other wavelength domains, from the ultra-violet to the infrared, which map different physical processes, and extending observations at higher redshift, in order to directly trace back galaxy evolution.

In the optical range it is worth mentioning two surveys which aims at obtaining spectra of tens of thousands of galaxies up to redshift of 5: the Vimos VLT Deep Survey (VVDS, Le Fèvre et al. 2004) and the Deep Extragalactic Evolutionary Probe (DEEP2, Davis et al. 2003). The VVDS is a spectroscopic survey that will provide a sample of 150,000 redshifts in the range  $0 < z < 5$  over 16 degrees of the sky in four separate fields. This survey will be comparable in size to the largest surveys underway (such as the SDSS) but will probe to much higher redshifts. The spectroscopic survey aims at measuring redshifts from magnitude selected samples of galaxies drawn from the imaging survey (in five optical bands). The spectra have a resolution is  $R \sim 250$ . A sub-sample will be observed at higher resolution of  $R \sim 2500 - 5000$ . The DEEP2 project uses the 10m Keck Telescopes and the Hubble Space Telescope to conduct a large-scale survey of distant, faint, field galaxies. It will obtain spectra of  $\sim 50,000$  galaxies with  $z > 0.7$ , at a resolution of  $R \sim 4000$ , that will allow the measurement of linewidths and rotation curves for a large fraction of objects. It will be complementary to VVDS, which will survey more galaxies in a larger region of the sky but with much lower spectral resolution and with fewer objects at high redshift.

The emission of galaxies in the UV regime reflects the radiation from young

## 1 Introduction

---

stars that escape the galaxy and is thus a useful tracer of the current star formation rate. Much information can thus be gained on the evolution of the star formation rate from UV observations of galaxies at different redshift. The first UV sky survey is being performed by the Galaxy Evolution Explorer (GALEX, Martin et al. 2004). Launched in April 2003, it includes imaging and grism spectroscopic surveys in a far-UV band (1350 – 1750Å) and a near-UV band (1750 – 2750Å). It includes an All-Sky Imaging Survey that will survey the entire sky down to a sensitivity comparable to the SDSS, a Medium Imaging Survey, that covers 1000 square degrees with extensive overlap of the SDSS, a Deep Imaging Survey over 80 square degrees in regions where major multiwavelength effort are underway, and a Nearby Galaxy Survey, with ~200 targets of diverse galaxy types and environment, including most galaxies from the *Spitzer* IR Nearby Galaxy Survey (SINGS, Kennicutt & SINGS Team 2005). GALEX will allow to map the history of star formation in the Universe over the redshift range  $0 < z < 2$ . The *James Webb Space Telescope*, scheduled for launch no earlier than 2013, will extend rest-frame UV selection to redshift of 5 – 20.

Complementary information can be gained from observations in near- and far-IR wavelength range, which is less sensitive to recent episodes of star formation, thus providing a better estimate of the total stellar mass, and reflects the amount of UV light absorbed and re-emitted by dust grains at longer wavelengths. The near-IR regime has been covered by the Two Micron All Sky Survey (2MASS), which uniformly scanned the sky in three near-IR bands from 1.25 $\mu\text{m}$  to 2.17 $\mu\text{m}$ . Started in 1997 and completed in 2001, it provided a catalog containing positions and total magnitudes for more than 1,000,000 galaxies and nebulae. In far-IR the Infrared Astronomical Satellite (IRAS) mission performed an unbiased sensitive all-sky survey at wavelengths 12, 25, 60 and 100  $\mu\text{m}$  and detected about 350,000 infrared sources.

A big step forward in our understanding of the infrared emission from galaxies will be represented by the *Spitzer* Space Telescope (formerly SIRTF, the Space Infrared Telescope Facility), which is the largest infrared telescope ever launched into space. *Spitzer* will be the final mission of the NASA's Great Observatories Program. Launched in August 2003, it will obtain imaging and spectra by detecting infrared emission in four short-wavelength channels (3.6, 4.5, 5.8, 8  $\mu\text{m}$ ) and three longer-wavelength channels (24, 70, 160  $\mu\text{m}$ ). It will thus measure the rest-frame near- and mid-IR emission from galaxies at  $1 < z < 6$ .

Two large and complementary *Spitzer* Legacy projects are SINGS and the Great Observatories Origins Deep Survey (GOODS, Dickinson et al. 2003). On one side, SINGS aims at characterising the infrared emission over the entire range of galaxy properties and star formation environments, from imaging

and low-resolution spectroscopy of 75 nearby galaxies obtained with Spitzer. These data will provide diagnostic tools for understanding Spitzer observations of the distant Universe, and an archive that combines optical, UV, IR and submillimeter studies into a self-consistent whole. On the other side, GOODS aims at studying galaxy formation and evolution over a wide range of redshift, tracing the mass assembly history of galaxies. It will survey  $\sim 300$  square arcmin divided into two fields, imaged from 3.6 to 8  $\mu\text{m}$  and at 24  $\mu\text{m}$ . These observations will allow to detect rest-frame near-IR light from progenitors of Milky Way-like galaxies out to  $z = 4$  and to detect dust-obscured star formation in ordinary galaxies out to  $z = 2.5$ . GOODS will also combine several observations to produce an archive from X-ray to radio wavelength for a large sample of objects out to very high redshifts.

It is worth mentioning other two high-redshift surveys that combine high-resolution optical imaging from the Hubble Space Telescope with spectroscopy and multiwavelength data. COSMOS surveys a 2 degree field with the Advanced Camera for Surveys (ACS) on board HST, with spectroscopic follow-up that will provide vary large samples of galaxies in the redshift range  $0.2 < z < 2.4$ . Complementary imaging data at X-ray, UV, IR and radio wavelengths are also available in this field. The Galaxy Evolution from Morphologies and SEDs (GEMS, Rix et al. 2004) is an imaging survey over a 800 square arcmin area that benefits of two-colour imaging from ACS on HST to derive morphologies and structural parameters of nearly 10,000 galaxies in the redshift range  $0.2 < z < 1.1$ . Redshifts, luminosities and SEDs are also available from medium-band imaging in 17 optical filters. The field surveyed is of particular interest for the intense focus of research at other wavelength, in particular X-ray and infrared.

Ongoing and planned surveys and facilities are operating in order to extend our knowledge of galaxy formation and evolution by collecting large samples of high-redshift galaxies, directly comparable to the large samples available in the local Universe. At the same time, a big effort is underway to cover as much as possible the entire wavelength range of galaxy Spectral Energy Distributions. This will provide different and complementary diagnostic tools for galaxy properties and star formation rates that should lead to a consistent picture of the history of star formation in the Universe.

## 1.5 The thesis

The aim of this thesis is to put new and more robust constraints on our understanding of galaxy formation processes, by studying in detail the physical properties of the stellar populations in present-day galaxies. The advent

## 1 Introduction

---

of large spectroscopic surveys providing hundreds thousands of galaxies and the progresses in population synthesis models make this a right time to re-address with increased accuracy galaxy evolution studies through the ‘fossil cosmology’. The goal is to provide a complete census of the mean stellar ages and metallicities of galaxy populations in the local Universe. While carrying important information in itself, this will provide a fundamental calibration measurement for similar studies at higher redshifts.

In this work I analyse a magnitude limited sample of galaxies drawn from the spectroscopic dataset of the second data release of the SDSS, including both early-type quiescent galaxies and actively star-forming galaxies. I make use of the recent Bruzual & Charlot (2003) population synthesis code to interpret the optical spectra of these galaxies in terms of the light-weighted age, stellar metallicity and stellar mass of their composite stellar populations. A new statistical technique has been developed and adopted, based on the Bayesian statistics, which provides the entire probability density function (PDF) of the physical parameters of interest. The PDF allows to derive a median-likelihood estimate of each parameter and the associated uncertainty. To obtain the PDF each observed spectrum is compared to a library of model spectra, generated by convolving the Bruzual & Charlot (2003) SSP models with a Monte-Carlo library of star formation histories (SFH) encompassing the full range of physically plausible SFHs. In practice, the comparison is focused on a limited set of absorption features, selected among those defined in the Lick system to have distinct sensitivities to age and metallicity and negligible dependence on the  $\alpha/\text{Fe}$  ratio (because the models are based on scaled-solar abundance ratios stellar spectra).

An important specificity of this work is that, contrary to most previous studies on the stellar populations in nearby galaxies, it is extended to star-forming galaxies with young stars. This is possible thanks to the full temperature coverage and the  $3\text{\AA}$  resolution of the models. The high resolution of the models, which matches the resolution of the SDSS, allows to measure accurately the emission lines in the spectra of star-forming galaxies. These are then subtracted to obtain a pure absorption-line spectrum. Moreover, an advantage with respect to previous works is that there is no need to degrade the observed spectra to the lower resolution of the Lick spectrograph for calibration onto the Lick system, instead the absorption indices are measured directly from the spectra using the bandpass definitions, in the same way in model and observed spectra.

The method allows to derive robust statistical estimates of the ages and metallicities for large samples of galaxies. I exploit these estimates to give a detailed description of the full distribution of galaxies in the age-metallicity-mass plane, for the sample as a whole and as a function of the galaxy mor-

phology. In particular, I focus on the relation between age and stellar mass and between stellar metallicity and stellar mass, identifying a transition mass, compatible with the characteristic mass of other bimodalities in galaxy properties. I also compare the stellar and gas-phase metallicities for star-forming galaxies only, and re-address the age-metallicity relation for different galaxy types and stellar masses. The methodology and the results of the first part of the work are described in Chapter 2 as published in Gallazzi et al. (2005).

I then focus on the properties of a sample of early-type galaxies (selected on the basis of the concentration of their surface brightness profile), which sample the high-mass end of the mass-metallicity relation and represent a fundamental element of comparison for models of galaxy evolution. I re-address the physical origin of the colour-magnitude relation and the relation between the  $Mg_2$  absorption strength and velocity dispersion. The aim is to provide a quantitative estimate of the relative role of age, metallicity and  $\alpha/Fe$  abundance ratio (for which I use an empirical estimator) in driving the relations and their relative contribution to the scatter in observed quantities at fixed mass. This gives information about the timescales and the modes of star formation as a function of mass. I also study the relation between the stellar mass and the dynamical mass (a measure of the total potential well inside the optical radius of the galaxy), which can bring records of the assembly history of early-type galaxies. This analysis and the implications of the results are discussed in Chapter 3, as published in Gallazzi et al. (2006).

The SDSS sample span large ranges in galaxy properties and can thus be regarded as a representative sample of the local Universe. I use the new stellar metallicity and stellar mass estimates to derive the total density of mass and metals locked up in stars today. These quantities represent the product of star formation and stellar nucleosynthesis over the entire history of the Universe, and are thus fundamental constraints to the cosmic star formation and chemical evolution histories. The extremely good statistics allows me to give accurate descriptions of the distribution of metals as a function of various galaxy properties, such as mass, morphology and mean stellar age. Such distributions, and the amount of metals and mass provided by different galaxy types, encode important information about when and in which galaxies the bulk of the stars and metals were produced. This constitutes the topic of Chapter 4.

The main results of the thesis are summarised and discussed in Chapter 5, where I also give an overview of the possible extensions and applications of the methodology adopted in this work. I focus in particular on the refinements in the models, and on the application to large spectroscopic or photometric samples of high-redshift galaxies.

## 1 Introduction

---

## Bibliography

- Arimoto N., Yoshii Y., 1987, *A&A*, 173, 23
- Baldry I. K., Balogh M. L., Bower R., Glazebrook K., Nichol R. C., 2004, in Allen R. E., Nanopoulos D. V., Pope C. N., eds, *AIP Conf. Proc. 743: The New Cosmology: Conference on Strings and Cosmology* Color bimodality: Implications for galaxy evolution. pp 106–119
- Baldry I. K., Glazebrook K., Brinkmann J., Ivezić Ž., Lupton R. H., Nichol R. C., Szalay A. S., 2004, *ApJ*, 600, 681
- Baugh C. M., Cole S., Frenk C. S., 1996, *MNRAS*, 283, 1361
- Baum W. A., 1959, *PASP*, 71, 106
- Bender R., Burstein D., Faber S. M., 1992, *ApJ*, 399, 462
- Bender R., Burstein D., Faber S. M., 1993, *ApJ*, 411, 153
- Bennett C. L., Bay M., Halpern M., Hinshaw G., Jackson C., Jarosik N., Kogut A., Limon M., Meyer S. S., Page L., Spergel D. N., Tucker G. S., Wilkinson D. T., Wollack E., Wright E. L., 2003, *ApJ*, 583, 1
- Bruzual G., Charlot S., 2003, *MNRAS*, 344, 1000
- Bruzual A. G., Charlot S., 1993, *ApJ*, 405, 538
- Burstein D., Faber S. M., Gaskell C. M., Krumm N., 1984, *ApJ*, 287, 586
- Chabrier G., 2003, *PASP*, 115, 763
- Cole S., Lacey C. G., Baugh C. M., Frenk C. S., 2000, *MNRAS*, 319, 168
- Colless M., et al 2001, *MNRAS*, 328, 1039
- Davis M., et al. 2003, in *Discoveries and Research Prospects from 6- to 10-Meter-Class Telescopes II*. Edited by Guhathakurta, Puragra. *Proceedings of the SPIE*, Volume 4834, pp. 161-172 (2003). *Science Objectives and Early Results of the DEEP2 Redshift Survey*. pp 161–172

## Bibliography

---

- De Lucia G., Kauffmann G., White S. D. M., 2004, MNRAS, 349, 1101
- Dekel A., Birnboim Y., 2004, in AIP Conf. Proc. 743: The New Cosmology: Conference on Strings and Cosmology Characteristic Scale and Bimodality in Galaxies: Cold Streams, Shock Heating, Feedback and Clustering. pp 162–189
- Dickinson M., Papovich C., Ferguson H. C., Budavári T., 2003, ApJ, 587, 25
- Edmunds M. G., 1990, MNRAS, 246, 678
- Eggen O. J., Lynden-Bell D., Sandage A. R., 1962, ApJ, 136, 748
- Ellison S. L., Kewley L. J., Mallén-Ornelas G., 2005, MNRAS, 357, 354
- Faber S. M., 1973, ApJ, 179, 731
- Faber S. M., Friel E. D., Burstein D., Gaskell C. M., 1985, ApJS, 57, 711
- Fioc M., Rocca-Volmerange B., 1997, A&A, 326, 950
- Gallazzi A., Charlot S., Brinchmann J., White S. D. M., Tremonti C. A., 2005, MNRAS, 362, 41
- Gallazzi A., Charlot S., Brinchmann J., White S. D. M., 2006, MNRAS, 370, 1106
- Garnett D. R., 2002, ApJ, 581, 1019
- Guiderdoni B., Rocca-Volmerange B., 1987, A&A, 186, 1
- Huchra J., Davis M., Latham D., Tonry J., 1983, ApJS, 52, 89
- Kannappan S. J., 2004, ApJ, 611, L89
- Kauffmann G., Charlot S., 1998, MNRAS, 294, 705
- Kauffmann G., et al. 2003, MNRAS, 341, 33
- Kauffmann G., White S. D. M., Guiderdoni B., 1993, MNRAS, 264, 201
- Kennicutt R. C., SINGS Team 2005, American Astronomical Society Meeting Abstracts, 207,
- Kobulnicky H. A., Zaritsky D., 1999, ApJ, 511, 118
- Kroupa P., 2001, MNRAS, 322, 231

- Larson R. B., 1974, MNRAS, 166, 585
- Le Fèvre O., et al 2004, A&A, 428, 1043
- Lilly S. J., Le Fevre O., Crampton D., Hammer F., Tresse L., 1995, ApJ, 455, 50
- Lilly S. J., Le Fevre O., Hammer F., Crampton D., 1996, ApJ, 460, L1+
- Lin H., 1995, Ph.D. Thesis
- Lupton R., Gunn J. E., Ivezić Z., Knapp G. R., Kent S., Yasuda N., 2001, in Harnden F. R., Primini F. A., Payne H. E., eds, ASP Conf. Ser. 238: Astronomical Data Analysis Software and Systems X The SDSS Imaging Pipelines. pp 269–+
- Madau P., Ferguson H. C., Dickinson M. E., Giavalisco M., Steidel C. C., Fruchter A., 1996, MNRAS, 283, 1388
- Madau P., Pozzetti L., Dickinson M., 1998, ApJ, 498, 106
- Maraston C., 1998, MNRAS, 300, 872
- Martin C. D., et al. 2004, astro-ph/0411302
- Mather J. C., Fixsen D. J., Shafer R. A., Mosier C., Wilkinson D. T., 1999, ApJ, 512, 511
- Pagal B. E. J., 1997, Nucleosynthesis and Chemical Evolution of Galaxies. Nucleosynthesis and Chemical Evolution of Galaxies, by Bernard E. J. Pagel, pp. 392. ISBN 0521550610. Cambridge, UK: Cambridge University Press, October 1997.
- Pagal B. E. J., 2002, in ASP Conf. Ser. 253: Chemical Enrichment of Intracluster and Intergalactic Medium Metals in the Universe and Diffuse Background Radiation. (I). pp 489–+
- Pagal B. E. J., Edmunds M. G., Blackwell D. E., Chun M. S., Smith G., 1979, MNRAS, 189, 95
- Peacock J. A., 1999, Cosmological Physics. Cosmological Physics, by John A. Peacock, pp. 704. ISBN 052141072X. Cambridge, UK: Cambridge University Press, January 1999.
- Pei Y. C., Fall S. M., 1995, ApJ, 454, 69

## Bibliography

---

- Pettini M., Smith L. J., King D. L., Hunstead R. W., 1997, *ApJ*, 486, 665
- Rix H.-W., et al 2004, *ApJS*, 152, 163
- Salpeter E. E., 1955, *ApJ*, 121, 161
- Sandage A., 1986, *A&A*, 161, 89
- Scalo J., 1998, in Gilmore G., Howell D., eds, *ASP Conf. Ser. 142: The Stellar Initial Mass Function (38th Herstmonceux Conference) The IMF Revisited: A Case for Variations*. pp 201–+
- Smail I., Ivison R. J., Blain A. W., Kneib J.-P., 2002, *MNRAS*, 331, 495
- Somerville R. S., Primack J. R., 1999, *MNRAS*, 310, 1087
- Springel V., 2005, *MNRAS*, 364, 1105
- Springel V., Hernquist L., 2003, *MNRAS*, 339, 289
- Tegmark M., et al 2004, *ApJ*, 606, 702
- Thomas D., 1999, *MNRAS*, 306, 655
- Tinsley B. M., 1978, *ApJ*, 222, 14
- Tinsley B. M., 1980, *Fundamentals of Cosmic Physics*, 5, 287
- Tremonti C. A., et al. 2004, *ApJ*, 613, 898
- Vazdekis A., 1999, *ApJ*, 513, 224
- White S. D. M., Rees M. J., 1978, *MNRAS*, 183, 341
- Worthey G., 1994, *ApJS*, 95, 107
- Worthey G., Ottaviani D. L., 1997, *ApJS*, 111, 377
- York D. G., et al. 2000, *AJ*, 120, 1579
- Zwicky F., 1937, *ApJ*, 86, 217

*While the individual man is an insoluble puzzle, in the aggregate he becomes a mathematical certainty. You can, for example, never foretell what any one man will be up to, but you can say with precision what an average number will be up to. Individuals vary, but percentages remain constant. So says the statistician.*

Arthur Conan Doyle, The sign of four

# 2

## The Ages and Metallicities of Galaxies in the Local Universe

Gallazzi, A., Charlot, S., Brinchmann, J., White, S.D.M., Tremonti, C.A., 2005, MNRAS, 362, 41

### Abstract

We derive stellar metallicities, light-weighted ages and stellar masses for a magnitude-limited sample of 175,128 galaxies drawn from the Sloan Digital Sky Survey Data Release Two (SDSS DR2). We compute median-likelihood estimates of these parameters using a large library of model spectra at medium-high resolution, covering a comprehensive range of star formation histories. The constraints we derive are set by the simultaneous fit of five spectral absorption features, which are well reproduced by our population synthesis models. By design, these constraints depend only weakly on the  $\alpha/\text{Fe}$  element abundance ratio. Our sample includes galaxies of all types spanning the full range in star formation activity, from dormant early-type to actively star-forming galaxies. By analysing a subsample of 44,254 high-quality spectra, we show that, in the mean, galaxies follow a sequence of increasing stellar metallicity, age and stellar mass at increasing 4000 Å-break strength. For galaxies of intermediate mass, stronger Balmer absorption at fixed 4000 Å-break strength is associated with higher metallicity and younger age. We investigate how stellar metallicity and age depend on total galaxy stellar mass. Low-mass galaxies are typically young and metal-poor, massive galaxies old and metal-rich, with a rapid transition between these regimes over the stellar mass range  $3 \times 10^9 \lesssim M_* \lesssim 3 \times 10^{10} M_\odot$ . Both

## 2 The Ages and Metallicities of Galaxies in the Local Universe

---

high- and low-concentration galaxies follow these relations, but there is a large dispersion in stellar metallicity at fixed stellar mass, especially for low-concentration galaxies of intermediate mass. Despite the large scatter, the relation between stellar metallicity and stellar mass is similar to the correlation between gas-phase oxygen abundance and stellar mass for star-forming galaxies. This is confirmed by the good correlation between stellar metallicity and gas-phase oxygen abundance for galaxies with both measures. The substantial range in stellar metallicity at fixed gas-phase oxygen abundance suggests that gas ejection and/or accretion are important factors in galactic chemical evolution.

### **Keywords:**

galaxies: formation, galaxies: evolution, galaxies: stellar content

### **2.1 Introduction**

The ages and metallicities of stellar populations in nearby galaxies are direct tracers of the star formation and chemical enrichment histories of the Universe. Clues to the ages and metallicities of the stars may be inferred from the integrated spectra of galaxies, using ‘stellar population synthesis models’ (Tinsley 1978; Bruzual A. 1983; Bruzual A. & Charlot 1993; Bressan et al. 1994; Fioc & Rocca-Volmerange 1997; Maraston 1998; Vazdekis 1999). Analyses based on these models have been traditionally limited by the difficulty of deriving independent constraints on the age, star formation history, metallicity and dust content of a galaxy. For example, changes in age, metallicity and attenuation by dust all have similar effects on the colours and low-resolution spectra of galaxies. This gives rise to well-known ‘near-degeneracies’ in the constraints derived on these different parameters.

The expectation is that these degeneracies may be broken, at least in part, by appealing to refined spectral diagnostics which are not sensitive to attenuation by dust and have different sensitivities to age and metallicity. Studies in this area have focused on a set of 25 absorption features defined and calibrated in the spectra of 460 nearby Galactic stars obtained at Lick Observatory (e.g. Faber 1973; Worthey et al. 1994; Worthey & Ottaviani 1997). These studies all pertain to early-type galaxies, because the lack of hot stars in the Lick library does not allow the spectral interpretation of star-forming galaxies. The conclusion from these studies is that, for early-type galaxies, comparisons of the strengths of metallic lines and age-sensitive Balmer lines *can* break the age-metallicity degeneracy, but only in a relative way: the derived ages and metallicities appear to depend strongly on the specific choice of metal indices (e.g. Kuntschner et al. 2001; Eisenstein et al. 2003; Thomas et al. 2004). This

is because the Galactic stars used to calibrate the Lick indices have approximately solar metal abundance ratios at any metallicity, whereas the ratio of  $\alpha$ -elements to iron is seen to increase from dwarf to massive early-type galaxies (e.g. Worthey et al. 1992).

A main weakness of the original calibration of Lick indices is that it relies on spectra which were not calibrated in flux, and for which the resolution ( $\sim 9 \text{ \AA}$  FWHM) is three times lower than achieved by modern spectroscopic galaxy surveys, such as the Sloan Digital Sky Survey (SDSS; York et al. 2000). Thus, the high-quality spectra from these surveys must be degraded to the calibration and resolution of the original Lick spectra for index-strength analyses to be performed. The situation has changed recently with the development of medium-high resolution ( $\lesssim 3 \text{ \AA}$  FWHM), flux-calibrated population synthesis models including stars in the full temperature range (Vazdekis 2001; Bruzual & Charlot 2003). These models can be compared directly to high-quality observed spectra of both early-type and late-type galaxies. Several studies have also quantified the sensitivity of stellar absorption features to changes in element abundance ratios in galaxy spectra (Tantalo et al. 1998; Trager et al. 2000a; Thomas et al. 2003). These developments coincide with the advent of large homogeneous samples of galaxy spectra gathered by modern surveys such as the SDSS.

This is the first paper of a series in which we combine modern population synthesis techniques with the statistical power of the SDSS to investigate the connection between metallicity, age and stellar mass in nearby galaxies. Here, we use the medium-high resolution population synthesis code of Bruzual & Charlot (2003, hereafter BC03) to derive estimates of the metallicities, ages and stellar masses of a sample of  $\sim 2 \times 10^5$  nearby galaxies from the SDSS Data Release Two (DR2). We adopt a Bayesian statistical approach and derive full likelihood distributions for these physical parameters by comparing the observed spectrum of each galaxy with a comprehensive library of model spectra corresponding to different star formation histories. The comparison is driven by the strengths of 5 spectral features selected to depend only weakly on the  $\alpha/\text{Fe}$  ratio, which we measure in the same way in model and observed spectra.

An important specificity of our work is that we derive the above constraints not only for quiescent, early-type galaxies, but also for late-type, star-forming galaxies, for which the contamination of stellar absorption features by nebular emission must be removed. We explore the relationships between metallicity, age and stellar mass and the dependence of these relationships on galaxy structure. In a companion paper, we exploit these results to investigate the physical origin of the colour-magnitude relation and of the relation between  $\text{Mg}_2$ -index strength and velocity dispersion for early-type galaxies. The total

## 2 The Ages and Metallicities of Galaxies in the Local Universe

---

metal content of the local Universe and the distribution of metals as a function of galaxy properties will be the subject of a subsequent paper.

The paper is organized as follows. In Section 4.2 below, we present our sample of SDSS spectra and the models used to interpret them. We also describe our method for deriving metallicities, ages and stellar masses from observed galaxy spectra. The results are presented in Section 2.3, where we study the dependence of metallicity and age on total stellar mass and the age-metallicity relation as a function of galaxy structure. We also address in that section the influence of aperture bias on our derived parameters. We summarize and briefly discuss our results in Section 3.4.

### 2.2 The approach

In this section, we describe our approach for deriving estimates of light-weighted ages and metallicities from the observed spectra of SDSS galaxies. These spectra are discussed in Section 2.2.1, along with the models we use to interpret them. In Section 2.2.2, we select a set of spectral absorption features which we argue should most robustly constrain age and metallicity. Then, in Section 2.2.3, we outline the statistical approach we adopt to derive ages and metallicities from galaxy spectra. We also highlight the sensitivity of our constraints on age and metallicity to the observational signal-to-noise ratio (S/N) of the spectra.

#### 2.2.1 Observed and model spectra

The observed spectra we consider are drawn from the SDSS DR2 (Abazajian et al. 2004). The SDSS is an imaging and spectroscopic survey of the high Galactic latitude sky, which will obtain  $u$ ,  $g$ ,  $r$ ,  $i$  and  $z$  photometry of almost a quarter of the sky and spectra of at least 700,000 objects (York et al. 2000). The spectra are taken using 3''-diameter fibres, positioned as close as possible to the centres of the target galaxies. The flux- and wavelength-calibrated spectra cover the range from 3800 to 9200 Å with a resolution of  $\sim 1800$ . Our sample, drawn from the SDSS DR2, includes unique spectra of 196,673 galaxies with Petrosian  $r$ -band magnitudes in the range  $14.5 < r < 17.77$  (after correction for foreground Galactic extinction using the extinction maps of Schlegel et al. 1998). The galaxies span the full range of types, from actively star-forming, late-type galaxies to dormant, early-type galaxies. The median redshift is 0.13. A more detailed description of this sample is given in Section 2.3 below.

To interpret these observed spectra in terms of physical parameters such as age, metallicity and stellar mass, we use the recent population synthesis

models of BC03. These models are based on ‘STELIB’, a newly available library of observed stellar spectra assembled by Le Borgne et al. (2003). The models have a spectral resolution of  $3 \text{ \AA}$  FWHM across the whole wavelength range from 3200 to 9500  $\text{\AA}$ . They are thus ideally matched to the SDSS spectra.

We note that, to interpret the spectra of star-forming and active galaxies with these models, we must first remove the contamination of the observed spectra by nebular emission lines. This is achieved using the procedure outlined by Tremonti et al. (2004), which is optimized for use with SDSS galaxy spectra (see also Tremonti 2003). This consists in performing first a non-negative least-squares fit of the emission-line-free regions of the observed spectrum, using a set of model template spectra broadened to the observed velocity dispersion (the template spectra correspond to 30 instantaneous-burst models of different ages and metallicities computed using the BC03 code). Once the fitted spectrum is subtracted from the observed spectrum, the residuals can be fitted to Gaussian-broadened emission-line templates. The method assumes a single broadening width for all the Balmer lines, and another (independent) width for all the forbidden lines. The strength of each line is fitted independently. Then, the fitted emission lines are subtracted from the original observed spectrum to produce a ‘pure’ absorption-line spectrum suited to our analysis.

### 2.2.2 Stellar absorption diagnostics of age and metallicity

The strongest stellar absorption features in the optical spectra of galaxies form the basis of the Lick system of spectral indices (Burstein et al. 1984; Gorgas et al. 1993; Worthey et al. 1994; Worthey & Ottaviani 1997; Trager et al. 1998; see also Section 3.1). Each index in this system is defined by a central ‘feature bandpass’ and two adjacent ‘pseudo-continuum bandpasses’. The above studies have shown that some Lick indices are primarily sensitive to age, such as those based on H-Balmer lines, while others are primarily sensitive to metallicity, such as several Fe- and Mg-based indices at wavelengths between 4500 and 5700  $\text{\AA}$ . We also consider here the 4000- $\text{\AA}$  break index of Balogh et al. (1999), which we denote  $D_{4000}$ , which is defined as the ratio of the average flux densities in the narrow bands 4000–4100  $\text{\AA}$  and 3850–3950  $\text{\AA}$ .<sup>1</sup> This index depends somewhat on metallicity but correlates more with the ratio of present to past-averaged star formation rates in galaxies (see fig. 2 of Kauffmann et al. 2003 and fig. 27 of Brinchmann et al. 2004).

In previous studies based on models with low spectral resolution, the strengths of Lick indices had to be modelled analytically as functions of the effective

---

<sup>1</sup>This index is sometimes denoted by  $D_n(4000)$ .

## 2 The Ages and Metallicities of Galaxies in the Local Universe

---

temperatures, gravities and metallicities of the stars (Worthey et al. 1994; Worthey & Ottaviani 1997; Gorgas et al. 1999). These ‘fitting functions’ were not appropriate for hot stars, and hence, index-strength analyses had to be restricted to old stellar populations. Moreover, as mentioned in Section 3.1, the stellar spectra on which the Lick indices were originally calibrated had lower resolution than typical galaxy spectra today and were not flux-calibrated. These various weaknesses are resolved here by our adoption of the medium-high resolution, flux-calibrated BC03 models. These models can be compared directly to the SDSS spectra of galaxies with any star formation history, and the Lick indices can be measured in the same way in model and observed spectra.

Like previous models, however, the BC03 models rely on a spectral library of nearby stars with near solar metal abundance ratios at any metallicity. The models are therefore expected to show discrepancies when compared to galaxies where the abundance ratios differ from those of nearby stars.<sup>2</sup> In fact, such discrepancies appear to be responsible for the fact that some spectral features, such as CN<sub>1</sub>, CN<sub>2</sub>, TiO<sub>1</sub>, TiO<sub>2</sub>, Ca4227 and several Mg and Fe lines, were not well reproduced when BC03 compared their models with a sample of high-quality galaxy spectra drawn from SDSS Early Data Release (Stoughton et al. 2002).

Several studies have addressed the dependence of Lick index strengths on changes in the relative ratios of heavy elements (González 1993; Tripicco & Bell 1995; Tantalo et al. 1998; Trager et al. 2000a; Vazdekis 2001; Thomas et al. 2003; Tantalo & Chiosi 2004; Thomas et al. 2004, see also BC03). These studies have led to the identification of composite Mg+Fe indices, which are sensitive to metallicity (i.e. the fraction by mass of all elements heavier than helium over the total gas mass) but show little sensitivity to  $\alpha$ /Fe (i.e. the ratio of the total mass of  $\alpha$  elements to the mass of iron; see footnote 2). Among these, we use here

$$[\text{MgFe}]' = \sqrt{\text{Mgb} (0.72 \text{ Fe5270} + 0.28 \text{ Fe5335})}, \quad (2.1)$$

as proposed by Thomas et al. 2003, and

$$[\text{Mg}_2\text{Fe}] = 0.6 \text{ Mg}_2 + 0.4 \log(\text{Fe4531} + \text{Fe5015}), \quad (2.2)$$

as defined in BC03.

---

<sup>2</sup>The abundance ratio of  $\alpha$  elements (such as N, O, Mg, Ca, Na, Ne, S, Si, Ti), which are produced mainly by Type II supernovae, to Fe-peak elements (such as Cr, Mn, Fe, Co, Ni, Cu, Zn), which are produced mainly by Type Ia supernovae, is observed to vary in external galaxies (e.g., Worthey et al. 1992; Thomas et al. 2003a).

We wish to extract ages and metallicities from the SDSS galaxy spectra. We therefore fit simultaneously both metal-sensitive and age-sensitive indices. Among the 28 spectral indices studied by BC03, we concentrate on those that are best reproduced by the models. This requirement already excludes several Fe-based indices, the three Mg-based indices, Ca4227, Ca4455, the CN, TiO and NaD features (see fig. 18 of BC03). Among the remaining indices we identify those that are known to have at most a weak dependence on  $\alpha/\text{Fe}$ .  $[\text{Mg}_2\text{Fe}]$  and  $[\text{MgFe}]'$  are suitable metal-sensitive indices and  $\text{H}\beta$  is a suitable age-sensitive index. We also include D4000, which is sensitive to the ratio of present to past-averaged star formation rate (see above). We are not aware of any study indicating the dependence of this index on  $\alpha/\text{Fe}$ . Finally, to better constrain age we decided to include also the two higher-order Balmer lines,  $\text{H}\delta_A$  and  $\text{H}\gamma_A$ . These indices have been recently shown to depend on variations in element abundance ratios at metallicities around solar and above (Thomas et al. 2004; Korn et al. 2005). However, we find that including them in our procedure does not produce results systematically different from those obtained without them, while it provides smaller errors on both age and metallicity estimates. Therefore, we decide to use also  $\text{H}\delta_A + \text{H}\gamma_A$ . We choose the sum of  $\text{H}\delta_A$  and  $\text{H}\gamma_A$  because it is better reproduced by the models than the two indices separately (see fig. 18 of BC03). Thus, our final set of indices is composed of D4000,  $\text{H}\beta$ ,  $\text{H}\delta_A + \text{H}\gamma_A$ ,  $[\text{Mg}_2\text{Fe}]$  and  $[\text{MgFe}]'$ . This is the minimum set that allows us to derive good constraints on metallicity and age simultaneously and to recover well the parameters of simulated galaxies (see section 2.2.4 below).

The solid histograms in Fig. 2.1 show the distributions in ‘resolving power’ of these five spectral features for the galaxies in our sample. The resolving power is defined as the ratio between the 5–95 percent percentile range of the distribution of index strengths for all galaxies in the sample,  $\Delta_I$ , and the observational error for each galaxy,  $\sigma_I$ . The resolving power is largest ( $\sim 30$ ) for D4000 and slightly lower ( $\sim 10$ ) for the other indices. Also shown as dotted histograms in Fig. 2.1 are the analogous distributions in resolving power for a subsample of galaxies with mean signal-to-noise per pixel greater than 20. As expected, the distributions for these galaxies are shifted to higher values, because of the smaller observational errors.

We note that the strengths of some spectral absorption indices are sensitive to the stellar velocity dispersion in a galaxy (e.g. Davies et al. 1993; Longhetti et al. 1998; Trager et al. 1998; Kuntschner 2004). The indices that are most affected are those measured with the narrowest pseudo-continuum bandpass definitions. In particular this effect is seen in Fe-based indices and therefore also in the composite Mg+Fe indices. The BC03 population synthesis code provides SSP spectra broadened to different velocity dispersions. This allows

## 2 The Ages and Metallicities of Galaxies in the Local Universe

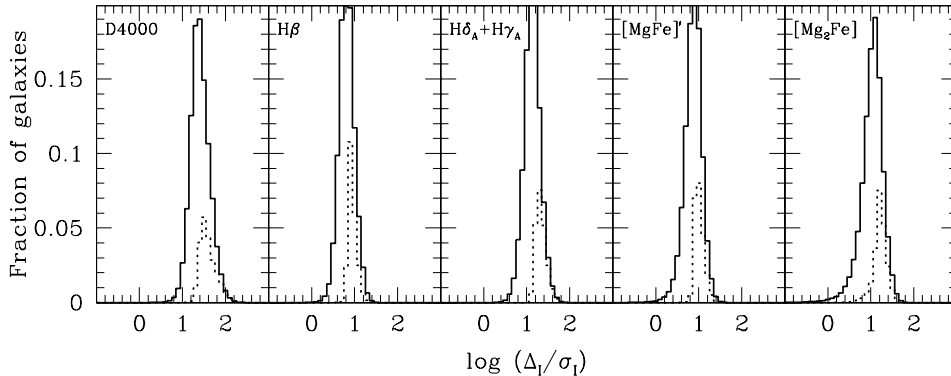


**Figure 2.1:** Distributions in ‘resolving power’ of the 5 spectral features selected to constrain the ages and metallicities of SDSS galaxies, as indicated. The resolving power is defined as the ratio between the 5%–95% percentile range  $\Delta_I$  of index strengths in the sample and the observational error  $\sigma_I$  of each galaxy. In each panel, the solid histogram shows the distribution for our sample of 196,673 SDSS-DR2 galaxies, and the dotted histogram the distribution for the subsample of 44,347 galaxies with mean signal-to-noise per pixel greater than 20.

us to compare each galaxy spectra with models that have a similar velocity dispersion (see Section 2.2.3).

### 2.2.3 Statistical estimates of age and metallicity

We wish to estimate not only the most likely values of the ages and metallicities of SDSS galaxies, but also the accuracy of these values. To this purpose, we adopt a Bayesian statistical approach, similar to the one outlined by Kauffmann et al. (2003). The goal is to obtain the likelihood distribution of a given parameter  $X$  in the space of all possible values of  $X$ . This is obtained by comparing the observational data with a set of models that populate the space of all possible  $X$  according to a prior distribution which represents our prejudice about the relative likelihood of different  $X$  values in absence of any data.

We generate a library of 150,000 Monte Carlo realizations of a full range of physically plausible star formation histories. Following Kauffmann et al. (2003), each star formation history is parametrized in terms of a continuous model in which stars are formed from the time  $t_{\text{form}}$  to the present according to the law  $\psi(t) \propto \exp(-\gamma t)$ . Random bursts of star formation are superposed on this continuous model. We take the formation time  $t_{\text{form}}$  to be uniformly

distributed between 13.5 and 1.5 Gyr and the star formation time-scale parameter  $\gamma$  to be uniform over the interval from 0 to 1 Gyr<sup>-1</sup>. The bursts can occur at all times after  $t_{\text{form}}$  with equal probability, set in such a way that 10 percent of the galaxies in the library experience a burst in the last 2 Gyr.<sup>3</sup> They are parametrized in terms of the fraction  $A$  of stellar mass produced during the burst relative to the total mass formed by the continuous model. The ratio  $A$  is logarithmically distributed between 0.03 and 4. During a burst, stars form at a constant rate for a time distributed uniformly in the range  $3 \times 10^7$ – $3 \times 10^8$  yr. The velocity dispersions of the models are distributed uniformly in the range 50–350 km s<sup>-1</sup>. We further take the models to be distributed logarithmically in metallicity in the range 0.2–2.5  $Z_{\odot}$  and make the density of models drop smoothly as  $(\log Z)^{1/3}$  at metallicities from 0.2 down to 0.02  $Z_{\odot}$ , in order not to overrepresent extremely metal-poor models. All stars in a given model have the same fixed metallicity, which we interpret as the ‘(optical) light-weighted’ metallicity.

For each model in the library we compute the following properties:

1. the strengths of the D4000, H $\beta$ , H $\delta_A$ +H $\gamma_A$ , [Mg<sub>2</sub>Fe] and [MgFe]’ spectral indices, measured in the same way as in the SDSS spectra;
2. the  $r$ -band light-weighted age, evaluated by the integral

$$t_r = \frac{\int_0^t d\tau \psi(t - \tau) f_r(\tau) \tau}{\int_0^t d\tau \psi(t - \tau) f_r(\tau)} \quad (2.3)$$

where  $f_r(\tau)$  is the total  $r$ -band flux produced by stars of age  $\tau$ . We refer below to the  $r$ -band light-weighted age simply as the ‘age’ of a galaxy;

3. the  $z$ -band stellar mass-to-light ratio  $M_*/L_z$ , which accounts for the gas mass returned to the ISM by evolved stars (see also section 3.1 of BC03);
4. the apparent  $u$ ,  $g$ ,  $r$ ,  $i$  and  $z$  magnitudes of the model at redshifts between 0 and 0.3 in steps of 0.01.

The models in the library provide accurate simultaneous fits to the strengths of the 5 spectral indices D4000, H $\beta$ , H $\delta_A$ +H $\gamma_A$ , [Mg<sub>2</sub>Fe] and [MgFe]’ that we have selected to derive age and metallicity estimates from SDSS galaxy spectra. To illustrate this, Fig. 2.2 shows the distribution of the differences between the best-fit and observed strengths of each index, in units of the

<sup>3</sup>In Kauffmann et al. (2003) this parameter was set such that 50 percent of the models in the library experienced a burst in the last 2 Gyr. We reduce this fraction to 10 percent because it provides a more uniform distribution of the models in light-weighted age. The influence on our results from changing this fraction is discussed in Section 2.2.4.2.

## 2 The Ages and Metallicities of Galaxies in the Local Universe

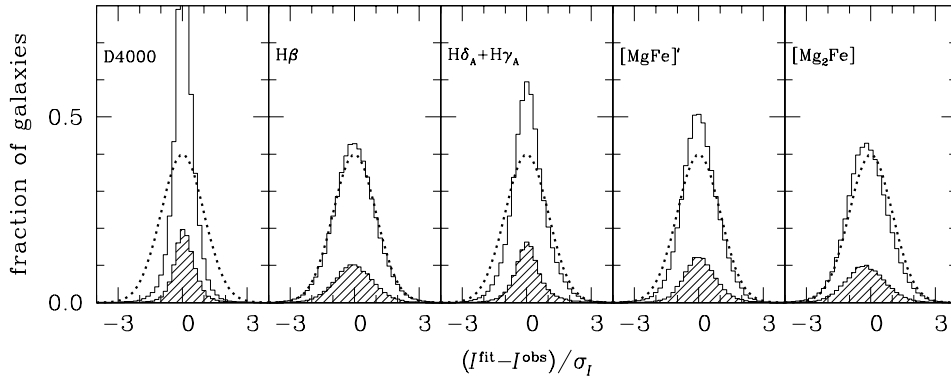


**Figure 2.2:** Simultaneous fit of the 5 spectral features chosen to derive age and metallicity estimates from SDSS galaxy spectra using the model library described in Section 2.2.3. The histograms show the distributions of the differences between the best-fit ( $I^{\text{fit}}$ ) and observed ( $I^{\text{obs}}$ ) strengths of each index (as indicated), in units of the observational error ( $\sigma_I$ ). The plain histograms are for the full sample of 196,673 galaxies, while the hatched histograms are for the subsample of 44,347 galaxies with mean S/N per pixel greater than 20. Only those models for which the stellar velocity dispersion is within  $\pm 15 \text{ km s}^{-1}$  of the observed one are included in the fit for each galaxy. For reference, the dotted line in each panel shows a Gaussian distribution with unit standard deviation.

observational error, for the galaxies in our sample. Because of the dependence of the composite Mg+Fe indices on stellar velocity dispersion, when fitting the index strengths of an observed galaxy, we only include those models for which the stellar velocity dispersion is within  $\pm 15 \text{ km s}^{-1}$  of the observed one.<sup>4</sup> The plain histograms in Fig. 2.2 show the distributions for the sample as a whole, while the hatched histograms show the distributions for those galaxies with a median S/N per pixel greater than 20. For both samples, the deviations between observations and best-fit models are within the observational errors for all indices, as indicated by the comparison with a Gaussian distribution of unit standard deviation (dotted line). There is no strong correlation between the residuals of the different indices.

The comparison of the strengths of D4000,  $H\beta$ ,  $H\delta_A + H\gamma_A$ ,  $[\text{Mg}_2\text{Fe}]$  and  $[\text{MgFe}]'$  in the spectrum of an observed SDSS galaxy with the strengths of

<sup>4</sup>The median uncertainty on velocity dispersion is  $\sim 15 \text{ km s}^{-1}$  for the full sample and only  $\sim 7 \text{ km s}^{-1}$  for galaxies with  $S/N > 20$ .

these indices in every model spectrum in the library allows us to construct the probability density functions (PDFs) of physical parameters (such as age, metallicity and mass-to-light ratio) for that galaxy. This is achieved by assigning to each model a weight  $w = \exp(-\chi^2/2)$ , where  $\chi^2$  is calculated by comparing the strengths of the 5 indices measured in the observed spectrum with those measured in the model spectrum, given the observational measurement errors. The PDF of a selected physical parameter is then simply given by the distribution in that parameter of the weights  $w$  of all the models in the library.

The PDF of a given parameter can then be characterized by its mode, which corresponds to the most likely value of the parameter, its median, which can differ from the mode for non-symmetric distributions, and by a confidence interval within which the parameter is constrained at a certain probability level. We often quote below the 68 percent confidence interval corresponding to the 16%–84% percentile range of the PDF, which would be equivalent to the  $\pm 1\sigma$  range for a Gaussian distribution.

### 2.2.4 Accuracy of the estimates

#### 2.2.4.1 Dependence on observational properties

We now want to illustrate the kind of constraints that can be obtained on the ages and metallicities of SDSS galaxies with different spectral properties using the method outlined above. Kauffmann et al. (2003) have shown that the combination of H-Balmer lines and D4000 is a discriminating diagnostic of the recent star formation activity in galaxies. We therefore draw 4 galaxies from our sample with high-quality spectra (median S/N per pixel larger than 30) located at different positions along the sequence occupied by SDSS galaxies in the  $H\delta_A+H\gamma_A$  versus D4000 diagnostic diagram.

The solid distributions in Fig. 2.3 show the constraints obtained on the metallicities (left-hand plot) and ages (right-hand plot) of these galaxies in two cases: when including only the age-sensitive indices D4000,  $H\beta$  and  $H\delta_A+H\gamma_A$  to constrain the fits (bottom panels), and when including also the metal-sensitive indices  $[Mg_2Fe]$  and  $[MgFe]'$  (top panels). As expected, the ages are well constrained by D4000,  $H\beta$  and  $H\delta_A+H\gamma_A$  alone, and the corresponding PDFs do not change appreciably when including also the constraints from metal-sensitive indices. In contrast, the metallicities are well constrained only when the metal-sensitive indices are included in the fit. In each panel in Fig. 2.3, the arrows indicate the median (longer one) and the 16<sup>th</sup> and 84<sup>th</sup> percentiles (shorter ones) of the PDF. The 68 percent confidence interval becomes narrower when all the five indices are included, and the median of

## 2 The Ages and Metallicities of Galaxies in the Local Universe

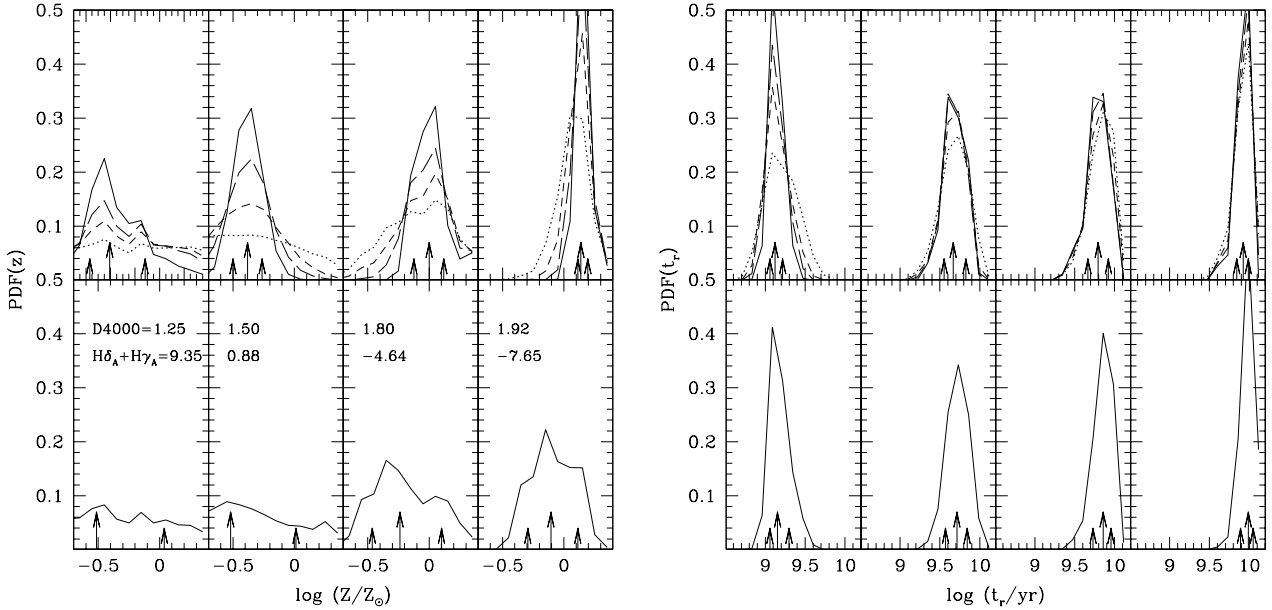


**Figure 2.3:** Probability density functions of stellar metallicity (left-hand plot) and  $r$ -band light-weighted age (right-hand plot) for 4 SDSS galaxies with high-quality spectra (median S/N per pixel larger than 30) and different D4000 and  $H\delta_A+H\gamma_A$  strengths (indicated in the bottom panels of the left-hand plot). The solid PDFs in the bottom panels were obtained when including only the age-sensitive indices D4000,  $H\beta$  and  $H\delta_A+H\gamma_A$  to constrain the fits. Those in the top panels were obtained after including also the metal-sensitive indices  $[Mg_2Fe]$  and  $[MgFe]'$ . In each panel, the arrows indicate the median (longer one) and the 16<sup>th</sup> and 84<sup>th</sup> percentiles (shorter ones) of the PDF. The long-dashed, short-dashed and dotted PDFs in the top panels show the constraints obtained when degrading the original galaxy spectra to a median S/N per pixel of 30, 20 and 10, respectively (see text for detail).

the distribution in this case is consistent with that obtained when including only the age-sensitive indices. We note that age and metallicity appear to correlate with D4000 (indicated on the figure) for these 4 galaxies, and that the constraints on metallicity are weakest for the galaxy with the lowest D4000. This is not a coincidence, as we shall see in Section 2.3 below.

It is important to note that the observed S/N directly influences the uncertainties in the age and metallicity estimates. To investigate this, we consider a set of galaxies with index strengths similar to those of the galaxies in Fig. 2.3, but with lower median S/N per pixel, e.g. 20. We take the average errors in the index strengths of these low-S/N galaxies to be typical of errors that

## 2.2 The approach

**Table 2.1:** Median-likelihood estimates of metallicity and age for the four galaxies shown in Fig. 2.3, obtained by degrading the actual signal-to-noise ratio of the spectrum ( $S/N_{\text{obs}}$ ) to 30, 20 and 10. The quoted errors are one half the 68 percent confidence range of the PDFs in the upper panels of Fig. 2.3. Each column corresponds to a galaxy, ordered from left to right as in Fig. 2.3.

$\log(Z/Z_{\odot})$				
S/N = 10	$-0.43 \pm 0.57$	$-0.42 \pm 0.43$	$-0.07 \pm 0.27$	$0.09 \pm 0.12$
S/N = 20	$-0.36 \pm 0.44$	$-0.39 \pm 0.27$	$-0.02 \pm 0.21$	$0.12 \pm 0.08$
S/N = 30	$-0.34 \pm 0.35$	$-0.37 \pm 0.17$	$0.00 \pm 0.16$	$0.13 \pm 0.06$
S/N <sub>obs</sub>	$-0.41 \pm 0.22$	$-0.38 \pm 0.12$	$0.00 \pm 0.12$	$0.14 \pm 0.04$
$\log(t_r/yr)$				
S/N = 10	$9.19 \pm 0.21$	$9.68 \pm 0.18$	$9.84 \pm 0.15$	$9.92 \pm 0.11$
S/N = 20	$9.12 \pm 0.15$	$9.68 \pm 0.15$	$9.83 \pm 0.14$	$9.92 \pm 0.10$
S/N = 30	$9.12 \pm 0.12$	$9.66 \pm 0.13$	$9.79 \pm 0.14$	$9.92 \pm 0.09$
S/N <sub>obs</sub>	$9.12 \pm 0.08$	$9.66 \pm 0.13$	$9.79 \pm 0.13$	$9.92 \pm 0.07$

would be measured at the same S/N for the galaxies in Fig. 2.3. We then mimic 100 realizations of ‘degraded spectra’ of the high-S/N galaxies by randomly drawing index strengths from Gaussian distributions centered on their index values, of widths the typical errors obtained from the lower-S/N galaxies. The PDFs of age and metallicity may be computed for each realization, and the average PDF of the 100 realizations is a good estimator of the results that would be obtained at low S/N for these galaxies.

In the upper panels of Fig. 2.3, we show the average PDFs obtained in this way when the median S/N per pixel of each galaxy is degraded to 30 (long-dashed line), 20 (short-dashed line) and 10 (dotted line). A median S/N per pixel of 10 is not sufficient to constrain metallicity well (except for the most metal-rich galaxy, which has the spectrum with the strongest absorption features). As we increase the S/N, the distributions narrow down and converge to the PDFs obtained from the original high-S/N spectra. We conclude that a median S/N per pixel of at least 20 is required to reliably constrain metallicity. This is higher than the median value of  $\sim 15$  for the SDSS-DR2 sample. The age estimates do not appear to be significantly affected by low S/N (except for the youngest galaxy), probably because they are constrained strongly by D4000, which has small errors. The results of this exercise are summarized in Table 2.1.

The results of Fig. 2.3 would not change dramatically if we restricted the fit to only a subset of the selected spectral indices. We have checked this by using only H $\beta$  to derive age estimates for the galaxies in Fig. 2.3, and only [MgFe]’ to derive metallicity estimates. The median-likelihood estimates of age and

## 2 The Ages and Metallicities of Galaxies in the Local Universe

---

metallicity obtained in this way fall within the  $1\sigma$  errors of those shown in Fig. 2.3. The main effect of reducing the number of indices included in the fitting is to broaden the derived likelihood distributions. For the galaxies of Fig. 2.3, the average error on age increases from 0.10 dex to 0.14 dex when fitting  $H\beta$  alone<sup>5</sup>, while the average error on metallicity increases from 0.13 dex to 0.29 dex when fitting  $[MgFe]'$  alone.

### 2.2.4.2 Possible systematic uncertainties

To identify any potential bias in our method, we also tested how well it can recover ages and metallicities of model galaxies for which these parameters are known. We selected 3000 models at random from the library described in Section 2.2.3. We added Gaussian noise to the index strengths of these models to reflect the average observational errors of our SDSS sample. The ages and metallicities recovered by our method for these models showed no systematic deviation from the true values. For both age and metallicity, the deviations  $\Delta \log Z$  and  $\Delta \log t_r$  for the 3000 models followed Gaussian distributions centred on zero of width  $\sim 0.15$ . Interestingly, the deviations in age and metallicity appear to correlate with each other with a slope  $\Delta \log Z / \Delta \log t_r \approx -0.74$ . This is consistent with the age-metallicity degeneracy identified in Section 2.3.3 below. We have checked that the way in which  $\Delta \log Z$  and  $\Delta \log t_r$  respond to (noise-induced) changes in metal-sensitive and age-sensitive indices for galaxies with different star formation histories cannot lead to spurious correlations between index strengths and metallicity/age residuals.

We mentioned above that higher-order Balmer lines may be sensitive to the  $\alpha/Fe$  ratio. To quantify the potential error on our metallicity and age estimates for galaxies with enhanced  $\alpha/Fe$  relative to solar, we compared the predictions of the Thomas et al. (2004) stellar populations models at solar element abundance ratio,  $\alpha/Fe = 0$ , with those for  $\alpha/Fe = 0.3$  (a typical ratio for massive elliptical galaxies). We chose 3000 models at random from our library and perturbed their index strengths with Gaussian noise, as above. In addition, we increased the values of  $H\delta_A$  and  $H\gamma_A$  to reflect the difference between the  $\alpha/Fe = 0$  and  $\alpha/Fe = 0.3$  tracks, interpolating in metallicity and age to the values for each model considered. The distributions in  $\Delta \log Z$  and  $\Delta \log t_r$  are well represented by Gaussian centred on  $+0.05$  and  $-0.05$ , respectively, of width given by the average error on metallicity and age (0.2

---

<sup>5</sup>It has been noticed that higher-order Balmer lines can yield younger ages than those predicted by  $H\beta$ , presumably because of the dependence of higher-order lines on  $\alpha/Fe$  (e.g. Kuntschner 2000; Eisenstein et al. 2003). However, we do not see any significant difference in the results when using either  $H\delta_A + H\gamma_A$  only or  $H\beta$  only.

and 0.13 respectively). This test indicates that we tend to overestimate the stellar metallicities and underestimate the light-weighted ages of galaxies with supersolar abundance ratios by  $\sim 0.05$  dex. However, this seems in contradiction with the fact that the results on the galaxies in our sample do not vary systematically if we include or exclude  $H\delta_A+H\gamma_A$  in the fit. This is true also for massive early-type galaxies, which are likely to be  $\alpha$ -enhanced (e.g. Worthey et al. 1992). The offset of  $\sim 0.05$  dex may thus be regarded as an upper limit to the error in the ages and metallicities derived from our analysis in the case of non-solar abundance ratios.

Another possible source of systematic error is the choice of prior according to which our model library populates the parameter space. In particular, the mix of continuous and bursty star formation histories may influence the physical parameters in which we are interested, mainly the light-weighted age. To test for this effect, we generated a Monte Carlo library with a modified prior, by increasing to 50 percent (instead of 10 percent) the fraction of models that can undergo a burst of star formation in the last 2 Gyrs. We then compared the (median-likelihood) estimates of light-weighted age and stellar metallicity derived with this modified prior and with our standard prior. Increasing the fraction of bursts, we derive ages  $\sim 0.07$  dex younger, on average, than those derived with our standard prior. This bias mainly affects old, early-type galaxies. Similarly the metallicities are on average 0.04 dex higher than those derived with the standard prior. The effect of these offsets on the relations between age, metallicity and stellar mass that we discuss in Section 2.3.2 is very small. The zeropoint of the relations changes according to the offsets in metallicity and age reported above, but the shape of the relations remains identical.

### 2.2.4.3 Stellar mass estimates

In the remainder of this paper, we will be interested in the dependence of age and metallicity not only on directly observed properties, such as spectral features and morphology, but also on ‘derived’ quantities, such as stellar mass. Kauffmann et al. (2003) derived Bayesian likelihood estimates of the stellar masses of a sample of SDSS galaxies, based on fits of the  $H\delta_A$  and D4000 absorption indices. We use a similar approach here and estimate stellar masses for all the galaxies in our sample, based on the fits of D4000,  $H\beta$ ,  $H\delta_A+H\gamma_A$ ,  $[Mg_2Fe]$  and  $[MgFe]'$ . We compute the PDF of the stellar mass for each galaxy by scaling the  $z$ -band mass-to-light ratio  $M_*/L_z$  of each model to the observed, total  $z$ -band luminosity of the galaxy.<sup>6</sup> We compute  $M_*/L_z$  at the

---

<sup>6</sup>We assume that the  $M_*/L_z$  ratio is the same for the whole galaxy as it is in the region sampled by the fibre. See Fig. 2.13 for the typical fraction of light that enters the fibre.

## 2 The Ages and Metallicities of Galaxies in the Local Universe

---

observed galaxy redshift and include the effects of attenuation by dust. The  $z$ -band attenuation  $A_z$  is inferred from the difference between the emission-line corrected fibre  $r-i$  colour<sup>7</sup> of the galaxy and the  $r-i$  colour of the redshifted (dust-free) model, assuming a single power law ( $\propto \lambda^{-0.7}$ ) attenuation curve (Charlot & Fall 2000).

The true attenuation can of course not be negative, but imposing strictly  $A_z > 0$  would not account for the errors affecting the measurements of indices and magnitudes. Moreover, at high metallicities, there is a potential problem that the dust-free models providing the best fits to the observed absorption-line strengths can be *redder* than the observed galaxy (implying negative apparent attenuations). This problem arises because of a discrepancy between the spectral absorption features and the integrated colours of the BC03 models at the metallicity  $2.5 Z_\odot$ . The colours of these models correspond to stellar evolutionary tracks with (and colour-temperature calibrations for)  $Z = 2.5 Z_\odot$ , but the absorption-line strengths had to be calibrated using stellar spectra for slightly lower metallicity,  $1.6 \lesssim Z/Z_\odot \lesssim 2$  (see Appendix A of BC03). Hence, the metallicity scale, which is linked to the evolutionary tracks and colours, may be biased high at supra-solar metallicities. This problem affects mainly the most metal-rich, early-type galaxies. To account for this bias, we include models producing dust attenuations down to  $A_z = -0.1$  when computing the PDFs of stellar mass, stellar metallicity and age.<sup>8</sup>

A comparison of our stellar mass estimates with those derived by Kauffmann et al. (2003, which were based on a preliminary version of the BC03 models and an early calibration of the SDSS spectra) for the galaxies in common between the two samples shows overall consistency, with a scatter of  $\sim 0.16$  dex. Our stellar mass estimates tend to be systematically larger than theirs by  $\sim 0.1$  dex. A difference of almost  $+0.04$  dex can be attributed to the different prior used to generate the Monte Carlo library. The remaining offset is likely to originate from their exclusion of all models with  $r-i$  colour redder than that observed, while we include models which imply  $A_z$  ‘attenuations’ down to  $-0.1$ .

---

<sup>7</sup>Fibre magnitudes are obtained using the SDSS photometry directly out to the radius covered by the fibre. They are thus directly comparable to quantities derived from spectroscopy, provided that the fibre is positioned at the centre of the galaxy. Corrections for emission lines are obtained by comparing the magnitudes measured off the spectrum before and after removing emission lines.

<sup>8</sup>The difference in  $r-i$  colour between two old stellar populations of metallicities  $2.5 Z_\odot$  and  $2 Z_\odot$ , when interpreted as a colour excess, corresponds to a  $z$ -band attenuation  $A_z \sim 0.1$ .

## 2.3 The ages and metallicities of nearby galaxies

We now use the models described in Section 4.2 to estimate ages and metallicities for a sample of 196,673 galaxies drawn from the SDSS-DR2 (Abazajian et al. 2004, see also Section 2.2.1 above). Fig. 2.4 shows the distributions in median S/N per pixel (upper panel) and in redshift (lower panel) of this sample. Although the distribution in redshift extends up to 0.3, in what follows we discuss results only for galaxies in the redshift range  $0.005 < z \leq 0.22$ . The lower limit is intended to avoid redshifts for which deviations from the Hubble flow can be substantial, but still allows us to include galaxies at very low luminosity (corresponding roughly to a lower mass limit of  $\sim 10^8 M_\odot$ ). The upper limit corresponds roughly to the redshift at which a typical  $10^{11} M_\odot$  galaxy is detected with median S/N per pixel greater than 20. These cuts leave us with 175,128 galaxies.

In some applications below, it will be useful to distinguish between different morphological types of galaxies. This can be achieved on the basis of the ‘concentration parameter’  $C = R_{90}/R_{50}$ , defined as the ratio of the radii enclosing 90 and 50 percent of the Petrosian  $r$ -band luminosity of a galaxy. Strateva et al. (2001) and Shimasaku et al. (2001) have shown that the concentration parameter allows a rough classification into galaxy morphological types. Strateva et al. (2001) propose a cut at  $C = 2.6$  to separate early- from late-type galaxies. To limit the contamination between the two types, here we define those galaxies with  $C \geq 2.8$  to be ‘early-type’ and those galaxies with  $C \leq 2.4$  to be ‘late-type’. The dotted and dashed lines in Fig. 2.4 show separately the distributions in median S/N per pixel and in redshift of the resulting subsamples of early- and late-type galaxies, respectively. Early-type galaxies generally have a higher median S/N per pixel and are detected out to higher redshifts than late-type galaxies, as expected from their higher surface brightnesses.

We have shown in Section 2.2.4.1 and Fig. 2.3 the impact of the signal-to-noise ratio on our ability to derive reliable constraints on age and, especially, metallicity. In the remainder of this paper we focus on the subsample of 44,254 galaxies with median S/N per pixel greater than 20, for which the constraints on metallicity are the most accurate. The properties of these high-S/N galaxies are summarized in Fig. 2.5 where we show their distribution (shaded histogram) in  $z$ -band surface brightness (averaged within the Petrosian  $R_{50}$  radius), Petrosian  $r$ -band absolute magnitude, redshift and D4000, compared to the distributions for the original sample (dot-dashed line). The red and blue lines distinguish early-type from late-type (high-S/N) galaxies. The S/N requirement excludes about 75 percent of our sample. As can be seen from Fig. 2.5, this biases the sample toward higher-surface brightness, more concen-

## 2 The Ages and Metallicities of Galaxies in the Local Universe

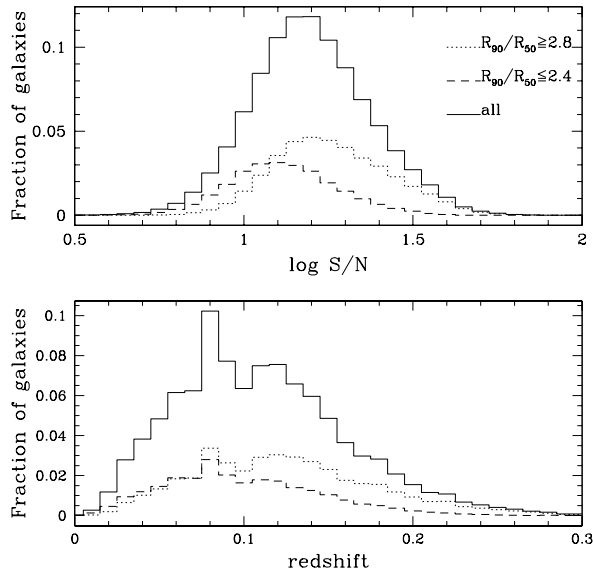


**Figure 2.4:** Distributions in median S/N per pixel (upper panel) and in redshift (bottom panel) of the sample of 196,673 SDSS-DR2 galaxies (solid histograms). In each panel, the dotted and dashed histograms show the corresponding distributions for the subsamples of high-concentration ( $C \geq 2.8$ ), early-type galaxies and low-concentration ( $C \leq 2.4$ ), late-type galaxies, respectively.

trated, lower-redshift galaxies. There is not a bias instead in the luminosity distribution. In the redshift range  $0.005 < z \leq 0.22$ , high-S/N galaxies typically have  $z$ -band surface brightnesses brighter than  $21 \text{ mag arcsec}^{-2}$ . They lie primarily at redshifts less than 0.15, where they account for about 40 percent of the galaxies. They also represent roughly 40 percent of the high-concentration sample but only 10 percent of the low-concentration sample. Similarly, they constitute about 30 percent of the galaxies with  $D4000 > 1.6$  and 15 percent of those with  $D4000 < 1.6$ . Our selection in S/N therefore excludes a substantial fraction of diffuse systems, with potentially subsolar metallicities. We will turn our attention to these systems in the third paper of this series. Their omission here does not alter significantly the results presented in the next sections. In particular, we have checked that the median ages and metallicities found for galaxies with stellar masses less than  $\sim 2 \times 10^9 M_\odot$  in Sections 2.3.2 and 2.3.3 below would change by at most 0.2 dex if we included galaxies with low S/N in our sample.

## 2.3 The ages and metallicities of nearby galaxies

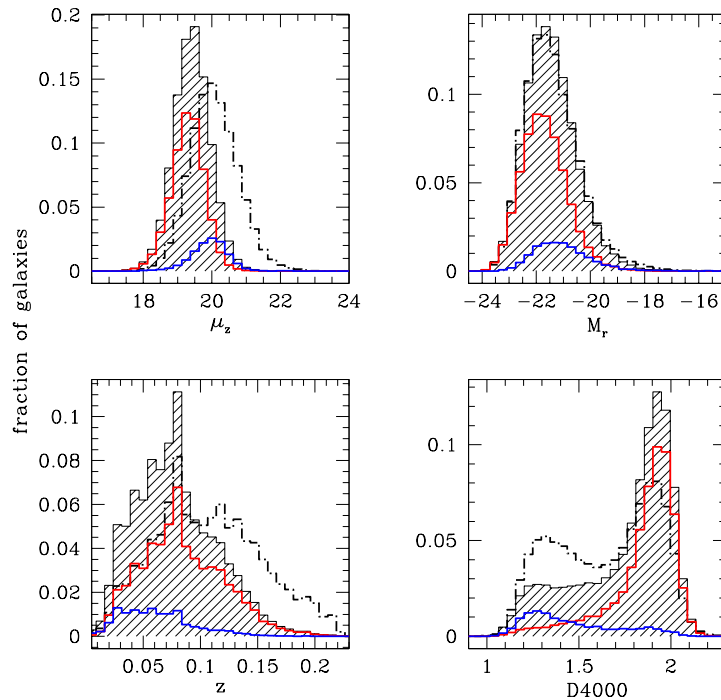


**Figure 2.5:** From top-left to bottom-right: distribution in  $z$ -band surface brightness,  $r$ -band absolute Petrosian magnitude (k-corrected at  $z = 0$ ), redshift and 4000Å-break strength for the galaxies in our sample. The dot-dashed line represents the distribution for the original sample of 175,128 galaxies in the redshift range  $0.005 < z \leq 0.22$ . The shaded histogram describes the distribution for the final sample of 44,254 high-S/N galaxies, while the red and blue histograms separate (high-S/N) early-type ( $C \geq 2.8$ ) and late-type ( $C \leq 2.4$ ) galaxies, respectively. (Note that the dot-dashed and the shaded histograms are both normalized to unit area.)

### 2.3.1 Age, metallicity and mass distributions

We present here the distributions in age, metallicity and stellar mass of the 44,254 galaxies in our final sample. We recall that we estimate  $r$ -band light-weighted ages but assume that all stars in a given galaxy have a single metallicity (interpreted as the optical light-weighted metallicity). The left-hand panels of Fig. 2.6 show, from top to bottom, the distributions of the median-likelihood estimates of stellar metallicity, age and stellar mass for the galaxies in our sample (solid histograms). The distribution in metallicity peaks around  $\log(Z/Z_{\odot}) \sim 0.1$ , the number of galaxies with sub-solar metallicities

## 2 The Ages and Metallicities of Galaxies in the Local Universe

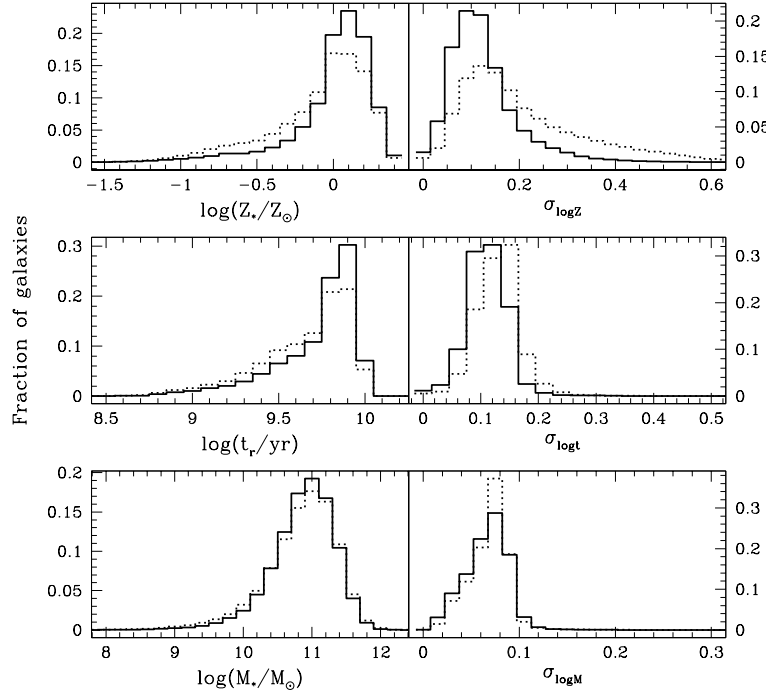


**Figure 2.6:** Distributions of the median-likelihood estimates of stellar metallicity (top-left panel), age (middle-left panel) and stellar mass (bottom-left panel) for 44,254 SDSS-DR2 galaxies with redshifts in the range  $0.005 < z \leq 0.22$  and median S/N per pixel greater than 20 (solid histograms). The right-hand panels show the corresponding distributions of errors, computed as one half the 68 percent confidence ranges in the estimates of  $\log(Z/Z_\odot)$ ,  $\log(t_r/\text{yr})$  and  $\log(M_*/M_\odot)$ . The dotted histograms are for the original sample of 175,128 galaxies (all histograms are normalized to unit area).

decreasing smoothly down to 10 percent of solar. The distribution in age indicates that most of the galaxies have fairly old mean stellar populations, with  $t_r \sim 7 - 8$  Gyr. The distribution in stellar mass reveals that our sample is dominated by relatively massive galaxies, with  $M_* \sim 10^{11} M_\odot$ , while only a small fraction of the sample has masses below  $10^{10} M_\odot$ .

The right-hand panels of Fig. 2.6 show the distributions of one half the 68 percent confidence range in the estimates of  $\log(Z/Z_\odot)$ ,  $\log(t_r/\text{yr})$  and  $\log(M_*/M_\odot)$ . Stellar mass is the best constrained parameter, with a typical random uncertainty of  $\sim 0.08$  dex. Almost all the galaxies in the sample have a stellar mass estimate with an uncertainty less than 0.1 dex. Also, the ages are

## 2.3 The ages and metallicities of nearby galaxies

---

constrained within 0.2 dex for almost all the galaxies, the typical uncertainty being  $\sim 0.12$  dex. Similarly the average error on stellar metallicity is 0.12 dex, but the distribution extends to larger errors ( $\sim 0.3$ ) than for light-weighted age.

As a comparison, the dotted histograms show the distributions in the derived parameters and the associated uncertainties for the original sample of 175,128 galaxies. There is a significant tail of galaxies with very broad stellar metallicity PDFs, resulting in uncertainties greater than 0.25 dex. This further demonstrates that the uncertainties in metallicity estimates depend sensitively on the S/N in the observed spectra, as discussed in Section 2.2.4. Also, the distribution in stellar metallicity shows that with our S/N cut we have excluded preferentially galaxies with subsolar metallicity. High-metallicity galaxies tend to be associated with small errors and low-metallicity galaxies with large errors (presumably because of their weaker absorption lines). Including low-S/N galaxies also increases the average error on light-weighted age to  $\sim 0.15$  dex, but the trend of increasing error with decreasing age is less strong than the analogous trend for metallicity.

### 2.3.2 Relations between age, stellar metallicity, stellar mass and gas-phase metallicity

It is interesting to examine how age, metallicity and stellar mass (and the errors on these quantities) are distributed among galaxies with different star formation histories. As shown by Kauffmann et al. (2003), galaxies with different star formation histories populate different areas of a diagram defined by D4000 and the strength of a H-Balmer absorption line (they illustrated this result for  $H\delta_A$ ). Galaxies with smooth star formation histories form a sequence extending from actively star-forming galaxies (corresponding to small D4000 and strong H-Balmer absorption) to quiescent early-type galaxies (corresponding to large D4000 and weak H-Balmer absorption). Galaxies which experienced recent bursts of star formation exhibit the strongest H-Balmer absorption at fixed D4000.

We now explore how the 44,254 high-S/N galaxies in our sample populate such a diagram as a function of their physical parameters derived in Section 2.3.1 above. We consider here for consistency the diagram defined by D4000 and the  $H\delta_A+H\gamma_A$  absorption index. In the left-hand panels of Fig. 2.7, we have binned and colour-coded this diagram in order to reflect, from top to bottom, the average stellar metallicity, the average age and the average stellar mass of the galaxies falling into each bin. The widths of the bins in D4000 and  $H\delta_A+H\gamma_A$  correspond roughly to the mean observational errors in the two quantities for galaxies with median S/N per pixel greater

## 2 The Ages and Metallicities of Galaxies in the Local Universe

---

than 20 (0.04 and 0.4, respectively).

The bottom-left panel of Fig. 2.7 shows that stellar mass increases with D4000 along the sequence populated by SDSS galaxies in the  $H\delta_A+H\gamma_A$  versus D4000 diagram. The average mass of galaxies with  $D4000 \lesssim 1.2$  is less than  $10^{10}M_\odot$ , while that of galaxies with  $D4000 \gtrsim 1.9$  reaches  $10^{11}M_\odot$ . There is a smooth transition between these two regimes in the central region of the diagram. This confirms the trends in D4000 and  $H\delta_A$  as functions of stellar mass observed by Kauffmann et al. (2003) (see their fig. 1). Both stellar metallicity and age also appear to increase with increasing D4000 (upper- and middle-left panels of Fig. 2.7). The variation in age is very smooth. In the intermediate regime, age appears to decrease with increasing  $H\delta_A+H\gamma_A$  at almost fixed D4000. The variation in metallicity is more noisy, partly because of the larger errors associated with metallicity estimates, especially for low D4000 (see Section 2.3.1). Near the middle of the galaxy sequence, i.e., for  $1.4 \lesssim D4000 \lesssim 1.8$ , stronger H-Balmer absorption appears to be associated to not only younger but also more metal-rich stellar populations. This is consistent with the idea that these galaxies could have experienced a burst of metal-enriched star formation about 1–2 Gyr ago.<sup>9</sup>

We have checked that the above trends in stellar metallicity, age and stellar mass do not change significantly if we include galaxies with lower S/N values. The main effect is to increase the scatter in these physical parameters along the  $H\delta_A+H\gamma_A$  versus D4000 sequence, mainly because of the larger observational errors in these two indices. Moreover, the average S/N for the full sample does not vary significantly along the relation. For these reasons, we believe that our results are not strongly biased by our cut in S/N.

In the right-hand panels of Fig. 2.7, we have colour-coded the  $H\delta_A+H\gamma_A$  versus D4000 diagram to reflect the average uncertainties in the determinations of stellar metallicity, age and stellar mass (from top to bottom) for the galaxies falling into each bin. These diagrams illustrate how the tightness of the constraints derived on the various physical parameters depends on the strengths of  $H\delta_A+H\gamma_A$  and D4000. The errors in all three parameters tend to be larger at lower D4000, the trend being especially strong for stellar metallicity. We emphasize that the right-hand panels of Fig. 2.7 do *not* reflect the rms scatter in the various physical parameters, but rather the average uncertainties associated with determinations of these parameters. For reference, the rms scatter is typically comparable to (or smaller than) the average uncertainty for stellar metallicity and age, but always larger than the average uncertainty for stellar mass.

---

<sup>9</sup>At fixed  $D4000 \sim 1.5$ , this trend in age and metallicity is not consistent with (and more pronounced than) the age-metallicity degeneracy described in Section 2.3.3.

### 2.3 The ages and metallicities of nearby galaxies

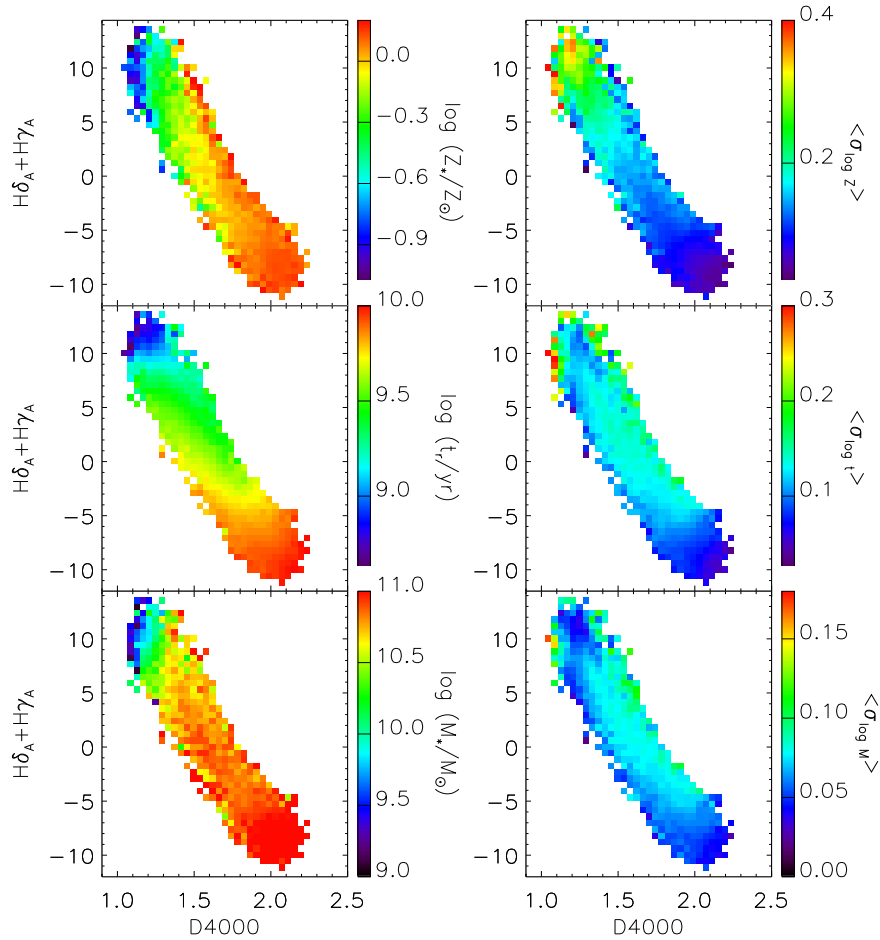


**Figure 2.7:** Physical parameters of 44,254 SDSS-DR2 galaxies with median S/N per pixel greater than 20 as a function of position in the  $H\delta_A + H\gamma_A$  versus D4000 diagram. In the left-hand panels, the diagram has been binned and colour-coded in order to reflect the average stellar metallicity (top), age (middle) and stellar mass (bottom) of the galaxies falling into each bin. In the right-hand panels, the diagram has been binned and colour-coded to reflect the average uncertainty (corresponding to one half the 68 percent confidence interval) in the derived stellar metallicities (top), ages (middle) and stellar masses (bottom) of the galaxies falling into each bin. The widths of the bins in D4000 and  $H\delta_A + H\gamma_A$  correspond roughly to the mean observational errors in these quantities (0.04 and 0.4, respectively).

## 2 The Ages and Metallicities of Galaxies in the Local Universe

---

The results of Fig. 2.7 suggest that both stellar metallicity and age correlate with stellar mass. We investigate this further in Fig. 2.8, where we show the distributions of metallicity (panel a) and age (panel b) as function of stellar mass for the 44,254 high-S/N galaxies in our sample. Rather than assigning each galaxy its median-likelihood estimate of each of the three parameters, we keep here the whole information contained in the PDFs. In Fig. 2.8a, the likelihood distribution of stellar metallicity as a function of stellar mass was obtained by coadding the normalized 2-D likelihood distributions of metallicity and stellar mass for all the galaxies and then re-normalizing along the metallicity axis in bins of stellar mass (we adopted a bin width of 0.2 dex, roughly comparable to the 68 percent confidence range in stellar mass estimates). The solid line indicates the median of the final conditional distribution, and the dashed lines the 16<sup>th</sup> and 84<sup>th</sup> percentiles. The percentiles of the metallicity and age distributions at fixed stellar mass are provided in Table 2.2.

The median shows that metallicity increases with stellar mass, from roughly 20 percent of solar for galaxies with masses below  $10^{10}M_{\odot}$  to about 1.4 times solar for those with masses above  $10^{11}M_{\odot}$ . In between, stellar metallicity increases rapidly with stellar mass, the trend becoming shallower at  $M_{*} \gtrsim 10^{10.5}M_{\odot}$ . Fig. 2.8b shows the analogous conditional distribution of age as a function of stellar mass. The median (*r*-band light-weighted) age increases from roughly 1 Gyr for galaxies with masses around  $10^9M_{\odot}$  to about 6.5 Gyr for those with masses around  $10^{10.5}M_{\odot}$ . For more massive galaxies, the median age continues to increase, but only by about 0.2 dex ( $\sim 1.6$  Gyr) over one order of magnitude in stellar mass.

Although the median metallicity and age both increase with increasing stellar mass, the probability levels (indicated by the colour) and the 68 percent confidence ranges reveal broad distributions in the estimates of both parameters. We now explore whether the larger scatter in both distributions at smaller masses can be accounted for by the larger uncertainties in metallicity and age estimates for more metal-poor and younger galaxies, or whether it is indicative of an intrinsically broad distribution in metallicity and age for low-mass galaxies. In the bottom panels of Fig. 2.8, we compare the scatter in these relations with the uncertainties in the estimates of metallicity (panel c) and age (panel d) at fixed stellar mass. In each panel, the diamonds show the difference between the 16<sup>th</sup> and 84<sup>th</sup> percentiles of the conditional distribution shown above as a function of stellar mass. The stars show the mean 68 percent confidence range in the individual estimates of metallicity or age for the galaxies falling into each stellar-mass bin.<sup>10</sup> Fig. 2.8c shows that the

---

<sup>10</sup>The stars in Fig. 2.8c,d are not computed using the joint likelihood distribution, but rather by adopting the median of the  $M_{*}$  PDF as our estimate of stellar mass. The comparison

### 2.3 The ages and metallicities of nearby galaxies

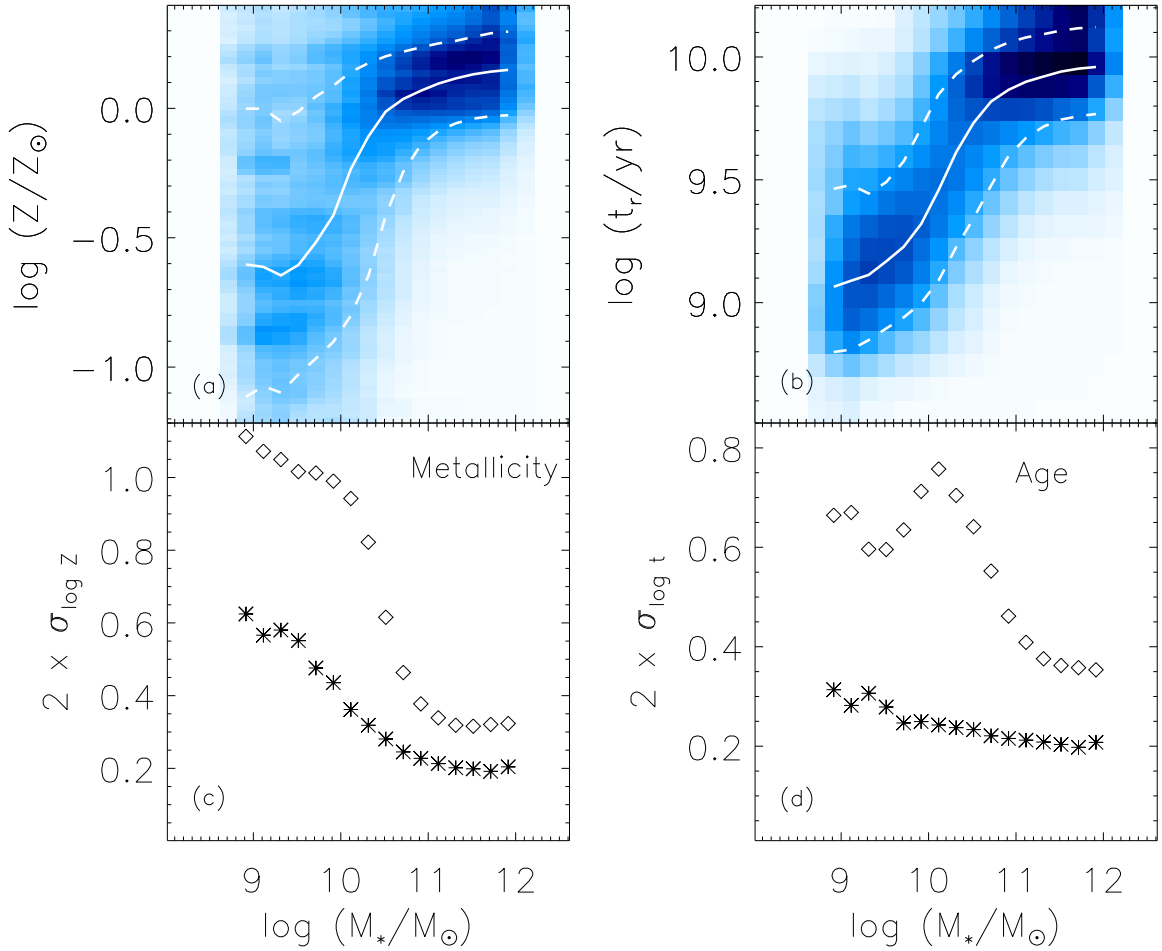


**Figure 2.8:** Panels a and b: conditional distribution of stellar metallicity and age as a function of stellar mass for 44,254 SDSS-DR2 galaxies with median S/N per pixel greater than 20. Each distribution was obtained by coadding the normalized 2-D likelihood distributions of the desired parameter (stellar metallicity or age) and stellar mass for all the galaxies and then re-normalizing along the y-axis in bins of stellar mass (of width 0.2 dex). The solid line indicates the median of the final conditional distribution, and the dashed lines the 16<sup>th</sup> and 84<sup>th</sup> percentiles. Panels c and d: comparison of the scatter in the metallicity and age distributions with the mean uncertainty of the metallicity and age estimates as a function of stellar mass. The diamonds show the difference in  $\log(Z/Z_\odot)$  or  $\log(t_r/\text{yr})$  between the 16<sup>th</sup> and 84<sup>th</sup> percentiles of the conditional distributions of panels a and b, while the stars represent the mean 68 percent confidence range in  $\log(Z/Z_\odot)$  or  $\log(t_r/\text{yr})$  for the galaxies in each stellar mass bin.

## 2 The Ages and Metallicities of Galaxies in the Local Universe

**Table 2.2:** Median (P50) and percentiles (P16, P84) of the distributions in stellar metallicity and age as a function of stellar mass (Fig. 2.8a,b).

$\log(M_*/M_\odot)$	$\log(Z/Z_\odot)$			$\log(t_r/yr)$		
	P50	P16	P84	P50	P16	P84
8.91	-0.60	-1.11	-0.00	9.06	8.80	9.46
9.11	-0.61	-1.07	-0.00	9.09	8.81	9.48
9.31	-0.65	-1.10	-0.05	9.11	8.85	9.44
9.51	-0.61	-1.03	-0.01	9.17	8.89	9.49
9.72	-0.52	-0.97	0.05	9.23	8.94	9.57
9.91	-0.41	-0.90	0.09	9.32	9.00	9.71
10.11	-0.23	-0.80	0.14	9.46	9.09	9.85
10.31	-0.11	-0.65	0.17	9.61	9.23	9.93
10.51	-0.01	-0.41	0.20	9.73	9.34	9.98
10.72	0.04	-0.24	0.22	9.82	9.48	10.03
10.91	0.07	-0.14	0.24	9.87	9.60	10.06
11.11	0.10	-0.09	0.25	9.90	9.67	10.08
11.31	0.12	-0.06	0.26	9.92	9.72	10.09
11.51	0.13	-0.04	0.28	9.94	9.75	10.11
11.72	0.14	-0.03	0.29	9.95	9.76	10.12
11.91	0.15	-0.03	0.30	9.96	9.77	10.12

scatter in the mass-metallicity relation is always larger than the uncertainties in the metallicity estimates, by at least 0.1 dex, and is largest (compared to the error) at about  $10^{10}M_\odot$ . Similarly, the scatter in the mass-age relation (Fig. 2.8d) is always larger than the uncertainties in the age estimates and is also largest at about  $10^{10}M_\odot$ . Fig. 2.8 clearly indicates that more massive galaxies are older and more metal-rich, while less massive galaxies are younger and more metal-poor. Metallicity and age, however, are not uniquely determined by stellar mass. There is an intrinsic scatter in both parameters, which is particularly evident at intermediate stellar masses. The results of Section 2.3.3 below indicate that part of this intrinsic scatter can be accounted for by differences in galaxy morphology, the intermediate-mass regime corresponding to the transition between disc-dominated and bulge-dominated galaxies. However, a significant scatter persists even when considering the two classes of galaxies separately.

Tremonti et al. (2004) have shown that the emission-line galaxies in the

---

of the stars with the diamonds is consistent, given that the width of the stellar mass bins is comparable with the error in stellar mass estimates.

### 2.3 The ages and metallicities of nearby galaxies

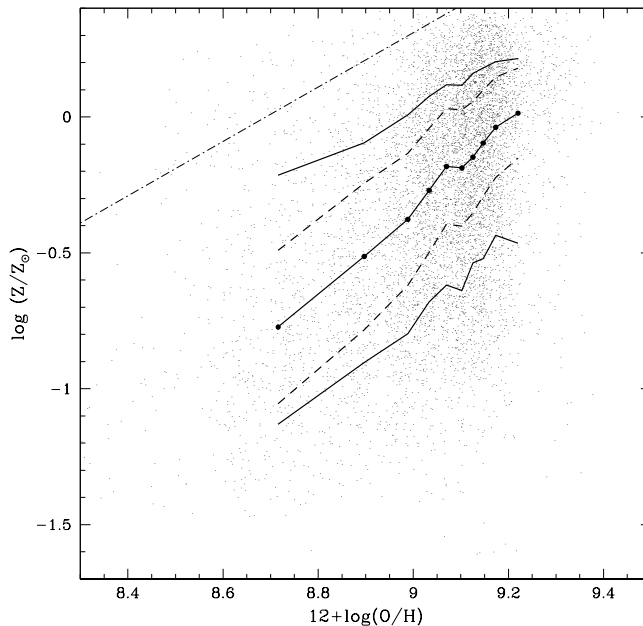


**Figure 2.9:** Stellar metallicity estimates (present work) plotted against gas-phase oxygen abundance  $12+\log(\text{O}/\text{H})$  (Tremonti et al. 2004) for 7462 high-S/N SDSS-DR2 galaxies for which both measures are available. The small dots show the median-likelihood estimates of the two parameters for each galaxy. The larger points (joined by a solid line) show the median stellar metallicity in bins of  $12+\log(\text{O}/\text{H})$  (each bin containing  $\sim 300$  galaxies), while the outer solid lines show the corresponding 16<sup>th</sup> and 84<sup>th</sup> percentiles. The dashed lines indicate the mean 68 percent confidence range in the stellar metallicity estimates for the galaxies in each bin of  $12+\log(\text{O}/\text{H})$ . Solar metallicity is 8.69 in these units (Allende Prieto et al. 2001). The dot-dashed line represents the one-to-one relation, showing that stellar metallicity is always lower than gas-phase metallicity.

DR2 sample exhibit a tight relation between stellar mass and gas-phase oxygen abundance, as determined from their nebular spectra. The gas-phase oxygen abundance increases steadily from low to high stellar masses, and then gradually flattens around masses of  $10^{10.5} M_{\odot}$ . There is a striking similarity between the relation Tremonti et al. (2004) found for star forming galaxies and the relation found in Fig. 2.8 above between stellar metallicity and stellar mass, which includes both star-forming and quiescent galaxies. However, the dispersion in the stellar metallicity versus stellar mass relation is much larger than that in the relation between gas-phase oxygen abundance and stellar

## 2 The Ages and Metallicities of Galaxies in the Local Universe

---

mass ( $\pm 0.1$  dex). This may partly reflect the larger errors associated with stellar metallicity determinations.

In Fig. 2.9, we plot stellar metallicity against gas-phase oxygen abundance,  $12+\log(\text{O}/\text{H})$ , for the 7462 high-S/N galaxies of our sample for which both measures are available. We note that gas-phase metallicity is best determined for star-forming galaxies, whereas stellar metallicity is best determined for early-type galaxies. The small dots show the median-likelihood estimates of the stellar and gas-phase metallicities for each galaxy. The larger points indicate the median stellar metallicity in bins of  $12+\log(\text{O}/\text{H})$ , while the outer solid lines show the corresponding 16<sup>th</sup> and 84<sup>th</sup> percentiles. There is a relation between the two parameters with approximately unit slope. However, the stellar metallicity is generally lower than the gas-phase metallicity (by  $\sim 0.5$  dex), as demonstrated by the one-to-one relation (dot-dashed line). This is expected since the nebular metallicity traces the metallicity of the last generations of stars to form, whereas the stellar metallicity represents an average over the entire star formation history of the galaxy. Notably, the large scatter in stellar metallicity at fixed gas-phase oxygen abundance (solid lines) cannot be solely accounted for by the errors in stellar metallicity estimates (indicated by the dashed lines).

To investigate the origin of this scatter, we compute the residuals in  $\log(Z/Z_{\odot})$  with respect to a simple linear fit of the median relation (large dots) in Fig. 2.9. The residuals are plotted in Fig. 2.10 as a function of various galaxy properties, including the star formation rate (from Brinchmann et al. 2004) and an indirect estimate of the gas mass fraction inferred from the star formation rate (see eq. 5 of Tremonti et al. 2004). In each panel, we indicate the median trend of the residuals as a function of the property under consideration for galaxies in five bins of gas-phase oxygen abundance, from  $8.70 \pm 0.075$  (blue) to  $9.3 \pm 0.075$  (red). The  $\log(Z/Z_{\odot})$  residuals show positive correlations with stellar mass, surface mass density, concentration parameter and D4000 and negative correlations with specific star formation rate, gas mass fraction and  $\text{H}\delta_A + \text{H}\gamma_A$ . These various trends are almost independent of gas-phase oxygen abundance.<sup>11</sup> They imply that, at fixed  $12+\log(\text{O}/\text{H})$ , the stars are most metal-rich in massive, high-concentration galaxies, which have exhausted most of their gas and form stars at a lower rate than in the past. The existence of a substantial range of stellar metallicities at fixed gas-phase oxygen abundance in Fig. 2.9 further suggests that the galaxies in our sample are not well approximated by ‘closed-box’ systems, for which stellar and interstellar metallicities

---

<sup>11</sup>We checked that the trends of  $\log(Z/Z_{\odot})$  residuals with the strengths of D4000 and  $\text{H}\delta_A + \text{H}\gamma_A$  are not caused by any bias in our estimates of stellar metallicity (see Section 2.2.4.2).

## 2.3 The ages and metallicities of nearby galaxies

---

should be tightly related (e.g., Tinsley 1980). This indicates that gas ejection and/or accretion may be important factors in galaxy chemical evolution.

### 2.3.3 Age versus metallicity

Most previous population synthesis studies of the age-metallicity relation for nearby galaxies have focused on early-type galaxies (e.g. Gonzalez et al. 1993; Worthey 1997; Bernardi et al. 1998; Terlevich et al. 1999; Ferreras et al. 1999; Trager et al. 2000a). A few studies have also included the bulges of spiral galaxies (Jablonka et al. 1996; Goudfrooij et al. 1999; Terlevich & Forbes 2002; Proctor & Sansom 2002). Our determination, with a new method, of the ages and metallicities of a large sample of nearby galaxies spanning a wide range of star formation activities allows us to re-assess the relation between these two physical parameters.

We separate here high-concentration, bulge-dominated early-type galaxies and low-concentration, disk-dominated late-type galaxies as described above to understand whether different conclusions can be drawn for different types of galaxies. We have shown in Fig. 2.8 that both metallicity and age increase with stellar mass. We may therefore expect that the distribution of galaxies over metallicity and age will change when different masses are considered. This mass dependence may also be different for different types of galaxies. For this reason, we divide each morphological subsample into six bins of stellar mass. Figs 2.11 and 2.12 show the age-metallicity relation in these different stellar-mass bins for late-type and early-type galaxies, respectively. The stellar mass increases from  $\log(M/M_\odot) \leq 10$  in the top-left panel to  $\log(M/M_\odot) > 11$  in the bottom-right panel. These relations were obtained by simply coadding the normalized joint likelihood distributions of age and metallicity for individual galaxies, without further normalization. The grey levels indicate the probability associated with each value of metallicity and age in a square-root scale, while the contours enclose 26, 68, 95 and 99 percent of the total probability.

Fig. 2.11 shows that the ages and metallicities of low-concentration, late-type galaxies change significantly as a function of stellar mass. Galaxies less massive than  $10^{10}M_\odot$  have typically low metallicities ( $Z \approx 10^{-0.6}Z_\odot$ ) and young ages ( $0.8 \lesssim t_r/\text{Gyr} \lesssim 2.5$ ). At intermediate stellar masses, i.e. for  $10^{10} \lesssim M_*/M_\odot \lesssim 10^{10.5}$ , the distribution in metallicity becomes broader and shifts gradually to higher metallicities. The overall spread in age is roughly 0.8 dex, and the distribution shifts slightly to older ages. Late-type galaxies more massive than  $10^{10.5}M_\odot$  have predominantly high metallicities ( $Z \gtrsim Z_\odot$ ) and old ages ( $3.2 \lesssim t_r/\text{Gyr} \lesssim 10$ ). The fraction of young metal-poor galaxies nearly vanishes at the highest masses.

Fig. 2.12 shows that the ages and metallicities of high-concentration, early-

## 2 The Ages and Metallicities of Galaxies in the Local Universe

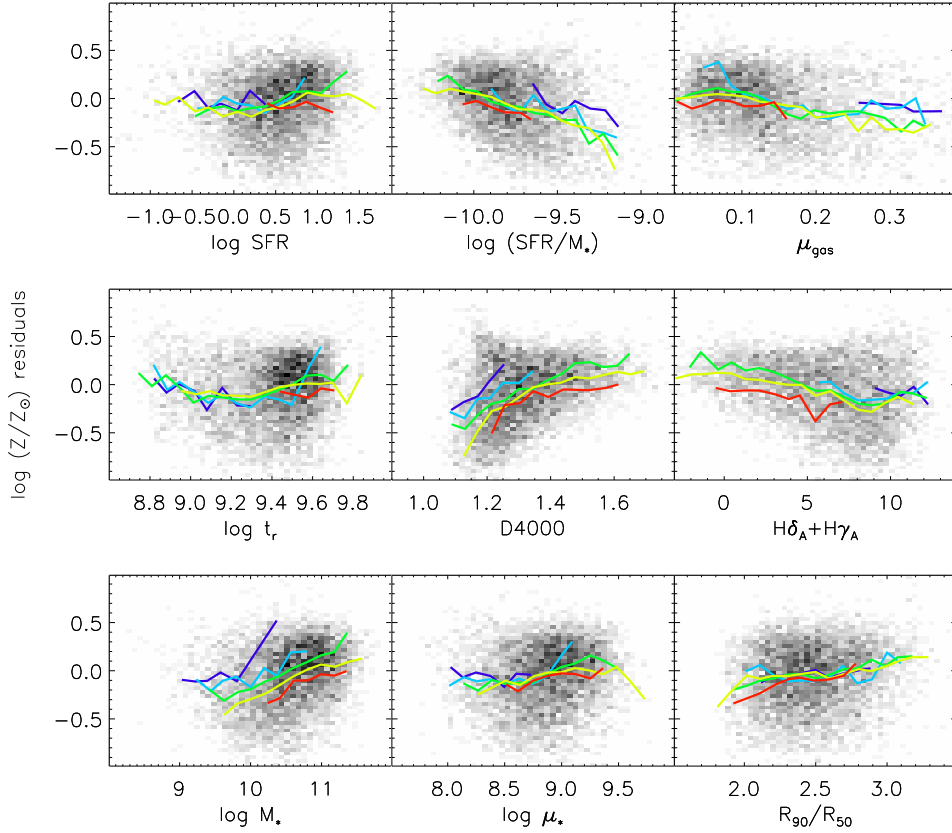


**Figure 2.10:** Residuals in  $\log(Z/Z_{\odot})$  with respect to a simple linear fit of the median relation between stellar metallicity and gas-phase oxygen abundance in Fig. 2.9, plotted against various galaxy properties. From left to right, top row: star formation rate (in units of  $M_{\odot}\text{yr}^{-1}$ ), specific star formation rate (in units of  $\text{yr}^{-1}$ ) and gas mass fraction. Middle row:  $r$ -band light-weighted age (in units of yr), D4000 and  $H\delta_A+H\gamma_A$  index strengths. Bottom row: total stellar mass (in units of  $M_{\odot}$ ), surface mass density within the Petrosian  $r$ -band  $R_{50}$  radius (in units of  $M_{\odot}\text{kpc}^{-2}$ ) and  $r$ -band concentration parameter. In each panel, curves of different colors indicate the median relations in different bins of gas-phase oxygen abundance, increasing from  $8.7\pm 0.075$  (blue) to  $9.3\pm 0.075$  (red).

type galaxies depend much more weakly on stellar mass than those of low-concentration, late-type galaxies. The gradual increase of metallicity with stellar mass is still appreciable for early-type galaxies. Galaxies less massive than  $10^{10}M_{\odot}$  have metallicities typically in the range  $10^{-0.4}-10^{0.1}Z_{\odot}$ , while

### 2.3 The ages and metallicities of nearby galaxies

---

galaxies more massive than  $10^{11}M_{\odot}$  have metallicities typically above solar. The age range does not exhibit any significant variation with stellar mass, except for a population of young metal-poor galaxies in the lowest-mass bin, which does not show up at higher masses. At low stellar masses, we also notice a small fraction ( $\sim 1$  percent) of galaxies clumping at much higher metallicities and younger ages than the bulk of the early-type galaxy sample. Detailed inspection reveals that these galaxies are photometric outliers, for which we are uncertain of the accuracy of our fits. Follow-up observations would be required to understand whether the unusual metallicities and ages of these galaxies are consistent with a substantial recent episode of metal-enriched star formation.

We note that the typical light-weighted age for the massive early-type galaxies in our sample is  $\sim 8$  Gyr, which is somewhat younger than the ages usually quoted for (cluster) ellipticals. Differences can arise from differences in the adopted methods. In particular, the ages usually quoted in the literature are derived by comparing the observed distributions in spectral indices with simple stellar population predictions. What we quote here is a proper light-weighted age, calculated by weighting the age of each generation of stars by their luminosity along the entire SFH of each model galaxy. Nevertheless, the relatively young ages we find could reflect an environmental dependence, since the SDSS sample is composed predominantly of galaxies in lower density regions than those used in most studies of early-type galaxies. Indeed, several studies have reported an age difference between early-type galaxies in clusters and in low-density regions from  $\sim 1.2$  Gyr (Bernardi et al. 1998) up to  $2 - 3$  Gyr (Kuntschner et al. 2002; Thomas et al. 2005). We will discuss the properties of the early-type galaxies in our sample in more detail in the second paper of this series.

A comparison of Figs 2.11 and 2.12 suggests that the ages and metallicities of late- and early-type galaxies differ primarily at the low-mass end. Low-mass late-type galaxies tend to be younger and more metal-poor than their early-type counterparts (by about 0.6 dex in both age and metallicity). In contrast, massive late-type galaxies tend to have old ages and high metallicities similar to those of their early-type counterparts, even though there is a tail of young ( $t_r \lesssim 10^{9.5}$  yr), metal-poor ( $Z \approx 10^{-0.5}Z_{\odot}$ ) late-type galaxies with masses greater than  $10^{11}M_{\odot}$  in our sample. The high metallicities of most massive late-type galaxies might reflect the influence of their metal-rich bulges. This may be enhanced by the fact that the SDSS spectra sample only the inner regions of the galaxies (see Section 2.3.4 below).

Figs 2.11 and 2.12 also indicate that the relation between stellar metallicity and stellar mass discussed in Section 2.3.2 holds for both late-type and early-type galaxies. In contrast, the relation between age and stellar mass is much

## 2 The Ages and Metallicities of Galaxies in the Local Universe

---

more pronounced for late-type galaxies, which cover a significant range in age ( $\sim 9$  Gyr). Early-type galaxies do not show such a clear trend, at least above  $10^{10.5}M_{\odot}$ . This is in agreement with previous findings of no significant relation between the ages of early-type galaxies and luminosity (Kuntschner & Davies 1998; Kuntschner 1998; Terlevich & Forbes 2002). At fainter luminosities, however, there are indications of a spread to younger ages (see also Worthey & Ottaviani 1997; Caldwell & Rose 1998). We also find that the fraction of young early-type galaxies increases at lower stellar masses. This is true in particular below  $10^{10}M_{\odot}$ , reflecting a possible contamination by S0 galaxies (e.g. Poggianti et al. 2001). Finally, we note that for both early-type galaxies and high-mass late-type galaxies, the probability contours of Figs 2.11 and 2.12 hint at an anticorrelation between age and stellar metallicity, at given mass. Other workers have pointed out this anticorrelation (e.g. Worthey et al. 1995; Colless et al. 1999; Jørgensen 1999; Rakos et al. 2001; Poggianti et al. 2001), but it is difficult to assess its significance here because of the correlated errors on age and metallicity (see below).

The dependence of the properties of SDSS galaxies on stellar mass has been addressed in previous studies (e.g. Shen et al. 2003; Brinchmann et al. 2004; Tremonti et al. 2004; Kannappan 2004; Salim et al. 2005; Jimenez et al. 2005). In particular, Kauffmann et al. (2003) point out that, at masses around  $\sim 10^{10.5}M_{\odot}$ , galaxies separate into two distinct classes of spectral and structural properties. Baldry et al. (2004) have recently shown that this transition around  $(2 - 3) \times 10^{10}M_{\odot}$  can be seen directly from the colour-magnitude relation. Moreover, this mass range seems also to correspond to a shift in gas richness (Kannappan 2004). It is interesting to note that, around the same value of stellar mass, there appears to be also a gradual transition in the ages and metallicities of the galaxies. This transition, which is particularly evident for late-type galaxies, causes the dispersion in age and metallicity to be highest for galaxies of intermediate mass.

We have not mentioned so far the potential influence of the ‘age-metallicity degeneracy’ on the results of Figs 2.11 and 2.12 (see Section 3.1). This degeneracy, which arises from the competing effects of age and metallicity on absorption-line strengths, can cause the confusion between old, metal-poor galaxies and young, metal-rich ones (Worthey 1994). To address this issue, we first evaluate the slope of the age-metallicity degeneracy from the two-dimensional likelihood distribution of each individual galaxy in our sample. This is achieved by computing the matrix of second moments of the likelihood distribution (inside the 68 percent probability contour) with respect to the median  $\log Z$  and  $\log t_r$  values. The direction of the eigenvector corresponding to the largest eigenvalue of this matrix defines the slope  $\Delta \log Z / \Delta \log t_r$  of the age-metallicity degeneracy. In each panel of Figs 2.11 and 2.12, the straight

### 2.3 The ages and metallicities of nearby galaxies

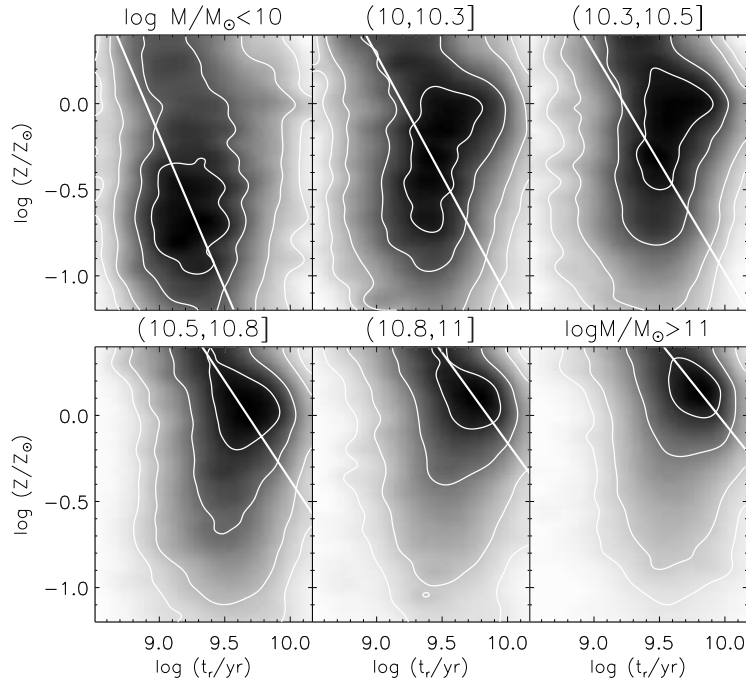


**Figure 2.11:** Two-dimensional distribution of stellar metallicity and age in 6 bins of stellar mass (as indicated) for the subsample of 5616 late-type ( $C \leq 2.4$ ) SDSS-DR2 galaxies with median S/N per pixel greater than 20. Each distribution was obtained by coadding the normalized joint likelihood distributions of age and metallicity for individual galaxies. The grey levels indicate the probability associated with each value of metallicity and age in a square-root scale, while the contours enclose 26, 68, 95 and 99 percent of the total probability. The straight line (which intersects the peak of the probability distribution) indicates the mean slope of the age-metallicity degeneracy for the galaxies falling into each stellar-mass bin.

line indicates the mean  $\Delta \log Z / \Delta \log t_r$  for the galaxies falling into the corresponding bin of stellar mass. The slopes are listed in Table 2.3.<sup>12</sup> They tend to be steeper for low-concentration galaxies ( $-1.78$  to  $-0.95$ ) than for high-concentration ones ( $-1.29$  to  $-0.75$ ).

The orientation of the age-metallicity degeneracy in Figs 2.11 and 2.12 indicates that it cannot be responsible for the trends in age and metallicity

<sup>12</sup>These values are consistent with the results of Worthey (1996), which imply that the change in metallicity needed to compensate a change in age at fixed index strength in the spectrum of an old stellar population should correspond to values of  $\Delta \log Z / \Delta \log t_r$  ranging from  $-1.7$  for age-sensitive indices to  $-0.2$  for metal-sensitive indices.

## 2 The Ages and Metallicities of Galaxies in the Local Universe

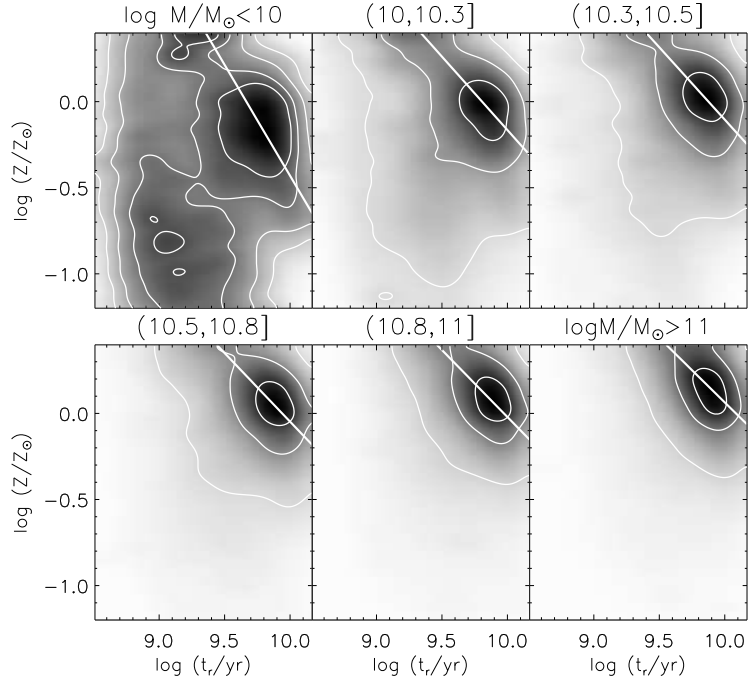


**Figure 2.12:** Same as Fig. 2.11, but for the subsample of 26,003 early-type ( $C \geq 2.8$ ) SDSS-DR2 galaxies with median S/N per pixel greater than 20.

**Table 2.3:** Average slope of the age-metallicity degeneracy in different bins of stellar mass, for the low-concentration and high-concentration galaxies of Figs 2.11 and 2.12.

Stellar mass ( $M_\odot$ )	$\Delta \log Z / \Delta \log t_r$	
	$C \leq 2.4$	$C \geq 2.8$
$\log M_* \leq 10$	-1.78	-1.29
$10 < \log M_* \leq 10.3$	-1.41	-0.85
$10.3 < \log M_* \leq 10.5$	-1.28	-0.84
$10.5 < \log M_* \leq 10.8$	-1.15	-0.80
$10.8 < \log M_* \leq 11$	-1.05	-0.78
$\log M_* > 11$	-0.95	-0.75

as a function of stellar mass identified above. However, it can account for the shape of the joint age-metallicity probability contours for early-type galaxies and the most massive late-type galaxies at high metallicities ( $Z \gtrsim Z_\odot$ ).

### 2.3.4 Aperture bias

The SDSS galaxy spectra on which our analysis is based are taken using 3''-diameter fibres, which collect only the light coming from limited inner regions of the galaxies. We can estimate the fraction of the total galaxy light entering a fibre from the ratio between the fibre flux and the total Petrosian flux. Fig. 2.13 shows the distribution of this ratio for the 44,254 high-S/N galaxies in our sample. The median value is about 30 percent, and the maximum value about 60 percent. The dashed and dotted lines show the distributions for low-concentration, late-type galaxies and high-concentration, early-type galaxies, respectively. As expected, the fibre tends to collect a smaller fraction of the total light for low-concentration galaxies than for high-concentration galaxies.

Radial gradients in the properties of stellar populations are known to exist for both bulge-dominated (Henry & Worthey 1999; Saglia et al. 2000; Mehlert et al. 2003) and disk-dominated (Bell & de Jong 2000; MacArthur et al. 2004) galaxies. Thus, aperture effects are a significant concern for our age and metallicity estimates. Fortunately, the distribution of the fraction of total galaxy light that enters an SDSS fibre does not vary appreciably with redshift (except at very low redshift), because larger galaxies are also brighter and hence selected out to larger distances.

One way to test for the effects of aperture bias on our results is to compare the ages and metallicities of galaxies of similar luminosity located at different redshifts. Because of the presence of both a faint and a bright magnitude cut-off in the SDSS survey, this comparison is possible only for galaxies in a limited absolute-luminosity range, if we want to span a reasonably large redshift range. We consider galaxies with  $r$ -band absolute magnitudes in the narrow range  $-21 \leq r \leq -22$ , which are observed at redshifts between 0.02 and 0.12. At fixed absolute magnitude within this range, both low- and high-concentration galaxies show a decrease (by  $\sim 0.15$  dex) in typical metallicity from redshift 0.02 to 0.12. High-concentration galaxies do not exhibit any significant trend in age, but the typical age of low-concentration galaxies decreases by about 0.2 dex over the same redshift range.

Another way to examine the potential effects of aperture bias on our results is to compare the age and metallicity distributions of galaxies with similar properties as a function of  $z/z_{\max}$ , where  $z_{\max}$  is the minimum of the redshift at which the galaxy reaches the survey faint-magnitude limit and that at which its median S/N per pixel drops below 20 (we assume Poissonian noise, i.e. that the median S/N per pixel scales as the square root of the apparent fibre luminosity). With this approach, we can avoid restricting our test to galaxies in a narrow magnitude range. Also, since we are interested in possible effects of aperture bias on trends with galaxy mass, we divide our sample into the

## 2 The Ages and Metallicities of Galaxies in the Local Universe

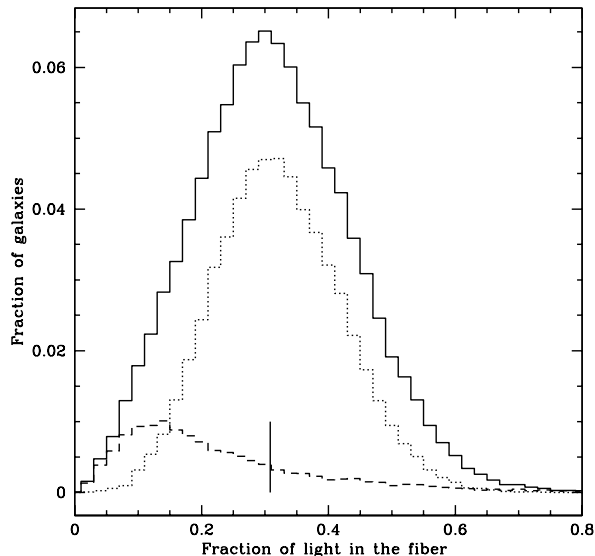


**Figure 2.13:** Distribution of the fraction of the total  $r$ -band flux collected by the SDSS fibre, computed as the ratio between the fibre flux and the Petrosian flux, for 44,254 high-S/N galaxies in the SDSS DR2. The vertical bar indicates the median fraction for this sample. The dashed and dotted lines show the distributions of low-concentration, late-type galaxies and high-concentration, early-type galaxies, respectively.

same 6 bins of stellar mass as in Figs 2.11 and 2.12 above.

Fig. 2.14 shows the dependence on  $z/z_{\max}$  of the median (thick line) and the 16<sup>th</sup> and 84<sup>th</sup> percentiles (thin lines) of the distributions in stellar metallicity (left-hand plot) and age (right-hand plot) of the high-S/N galaxies in our sample. The solid lines correspond to the subsample of 26,003 early-type galaxies, while the dot-dashed lines correspond to the subsample of 5616 late-type galaxies. For early-type galaxies of different masses, the largest change in median metallicity from one edge of the survey to the other is about 0.2 dex. This is comparable to the error associated with the metallicity estimates of most galaxies and smaller than the overall metallicity change with galaxy mass (see Fig. 2.8). This variation is also consistent with the metallicity gradient of  $-0.2$  dex per decade in radius reported by several studies of bulge-dominated galaxies (see Henry & Worthey 1999; Wu et al. 2004). We note that the largest variation arises for galaxies with intermediate stellar masses, which often have both a prominent bulge and a disk. For disk-dominated, late-type galaxies, the trends in median metallicity with  $z/z_{\max}$  are weaker than for early-type

### 2.3 The ages and metallicities of nearby galaxies

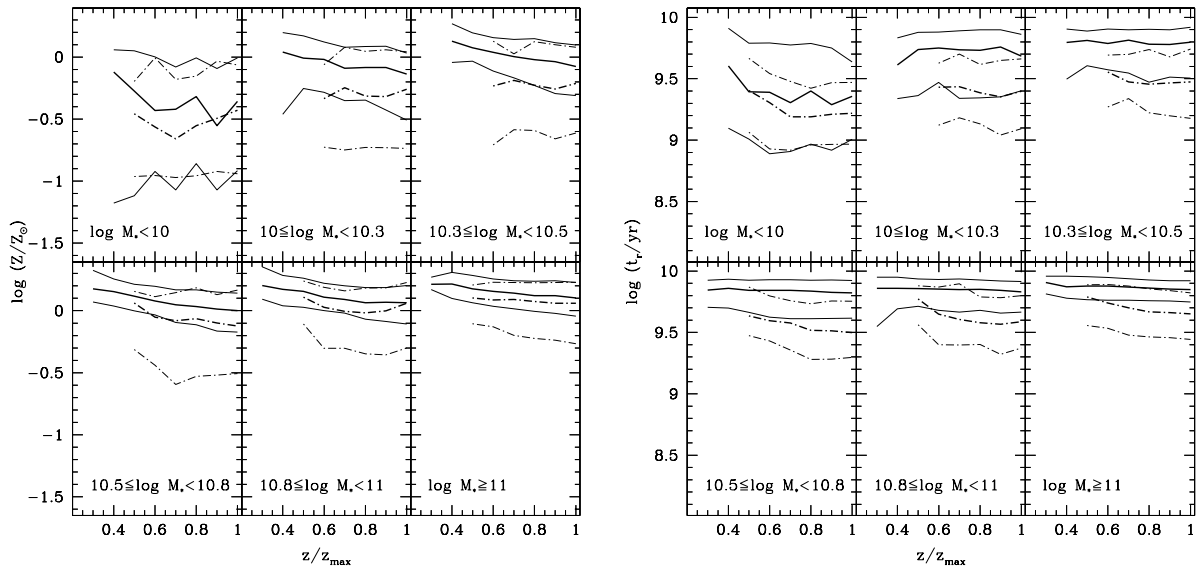


**Figure 2.14:** Dependence on  $z/z_{\max}$  of the median (thick line) and the 16<sup>th</sup> and 84<sup>th</sup> percentiles (thin lines) of the distributions in stellar metallicity (left-hand plot) and age (right-hand plot) of SDSS-DR2 galaxies with median S/N per pixel greater than 20. The quantity  $z_{\max}$  is the minimum of the redshift at which the galaxy reaches the survey magnitude limit and that at which its median S/N per pixel drops below 20. The solid lines correspond to the subsample of 26,003 early-type ( $C \geq 2.8$ ) galaxies, while the dot-dashed lines correspond to the subsample of 5616 late-type ( $C \leq 2.4$ ) galaxies.

galaxies, although the distributions are broader.

The median age of early-type galaxies does not show any significant trend with  $z/z_{\max}$  in any mass range in Fig. 2.14. This is in agreement with earlier findings of negligible age gradients in such galaxies (Mehlert et al. 2003; Wu et al. 2004). Late-type galaxies of low and intermediate mass show a similar behaviour. Only the most massive late-type galaxies show a significant decrease (by about 0.2 dex) in median age as a function of  $z/z_{\max}$ , as expected if age gradients in spiral galaxies are stronger for larger galaxies (MacArthur et al. 2004).

The occurrence of negative radial age and metallicity gradients in different types of galaxies and the fact that the SDSS spectra sample no more than 50–60 percent of the total light of a galaxy are likely to cause overestimates of the stellar metallicities and ages of some galaxies in our sample. However, the weak trends in  $\log Z$  and  $\log t_r$  as a function of  $z/z_{\max}$  in Fig. 2.14 suggest

## 2 The Ages and Metallicities of Galaxies in the Local Universe

---

that aperture biases are unlikely to have a significant effect on the trends we have found previously for metallicity and age as a function of stellar mass.

### 2.4 Summary and conclusions

We have used a new approach to derive estimates of light-weighted stellar metallicity, age and stellar mass from the optical spectra of a sample of  $\sim 200,000$  nearby galaxies ( $0.005 < z \leq 0.22$ ) drawn from the SDSS DR2. Our method relies on the comparison of the galaxy spectra to a large library of model spectra at medium-high resolution, based on Monte Carlo star formation histories spanning the full physically plausible range. Extending earlier work by Kauffmann et al. (2003), we have adopted a Bayesian approach to derive the a posteriori likelihood distribution of each physical parameter by computing the goodness of fit of the observed spectrum for all the models in the library. In practice, we compute only the strengths of a set of carefully selected spectral absorption features.

Our analysis shows that stellar absorption features with different sensitivities to age and metallicity must be fitted simultaneously in galaxy spectra to obtain good constraints on both age and metallicity. We focus on several newly calibrated Lick indices and the 4000 Å break (see below). The resolution of our models is higher than that used in most previous studies and is well matched to the resolution of the SDSS spectra. This allows us to measure the indices in the same way in model and galaxy spectra, avoiding any loss of information from the observed spectra. We emphasize that, while most previous studies were restricted to the analysis of old stellar populations, our sample includes galaxies in the full range of star formation activities. For actively star-forming galaxies, the higher resolution of the models is crucial to separate strong emission lines from the underlying stellar absorption.

Using this approach, we are able to constrain stellar metallicity and light-weighted age to within  $\pm 0.15$  dex for the majority of the galaxies in the sample. Our stellar-mass estimates, determined within less than  $\pm 0.1$  dex for the whole sample, are in good agreement with those derived by Kauffmann et al. (2003). While the uncertainties on the stellar mass are almost independent of galaxy type, we find that, as expected, the smallest errors on age and especially metallicity are obtained for galaxies with the strongest absorption lines.

The estimates we derive of galaxy parameters are affected by limitations of both model and observed spectra. For example, the models do not include the effects of variations in heavy-element abundance ratios, while systematic deviations from the solar abundance ratios are known to arise in external galaxies (e.g. Worthey et al. 1992). When estimating metallicity, we therefore

## 2.4 Summary and conclusions

---

consider only those spectral features that have been shown by previous studies to depend negligibly on  $\alpha/\text{Fe}$  abundance ratio (Trager et al. 2000a; Thomas et al. 2003; Tantalo & Chiosi 2004). The inclusion of higher-order Balmer lines, which may depend on element abundance ratio at high metallicities (Thomas et al. 2004), could lead to an overestimate of the metallicity and an underestimate of the age by  $\sim 0.05$  dex for galaxies with non-solar abundance ratios in our sample. Another systematic uncertainty in our metallicity and age estimates comes from the discrepancy between integrated colours and spectral index strengths for supra-solar metallicity models (the model spectral indices correspond to lower metallicities than the colours). Therefore, we expect metallicities inferred using these models to be biased toward high values at high metallicities. This problem mainly affects massive, early-type galaxies with strong absorption lines.

We have shown that, in addition to these model uncertainties, the signal-to-noise ratio in a galaxy spectrum strongly affects our estimates of age and especially metallicity. We choose to rely primarily on results for galaxies with median S/N per pixel greater than 20. This cut reduces the original sample by about 75 percent and biases our analysis toward high surface brightness, high concentration galaxies. Our main results appear unaffected by this cut in S/N; including lower-S/N galaxies mainly increases the scatter in the relations we find, because of the larger associated uncertainties on metallicity.

Another observational limitation is the small aperture sampled by the SDSS spectra. The fraction of light collected by an SDSS fibre depends on the apparent size of the target galaxy, and this fraction is less than 30 percent for most galaxies in our sample. The stellar mass we derive from the spectrum has been scaled to the total luminosity of the galaxy, and hence, it represents the total stellar mass of that galaxy. However, the age and the metallicity derived from the fibre spectrum cannot be easily extrapolated to total values without information about radial gradients. We have shown that these two parameters vary weakly as a function of the fraction of light entering the fibre. This reassures us that aperture bias does not have a major effect on the relations between metallicity, age and stellar mass that we derive.

We have explored how galaxies are distributed in metallicity, age and stellar mass in the diagram defined by 4000-Å break and Balmer-line strength. As shown by Kauffmann et al. (2003) the principal sequence in this plane reflects an increase in present to past-averaged star formation rate with decreasing D4000 (see also Brinchmann et al. 2004). Galaxies with particularly strong Balmer absorption at given D4000 have undergone recent starbursts. By including metallicity dependence in the modelling, we have shown that:

- In this diagram, the average stellar mass increases along the sequence

## 2 The Ages and Metallicities of Galaxies in the Local Universe

---

populated by galaxies in our sample, from less than  $10^{10}M_{\odot}$  to more than  $10^{11}M_{\odot}$  from end to end of the sequence. The transition at intermediate D4000 is smooth between the two regimes. These results are in agreement with those of Kauffmann et al. (2003).

- Both stellar metallicity and light-weighted age also increase with D4000. Galaxies with particularly strong Balmer absorption at intermediate 4000-Å breaks (D4000  $\sim$  1.5) are on average younger and more metal-rich than the bulk of the sequence. This supports the idea that these galaxies may have recently undergone a burst of metal-enriched star formation.

In addition, we have constructed the conditional distributions of metallicity and age estimates as a function of stellar mass. This analysis shows that:

- Both stellar metallicity and light-weighted age increase with stellar mass, the increase being rapid at intermediate masses. At masses above  $\sim 3 \times 10^{10}M_{\odot}$ , a gradual flattening occurs in both relations. This stellar mass corresponds to the transition mass identified by Kauffmann et al. (2003) in plots of D4000, surface mass density and concentration against stellar mass.
- Despite the above clear relations, metallicity and age are not uniquely determined by mass; there is an intrinsic scatter in both relations, which is largest at stellar masses around  $10^{10}M_{\odot}$ . This scatter persists even when considering low- and high-concentration galaxies separately.
- The relation we find between stellar metallicity and stellar mass is similar to that found by Tremonti et al. (2004) between gas-phase oxygen abundance and stellar mass. We confirm that higher stellar metallicities are indeed associated with higher gas-phase metallicities. However, the relation between stellar and gas-phase metallicities has a substantial scatter, which can only partly be attributed to the uncertainties in stellar-metallicity estimates. This suggests that a simple ‘closed-box’ scenario is not sufficient to explain the relation, and that a variety of gas accretion/ejection histories may be required.

We have also explored relationships between metallicity, age and stellar mass for separate subsamples of high-concentration, early-type galaxies and low-concentration, late-type galaxies. The distribution in age-metallicity space in bins of stellar mass shows that (Figs 2.11 and 2.12):

- Relations between stellar metallicity, age and stellar mass hold for both early- and late-type galaxies. However, the age range of the sample is less mass-dependent for early-type than for late-type galaxies.

## 2.4 Summary and conclusions

---

- At masses below  $10^{10}M_{\odot}$ , late-type galaxies are younger and more metal-poor than early-type galaxies. At masses above  $10^{11}M_{\odot}$  the metallicities and ages of late-type galaxies are similar to those of early-type galaxies.

The above results indicate that young, metal-poor stellar populations are found predominantly in low-mass galaxies. This is consistent with a ‘downsizing’ scenario, in which the mass and luminosity of the galaxies undergoing active star formation become progressively lower as the Universe becomes older (Cowie et al. 1996). Taken at face value, this would imply that the low metallicities of low-mass galaxies just reflect the fact that these galaxies have had less time to produce metals. This naive conclusion is not consistent with that of Tremonti et al. (2004), who showed that the effective yields (from indirect gas-mass fraction measurements) of low-mass, star-forming galaxies in the SDSS DR2 are too low for these galaxies to be interpreted as young closed-box systems. This led Tremonti et al. (2004) to favor galactic winds as the most likely origin of the relation between gas-phase metallicity and stellar mass. This interpretation is supported here by the fact that galaxies with no H $\alpha$  emission in our sample (which have presumably completed their star formation) also show a trend of decreasing stellar metallicity with decreasing stellar mass for  $M_{*} \lesssim 2 \times 10^{10}M_{\odot}$  (the metallicity of closed-box galaxies should tend to the yield near gas exhaustion, independently of mass). The large scatter present in all relations between stellar metallicity, age and stellar mass (even when separated into late-type and early-type galaxies) further indicates that stellar mass is not the unique parameter determining the star formation history and hence the physical parameters of present-day galaxies. Additional variations in star formation and enrichment history (e.g. driven by gas infall or outflow) are required to explain these parameters.

An advantage of the large samples available from the SDSS is that they allow us to study not only the mean relations between physical parameters of galaxies, but also the dependence of these parameters on various galaxy properties. Our results are particularly useful for studying the physical origin of well-known observed relations, such as for example the colour-magnitude relation and the relation between Mg<sub>2</sub>-index strength and velocity dispersion for early-type galaxies. Our analysis also enables us to estimate the total metal content of the local Universe and the distribution of these metals over different galaxy types. We will address these questions in forthcoming papers.

A complete census of the physical parameters of galaxies out to  $z \sim 0.1$  is essential for constraining models of the star formation and chemical enrichment histories of galaxies. The application of our method to large samples of galaxies at higher redshifts will enable us to study how the distribution of the physical parameters of galaxies evolves with lookback time. Ongoing deep

## 2 The Ages and Metallicities of Galaxies in the Local Universe

---

redshift surveys, such as VVDS (Le Fèvre et al. 2004) and DEEP2 (Davis et al. 2003) in the optical and *GALEX* in the ultraviolet (Martin et al. 2004), are already assembling large samples of high-redshift galaxies. Quantitative comparison with the SDSS samples should substantially deepen our understanding of galaxy evolution.

### Acknowledgments

We thank Guinevere Kauffmann and an anonymous referee for useful comments. A.G. thanks Stefano Zibetti and Gabriella De Lucia for useful discussions. A.G. and S.C. thank the Alexander von Humboldt Foundation, the Federal Ministry of Education and Research, and the Programme for Investment in the Future (ZIP) of the German Government for funding through a Sofja Kovalevskaja award. J.B. acknowledges the support of an ESA post-doctoral fellowship.

Funding for the creation and distribution of the SDSS Archive has been provided by the Alfred P. Sloan Foundation, the Participating Institutions, the National Aeronautics and Space Administration, the National Science Foundation, the US Department of Energy, the Japanese Monbukagakusho, and the Max Planck Society. The SDSS Web site is <http://www.sdss.org/>. The Participating Institutions are the University of Chicago, Fermilab, the Institute for Advanced Study, the Japan Participation Group, the Johns Hopkins University, the Max Planck Institute for Astronomy (MPIA), the Max Planck Institute for Astrophysics (MPA), New Mexico State University, Princeton University, the United States Naval Observatory, and the University of Washington.

## Bibliography

- Abazajian K., et al. 2004, AJ, 128, 502
- Allende Prieto C., Lambert D. L., Asplund M., 2001, ApJ, 556, L63
- Baldry I. K., Glazebrook K., Brinkmann J., Ivezić Ž., Lupton R. H., Nichol R. C., Szalay A. S., 2004, ApJ, 600, 681
- Balogh M. L., Morris S. L., Yee H. K. C., Carlberg R. G., Ellingson E., 1999, ApJ, 527, 54
- Bell E. F., de Jong R. S., 2000, MNRAS, 312, 497
- Bernardi M., Renzini A., da Costa L. N., Wegner G., Alonso M. V., Pellegrini P. S., Rit  C., Willmer C. N. A., 1998, ApJ, 508, L143
- Bressan A., Chiosi C., Fagotto F., 1994, ApJS, 94, 63
- Brinchmann J., Charlot S., White S. D. M., Tremonti C., Kauffmann G., Heckman T., Brinkmann J., 2004, MNRAS, 351, 1151
- Bruzual G., Charlot S., 2003, MNRAS, 344, 1000
- Bruzual A. G., 1983, ApJ, 273, 105
- Bruzual A. G., Charlot S., 1993, ApJ, 405, 538
- Burstein D., Faber S. M., Gaskell C. M., Krumm N., 1984, ApJ, 287, 586
- Caldwell N., Rose J. A., 1998, AJ, 115, 1423
- Charlot S., Fall S. M., 2000, ApJ, 539, 718
- Colless M., et al 1999, MNRAS, 303, 813
- Cowie L. L., Songaila A., Hu E. M., Cohen J. G., 1996, AJ, 112, 839
- Davies R. L., Sadler E. M., Peletier R. F., 1993, MNRAS, 262, 650

## Bibliography

---

- Davis M., et al. 2003, in Discoveries and Research Prospects from 6- to 10-Meter-Class Telescopes II. Edited by Guhathakurta, Puragra. Proceedings of the SPIE, Volume 4834, pp. 161-172 (2003). Science Objectives and Early Results of the DEEP2 Redshift Survey. pp 161–172
- Eisenstein D. J., et al. 2003, ApJ, 585, 694
- Faber S. M., 1973, ApJ, 179, 731
- Ferreras I., Charlot S., Silk J., 1999, ApJ, 521, 81
- Fioc M., Rocca-Volmerange B., 1997, A&A, 326, 950
- González J. J., 1993, Ph.D. Thesis
- Gonzalez J. J., Faber S. M., Worthey G., 1993, Bulletin of the American Astronomical Society, 25, 1355
- Gorgas J., Cardiel N., Pedraz S., González J. J., 1999, A&AS, 139, 29
- Gorgas J., Faber S. M., Burstein D., Gonzalez J. J., Courteau S., Prosser C., 1993, ApJS, 86, 153
- Goudfrooij P., Gorgas J., Jablonka P., 1999, Ap&SS, 269, 109
- Henry R. B. C., Worthey G., 1999, PASP, 111, 919
- Jablonka P., Martin P., Arimoto N., 1996, AJ, 112, 1415
- Jimenez R., Panter B., Heavens A. F., Verde L., 2005, MNRAS, 356, 495
- Jørgensen I., 1999, MNRAS, 306, 607
- Kannappan S. J., 2004, ApJ, 611, L89
- Kauffmann G., et al. 2003a, MNRAS, 341, 33
- Kauffmann G., et al. 2003b, MNRAS, 341, 54
- Korn A. J., Maraston C., Thomas D., 2005, astro-ph/0504574
- Kuntschner H., 1998, Ph.D. Thesis
- Kuntschner H., 2000, MNRAS, 315, 184
- Kuntschner H., 2004, A&A, 426, 737
- Kuntschner H., Davies R. L., 1998, MNRAS, 295, L29+

- Kuntschner H., Lucey J. R., Smith R. J., Hudson M. J., Davies R. L., 2001, MNRAS, 323, 615
- Kuntschner H., Smith R. J., Colless M., Davies R. L., Kaldare R., Vazdekis A., 2002, MNRAS, 337, 172
- Le Borgne J.-F., Bruzual G., Pelló R., Lançon A., Rocca-Volmerange B., Sanahuja B., Schaerer D., Soubiran C., Vílchez-Gómez R., 2003, A&A, 402, 433
- Le Fèvre O., et al. 2004, A&A, 417, 839
- Longhetti M., Rampazzo R., Bressan A., Chiosi C., 1998, A&AS, 130, 251
- MacArthur L. A., Courteau S., Bell E., Holtzman J. A., 2004, ApJS, 152, 175
- Maraston C., 1998, MNRAS, 300, 872
- Martin C. D., et al. 2004, astro-ph/0411302
- Mehlert D., Thomas D., Saglia R. P., Bender R., Wegner G., 2003, A&A, 407, 423
- Poggianti B. M., Bridges T. J., Carter D., Mobasher B., Doi M., Iye M., Kashikawa N., Komiyama Y., Okamura S., Sekiguchi M., Shimasaku K., Yagi M., Yasuda N., 2001, ApJ, 563, 118
- Poggianti B. M., Bridges T. J., Mobasher B., Carter D., Doi M., Iye M., Kashikawa N., Komiyama Y., Okamura S., Sekiguchi M., Shimasaku K., Yagi M., Yasuda N., 2001, ApJ, 562, 689
- Proctor R. N., Sansom A. E., 2002, MNRAS, 333, 517
- Rakos K., Schombert J., Maitzen H. M., Prugovecki S., Odell A., 2001, AJ, 121, 1974
- Saglia R. P., Maraston C., Greggio L., Bender R., Ziegler B., 2000, A&A, 360, 911
- Salim S., et al. 2005, ApJ, 619, L39
- Schlegel D. J., Finkbeiner D. P., Davis M., 1998, ApJ, 500, 525
- Shen S., et al. 2003, MNRAS, 343, 978
- Shimasaku K., et al. 2001, AJ, 122, 1238

## Bibliography

---

- Stoughton C., et al. 2002, *AJ*, 123, 485
- Strateva I., et al. 2001, *AJ*, 122, 1861
- Tantalo R., Chiosi C., 2004, *MNRAS*, 353, 917
- Tantalo R., Chiosi C., Bressan A., 1998, *A&A*, 333, 419
- Terlevich A. I., Forbes D. A., 2002, *MNRAS*, 330, 547
- Terlevich A. I., Kuntschner H., Bower R. G., Caldwell N., Sharples R. M., 1999, *MNRAS*, 310, 445
- Thomas D., Maraston C., Bender R., 2003a, *MNRAS*, 343, 279
- Thomas D., Maraston C., Bender R., 2003b, *MNRAS*, 339, 897
- Thomas D., Maraston C., Bender R., de Oliveira C. M., 2005, *ApJ*, 621, 673
- Thomas D., Maraston C., Korn A., 2004, *MNRAS*, 351, L19
- Tinsley B. M., 1978, *ApJ*, 222, 14
- Tinsley B. M., 1980, *Fundamentals of Cosmic Physics*, 5, 287
- Trager S. C., Faber S. M., Worthey G., González J. J., 2000, *AJ*, 120, 165
- Trager S. C., Worthey G., Faber S. M., Burstein D., Gonzalez J. J., 1998, *ApJS*, 116, 1
- Tremonti C. A., 2003, Ph.D. Thesis
- Tremonti C. A., et al. 2004, *ApJ*, 613, 898
- Tripicco M. J., Bell R. A., 1995, *AJ*, 110, 3035
- Vazdekis A., 1999, *ApJ*, 513, 224
- Vazdekis A., 2001, *Ap&SS*, 276, 921
- Worthey G., 1994, *ApJS*, 95, 107
- Worthey G., 1996, in *ASP Conf. Ser. 98: From Stars to Galaxies: the Impact of Stellar Physics on Galaxy Evolution Elliptical Galaxies: Abundance Ratio Trends and Implications*. pp 467–+
- Worthey G., 1997, in *American Institute of Physics Conference Series Star Formation History of Elliptical Galaxies from Low-Redshift Evidence*. pp 525–+

- Worthey G., Faber S. M., Gonzalez J. J., 1992, ApJ, 398, 69
- Worthey G., Faber S. M., Gonzalez J. J., Burstein D., 1994, ApJS, 94, 687
- Worthey G., Ottaviani D. L., 1997, ApJS, 111, 377
- Worthey G., Trager S. C., Faber S. M., 1995, in ASP Conf. Ser. 86: Fresh Views of Elliptical Galaxies The Galaxian Age-Metallicity Relation. pp 203–  
+
- Wu H., Shao Z., Mo H. J., Xia X., Deng Z., 2004, astro-ph/0404226
- York D. G., et al. 2000, AJ, 120, 1579

## Bibliography

---

*Das Fürwahrhalten, oder die subjektive Gültigkeit des Urteils, in Beziehung auf die Überzeugung (welche zugleich objektiv gilt), hat folgende drei Stufen: Meinen, Glauben und Wissen. Meinen ist ein mit Bewußtsein sowohl subjektiv, als objektiv unzureichendes Fürwahrhalten. Ist das letztere nur subjektiv zureichend und wird zugleich für objektiv unzureichend gehalten, so heißt es Glauben. Endlich heißt das sowohl subjektiv als objektiv zureichende Fürwahrhalten das Wissen.*

Immanuel Kant, Kritik der reinen Vernunft

# 3

## Early-type galaxies: new insight into the physical origin of the colour-magnitude and the $Mg_2-\sigma_V$ relations

Gallazzi, A., Charlot, S., Brinchmann, J., White, S.D.M., 2006, MNRAS, 370, 1106

### Abstract

We exploit recent constraints on the ages and metallicities of early-type galaxies in the Sloan Digital Sky Survey (SDSS) to gain new insight into the physical origin of two fundamental relations obeyed by these galaxies: the colour-magnitude and the  $Mg_2-\sigma_V$  relations. Our sample consists of 26,003 galaxies selected from the SDSS Data Release Two (DR2) on the basis of their concentrated light profiles, for which we have previously derived median-likelihood estimates of stellar metallicity, light-weighted age and stellar mass. Our analysis provides the most unambiguous demonstration to date of the fact that both the colour-magnitude and the  $Mg_2-\sigma_V$  relations are primarily sequences in stellar mass and that total stellar metallicity,  $\alpha$ -elements-to-iron abundance ratio and light-weighted age all increase with mass along the two relations. For high-mass ellipticals, the dispersion in age is small and consistent with the error. At the low-mass end, there is a tail towards younger ages, which dominates the scatter in colour and index strength at fixed mass. A small, but detectable, intrinsic scatter in the mass-metallicity

### 3 Physical origin of the colour-magnitude and the $Mg_2$ - $\sigma_V$ relations for early-type galaxies

---

relation also contributes to the scatter in the two observational scaling relations, even at high masses. Our results suggest that the chemical composition of an early-type galaxy is more tightly related to its dynamical mass (including stars and dark matter) than to its stellar mass. The ratio between stellar mass and dynamical mass appears to decrease from the least massive to the most massive galaxies in our sample.

**Keywords:**

galaxies: formation, galaxies: evolution, galaxies: stellar content

#### 3.1 Introduction

The observed properties of early-type galaxies obey several fundamental relations, which have long been thought to hide important clues about the physical processes that influenced the formation and evolution of these galaxies. For example, luminosity, central velocity dispersion  $\sigma_V$ , mean surface brightness, brightness profile, colours and  $Mg_2$  absorption-line index all appear to be tightly related to each other in early-type galaxies (Baum 1959; Faber & Jackson 1976; Visvanathan & Sandage 1977; Kormendy 1977; Bender et al. 1993; Djorgovski & Davis 1987). The colour-magnitude and the  $Mg_2$ - $\sigma_V$  relations are particularly interesting in that they connect the luminous and dynamical masses of the galaxies with the physical properties of their stellar populations. The tightness and homogeneity of these two relations must be telling us something fundamental about the epoch and the process of formation of early-type galaxies (see for a review Renzini 2006).

The physical interpretation of the above observational relations is still a subject of debate. The colour-magnitude relation is often interpreted as a sequence of increasing metallicity with increasing luminosity (Faber 1973; Worthey 1994; Kodama & Arimoto 1997; Kodama et al. 1999). However, it has been proposed that, in addition to metallicity, age could at least in part drive the relation (Gonzalez et al. 1993; Terlevich et al. 1999; Ferreras et al. 1999; Poggianti et al. 2001). Studies of evolution with cosmic time indicate that the slope of the colour-magnitude relation has changed little since  $z \sim 1$  (Kodama & Arimoto 1997; Kodama et al. 1998; Stanford et al. 1998; Blakeslee et al. 2003). This has been used as an argument against age as the primary driver of the relation, since the colours of young stellar populations evolve faster than those of old stellar populations. Similar interpretations have been proposed for the relation between  $Mg_2$  index strength and central velocity dispersion  $\sigma_V$ , which is generally thought to arise from a combination of age and metallicity variations (Colless et al. 1999; Trager et al. 2000a; Kuntschner et al. 2001).

The difficulty of obtaining unambiguous constraints on the relative influence of age and metallicity on the colour-magnitude and the  $\text{Mg}_2\text{-}\sigma_V$  relations is a consequence of the difficulty of deriving accurate ages and metallicities for large samples of early-type galaxies: age and metallicity both tend to redden the colours and strengthen the  $\text{Mg}_2$  absorption line in similar ways (e.g., Worthey 1994). In addition, at fixed metallicity, the  $\alpha$ -element-to-iron ( $\alpha/\text{Fe}$ ) abundance ratio appears to be larger in the most massive early-type galaxies than in the nearby stars used to calibrate age and metallicity estimates (Worthey et al. 1992; Vazdekis et al. 2001). This has been explored recently by Thomas et al. (2004), who used ‘closed-box’ chemical evolution models with variable heavy-element abundance ratios to analyse a heterogeneous sample of 124 nearby early-type galaxies, in both low-density and high-density environments. According to these models, massive galaxies formed earlier and more rapidly than low-mass galaxies, while both the colour-magnitude and the  $\text{Mg}_2\text{-}\sigma_V$  relations are primarily driven by metallicity. Bernardi et al. (2003a,b,c,d) carried out a more observationally oriented analysis on a sample of nearly 9000 early-type galaxies from the Sloan Digital Sky Survey (SDSS). They showed that the colour-magnitude relation reflects a dependence of both colour and luminosity on velocity dispersion. By *assuming* that luminosity traces metallicity and that the scatter in colour at fixed luminosity traces age, Bernardi et al. (2005) explored how age and metallicity may be related to velocity dispersion in early-type galaxies.

In this paper, we re-examine the physical origin of the colour-magnitude and the  $\text{Mg}_2\text{-}\sigma_V$  relations using a different approach. Our starting point is a set of statistical estimates of light-weighted age, stellar metallicity and stellar mass for a large sample of 26,003 early-type galaxies drawn from the SDSS Data Release Two (DR2). We derived these constraints in earlier work by using a comprehensive library of model spectra at medium-high resolution (Gallazzi et al. 2005, hereafter Paper I), to interpret the strengths of five spectral absorption features with negligible dependence on the  $\alpha/\text{Fe}$  ratio. We use here this dataset, together with an observational tracer of the  $\alpha/\text{Fe}$  ratio, to demonstrate unambiguously that both the colour-magnitude and the  $\text{Mg}_2\text{-}\sigma_V$  relations of early-type galaxies are primarily sequences in stellar mass and that both the total stellar metallicity and the  $\alpha/\text{Fe}$  ratio increase with mass along the two relations. Light-weighted age increases from the least massive to the most massive early-type galaxies, with a larger spread at low masses that dominates the scatter in the colour-magnitude and  $\text{Mg}_2\text{-}\sigma_V$  relations. The small intrinsic scatter in metallicity at fixed mass also contributes to the scatter in the two scaling relations.

We present our sample in Section 4.2.1 below, along with a brief description of the method adopted in Paper I to derive statistical estimates of the

### 3 Physical origin of the colour-magnitude and the $Mg_2-\sigma_V$ relations for early-type galaxies

ages, metallicities and stellar masses of the galaxies. The influence of these parameters on the colour-magnitude and the  $Mg_2-\sigma_V$  relations is explored in Sections 3.3.1 and 3.3.2, respectively, and their possible dependence on galaxy environment is addressed in Section 3.3.3. In Section 3.3.4 we discuss some implications on the relations between physical parameters and dynamical mass. Section 3.4 summarises our conclusions. Throughout the paper we use  $\Omega_m = 0.3$ ,  $\Omega_\Lambda = 0.7$  and  $H_0 = 70 \text{ km s}^{-1} \text{ Mpc}^{-1}$

## 3.2 Observational sample

We select our sample from the main spectroscopic sample of the SDSS DR2 (Abazajian et al. 2004). The SDSS is an imaging and spectroscopic survey of the high Galactic latitude sky, which will obtain  $u$ ,  $g$ ,  $r$ ,  $i$  and  $z$  photometry of almost a quarter of the sky and spectra of at least 700,000 objects (York et al. 2000). The spectra are taken using  $3''$ -diameter fibres, positioned as close as possible to the centres of the target galaxies. Stellar metallicity, light-weighted age and stellar mass estimates are available from Paper I for a sample of 175,128 galaxies with Petrosian  $r$ -band magnitudes in the range  $14.5 < r < 17.77$  (after correction for foreground Galactic extinction) and in the redshift range  $0.005 < z \leq 0.22$ . The lower redshift limit allows us to include low-luminosity galaxies (corresponding to a stellar mass of  $\sim 10^8 M_\odot$ ), while still avoiding redshifts for which deviations from the Hubble flow can be substantial. The upper limit corresponds roughly to the redshift at which a typical  $10^{11} M_\odot$  galaxy is detected with median S/N per pixel greater than 20.

We select early-type galaxies on the basis of the light concentration index  $C = R_{90}/R_{50}$ , defined as the ratio of the radii enclosing 90 and 50 percent of the total Petrosian  $r$ -band luminosity of a galaxy. This parameter has been shown to correlate well with morphological type (Strateva et al. 2001; Shimasaku et al. 2001). Thus, it allows a rough morphological classification of SDSS galaxies. Strateva et al. (2001) propose a cut at  $C = 2.6$  to separate early- from late-type galaxies. To limit the contamination by disc galaxies with large bulges, we define here as ‘early-type’ those galaxies with concentration index  $C \geq 2.8$ . In this way, we select 67,411 early-type galaxies in the redshift range  $0.005 < z \leq 0.22$ . We note that we decided against further limiting the contamination of our sample by systems with residual star formation by imposing a lower cutoff in 4000-Å break strength or an upper limit on emission lines equivalent width. Since these quantities correlate with colour, such limits would introduce an unwanted cutoff in the colour-magnitude relation.<sup>1</sup>

<sup>1</sup>Bernardi et al. (2005) adopted a different criterion to select early-type galaxies from the

## 3.2 Observational sample

---

Bayesian-likelihood estimates of the  $r$ -band light-weighted ages, stellar metallicities and stellar masses of the 67,411 galaxies in our sample are available from Paper I. These estimates were derived by comparing the spectrum of each galaxy to a library of Bruzual & Charlot (2003) models at medium-high spectral resolution, encompassing the full range of physically plausible star formation histories. In practice, we compared the strengths of five spectral absorption features in the spectrum of each observed galaxy to the strengths of these features in every model spectrum (broadened to the observed velocity dispersion) in the library. We used D4000, H $\beta$  and H $\delta_A$ +H $\gamma_A$  as age-sensitive indices and [Mg<sub>2</sub>Fe] and [MgFe]' as metal-sensitive indices, all of which depend negligibly on the  $\alpha$ /Fe ratio.<sup>2</sup> This comparison allowed us to construct the probability density functions of age, metallicity and stellar mass for every galaxy. The estimate of each parameter is given by the median of the corresponding probability distribution, while the  $\pm 1\sigma$  error on each parameter is given by half the 16–84 percent percentile range of the likelihood distribution (this would be equivalent to the  $\pm 1\sigma$  range for a Gaussian distribution).

We note that the stellar ages, as well as the other physical parameters, are derived by fitting the galaxy spectra as observed and so refer to the galaxies at the time they are observed. Because of the bright and faint magnitude limits in our sample, there is a strong correlation between luminosity and redshift. If uncorrected, it may introduce systematic effects in correlations between age and luminosity (or mass). To avoid this, we correct our measured ages so that they are relative to the present, rather than to the point of observation by adding to the measured age for each galaxy the look-back time to the redshift at which it is observed. The metallicity is left unchanged. This look-back time varies from 0.07 to 2.64 Gyr over the redshift range covered by our sample. The corrections mainly affect the most luminous galaxies, which are found out to higher redshifts. All light-weighted ages quoted throughout this paper refer to  $z = 0$ .

As described in Paper I, our constraints on metallicity and age are sensitive to the observational signal-to-noise ratio (S/N) of the spectra. A median S/N per pixel of at least 20 is required to constrain metallicity reliably. For this reason, we consider here only those galaxies with a median S/N per pixel

---

SDSS. They considered to be of early type those galaxies for which the  $r$ -band surface brightness profile is better described by a de Vaucouleurs law than by an exponential law (photometric parameter `fracDev` > 0.8) and that do not have emission lines (spectroscopic parameter `eclass` < 0).

<sup>2</sup>This might not be entirely correct for H $\delta_A$  and H $\gamma_A$ , which are suspected to depend on the  $\alpha$ /Fe ratio at high metallicity (Thomas et al. 2004; Korn et al. 2005). However, we did not find any discrepancy between the metallicities and ages derived including or excluding H $\delta_A$ +H $\gamma_A$  (see section 2.4.2 of Paper I).

### 3 Physical origin of the colour-magnitude and the $Mg_2-\sigma_V$ relations for early-type galaxies

greater than 20. This cut reduces our sample to 26,003 high-concentration galaxies in the redshift range  $0.005 < z \leq 0.22$ . This is the same sample of ‘early-type’ galaxies as analysed in section 3.3 of Paper I. As shown there, the S/N requirement biases the sample towards low-redshift, high-surface brightness galaxies, but it does not introduce any bias in the luminosity, colour, velocity-dispersion and index-strength distributions of the early-type galaxy sample.

Our selection of early-type galaxies, based only on the concentration parameter, includes early-type spiral galaxies, galaxies with emission lines and active galactic nuclei (AGN). We can divide our sample into five subclasses according to the classification given by Brinchmann et al. (2004) on the basis of the emission-line properties of SDSS-DR2 galaxies. Following their notation, we label as (1) unclassifiable (‘Unclass.’) those galaxies which cannot be classified using the Baldwin et al. (1981) diagram, i.e. mostly galaxies with no or weak emission lines; (2) AGN those galaxies with a substantial AGN contribution to their emission-line fluxes; (3) star forming (‘SF’) those galaxies with  $S/N > 3$  in  $H\beta$ ,  $H\alpha$ , [OIII]5007, [NII]6564 emission lines and for which the contribution to  $H\alpha$  from AGN is less than 1 percent; (4) composite (‘C’) those galaxies with  $S/N > 3$  in the same four lines, but for which the AGN contribution to  $H\alpha$  luminosity can be up to 40 percent; (5) low-S/N star forming (‘low-S/N SF’) those galaxies with  $S/N > 2$  in  $H\alpha$  but without AGN contribution to their spectra. The sample includes 10,982 unclassifiable galaxies, 7782 AGN and 3018 low-S/N SF galaxies. There are 2858 composite and 1362 star-forming galaxies, accounting for roughly 11 and 5 percent of the total sample, respectively. As expected, most galaxies in the sample have specific star formation rates ( $SFR/M_*$ ) less than  $10^{-10.6} \text{ yr}^{-1}$ , which are in most cases consistent with zero. We note that the distribution in specific star formation rates for the subclasses of C and SF galaxies shows a peak at  $10^{-10.0} \text{ yr}^{-1}$ .

Fig. 3.1 shows the distributions of several observational quantities of interest to us for this sample: the  $r$ -band absolute magnitude  $M_r$ , the  $g-r$  colour, the logarithm of the velocity dispersion (in  $\text{km s}^{-1}$ ) and the  $Mg_2$  index strength. The magnitude  $M_r$  and the colour  $g-r$  represent rest-frame quantities. They are corrected for evolution following the prescription of Bernardi et al. (2005), as described in Section 3.3.1.1. Also the  $Mg_2$  index strength is corrected to  $z = 0$  assuming passive evolution, as described in Section 3.3.2. In each row, the solid histogram represents the distribution for each of the above subclasses (whose fractional contribution to the total sample is given in the leftmost panel), while the distribution for the sample as a whole is represented by the shaded grey histogram. The distributions for the unclassifiable, AGN and low-S/N SF galaxies agree well with the distributions for the sample

as a whole. In contrast, C and especially SF galaxies tend to concentrate in the low-luminosity, blue, low-velocity-dispersion and low-Mg<sub>2</sub> tails of the distributions.

The stellar metallicities, ages and stellar masses derived in Paper I for the galaxies in the sample are shown in Fig. 3.2 (shaded grey histograms). The distribution in metallicity extends from  $0.4 Z_{\odot}$  to  $2 Z_{\odot}$  with a peak around  $Z = 1.6 Z_{\odot}$ . The distribution in  $r$ -band light-weighted age extends from 2.5 to 12 Gyr with a peak around  $t_r = 9$  Gyr. The distribution in stellar mass extends from  $10^{10}$  to  $10^{12} M_{\odot}$  with a peak around  $M_* = 10^{11} M_{\odot}$ . The right-hand panels of Fig. 3.2 show the distributions of the associated errors, computed as one half the 68 percent confidence ranges in the estimates of  $\log(Z/Z_{\odot})$ ,  $\log(t_r/\text{yr})$  and  $\log(M_*/M_{\odot})$ . The typical uncertainty in both metallicity and age estimates is about  $\pm 0.1$  dex, while stellar mass is constrained to better than  $\pm 0.1$  dex for the majority of the galaxies in the sample. The same is true when considering Unclass., AGN and low-S/N SF galaxies only (solid histograms). The distributions for SF (dotted line) and C (dashed line) galaxies extend to lower stellar metallicities, ages and stellar masses than the bulk of the sample, with slightly higher errors in all three parameters.

In addition to the effects of age, metallicity and stellar mass, we are also interested in the influence of the  $\alpha/\text{Fe}$  ratio on the observed properties of early-type galaxies. This ratio can be empirically quantified by the relative strengths of Mg- and Fe-based absorption-line indices (Thomas et al. 2003). We use here  $\text{Mgb}/\langle\text{Fe}\rangle$ , where  $\langle\text{Fe}\rangle$  is the average of the Fe5270 and Fe5335 index strengths. In what follows, we compare the observed  $\text{Mgb}/\langle\text{Fe}\rangle$  ratio of a galaxy to that of the model that best reproduces the 5 spectral features mentioned above. Since the models have scaled-solar abundance ratios, any discrepancy  $\Delta(\text{Mgb}/\langle\text{Fe}\rangle)$  between observed and model index strengths can then be interpreted as a departure of the  $\alpha$ -elements-to-iron abundance ratio from solar in the observed galaxy.

Working with the difference in index ratio rather than with the observed value of  $\text{Mgb}/\langle\text{Fe}\rangle$  allows us to take into account the dependence of the index strength on age. It is also interesting to check whether the difference  $\Delta(\text{Mgb}/\langle\text{Fe}\rangle)$  traces linearly the true  $\alpha/\text{Fe}$  abundance ratio over the whole parameter space covered by our galaxies. It is not possible to check this self-consistently on our sample with our own models, since they do not include variations in element abundance ratios. For this test, we used Simple Stellar Population (SSP) models with variable element abundance ratios from Thomas et al. (2003). We have considered SSPs with different  $\alpha/\text{Fe}$  abundance ratios ( $[\alpha/\text{Fe}] = -0.2, 0, 0.2, 0.4, 0.6$ ), with age varying from 1 to 13 Gyr and metallicity varying from  $\log(Z/Z_{\odot}) = -0.6$  to 0.5. For each model we calcu-

### 3 Physical origin of the colour-magnitude and the $Mg_2$ - $\sigma_V$ relations for early-type galaxies

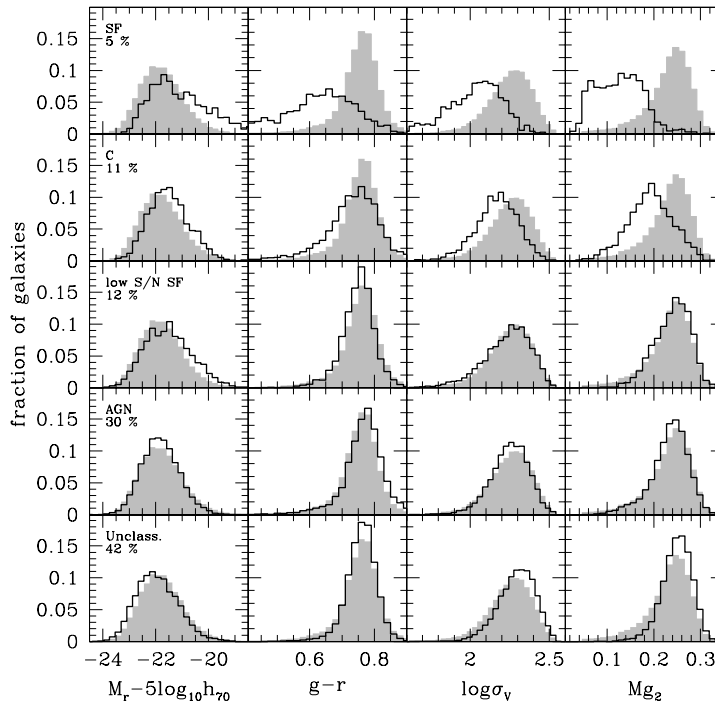


**Figure 3.1:** Distributions of the  $r$ -band absolute magnitude,  $g - r$  colour ( $k$ -corrected to  $z = 0$  and corrected for evolution following Bernardi et al. 2005), logarithm of velocity dispersion (in  $\text{km s}^{-1}$ ) and  $Mg_2$  index strength (in mag) for a sample of 26,003 early-type (high-concentration) SDSS-DR2 galaxies with median S/N per pixel greater than 20 (grey histograms, repeated in all rows). From top to bottom, solid histograms in each row show the distributions for subsamples of galaxies classified by Brinchmann et al. (2004) according to their emission-line properties as star-forming (‘SF’), composite (‘C’), low signal-to-noise star-forming (‘low-S/N SF’), AGN (‘AGN’) and unclassifiable (‘Unclass.’, these are mainly galaxies with no emission lines). The fractional contributions by the different classes to the total sample of 26,003 early-type galaxies are indicated in the left-most panels. All histograms are normalised to unit area.

late the difference in  $Mgb/\langle Fe \rangle$  with respect to the corresponding scaled-solar model at the same age and metallicity. We have looked at the relation between  $\Delta(Mgb/\langle Fe \rangle)$  and the abundance ratio  $[\alpha/Fe]$  at fixed metallicity. We do not find significant differences in the slope and zero-point of the linear relations, averaged over age, for different metallicities. Only at  $\log(Z/Z_\odot) \sim -0.5$  is the relation somewhat flatter; we note that this is not relevant for the galaxies in our sample, which predominantly have metallicities above  $\log(Z/Z_\odot) = -0.2$

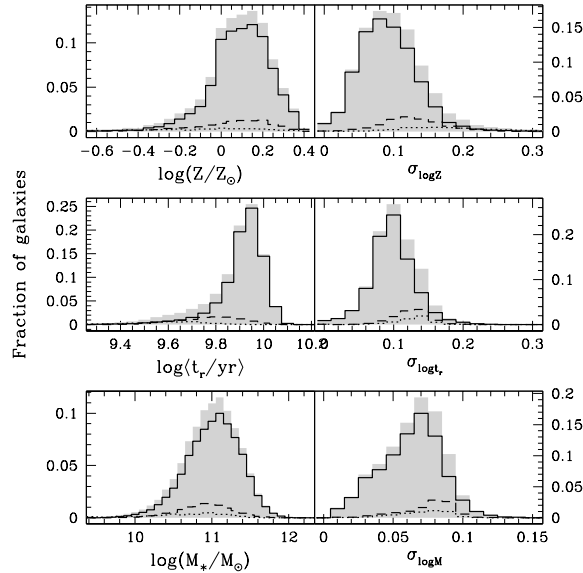


**Figure 3.2:** Left: distributions of the median-likelihood estimates of stellar metallicity (top),  $r$ -band light-weighted age (middle) and stellar mass (bottom) for the same sample of early-type galaxies as in Fig. 3.1. The dotted histogram shows the distribution for SF galaxies, the dashed histogram for C galaxies and the solid histogram for the rest of the sample (Unclass, AGN and low-S/N SF). Right: distributions of the associated errors, computed as one half the 68 percent confidence ranges in the estimates of  $\log(Z/Z_\odot)$ ,  $\log(t_r/\text{yr})$  and  $\log(M_*/M_\odot)$ .

(see Fig. 3.2). The proportionality between  $\Delta(\text{Mgb}/\langle\text{Fe}\rangle)$  and  $[\alpha/\text{Fe}]$  is confirmed by plotting  $\Delta(\text{Mgb}/\langle\text{Fe}\rangle)$  as a function of age and as a function of metallicity for SSPs with different  $\alpha/\text{Fe}$  ratio. At fixed  $[\alpha/\text{Fe}]$ , the measured  $\Delta(\text{Mgb}/\langle\text{Fe}\rangle)$  is constant over the age and metallicity ranges covered by our sample. These checks reassure us that the discrepancy  $\Delta(\text{Mgb}/\langle\text{Fe}\rangle)$  between the observed and the best-fit model index strengths has the same proportionality with  $[\alpha/\text{Fe}]$  over the age and metallicity ranges covered by the sample.

## 3.3 Physical origin of observed relations for early-type galaxies

We use here the sample of 26,003 early-type galaxies described above to investigate the physical origin of two fundamental relations obeyed by early-type galaxies: the colour-magnitude relation (Section 3.3.1) and the  $M_{g_2-\sigma_V}$  relation (Section 3.3.2). We address the environmental dependence of these relations and of galaxy physical parameters in Section 3.3.3. We then explore in more detail how physical parameters are related to the depth of a galaxy's potential well (Section 3.3.4).

### 3.3.1 The colour-magnitude relation

The optical colours of early-type galaxies are strongly correlated with absolute magnitude, in the sense that bright galaxies tend to be redder than faint galaxies (e.g. Baum 1959; de Vaucouleurs 1961; Faber 1973; Visvanathan & Sandage 1977; Bower et al. 1992). As mentioned in Section 3.1, the physical origin of this correlation is still a matter of controversy, mainly because of the lack of large samples of galaxies with accurate age and metallicity estimates.

#### 3.3.1.1 Observed colour-magnitude relation

We consider here the colour-magnitude relation (CMR) defined by the rest-frame  $g-r$  colour and the absolute  $r$ -band magnitude  $M_r$ . We compute these quantities using the SDSS `model` magnitudes, which are obtained from fits of the  $r$ -band surface brightness profile of each galaxy with either a de Vaucouleurs law or an exponential law (the best-fitting profile is also adopted in the other photometric bands). We  $k$ -correct the observed  $g-r$  colour and the  $M_r$  absolute magnitude to  $z=0$  using the model in the spectral library of Section 4.2.1 that best reproduces the spectral absorption features of the galaxy, reddened to reproduce the observed colours at the redshift of the galaxy (this reddening correction is typically small; see below). We also correct colours and magnitudes for evolution, adopting the correction estimated by Bernardi et al. (2005) from a sample of 39,320 SDSS early-type galaxies, i.e. we make the magnitudes fainter by  $0.85z$  and the colours redder by  $0.3z$ . From now on, we denote by  $M_r$  and  $g-r$  the  $k+e$ -corrected (but not dereddened) quantities.

Fig. 3.3 shows the  $g-r$ ,  $M_r$  colour-magnitude relation defined in this way by early-type galaxies in the sample described in Section 4.2.1. We have arranged galaxies in bins of absolute magnitude and colour (0.15 and 0.01 width respectively). The grey scale indicates, for each magnitude bin, the relative distribution of galaxies in the different colour bins (we do not show

### 3.3 Physical origin of observed relations for early-type galaxies

bins containing less than 2 percent of the total number of galaxies at a given magnitude). The straight line in Fig. 3.3 shows a ‘robust’ fit of these data, obtained by minimising the absolute deviation in colour as a function of magnitude. We note that this lies slightly to the blue of the ridge-line of the relation, reflecting the skewed colour distributions of Fig. 3.1. The robust fit has a slope<sup>3</sup> of  $-0.024 \pm 0.002$ . This slope is consistent with that of  $-0.024$  obtained previously by Bernardi et al. (2005)<sup>4</sup>. The dashed lines in Fig. 3.3 show the mean positive and negative absolute deviations in colour ( $\pm 0.050$ ) relative to this fit.

To better understand the influence of our galaxy selection criteria on our results, we constructed a second sample (we call this ‘sample B’) following the prescription by Bernardi et al.. We first select all objects classified as galaxies, with measured velocity dispersions and with Petrosian  $r$ -band magnitudes (corrected for galactic reddening) between 14.5 and 17.75 in the SDSS DR2. We then define as early-type those galaxies with `fracDev_r`  $> 0.8$  and `eClass`  $< 0$ . We select in this way 59,907 early-type galaxies, for which we have  $g - r$  colours and  $M_r$  absolute magnitudes.<sup>5</sup>

In Fig. 3.4, we compare the CMRs obtained from our primary sample and from sample B in different redshift bins (by analogy with fig. 2 of Bernardi et al. 2005). The black dot-dashed lines in Fig. 3.4 show robust fits to the relations for the two samples. The slope for sample B ( $-0.028 \pm 0.001$ , upper panel) is in good agreement with that obtained by Bernardi et al. (2005, black solid line) and with that derived for our primary sample ( $-0.024 \pm 0.002$ , lower panel). The colour-magnitude distributions of the galaxies in different redshift bins in sample B (upper panel) also agree reasonably well with those in fig. 2 of Bernardi et al. (2005). Thus, our results agree with those of Bernardi et al. (2005) under similar assumptions.

We note that our primary sample differs from sample B mainly through the inclusion of blue galaxies at intermediate-to-low luminosities. These are predominantly galaxies in the SF and C classes, which are likely to be bulge-dominated spiral galaxies with detectable emission lines (`eClass`  $> 0$ , which excludes them from sample B). The contamination of our primary sample by these galaxies also results from the fact that we do not make any distinction on

<sup>3</sup>The errors on the slopes of the fitted relations quoted throughout the paper have been estimated using a ‘jackknife’ method. The parameters of the fitted relations are summarised in Table 3.1.

<sup>4</sup>We estimated this slope as  $\xi_{CM} \sigma_{CC} / \sigma_{MM}$ , using the values reported in tables 1 and 2 of Bernardi et al. (2005, see their appendix B1).

<sup>5</sup>Note that the sample used by Bernardi et al. (2005) is slightly smaller than the SDSS DR2. Note also that sample B is larger than our primary sample, mainly because of our cut in S/N ratio.

### 3 Physical origin of the colour-magnitude and the $Mg_2-\sigma_V$ relations for early-type galaxies

the basis of galaxy environment. While the slope of the CMR in low-density environments is not significantly different from that found for cluster early-type galaxies, the scatter about the relation appears to increase from high- to low-density environments (Larson et al. 1980; Hogg et al. 2004). Also, at the median redshift  $z \sim 0.1$  of our sample, Pimblet et al. (2002) find that, at fixed luminosity, early-type galaxies tend to have bluer colours in the outskirts than in the centres of galaxy clusters (see also Abraham et al. 1996). They interpret this as a difference in age of the galaxies in different environments.

As in other work on early-type galaxies (e.g. Bernardi et al. 2005), we do not include any correction for dust attenuation in the CMR presented here. We can estimate the influence of dust on the CMR, using the model spectral fits described in Section 4.2.1. The  $g$ - and  $r$ -band dust attenuation can be estimated from the difference between the emission-line corrected  $r-i$  **fibres**<sup>6</sup> colour of the galaxy and the  $r-i$  colour of the redshifted, dust-free model, assuming a single power-law attenuation curve (see also Paper I). To quantify the effect of dust attenuation on the CMR, we show in Fig. 3.5 the average attenuation vectors (red arrows) for galaxies falling into different bins of  $g-r$  and  $M_r$  (dashed boxes). As expected, the average attenuation is reduced if C and SF galaxies are excluded (blue arrows). In both cases, attenuation by dust becomes more important at lower luminosities. Correcting for dust attenuation would thus steepen the relation. When de-reddening the colours and magnitudes of the galaxies in the sample according to the average attenuation vectors shown in Fig. 3.5, we derive a slope of  $-0.035 \pm 0.002$ . Table 3.1 summarizes the parameters of the fits to the ( $k$ -corrected) colour-magnitude relation, with and without evolution and dust corrections.

#### 3.3.1.2 Physical origin of the colour-magnitude relation

Fig. 3.6 shows how metallicity, age,  $\alpha/\text{Fe}$  ratio and stellar mass change along the colour-magnitude relation. We have binned the  $g-r$ ,  $M_r$  plane in the same way as in Fig. 3.3, the brightness of each  $g-r$  bin at a given  $M_r$  being proportional to the number of galaxies falling into this bin (see Section 3.3.1.1). In each panel, the colour code reflects the average properties of the galaxies falling into each colour-magnitude bin, as indicated. Panels (a)–(c) show how (the median-likelihood estimates of) age, metallicity and stellar mass are distributed along the CMR. Panel (d) shows the distribution of the offset  $\Delta(\text{Mgb}/\langle\text{Fe}\rangle)$  between observed and predicted  $\text{Mgb}/\langle\text{Fe}\rangle$  index strengths, which traces the  $\alpha$ -elements-to-iron abundance ratio (Section 4.2.1).

<sup>6</sup>**fibres** magnitudes are obtained from the flux measured within an aperture of radius 1.5 arcsec, i.e. equal to the fibre radius.

### 3.3 Physical origin of observed relations for early-type galaxies

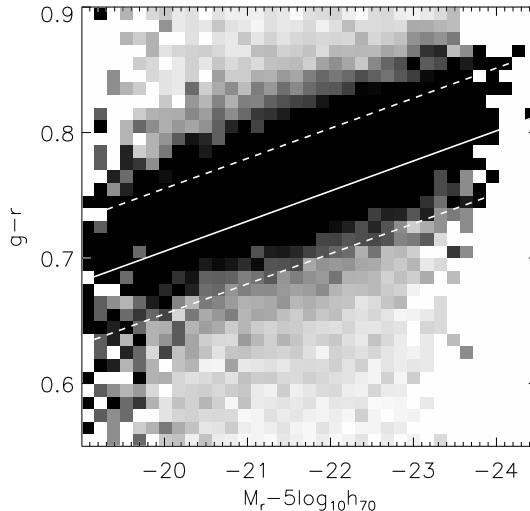


**Figure 3.3:** Relation between ( $k+e$ -corrected)  $g-r$  colour and  $r$ -band absolute magnitude for the same sample of early-type galaxies as in Fig. 3.1. The grey scale indicates, for each magnitude bin, the relative distribution of galaxies in the different colour bins (normalised along the colour axis). The solid line represents the relation between  $g-r$  and  $M_r$ , fitted as described in the text. The dashed lines show the vertical scatter about the relation.

The most remarkable result from Fig. 3.6 is that the colour-magnitude relation is primarily a sequence in the stellar mass of early-type galaxies (panel c; note that the gradient in stellar mass is not exactly parallel to the magnitude axis, reflecting a non-constant mass-to-light ratio in the optical bands). Another striking result is that the average metallicity increases from  $\sim 0.8Z_{\odot}$  to  $\sim 1.6Z_{\odot}$  from the faintest to the brightest galaxies along the relation, the average light-weighted age increasing by less than 3 Gyrs (from 6.5 and 9.0 Gyr) over the same interval of 5 magnitudes in  $M_r$  (panels a and b). The marked increase in metallicity is accompanied by an increase in the  $\alpha$ -elements-to-iron abundance ratio (panel d). This is consistent with the finding that giant elliptical galaxies have higher  $[\text{Mg}/\text{Fe}]$  than faint elliptical galaxies (e.g. Worthey et al. 1992; Trager et al. 2000a; Kuntschner et al. 2001; Thomas et al. 2004). The gradients in both metallicity and age are not exactly parallel to the relation, but at fixed magnitude, bluer galaxies are more metal-poor and younger than redder galaxies. Thus, both metallicity and age contribute to the scatter about the relation.

It is of interest to compare the relative contributions by age and metallicity to the scatter about the CMR. We note that we expect dust attenuation

### 3 Physical origin of the colour-magnitude and the $Mg_2-\sigma_V$ relations for early-type galaxies

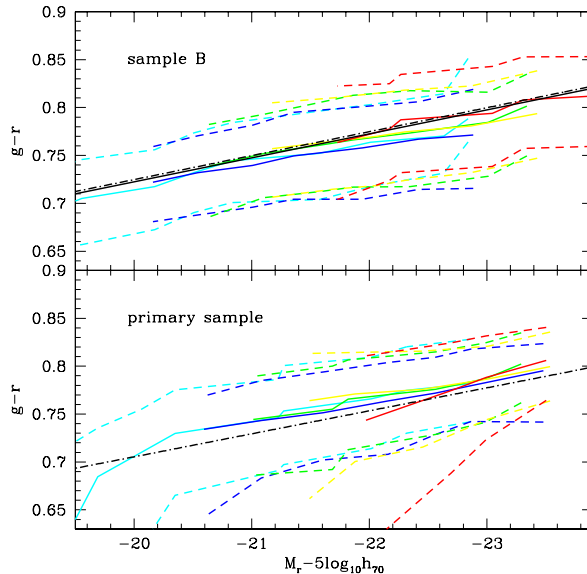


**Figure 3.4:** Colour-magnitude relation for the same sample of early-type galaxies as in Fig. 3.1 (lower panel) and for a sample obtained using the same selection criteria as in Bernardi et al. (2005) (upper panel). The colours and luminosities of the galaxies in both samples are corrected for evolution following Bernardi et al. (2005, i.e., making  $g - r$  redder by  $0.3z$  and  $M_r$  fainter by  $0.85z$ ). Different colours refer to different redshift intervals,  $0.02 < z < 0.07$  (cyan),  $0.07 < z < 0.09$  (blue),  $0.09 < z < 0.12$  (green),  $0.12 < z < 0.15$  (yellow),  $0.15 < z < 0.2$  (red). For each redshift bin, solid and dashed lines give the median and the 68 percent range in colour as a function of luminosity. Black dot-dashed lines show robust fits to the relations for the two samples (including galaxies at all redshifts), while the black solid line in the upper panel is the corresponding relation fitted by Bernardi et al. (2005) with a maximum-likelihood technique (see their fig. 2).

and changes in the  $[\alpha/\text{Fe}]$  ratio to contribute negligibly to the scatter, since the scatter in  $g - r$  colour of dust-free,  $[\alpha/\text{Fe}]=0$  models with the ages and metallicities of the galaxies in our sample ( $\pm 0.041$ )<sup>7</sup> is very similar to the

<sup>7</sup>This is estimated by adopting, for each galaxy in the sample, the median of the likelihood distribution in  $g - r$  obtained by weighting each model in the library of Section 4.2.1 by  $\chi^2 = [(\log Z_{mod} - \log Z)/\sigma_{\log Z}]^2 + [(\log t_{mod} - \log t_r)/\sigma_{\log t_r}]^2$ .

### 3.3 Physical origin of observed relations for early-type galaxies

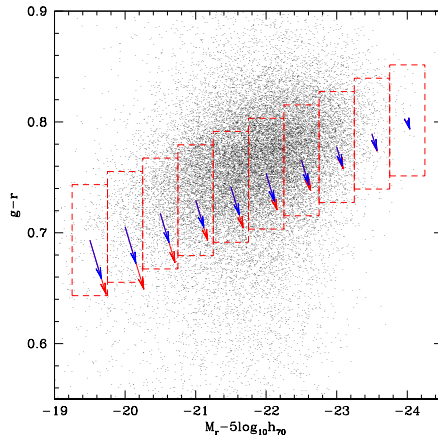


**Figure 3.5:** Relation between ( $k+e$ -corrected)  $g-r$  colour and  $r$ -band absolute magnitude for the same sample of early-type galaxies as in Fig. 3.1. The red arrows indicate the average correction for dust attenuation on the colour and absolute magnitude of the galaxies falling into different  $g-r, M_r$  bins (indicated by the dashed boxes) along the fitted relation. The blue arrows indicate the average dust correction when galaxies in the star-forming and composite classes are excluded.

observed scatter ( $\pm 0.050$ ). For comparison, the scatter in  $g-r$  colour of models with the metallicities of the galaxies in our sample but with a fixed imposed (average) age at fixed  $M_r$  is only  $\pm 0.022$ , while that of models with the ages of the galaxies in our sample but with a fixed imposed (average) metallicity at fixed  $M_r$  is  $\pm 0.028$ . This indicates that age and metallicity contribute a similar amount to the scatter in the colour-magnitude relation for early-type galaxies.

Figure 3.7 better quantifies the intrinsic scatter in the two physical parameters and how much it determines the scatter in colour as a function of stellar mass. The left-hand panels show the distribution in light-weighted age (or metallicity) as a function of  $g-r$  colour in six bins of stellar mass (the median and the 16–84 interpercentile range are given by the red points and associated error bars). The right-hand panels show the marginalized distribution in age (metallicity) compared with a Gaussian of width equal to the average error in age (metallicity) for the galaxies in each stellar mass bin (dotted curve). From the left-hand plot we can see that at masses above  $10^{11} M_{\odot}$  the scatter in light-weighted age can be entirely accounted for by the measurement errors,

### 3 Physical origin of the colour-magnitude and the $Mg_2-\sigma_V$ relations for early-type galaxies

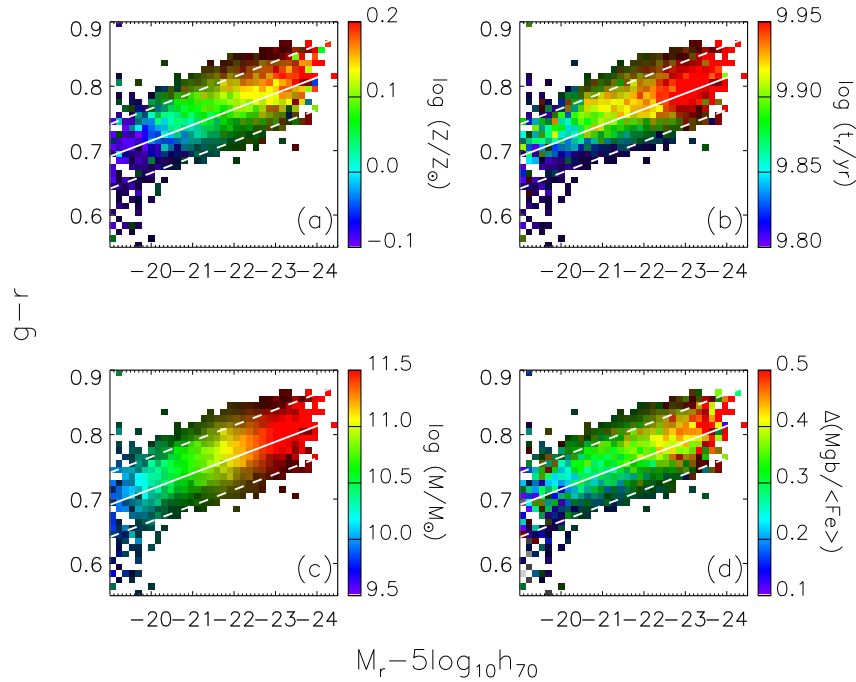


**Figure 3.6:** Relation between ( $k+e$ -corrected)  $g-r$  colour and  $M_r$  absolute magnitude for the same sample of early-type galaxies as in Fig. 3.1. The colour-magnitude relation has been binned and colour-coded to reflect the average stellar metallicity (panel a),  $r$ -band light-weighted age (panel b), stellar mass (panel c) and the  $\alpha/\text{Fe}$ -indicator  $\Delta(\text{Mgb}/\langle\text{Fe}\rangle)$  (panel d) of the galaxies falling into each bin. The shading indicates the fraction of galaxies populating each colour bin at fixed magnitude, according to the map of Fig. 3.3.

which are on average less than 0.1 dex. We can thus say that all massive ellipticals of given mass have the same mean age (within the errors). At lower masses the scatter in light-weighted age becomes larger than the typical error, and the distribution is skewed toward younger ages. At fixed mass, there is a correlation between age and colour, which saturates for the reddest galaxies. We also detect a small intrinsic scatter in the mass-metallicity relation in all mass bins (right-hand plot), which contributes to the scatter in the CMR at fixed mass, even at the high-mass end.

It is important to check that aperture effects do not introduce any spurious trend in Fig. 3.6. This could arise because colour, luminosity and stellar mass pertain to the galaxy as a whole, while age, metallicity and  $\Delta(\text{Mgb}/\langle\text{Fe}\rangle)$

### 3.3 Physical origin of observed relations for early-type galaxies

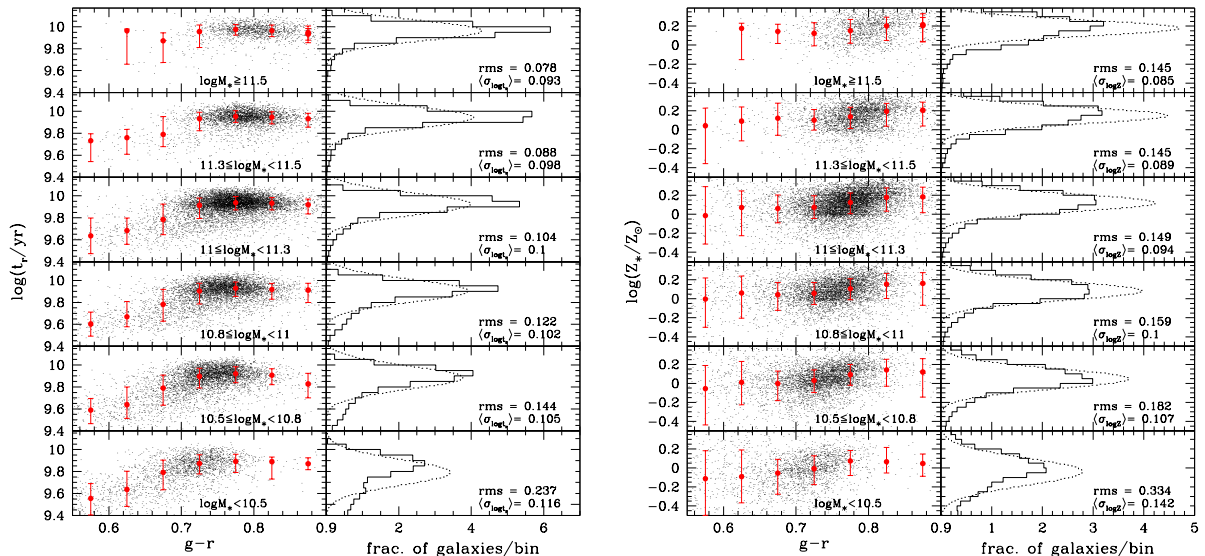


**Figure 3.7:** Left panels: distribution in light-weighted age (left plot) and stellar metallicity (right plot) as a function of  $g - r$  colour for different bins of stellar mass. The red dots are the median age (metallicity) at fixed colour, while the error bars give the 68 percent percentile range in the age (metallicity) distribution. Right panels: histogram of light-weighted age (metallicity) compared to a Gaussian (dotted curve) of width equal to the average error on age (metallicity) in each stellar mass bin. In each panel the rms scatter and the average error in age (metallicity) are also given.

are measured within a fixed fibre aperture of radius 1.5 arcsec, which samples different fractions of the total light in galaxies with different apparent sizes. In section 3.4 of Paper I, we already showed that aperture effects are not expected to affect significantly the ages and metallicities derived for the galaxies in our sample. To probe the influence of aperture effects on the results of Fig. 3.6, we have arranged galaxies in several bins of apparent size  $r_{50,r}$ , defined as the  $r$ -band Petrosian half-light radius. Galaxies with  $1.5 \lesssim r_{50,r} \lesssim 2.4$  arcsec are found out to redshift 0.2. We plotted the equivalent of Fig. 3.6 for each bin of  $r_{50,r}$  within this range. In all cases, we found the same increase in metallicity,  $\Delta(\text{Mgb}/\langle\text{Fe}\rangle)$  and age along the relation as in Fig. 3.6, although the trends were noisier because of the smaller numbers of galaxies in individual  $r_{50,r}$  bins. In our sample, galaxies along the CMR have a roughly constant apparent size  $r_{50,r} \sim 2.3$  arcsec at all magnitudes fainter than  $M_r = -23.5$  (corresponding roughly to stellar masses less than  $10^{11.5} M_\odot$ ). The brightest galaxies tend to have larger apparent sizes, but stellar metallicity, age and  $\Delta(\text{Mgb}/\langle\text{Fe}\rangle)$  do

### 3 Physical origin of the colour-magnitude and the $Mg_2-\sigma_V$ relations for early-type galaxies

not show any significant trend with apparent size. Thus, we are confident that aperture effects are not responsible for the trends seen in Fig. 3.6.

For completeness, we repeated the analysis of Fig. 3.6 using sample B in place of our primary sample (Section 3.3.1.1). We found no significant difference in this case with respect to the results described above. We also repeated the analysis using our primary sample, but correcting the observed CMR for the effects of dust attenuation (Section 3.3.1.1). Again, the main results in this case did not change. We further checked the influence of a possible contamination of the trends identified in Fig. 3.6 by late-type galaxies, in particular, with regard to the variation in age along the relation. Excluding SF and C galaxies (which tend to have younger ages than the bulk of the sample) had no significant effect on the results. In fact, C galaxies alone display the same trends as found in Fig. 3.6 for the sample as a whole. The average metallicity of SF galaxies also increases with luminosity along the CMR, although these tend to have light-weighted ages clustered around a mean value  $\log(t_r/\text{yr}) = 9.6$  almost independently of luminosity. We note that SF galaxies represent only about 5 percent of our primary sample, and they occupy  $g-r$ ,  $M_r$  bins where the fraction of galaxies at a given magnitude is less than 2 percent of the total sample (not displayed in Fig. 3.6).

In summary, we have shown that the colour-magnitude relation is primarily a sequence in galaxy stellar mass. Both the chemical composition (i.e. the total metallicity and the  $\alpha$ -elements-to-iron abundance ratio) and the age of elliptical galaxies depend mainly on stellar mass, increasing along the relation. At the high-mass end of the relation, the age spread is negligible and consistent with the errors. In this regime, the scatter in the CMR is determined by the small scatter in the mass-metallicity relation. At lower masses, the distribution in age becomes broader, with a spread toward younger ages, which correlates with colour and is thus the main contributor to the scatter about the colour-magnitude relation at the low luminosity end.

#### 3.3.2 The $Mg_2-\sigma_V$ relation

In this section, we focus on another observational relationship between the stellar populations and the structural properties of early-type galaxies: the relation between  $Mg_2$  index strength and galaxy velocity dispersion  $\sigma_V$  (Bender et al. 1993). The difficulty in interpreting this relation comes from the complex translation of  $Mg_2$  index strength and  $\sigma_V$  into physical parameters.

The  $Mg_2$  index strengths considered here are corrected for broadening due to velocity dispersion. They are normalised to a fixed velocity dispersion of  $\sigma_V = 200 \text{ km s}^{-1}$ , corresponding roughly to the average velocity dispersion of galaxies in our sample. The normalization is achieved by using the Bruzual

### 3.3 Physical origin of observed relations for early-type galaxies

& Charlot (2003) models to compute the difference in  $Mg_2$  index strength between the observed and reference velocity dispersion at the metallicity of each galaxy.<sup>8</sup> For a consistent comparison with the CMR and with the evolution-corrected light-weighted ages, we also correct the  $Mg_2$  index strengths so that they are relative to the present rather than to the redshift of observation, assuming passive evolution. The corrections are obtained by fitting simple linear relations between  $Mg_2$  index strength and time for SSPs of different metallicities and velocity dispersions. The  $Mg_2$  value measured for each galaxy is then corrected by adding the expected change in index strength over a time interval equal to the look-back time at the redshift of the galaxy.<sup>9</sup>

Fig. 3.8 shows the  $Mg_2$ - $\sigma_V$  relation defined by the early-type galaxies in our primary sample. We have arranged galaxies in narrow bins of  $Mg_2$  and  $\log \sigma_V$  (of widths 0.01 and 0.036, respectively). By analogy with Fig. 3.3, the grey scale in Fig. 3.8 indicates, for each  $\log \sigma_V$  bin, the relative distribution of galaxies in the different  $Mg_2$  bins (we do not show bins containing less than 2 percent of the total number of galaxies at given velocity dispersion). The solid straight line shows the result of a robust linear fit obtained by minimising the absolute deviation in  $Mg_2$  strength as a function of  $\log \sigma_V$ . This has a slope of  $0.25 \pm 0.01$ , i.e. very close to that found by Bernardi et al. (2003d) for a sample of co-added, high-quality spectra of SDSS early-type galaxies (see also Guzman et al. 1992; Colless et al. 1999). The dashed lines in Fig. 3.8 are the mean positive and negative absolute deviations in  $Mg_2$  strength ( $\pm 0.024$  mag) relative to this fit (also in agreement with previous work). These results are summarized in Table 3.1. We also indicate in the table the slightly lower slope of the  $Mg_2$ - $\sigma_V$  relation obtained for sample B ( $0.19 \pm 0.002$ ). This is because sample B includes fewer (emission-line) galaxies with weak  $Mg_2$  absorption than our primary sample at low  $\sigma_V$  and more (low-S/N) galaxies with weak  $Mg_2$  absorption at large  $\sigma_V$  (Section 3.3.1.1).

The tightness of the  $Mg_2$ - $\sigma_V$  relation has been used in the past to argue that early-type galaxies have nearly coeval stellar populations, perhaps within  $\sim 15$  percent, at given composition (e.g. Bender et al. 1993). However, as noted by Trager et al. (2000a), the small scatter about the relation could also conceal significant age spreads, if these are accompanied by metallicity spreads such that the  $Mg_2$  strength remains roughly constant at fixed velocity dispersion (see also Jørgensen 1999). Assuming a moderate anticorrelation between age

<sup>8</sup>This correction varies from  $-0.002$  to  $0.004$  over the range in velocity dispersion covered by the sample. The average absolute correction is only 0.8 percent of the 5 – 95 percent percentile range in  $Mg_2$  index strength.

<sup>9</sup>The fitted slopes, averaged over velocity dispersion, are 0.0056, 0.0044, 0.0064, 0.0077 mag Gyr<sup>-1</sup> for  $\log(Z/Z_\odot) = -0.7, -0.4, 0, 0.4$  respectively.

### 3 Physical origin of the colour-magnitude and the $Mg_2$ - $\sigma_V$ relations for early-type galaxies

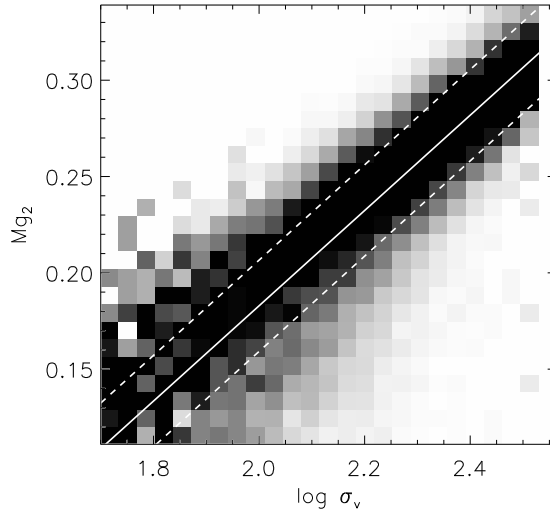


**Figure 3.8:** Relation between  $Mg_2$  index strength (mag) and velocity dispersion  $\log \sigma_V$  ( $\text{km s}^{-1}$ ) for the same sample of early-type galaxies as in Fig. 3.1. As in Fig. 3.3, the grey scale indicates, for each velocity dispersion bin, the relative distribution of galaxies in the different  $Mg_2$  bins.

and metallicity, Colless et al. (1999) find that the intrinsic scatter in the  $Mg_2$ - $\sigma_V$  relation translates into an upper limit of 40 (50) percent on the age (metallicity) spread. Moreover, it has been pointed out that, at fixed  $\sigma_V$ , the distribution of  $Mg_2$  residuals relative to the mean  $Mg_2$ - $\sigma_V$  relation is not symmetric but skewed toward low  $Mg_2$  values, and that this effect tends to increase at low velocity dispersion (Burstein et al. 1988; Bender et al. 1993; Jørgensen et al. 1996; Trager et al. 2000a; Worthey & Collobert 2003). Our data confirm this finding. Fig. 3.9 shows the distribution of  $Mg_2$  residuals at different velocity dispersions (increasing from the top-left to the bottom-right panels) for our primary sample. At large velocity dispersion, the distribution of residuals is symmetric and centred around zero, while at smaller velocity dispersions, a tail of negative residuals appears. This could result from either an age or a metallicity spread, or both. The observation that galaxies with negative residuals are often morphologically disturbed (presumably because of recent star formation) led to the idea that low  $Mg_2$  values at fixed  $\sigma_V$  are associated with younger ages (Schweizer & Seitzer 1992).

The availability of independent constraints on the ages and metallicities of early-type galaxies in our sample allows us to re-examine the physical origin of the  $Mg_2$ - $\sigma_V$  relation. Fig. 3.10 shows how metallicity, age,  $\alpha/\text{Fe}$  ratio and stellar mass change along this relation. We have binned and colour-coded the

### 3.3 Physical origin of observed relations for early-type galaxies

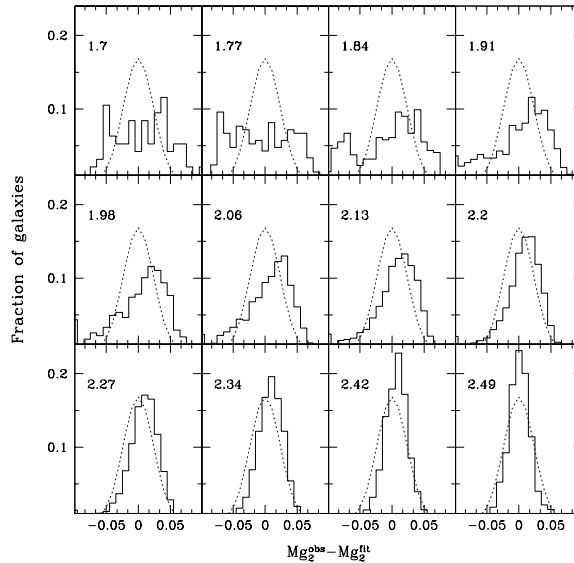


**Figure 3.9:** Distribution of residuals relative to the mean  $Mg_2$ - $\sigma_V$  relation fitted in Fig. 3.8, for different values of  $\log(\sigma_V/\text{km s}^{-1})$  (indicated in each panel). The number of galaxies is normalised to the total in each bin of velocity dispersion. The dotted curve (repeated in each panel) is a Gaussian distribution of width equal to the average absolute deviation in the  $Mg_2$ - $\sigma_V$  relation (see Table 3.1).

$Mg_2$ ,  $\sigma_V$  plane to reflect the average properties of the galaxies falling into each bin. As in Fig. 3.8, the brightness of each  $Mg_2$  bin at a given  $\sigma_V$  is proportional to the number of galaxies falling into this bin. Panels (a)–(c) show how (the median-likelihood estimates of) age, metallicity and stellar mass are distributed along the  $Mg_2$ - $\sigma_V$  relation. Panel (d) shows the distribution of the offset  $\Delta(Mgb/\langle Fe \rangle)$  between observed and predicted  $Mgb/\langle Fe \rangle$  index strengths, which traces the  $\alpha/Fe$  ratio (Section 4.2.1).

The most remarkable result from Fig. 3.10 is that, like the CMR, the  $Mg_2$ - $\sigma_V$  relation for early-type galaxies appears to be primarily a sequence in stellar mass (panel c). In fact, stellar mass correlates tightly with velocity dispersion, which is a tracer of dynamical mass (e.g., Cappellari et al. 2006). Panel (a) further shows that stellar metallicity increases along the relation, from  $\sim 0.8Z_\odot$  to  $1.6Z_\odot$  from low to high velocity dispersions. Galaxies with large  $\sigma_V$  are also older than those with low  $\sigma_V$ , though for  $\log \sigma_V \lesssim 2.3$  age appears to correlate with  $Mg_2$  index strength as well. Another striking result from Fig. 3.10 is the similarity between the metallicity and  $\Delta(Mgb/\langle Fe \rangle)$  gra-

### 3 Physical origin of the colour-magnitude and the $Mg_2$ - $\sigma_V$ relations for early-type galaxies

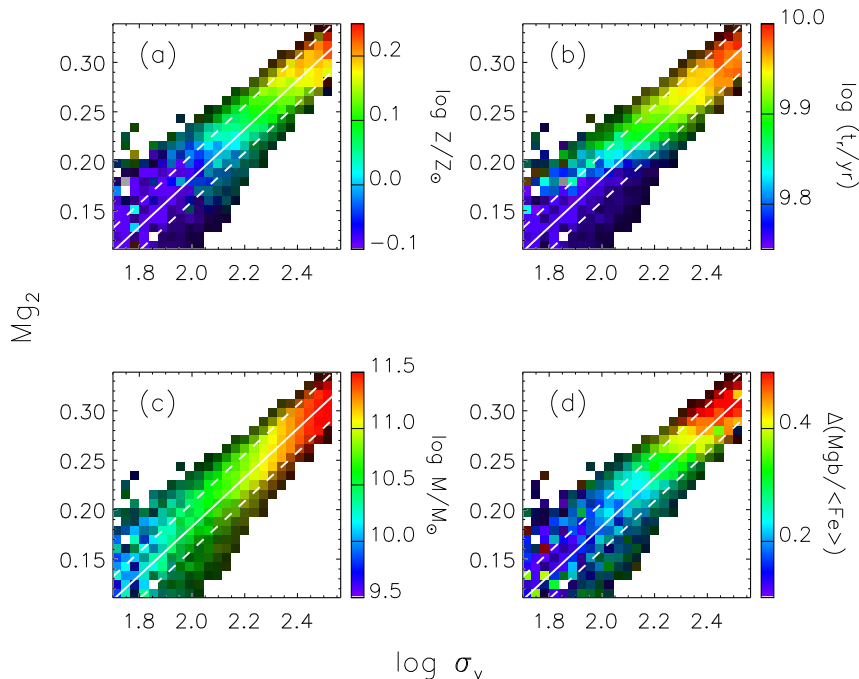


**Figure 3.10:** Relation between  $Mg_2$  index strength (mag) and velocity dispersion ( $\text{km s}^{-1}$ ) for the same sample of early-type galaxies as in Fig. 3.1. The relation has been binned and colour-coded to reflect the average stellar metallicity (panel a),  $r$ -band light-weighted age (panel b), stellar mass (panel c) and  $\alpha/\text{Fe}$ -estimator  $\Delta(\text{Mgb}/\langle\text{Fe}\rangle)$  (panel d) of the galaxies falling into each bin. The shading indicates the fraction of galaxies populating each  $Mg_2$  bin a fixed  $\log \sigma_V$ , according to the map of Fig. 3.8.

dients along the  $Mg_2$ - $\sigma_V$  relation (panels a and d). This shows that massive early-type galaxies with large velocity dispersions are both more metal-rich and more abundant in  $\alpha$  elements relative to iron than less massive galaxies.

As in the case of the CMR (Section 3.3.1.2), we have checked that the trends identified above are not caused by aperture effects. In particular, we find similar trends in stellar mass, metallicity, age and  $\Delta(\text{Mgb}/\langle\text{Fe}\rangle)$  along the  $Mg_2$ - $\sigma_V$  relation when considering galaxies in narrow ranges of  $r_{50,r}$ . Galaxies along the relation have roughly constant apparent size  $r_{50,r} \sim 2.3$  arcsec, implying that the average fraction of total galaxy flux sampled by the fibre is almost constant.

As above for the CMR, we can quantify the relative contribution of metallic-

### 3.3 Physical origin of observed relations for early-type galaxies

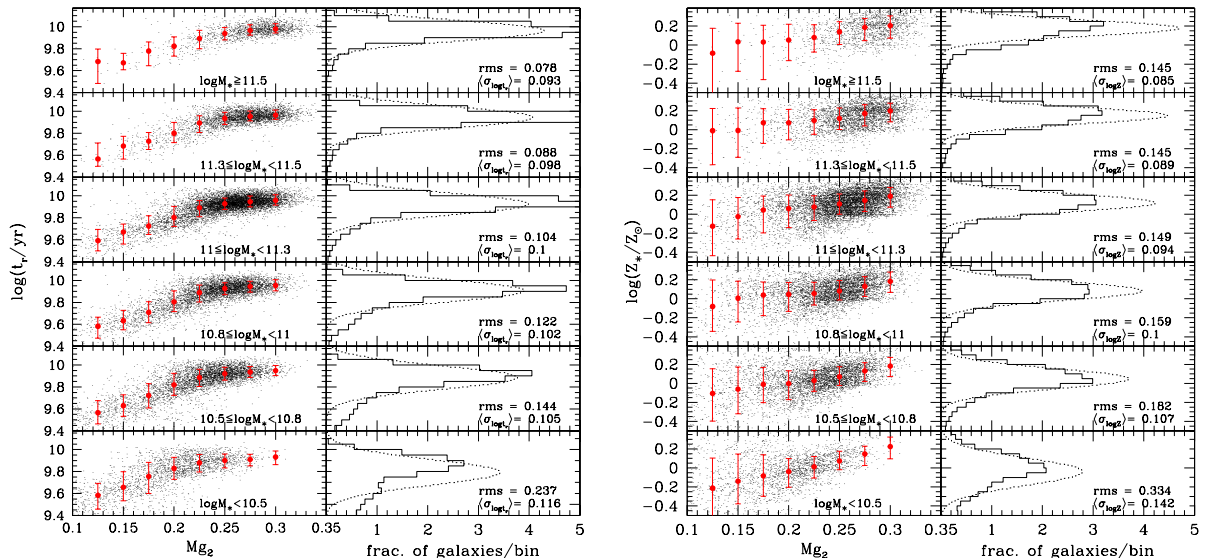


**Figure 3.11:** Left panels: light-weighted age (left plot) and stellar metallicity (right plot) as a function of  $\text{Mg}_2$  index strength (mag) in different bins of stellar mass. The red dots with error bars represent the median and the 68 percent percentile range of the age (metallicity) distribution at given  $\text{Mg}_2$  index strength. Right panels: histogram of light-weighted age (metallicity) compared to a Gaussian (dotted curve) of width given by the average error in age (metallicity) for the galaxies falling into each stellar mass bin. The scatter and the average error in age (metallicity) are also indicated.

ity and age to the scatter in the  $\text{Mg}_2$ - $\sigma_V$  relation. We note that there must be another parameter, most likely the  $\alpha$ -elements-to-iron abundance ratio, that is responsible for the scatter in the relation. In fact, the scatter in  $\text{Mg}_2$  of  $[\alpha/\text{Fe}]=0$  models with the ages and metallicities of the galaxies in our sample is only  $\pm 0.0118$ , i.e. much smaller than the observed scatter (0.0237).<sup>10</sup> We obtain a similar scatter ( $\pm 0.0116$ ) in the  $\text{Mg}_2$  index strength of models with the same metallicity as the galaxies in our sample but with a fixed imposed (average) age at fixed  $\log \sigma_V$ . On the other hand the scatter in  $\text{Mg}_2$  index strength of models with the ages of the galaxies in our sample but with a fixed imposed (average) metallicity at fixed  $\log \sigma_V$  is only  $\pm 0.007$ . This indicates that metallicity has a stronger influence than age on the scatter in the

<sup>10</sup>For each galaxy in the sample, we adopt here the median of the likelihood distribution in  $\text{Mg}_2$  obtained by weighting each model by  $\chi^2 = [(\log Z_{\text{mod}} - \log Z)/\sigma_{\log Z}]^2 + [(\log t_{\text{mod}} - \log t_r)/\sigma_{\log t_r}]^2$ .

### 3 Physical origin of the colour-magnitude and the $Mg_2-\sigma_V$ relations for early-type galaxies

$Mg_2-\sigma_V$  relation.

Figure 3.11 is obtained in a similar way as Fig. 3.7. As in Fig. 3.7, the left-hand panels of Fig. 3.11 show that the scatter in light-weighted age of high-mass ellipticals ( $M_* \geq 10^{11}M_\odot$ ) is negligible and consistent with the errors on the age estimates. Only at masses below  $10^{11}M_\odot$  does a significant tail of younger ages appear. These young galaxies are responsible for the scatter in  $Mg_2$  at fixed mass, but the relation between age and index strength saturates for  $Mg_2 \gtrsim 0.25$ . Also in agreement with Fig. 3.7, the right-hand plot shows that we detect (above the measurement error) a small scatter in metallicity at fixed mass in all mass bins. There is a correlation between metallicity and  $Mg_2$  at fixed mass, in particular for galaxies with  $Mg_2 \gtrsim 0.25$  (left-hand panels), where light-weighted age saturates to a constant mean value.

The  $Mg_2-\sigma_V$  relation is, therefore, primarily a sequence in galaxy stellar mass. It reflects the fact that early-type galaxies form a sequence of increasing total stellar metallicity and  $\alpha$ -elements to iron abundance ratio from shallow to deep potential wells. Our results also confirm the trend of increasing age with increasing velocity dispersion (e.g. Caldwell et al. 2003; Thomas et al. 2005; Nelan et al. 2005). At high masses, the small scatter in the relation correlates with the scatter in stellar metallicity at fixed stellar mass, while light-weighted age is almost independent of index strength. At the low-mass end of the relation, the fraction of young ellipticals increases and variations in age between  $\sim 4$  and  $\sim 8$  Gyr correlate with index strength at fixed mass.

#### 3.3.3 Environmental dependence

Several authors have addressed the dependence on environment of the properties of the stellar populations in early-type galaxies. Studies of the colour-magnitude relation and the relations between absorption indices and velocity dispersion on relatively small samples of early-type galaxies in different environments have shown that galaxies in low-density environments tend to be younger and more metal-rich than those in high-density environments (e.g. Kuntschner et al. 2002; Thomas et al. 2005; Denicoló et al. 2005). Bernardi et al. (1998), later confirmed by Bernardi et al. (2006) on a larger sample of SDSS early-type galaxies, found differences in the  $Mg_2-\sigma_V$  relation of galaxies in different environments, implying that galaxies in dense environments are at most 1 Gyr older than galaxies in low-density environments and that they have the same metallicity.

Kauffmann et al. (2004) provide estimates of environmental density for a sample of SDSS DR2 galaxies in the redshift range  $0.03 < z < 0.1$  and with apparent  $r$ -band magnitude in the range  $14.5 < r < 17.77$ , complete down to a stellar mass of  $2 \times 10^9 M_\odot$ . The density is expressed in terms of the

### 3.3 Physical origin of observed relations for early-type galaxies

**Table 3.1:** Parameters of the relations fitted by minimising the absolute vertical deviations. Sample A refers to our primary sample, while sample B is obtained by selecting galaxies according to Bernardi et al. (2005) criteria.

Sample	Slope	Intercept	Scatter
Colour-magnitude relation			
sample A <sup>a</sup>	$-0.015 \pm 0.001$	0.40	0.051
sample B <sup>a</sup>	$-0.014 \pm 0.002$	0.41	0.043
sample A <sup>b</sup>	$-0.024 \pm 0.002$	0.22	0.050
sample B <sup>b</sup>	$-0.028 \pm 0.001$	0.14	0.043
sample A <sup>c</sup>	$-0.025 \pm 0.001$	0.14	0.051
sample B <sup>c</sup>	$-0.015 \pm 0.002$	0.37	0.043
sample A <sup>d</sup>	$-0.035 \pm 0.002$	-0.05	0.050
sample B <sup>d</sup>	$-0.029 \pm 0.002$	0.09	0.044
Mg <sub>2</sub> - $\sigma_V$ relation			
sample A <sup>e</sup>	$0.23 \pm 0.01$	-0.29	0.024
sample B <sup>e</sup>	$0.17 \pm 0.003$	-0.15	0.023
sample A <sup>f</sup>	$0.25 \pm 0.01$	-0.31	0.024
sample B <sup>f</sup>	$0.19 \pm 0.00$	-0.18	0.023

<sup>a</sup>*k*-corrected colour and magnitude. <sup>b</sup>*k*+*e*-corrected colour and magnitude (the evolution correction is the one provided by Bernardi et al. 2005). <sup>c</sup>*k*-corrected colour and magnitude dereddened applying the average dust corrections of Fig. 3.5. <sup>d</sup>Fully corrected colour and magnitude. <sup>e</sup>Mg<sub>2</sub> index strength corrected for velocity dispersion. <sup>f</sup>Mg<sub>2</sub> index strength corrected for velocity dispersion and evolution.

number of spectroscopically-observed neighbouring galaxies (down to a fixed absolute magnitude) within 2 Mpc of projected radius and  $\pm 500$  km/s in velocity difference from the target galaxy, corrected for galaxies missed due to fibre collisions ( $N_{\text{neigh}}$ ). We take advantage of these density estimates to address any environmental dependence of the physical properties of the stellar populations for the galaxy sample studied here. This can be achieved for only 1765 galaxies in our sample, for which an estimate of  $N_{\text{neigh}}$  is available. We consider three bins in environmental density, defined by  $N_{\text{neigh}} < 4$ ,  $4 \leq N_{\text{neigh}} < 7$  and  $N_{\text{neigh}} \geq 7$ , which contain, respectively, 693, 388 and 684 galaxies. As mentioned in Section 4.2.1, we can classify the galaxies in our sample on the basis of their emission-line properties. As expected, the sample is dominated by ‘unclassifiable’ galaxies (without emission lines), but there is also contamination by galaxies with a low level of star formation (SF and C galaxies). Fig. 3.12 illustrates the fraction of unclassifiable, SF, low-S/N SF, C

### 3 Physical origin of the colour-magnitude and the $\text{Mg}_2-\sigma_V$ relations for early-type galaxies

and AGN galaxies as a function of environment. This plot quantifies the statement of Section 3.3.1.1 that the fraction of galaxies showing emission lines in our sample increases in lower-density environments. This class of galaxies also contributes to increase the scatter blueward of the colour-magnitude relation.

In Fig. 3.13, we explore how the CMR (left-hand panels) and the  $\text{Mg}_2-\sigma_V$  relation (right-hand panels) depend on environment. The relations found in the highest-density bin are compared to those defined in the lowest-density bin. The results of the linear fits (also for the intermediate bin of  $N_{\text{neigh}}$ ) are given in Table 3.2. Fig. 3.13 and Table 3.2 show that there is no systematic variation in the slope of the CMR as a function of environment, while the  $\text{Mg}_2-\sigma_V$  relation appears to steepen at low densities because of a larger fraction of galaxies with low  $\text{Mg}_2$  index strength at low velocity dispersions (columns 3 and 6). Between the two extreme density bins there are differences of  $0.006 \pm 0.003$  and  $0.007 \pm 0.003$  in the zero-points of the CMR and the  $\text{Mg}_2-\sigma_V$  relation, respectively (columns 4 and 7). This is in agreement with the small shift of  $0.007 \pm 0.002$  mag measured by Bernardi et al. (1998) in the  $\text{Mg}_2-\sigma_V$  relation of a sample of 931 early-type galaxies in different environments. We also identify a systematic increase of the scatter about both relations from high- to low-density environments, in agreement with earlier findings, as mentioned above (e.g. Hogg et al. 2004).

It is of interest to understand how the change in the scatter along the two scaling relations reflects differences in the physical parameters of galaxies in different environments. We note that the distribution in stellar mass does not vary significantly<sup>11</sup> with environment, but that the median stellar mass of galaxies in the lowest-density bin is lower by about 0.05 dex than the median stellar mass in the highest-density bin (it increases from  $8 \times 10^{10}$  to  $9 \times 10^{10} M_{\odot}$ ). Since stellar metallicity, age and element abundance ratio all increase with stellar mass, any effect induced by changes in stellar mass must be removed when quantifying variations in these parameters with environment. To do this, we calculate the median stellar metallicity, light-weighted age and element abundance ratio as a function of stellar mass for the sample as a whole (see Fig. 3.17). For the 1765 galaxies with an estimate of environmental density, we then consider the offsets in  $\log(Z/Z_{\odot})$ ,  $\log(t_r/yr)$ ,  $\Delta(\text{Mgb}/\langle\text{Fe}\rangle)$  from the median values of these parameters at fixed stellar mass in the whole sample. The distributions in  $\Delta[\log Z]$  and  $\Delta[\log t_r]$  are skewed toward negative values, independently of environment, and this effect is stronger at small masses. If galaxies at low densities are distributed preferentially to smaller

<sup>11</sup>When comparing the stellar mass distribution of galaxies in the low-density bin with that of galaxies in the high-density bin, the probability obtained from a Kolmogorov-Smirnov test is not low enough to reject the hypothesis that the two distributions are drawn from the same parent distribution.

### 3.3 Physical origin of observed relations for early-type galaxies

masses than galaxies in dense environments, the distributions in  $\Delta[\log Z]$  and  $\Delta[\log t_r]$  will show a stronger tail toward negative values in the low-density bin. To separate this effect from an intrinsic dependence of metallicity and age on environment, we further distinguish between galaxies with stellar masses above and below  $10^{11}M_{\odot}$ .

The result of this analysis is shown in Fig. 3.14 for the same three environmental bins as considered above. The distributions of the offsets in  $\log(Z/Z_{\odot})$ ,  $\log(t_r/yr)$  and  $\Delta(\text{Mgb}/\langle\text{Fe}\rangle)$  for the two low-density bins ( $N_{\text{neigh}} < 4$  and  $4 \leq N_{\text{neigh}} < 7$ , solid lines) are compared to the corresponding ones in the high-density bin ( $N_{\text{neigh}} \geq 7$ , dotted line in each panel), for massive and low-mass galaxies separately (red and blue histograms, respectively). The comparison is also summarized in Table 3.3, where we give the difference of the average parameter offset between the highest- and the lowest-density bins, for galaxies with stellar mass above and below  $10^{11}M_{\odot}$  separately. There, we also indicate the probability for the two distributions to be drawn from the same parent distribution, according to a Kolmogorov-Smirnov test. Element abundance ratio, as expressed by  $\Delta(\text{Mgb}/\langle\text{Fe}\rangle)$ , does not show any significant variation with environment, either in the average value or in the scatter. In contrast, light-weighted age (independently of mass) and metallicity (for massive galaxies) show a small dependence on environment in the sense that there is a higher fraction of young, metal-poor galaxies in low-density environments. Massive early-type galaxies in dense environments tend to be  $\sim 0.03$  dex more metal-rich than their field counterparts. Similarly, the light-weighted ages of galaxies in dense environments are  $\sim 0.02$  dex older than in the field. It is interesting to mention that we also find a systematic increase in the scatter of metallicity and age from dense to low-density environments. From the highest- to the lowest-density bins the scatter in both metallicity and age increases by about 0.02 dex for massive galaxies (from 0.118 to 0.135 for  $\log(Z/Z_{\odot})$ , from 0.083 to 0.103 for  $\log(t_r/yr)$ ) and by about 0.01 dex for  $M_* < 10^{11}M_{\odot}$  (from 0.16 to 0.17 for  $\log(Z/Z_{\odot})$  and from 0.12 to 0.136 for  $\log(t_r/yr)$ ). Although very small, these trends hint at a possibly very relevant environmental dependence of metallicity and age. Future analysis of larger samples of galaxies (provided, e.g., by the complete SDSS) with well characterized environmental properties will allow to draw firmer conclusions.

#### 3.3.4 Correlations between physical parameters

So far, we have considered separately the constraints set by the colour-magnitude and the  $\text{Mg}_2-\sigma_V$  relations on the ages, chemical compositions and stellar masses of early-type galaxies in our sample. Here, we explore in more detail the potential correlations between these different physical parameters,

### 3 Physical origin of the colour-magnitude and the $Mg_2-\sigma_V$ relations for early-type galaxies

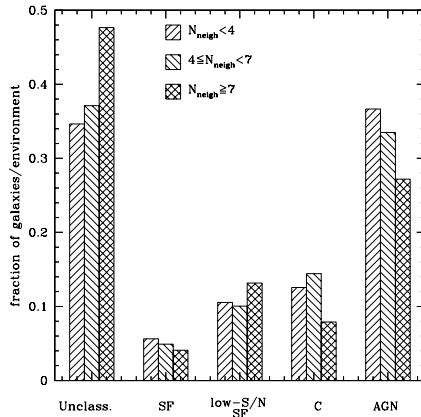


**Figure 3.12:** Fraction of unclassifiable (‘Unclass’), star-forming (‘SF’), low-S/N star-forming (‘low-S/N SF’), composite (‘C’) and AGN galaxies as a function of environment. Three different bins of environmental density are considered here, as given by  $N_{\text{neigh}}$  in the plot. Each histogram is normalised to the number of galaxies in the corresponding environmental bin. While the high-density environments are strongly dominated by galaxies without emission lines (unclassifiable), the fraction of star-forming, composite and AGN galaxies increases in lower-density environments.

**Table 3.2:** Parameters of the colour-magnitude relation (columns 3,4,5) and  $Mg_2-\sigma_V$  relation (columns 6,7,8) for a subsample of 1765 galaxies with environmental estimates. The relations are fitted separately for three different bins of environmental density (given by  $N_{\text{neigh}}$ , column 1). The number of galaxies in each bin is given in column 2. The intercepts are given at  $M_r = -21.5$  and  $\log \sigma_V = 2.25$ , which correspond roughly to the average magnitude and velocity dispersion of this subsample of galaxies.

Environment	$N_{\text{gal}}$	colour-magnitude			$Mg_2 - \sigma_V$		
		Slope	Intercept	Scatter	Slope	Intercept	Scatter
(1)	(2)	(3)	(4)	(5)	(6)	(7)	(8)
$N_{\text{neigh}} < 4$	693	$-0.021 \pm 0.004$	$0.755 \pm 0.002$	0.043	$0.27 \pm 0.03$	$0.244 \pm 0.002$	0.023
$4 \leq N_{\text{neigh}} < 7$	388	$-0.026 \pm 0.006$	$0.757 \pm 0.004$	0.041	$0.26 \pm 0.01$	$0.242 \pm 0.001$	0.020
$N_{\text{neigh}} \geq 7$	684	$-0.022 \pm 0.003$	$0.761 \pm 0.003$	0.036	$0.24 \pm 0.02$	$0.251 \pm 0.003$	0.019

the dynamical mass and the stellar surface mass density of galaxies.

We first turn our attention to the relation between age, luminosity, velocity dispersion and stellar mass inferred from the distribution in the full parameter space described by the colour-magnitude and the  $Mg_2-\sigma_V$  relations. Figs 3.6b and 3.10b taken together indicate that brighter galaxies or galaxies with large velocity dispersions are on average older than fainter or smaller velocity dis-

### 3.3 Physical origin of observed relations for early-type galaxies

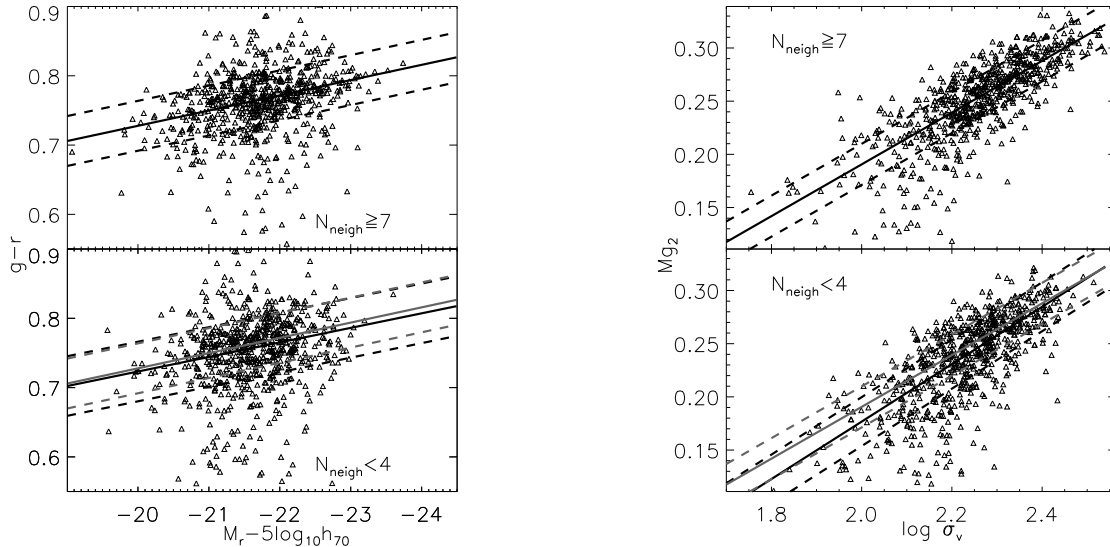


**Figure 3.13:** Colour-magnitude (left plot) and  $Mg_2 - \sigma_V$  relations (right plot) as a function of environment. Galaxies are divided into two disjoint bins of environmental density (increasing from bottom to top as indicated by  $N_{\text{neigh}}$  in each panel). The linear relation fitted for each subsample and the scatter about it are shown in each panel by the black solid and dashed lines. The grey lines reproduce the relation fitted in the highest density bin.

**Table 3.3:** Difference between the average parameter offset between the  $N_{\text{neigh}} < 4$  and  $N_{\text{neigh}} \geq 7$  environmental bins, distinguishing between galaxies with stellar masses above and below  $10^{11} M_{\odot}$ . For each parameter, the second row gives the probability from a Kolmogorov-Smirnov test that the two distributions are consistent with being drawn from the same parent distribution (we consider differences to be statistically significant only if the KS probability is below 1 percent).

	$M_* \geq 10^{11} M_{\odot}$	$M_* < 10^{11} M_{\odot}$
$\Delta[\log Z]$	$0.032 \pm 0.006$	$0.029 \pm 0.006$
	0.0030	0.0217
$\Delta[\log t_r]$	$0.019 \pm 0.005$	$0.023 \pm 0.006$
	0.0053	0.0017
$\Delta[\Delta(Mgb/\langle Fe \rangle)]$	$0.008 \pm 0.009$	$0.024 \pm 0.009$
	0.5321	0.1499

### 3 Physical origin of the colour-magnitude and the $Mg_2-\sigma_V$ relations for early-type galaxies

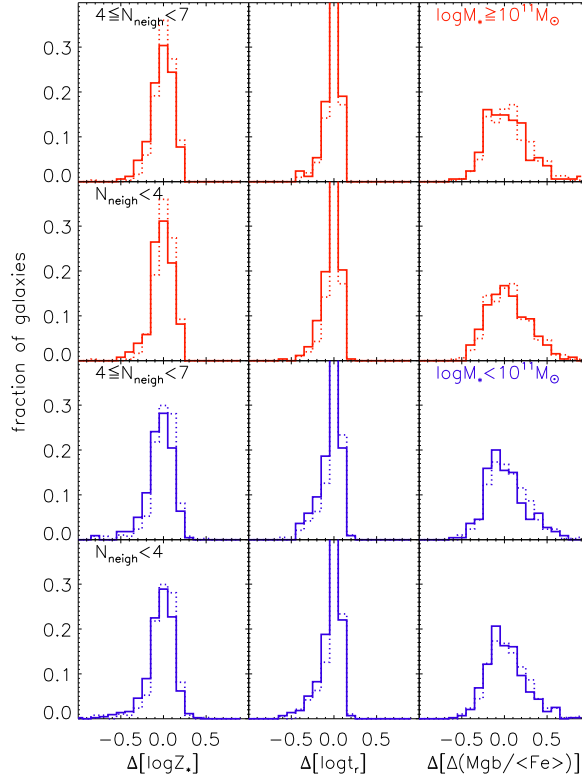


**Figure 3.14:** Stellar metallicity, age and element abundance ratio (expressed as  $\Delta(\text{Mgb}/\langle\text{Fe}\rangle)$ ) as a function of environment for the subsample of 1765 galaxies with environmental estimates. We have estimated the offset in  $\log(Z/Z_\odot)$ ,  $\log(t_r/\text{yr})$  and  $\Delta(\text{Mgb}/\langle\text{Fe}\rangle)$  from the median value at fixed stellar mass calculated for the sample as a whole. The distributions in the offsets are more skewed toward negative values at smaller masses. Thus, to further remove any effect induced by an environmental dependence of the mass, we analysed separately galaxies with masses above and below  $10^{11}M_\odot$  (shown in red and blue respectively). For each stellar mass bin, the distributions in the offsets are shown for galaxies with different environmental density ( $N_{\text{neigh}} < 4$  in the lower panels and  $4 \leq N_{\text{neigh}} < 7$  in the upper panels, solid line). Each distribution is compared to that for galaxies with  $N_{\text{neigh}} \geq 7$ , shown by the dotted line in each panel.

persion ones (consistent with the ‘downsizing’ scenario; Cowie et al. 1996, see also Section 3.4). In Fig. 3.15a, we show the relation between  $M_r$  absolute magnitude, velocity dispersion  $\sigma_V$  and light-weighted age for the galaxies in our primary sample. At fixed luminosity, galaxies with large  $\sigma_V$  tend to be

### 3.3 Physical origin of observed relations for early-type galaxies

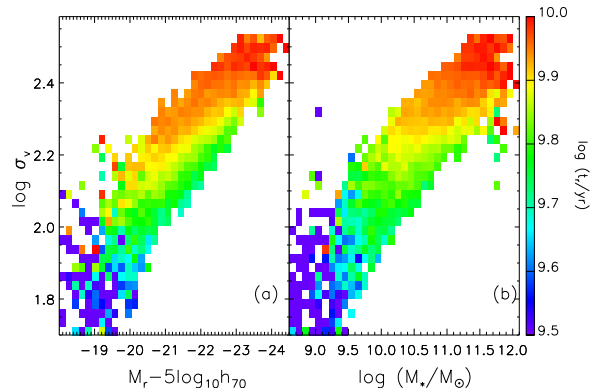


**Figure 3.15:** Relation between velocity dispersion and  $r$ -band absolute magnitude (panel a), colour-coded to reflect the average light-weighted age of the galaxies falling into each  $\log \sigma_V$ - $M_r$  bin. For  $M_r$  brighter than  $-20$ , lines of constant age are approximately parallel to the relation. Panel (b) shows the result of substituting absolute magnitude with stellar mass.

older than those with small  $\sigma_V$  (a result already pointed out by Forbes & Ponman 1999 and Bernardi et al. 2005). Conversely, at fixed velocity dispersion, luminous galaxies tend to be younger than faint galaxies. The dispersion in the  $M_r$ - $\sigma_V$  relation and the dependence of luminosity on age at fixed  $\sigma_V$  cannot be accounted for entirely by the fact that the stellar mass-to-light ratio  $M_*/L_r$  of an evolving stellar population increases with light-weighted age. This is shown in Fig. 3.15b, where we plot the relation between stellar mass and velocity dispersion for the same galaxies as in Fig. 3.15a. The scatter of 0.252 dex about this relation is consistent with the scatter of 0.579 mag in the relation between  $M_r$  and  $\sigma_V$ . There appears to be a real dependence of age on stellar mass at fixed velocity dispersion, in the sense that galaxies with large stellar masses tend to be slightly younger than those with low stellar masses (Table 3.4 provides simple linear fits to the relations shown in Figs 3.15a and b).

The results of Fig. 3.15 motivate us to investigate more closely the relation between stellar mass and dynamical mass for early-type galaxies. We can estimate the dynamical mass (including stars and dark matter) within the optical radius of a galaxy from a combination of velocity dispersion and optical size (Cappellari et al. 2006). Here we use the radius containing 50 percent of the Petrosian flux in the  $r$ -band ( $R_{50,r}$ ) rather than the effective de Vaucouleurs radius ( $r_{deV}$ ), because we do not explicitly select early-type galaxies on the

### 3 Physical origin of the colour-magnitude and the Mg<sub>2</sub>-σ<sub>V</sub> relations for early-type galaxies

**Table 3.4:** Linear fits to the relations plotted in Figs 3.15 and 3.17.

	Slope	Intercept	Scatter
log σ <sub>V</sub> vs M <sub>r</sub>	-0.125 ± 0.004	-0.464	0.073
log σ <sub>V</sub> vs log M <sub>*</sub>	0.286 ± 0.020	-0.895	0.071
log t <sub>r</sub> vs log M <sub>dyn</sub>	0.115 ± 0.056	8.628	0.085
log t <sub>r</sub> vs log M <sub>*</sub>	0.112 ± 0.098	8.678	0.088
log Z vs log M <sub>dyn</sub>	0.164 ± 0.010	-1.731	0.119
log Z vs log M <sub>*</sub>	0.168 ± 0.013	-1.757	0.122
Δ(Mgb/⟨Fe⟩) vs log M <sub>dyn</sub>	0.165 ± 0.012	-1.517	0.199
Δ(Mgb/⟨Fe⟩) vs log M <sub>*</sub>	0.128 ± 0.013	-1.107	0.204

basis of the shape of their light profile. Thus, a de Vaucouleurs profile may not always be an optimal fit to the photometric data, and the empirical half-light radius R<sub>50,r</sub> is more straightforward to interpret.<sup>12</sup> To estimate the dynamical mass within R<sub>50,r</sub>, we must also account for the fact that the velocity dispersion of SDSS galaxies is measured within a fixed 1.5 arcsec fibre radius. Following Jørgensen (1999), we assume that the radial profile of the velocity dispersion has a slope -0.04. The velocity dispersion at the radius R<sub>50,r</sub> is then given by

$$\frac{\sigma_V(r_{fibre})}{\sigma_V(R_{50,r})} = \left( \frac{r_{fibre}}{R_{50,r}} \right)^{-0.04}, \quad (3.1)$$

and the dynamical mass within R<sub>50,r</sub> by

$$\frac{M_{dyn}}{M_\odot} = \xi \frac{\sigma_V^2(R_{50,r}) R_{50,r}}{G}. \quad (3.2)$$

In this expression,  $G$  is the gravitational constant, and  $\xi$  is a scaling factor given in Table 3.5, which depends on the shape of the velocity dispersion profile (this factor would be equal to 5 if we estimated the dynamical mass within the effective de Vaucouleurs radius; see Cappellari et al. 2006).

In Fig. 3.16, we compare the dynamical masses obtained in this way to the stellar masses derived in Paper I for the early-type galaxies in our primary sample.<sup>13</sup> We focus on the slope of the relation, because the zero point is sensitive to our assumptions about the radius within which the dynamical

<sup>12</sup>The de Vaucouleurs effective radii of the galaxies in our sample are on average  $\sim 1.4$  times larger than the Petrosian half-light radii. This arises presumably from the fact that the Petrosian flux represents typically 80 percent of the total flux in the de Vaucouleurs model (Padmanabhan et al. 2004), but this could also result (at least for a class of objects) from forcing a de Vaucouleurs fit to a flatter galaxy light profile.

<sup>13</sup>We recall that the total stellar mass is obtained by multiplying the stellar mass-to-light

### 3.3 Physical origin of observed relations for early-type galaxies

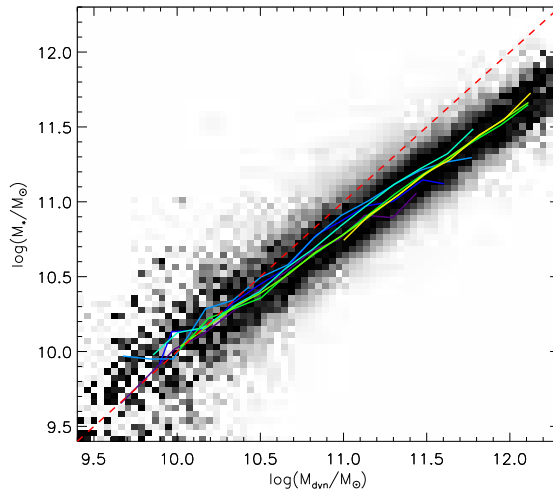


**Figure 3.16:** Relation between stellar mass and dynamical mass  $M_{dyn}$  estimated within the  $r$ -band Petrosian half-light radius (see equation 3.2). Lines of different colours represent the median relations in different bins of light-weighted age, increasing from  $\log(t_r/\text{yr}) = 9.5$  (purple) to 10.1 (yellow). The ratio between stellar and dynamical mass decreases with mass, as highlighted by the comparison with the one-to-one relation (dashed line).

mass is estimated, the conversion factor between dynamical and virial masses, and the stellar initial mass function (IMF; which we assume constant for all the galaxies). A linear fit to the relation in Fig. 3.16 yields

$$(M_*/M_\odot) \propto (M_{dyn}/M_\odot)^{(0.783 \pm 0.019)} \quad (3.3)$$

with a scatter of 0.13 dex. The specific correction applied to  $\sigma_V$  has little effect on the fitted slope. As a check, we tried steeper velocity dispersion profiles, with slopes  $-0.06$  (Mehlert et al. 2003) and  $-0.066$  (Cappellari et al. 2006). These yielded relations between  $\log M_*$  and  $\log M_{dyn}$  with slopes  $0.785 \pm 0.021$  and  $0.786 \pm 0.017$ , respectively, i.e. consistent within  $1\sigma$  with the slope of the relation in Fig. 3.16. We also tested the effect of estimating the dynamical mass within the effective de Vaucouleurs radius  $r_{deV}$  instead of  $R_{50,r}$ . The dynamical masses obtained in this case were systematically higher, by  $\sim 0.13$  dex, than those derived within  $R_{50,r}$ . The relation between  $\log M_*$  and  $\log M_{dyn}$  had a slope of  $0.808 \pm 0.026$ , i.e. slightly higher but consistent within  $1\sigma$

---

ratio derived from a fit of the fibre spectrum by the total luminosity of the galaxy. This assumes that the stellar mass-to-light ratio outside the fibre is the same as that inside the fibre (see Paper I).

### 3 Physical origin of the colour-magnitude and the $Mg_2$ - $\sigma_V$ relations for early-type galaxies

**Table 3.5:** Correlation between stellar and dynamical mass. The first two columns give the radius within which the dynamical mass is estimated and the slope of the velocity dispersion profile assumed to correct for aperture effects.

Radius	$\sigma_V$ profile	$\xi$	Slope	Intercept	Scatter
$R_{50,r}$	-0.040	7.14	$0.783 \pm 0.019$	2.19	0.127
$R_{50,r}$	-0.060	6.98	$0.785 \pm 0.021$	2.18	0.128
$R_{50,r}$	-0.066	7.02	$0.786 \pm 0.017$	2.17	0.128
$r_{deV}$	-0.040	5.00	$0.808 \pm 0.026$	1.93	0.113

with the slope of the relation in Fig. 3.16. These results are summarised in Table 3.5.

A robust result from Fig. 3.16, therefore, is that the ratio between dynamical mass and stellar mass increases from the least massive to the most massive early-type galaxies in our sample. Structural non-homology does not appear to be responsible for this effect. We have built different subsamples of galaxies, based on the value of the Sersic index  $n$  fitted to the light profile in the SDSS database. The slope of the relation between  $\log M_*$  and  $\log M_{dyn}$  within each subsample remains close to that of the relation in Fig. 3.16, changing from 0.847 for  $n = 3$  to 0.801 for  $n = 5.5$  (a de Vaucouleurs profile corresponding to  $n = 4$ ). Instead, the decrease in  $M_*/M_{dyn}$  with stellar mass in Fig. 3.16 is consistent with the increase in the dynamical mass-to-light ratio ( $M_{dyn}/L$ ) of early-type galaxies implied by the Fundamental Plane under the assumption of structural homology (Bender et al. 1992; Pierini et al. 2002; Zibetti et al. 2002; see also Cappellari et al. 2006, where no assumption on homology is made). This is also consistent with the increase in  $M_{dyn}/L$  with luminosity found by Padmanabhan et al. (2004) for a sample of 29,469 SDSS elliptical galaxies. The decrease of  $M_*/M_{dyn}$  with stellar mass could result from a more efficient mixing of dark matter and stars within the optical radius of massive galaxies relative to low-mass galaxies, as expected if the most massive early-type galaxies assembled through multiple mergers of dissipationless systems (see for discussion White 1980; Humphrey et al. 2005; De Lucia et al. 2006; Boylan-Kolchin, Ma & Quataert 2005).

The trend in  $M_*/M_{dyn}$  with stellar mass shows a weak dependence on galaxy light-weighted age. This is shown in Fig. 3.16, where lines of different colours indicate the median stellar mass as a function of dynamical mass for galaxies in various age bins, from  $\log(t_r/\text{yr}) = 9.5$  (purple) to 10.1 (yellow). Lines of constant age run parallel to the relation and, in spite of the small scatter, it appears that, at given dynamical mass, galaxies with more mass in stars are younger than those with small stellar mass (see also Fig. 3.15b). This weak trend cannot be accounted for entirely by the larger amount of mass re-

### 3.3 Physical origin of observed relations for early-type galaxies

turned to the interstellar medium by evolved stars in older galaxies relative to younger ones. For the Chabrier (2003) IMF adopted here, the returned stellar mass fraction of a simple stellar population increases by about 0.03 dex from  $\log(t_r/\text{yr}) = 9.5$  to 10 (with little dependence on metallicity; the differential change is similar for a Salpeter 1955 IMF). This effect can thus account for only about 10 percent of the trend in  $M_*/M_{dyn}$  with age in Fig. 3.16.<sup>14</sup> The bulk of the trend might result from a systematically higher baryonic fraction and/or higher efficiency of conversion of baryons into stars in young early-type galaxies relative to old ones. For example, if many of our early-types form by a merger of star-forming systems, those which currently have the youngest populations are presumably the most recently merged and so spent the longest time in the star-forming phase.

We now examine in more detail how age, stellar metallicity and  $\alpha/\text{Fe}$  ratio depend on stellar and dynamical mass. This is shown in Fig. 3.17 for the early-type galaxies in our primary sample (Table 3.4 provides simple linear fits to the relations shown in the figure). The relations followed by age, metallicity and  $\alpha/\text{Fe}$  ratio as a function of stellar mass (right-hand panels) reflect the conclusions drawn from our analysis of the CMR and  $\text{Mg}_2-\sigma_V$  relations in Section 3.3.1 and 3.3.2. In particular, we find that light-weighted age increases (with a small scatter) with stellar mass in galaxies more massive than  $10^{11}M_\odot$ , while there is a clear indication of a tail towards younger ages in less massive galaxies (Panel d; see also fig.12 of Paper I). This confirms the results of several previous studies of smaller samples of early-type galaxies at low- and slightly higher redshifts (e.g. Caldwell & Rose 1998; Poggianti et al. 2001; Thomas et al. 2005; van Dokkum & Ellis 2003; Treu et al. 2005). Stellar metallicity increases all the way from the least massive to the most massive galaxies in our sample (Panel e). The relation tends to steepen at stellar masses less than about  $\sim 3 \times 10^{10}M_\odot$ , i.e. the characteristic mass scale of several observed bimodalities (see Paper I, Kauffmann et al. 2003; Baldry et al. 2004). We note that the dependence of stellar metallicity on stellar mass found here for early-type galaxies resembles quite closely the relation presented by Tremonti et al. (2004) for a sample of SDSS star-forming galaxies.

The increase in metallicity with stellar mass, and hence the CMR, is a natural prediction of different scenarios of early-type galaxy formation. In models in which the galaxies form monolithically in a single dissipationless collapse, star formation and chemical enrichment are generally assumed to be interrupted by the onset of galactic winds following the major episode of star formation. Since massive galaxies with deep potential wells are able to retain

<sup>14</sup>For example, at  $M_{dyn} \sim 10^{11}M_\odot$ , stellar mass increases from  $\log M_*/M_\odot \sim 10.75$  for  $\log(t_r/\text{yr}) = 10$  to  $\sim 10.9$  for  $\log(t_r/\text{yr}) = 9.5$ .

### 3 Physical origin of the colour-magnitude and the $Mg_2-\sigma_V$ relations for early-type galaxies

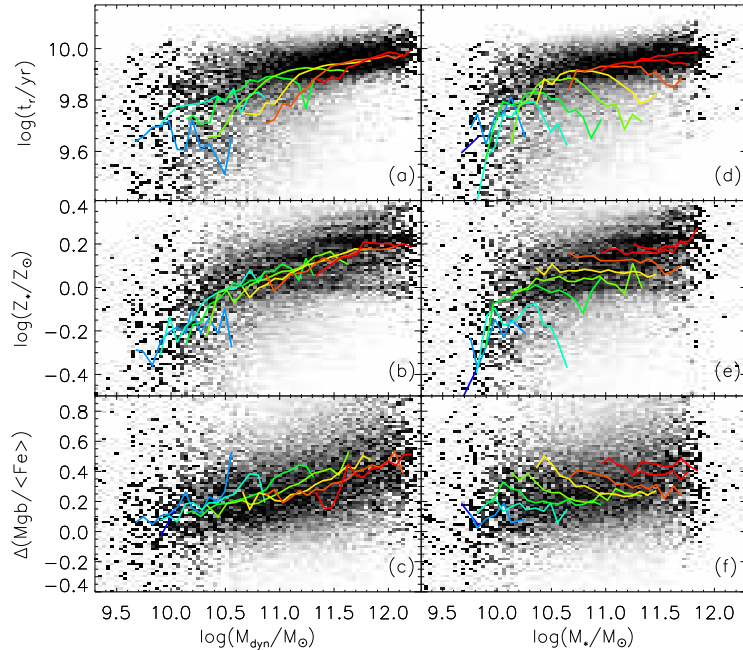


**Figure 3.17:** Left: Correlations between different physical parameters and the dynamical mass estimated within the  $r$ -band Petrosian half-light radius (see equation 3.2): (a) Light-weighted age; (b) stellar metallicity; (c)  $\alpha$ /Fe-estimator  $\Delta(Mgb/\langle Fe \rangle)$ . The grey scale indicates the density of points at each location in the diagram, normalised to the total number of galaxies at fixed  $\log(M_{dyn}/M_{\odot})$ . The solid lines represent the median relations for galaxies in different bins of stellar mass, centred on  $\log(M_*/M_{\odot}) = 9.6, 9.9, 10.2, 10.5, 10.8, 11.1, 11.4, 11.7$  (increasing from blue to red). Right: Correlations between the same physical parameters and stellar mass. In this case, the solid lines represent the median relations for galaxies in different bins of dynamical mass, centred on  $\log(M_{dyn}/M_{\odot}) = 9.6, 9.9, 10.2, 10.5, 10.8, 11.1, 11.4, 11.7, 12$  (increasing from blue to red).

their gas for much longer times and so to reach higher metallicities than less massive galaxies, this scenario accounts for the CMR as a metallicity sequence (Larson 1974; Bressan et al. 1994; Tantalo et al. 1996; Arimoto & Yoshii 1987). Early models of hierarchical galaxy formation neglected chemical enrichment and failed to produce sufficiently red, luminous elliptical galaxies (Kauffmann et al. 1993; Cole et al. 1994). However, subsequent renditions of these models have been able to reproduce the observed slope and scatter of the CMR and of the  $Mg_2-\sigma_V$  relation by including chemical evolution and strong feedback even in massive galaxies together with metallicity-dependent population synthesis

### 3.3 Physical origin of observed relations for early-type galaxies

models (Kauffmann & Charlot 1998; De Lucia et al. 2004). In this respect, the CMR of early-type galaxies does not represent a powerful tool to discriminate between the monolithic and merger formation scenarios (Kaviraj et al. 2005).

Additional clues about the formation of early-type galaxies may lie in their chemical abundance patterns. Fig. 3.17f shows that the  $\alpha/\text{Fe}$  abundance ratio, as traced by the quantity  $\Delta(\text{Mgb}/\langle\text{Fe}\rangle)$  (Section 4.2.1), increases linearly with  $\log M_*$ . This result, which was anticipated in several previous studies of early-type galaxies (Worthey et al. 1992; Jørgensen 1999; Greggio 1997), has been quantified using stellar population models with variable metal abundance ratios (Trager et al. 2000b; Mehlert et al. 2003; Thomas et al. 2005). If we consider as  $\alpha$ -enhanced those galaxies with  $\Delta(\text{Mgb}/\langle\text{Fe}\rangle) > 0.2$  (to account for the typical observational error on  $\text{Mgb}/\langle\text{Fe}\rangle$ ), Fig. 3.17f indicates that early-type galaxies with solar abundance ratios are found only at  $M_* \lesssim 10^{10.5} M_\odot$ , corresponding roughly to velocity dispersions  $\sigma_V \lesssim 100 \text{ km s}^{-1}$ . This is similar to the conclusion drawn by Kuntschner et al. (2001), based on the analysis of a sample of 72 early-type galaxies in groups and clusters.

The observed range in  $\alpha/\text{Fe}$  abundance ratio and the increase of this ratio with stellar mass constitute a challenge for galaxy formation models. If the enrichment in  $\alpha$  elements relative to iron reflects the star formation timescale, as is assumed in standard chemical evolution models, the values  $\Delta(\text{Mgb}/\langle\text{Fe}\rangle) > 0.2$  found in high-mass early-type galaxies require star formation timescales of the order 1–2 Gyr (see Section 3.4). Such short timescales are plausible for the onset of galactic winds in the classical monolithic collapse scenario. Hierarchical models can also produce star formation histories which are peaked at high redshift for massive early-type galaxies, although subsequent star formation is expected at lower redshift in most models (Kauffmann 1996; Thomas 1999). A possible solution to this problem may be the suppression of late gas cooling (and hence star formation) by AGN-driven outflows in massive early-type galaxies. As shown by various recent models of hierarchical galaxy formation accounting for the combined effects of star formation and black hole accretion, the feedback provided by active galactic nuclei can halt star formation on short timescales (Granato et al. 2001, 2004; Springel et al. 2005; Croton et al. 2006; De Lucia et al. 2006). This mechanism is expected to be most effective in massive halos hosting supermassive black holes, for which the timescale to drive outflows could be as short as 1 Gyr (Granato et al. 2004). Hence, the increase in the  $\alpha/\text{Fe}$  abundance ratio with stellar mass adds important constraints to models of early-type galaxy formation.

Fig. 3.17 also allows us to compare how age, metallicity and  $\alpha/\text{Fe}$  ratio vary with dynamical mass (left-hand panels) versus stellar mass (right-hand panels). In the left-hand panels, lines of different colours show the median relations between each parameter and  $M_{\text{dyn}}$  followed by galaxies in different

### 3 Physical origin of the colour-magnitude and the $\text{Mg}_2\text{-}\sigma_V$ relations for early-type galaxies

bins of stellar mass, increasing from  $\log(M_*/M_\odot) = 9.6$  to 11.7 in steps of  $\sim 0.3$  dex (from blue to red). In the right-hand panels, analogous lines show the median relations between each parameter and  $M_*$  followed by galaxies in different bins of dynamical mass. Fig. 3.17d shows that, at fixed dynamical mass, galaxies with large  $M_*$  tend to be younger than those with small  $M_*$  (in agreement with the result of Fig. 3.15b above). This trend is noticeable for dynamical masses in the range  $10^{10} \lesssim M_{\text{dyn}} \lesssim 10^{11.5} M_\odot$ . In contrast, at fixed dynamical mass, stellar metallicity is almost independent of  $M_*$  (Fig. 3.17e). In Fig. 3.17f, galaxies with large  $M_*$  tend to have slightly lower  $\Delta(\text{Mgb}/\langle\text{Fe}\rangle)$  and hence  $\alpha/\text{Fe}$  than those with small  $M_*$  at fixed  $M_{\text{dyn}}$ . This is consistent with the trend between  $\Delta(\text{Mgb}/\langle\text{Fe}\rangle)$  and age identified in Fig. 3.18 below. A remarkable conclusion from the comparison between the right- and left-hand panels in Fig. 3.17 is that the chemical composition of early-type galaxies appears to depend primarily on dynamical mass rather than stellar mass.

It is also of interest to examine the relations between age, metallicity and  $\alpha/\text{Fe}$  ratio. These are shown in Fig. 3.18 for our primary sample of early-type galaxies. In each panel, lines of different colours indicate the median trends followed by galaxies in different bins of velocity dispersion, from  $\sigma_V \sim 80 \text{ km s}^{-1}$  (purple) to  $\sim 300 \text{ km s}^{-1}$  (yellow). Fig. 3.18b shows that, at fixed velocity dispersion, age and metallicity are strongly anticorrelated for galaxies older than  $\log(t_r/\text{yr}) = 9.8$ . Bernardi et al. (2005), who *assume* that the scatter about the CMR is caused entirely by age variations, suggest that young galaxies may be more metal-rich than older galaxies at fixed velocity dispersion. Other previous studies also invoked an age-metallicity anticorrelation to explain the tightness of the colour-magnitude and the  $\text{Mg}_2\text{-}\sigma_V$  relations (e.g., Jørgensen 1999; Ferreras et al. 1999; Trager et al. 2000a; Terlevich & Forbes 2002, but see Kuntschner et al. 2001). However, the slope of this anticorrelation in Fig. 3.18b is consistent with the slope of the age-metallicity degeneracy for individual galaxies quantified in Paper I using the same sample of early-type galaxies. Thus, we cannot conclude here whether this anticorrelation is real or induced by correlated errors, but we note that the apparent scatter in age of massive, old ellipticals is consistent with the measurement error and the scatter in metallicity is quite small.

Fig. 3.18c shows the relation between  $\Delta(\text{Mgb}/\langle\text{Fe}\rangle)$  and metallicity for the galaxies in our sample. Interestingly, even though both the colour-magnitude and the  $\text{Mg}_2\text{-}\sigma_V$  relations imply an increase in both total metallicity and  $\alpha/\text{Fe}$  with mass, we do not identify any significant correlation between these two quantities (but see Fig. 3.19a below). This is true for the sample as a whole and for subsets of galaxies with fixed velocity dispersion. Instead,  $\Delta(\text{Mgb}/\langle\text{Fe}\rangle)$  appears to correlate more strongly with light-weighted age for  $\log(t_r/\text{yr}) \gtrsim 9.7$ , independent of galaxy velocity dispersion (Fig. 3.18a). Old galaxies appear

### 3.3 Physical origin of observed relations for early-type galaxies

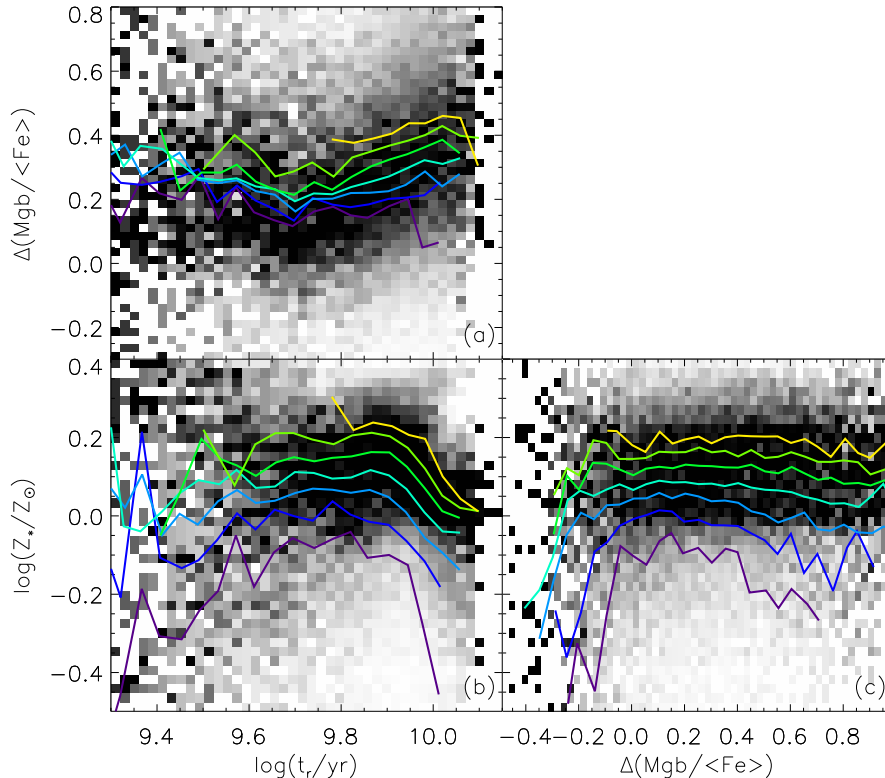


**Figure 3.18:** Correlations between stellar metallicity, light-weighted age and  $\alpha/\text{Fe}$ -estimator  $\Delta(\text{Mgb}/\langle\text{Fe}\rangle)$ . The solid lines represent the median relations for galaxies in different bins of velocity dispersion, centred on  $\log(\sigma_V/\text{km s}^{-1}) = 1.9, 2, 2.1, 2.2, 2.3, 2.4, 2.5$  (increasing from purple to yellow). The grey scale indicates the density of galaxies with respect to the total at fixed abscissa.

to have larger  $\alpha/\text{Fe}$  ratio than younger ones. This may be expected from the late enrichment in iron by Type Ia supernovae in galaxies which completed their star formation more recently, if the  $\alpha/\text{Fe}$  ratio reflects the star formation timescale. We might be tempted to relate star formation efficiency (and hence  $\alpha$ -enhancement) to stellar surface mass density, if the scaling between star formation rate and gas surface mass density in spiral galaxies can be extended to the progenitors of early-type galaxies (e.g. Schmidt 1959; Kennicutt 1998). Fig. 3.19b shows  $\Delta(\text{Mgb}/\langle\text{Fe}\rangle)$  as a function of surface stellar mass density for the galaxies in our sample. The lines of different colours indicate the median trends followed by galaxies in different age bins, from  $t_r \sim 3$  to 10 Gyr. We do not detect any significant correlation between  $\Delta(\text{Mgb}/\langle\text{Fe}\rangle)$  and

### 3 Physical origin of the colour-magnitude and the $Mg_2-\sigma_V$ relations for early-type galaxies

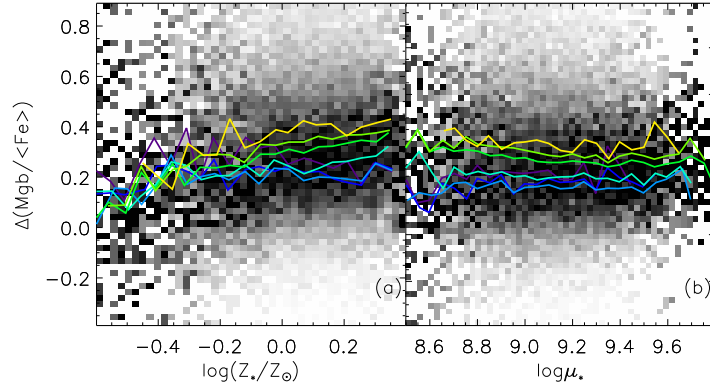


**Figure 3.19:**  $\alpha$ /Fe-estimator  $\Delta(\text{Mgb}/\langle\text{Fe}\rangle)$  plotted against (a) stellar metallicity and (b) surface stellar mass density within the  $r$ -band Petrosian half-light radius  $R_{50,r}$ . The solid lines represent the median relations for galaxies in different bins of light-weighted age, centred on  $\log(t_r/\text{yr}) = 9.5, 9.6, 9.7, 9.8, 9.9, 10, 10.1$  (increasing from purple to yellow).

surface stellar mass density. For completeness, in Fig. 3.19a, we show again  $\Delta(\text{Mgb}/\langle\text{Fe}\rangle)$  as a function of metallicity, as in Fig. 3.18c (the grey scale in this case indicates the distribution of galaxies as a function of  $\Delta(\text{Mgb}/\langle\text{Fe}\rangle)$  at fixed metallicity). There appears to be a mild correlation between  $\alpha$ /Fe and metallicity for galaxies in fixed age bins, in agreement with the results of Trager et al. (2000b).

### 3.4 Summary and conclusions

We have analysed a sample of 26,003 early-type galaxies selected from the SDSS DR2 on the basis of their light concentration. Light-weighted ages, stellar metallicities and stellar masses for this sample were previously derived through the comparison of a set of carefully selected spectral absorption features with a comprehensive library of high-resolution population synthesis models, encompassing the full range of physically plausible star formation histories (paper I). In addition to these physical parameters, we have considered here an empirical estimate of the  $\alpha$ -elements-to-iron abundance ratio, given by the offset  $\Delta(\text{Mgb}/\langle\text{Fe}\rangle)$  between the observed ratio of the Mgb and  $\langle\text{Fe}\rangle$  indices of a galaxy and that predicted by the best fitting model in the library (which has scaled-solar abundance ratios). We have used these data to investigate the physical origin of two well-known scaling relations for early-type galaxies: the colour-magnitude and the  $Mg_2-\sigma_V$  relations.

Our analysis demonstrates unambiguously and with unprecedentedly good statistics that both the colour-magnitude and the  $Mg_2-\sigma_V$  relations are primarily sequences in galaxy stellar mass. At increasing stellar mass, as traced by either luminosity or velocity dispersion, the increasing colour and  $Mg_2$ -absorption line strength along the relations reflect an increase in both total metallicity and  $\alpha/Fe$  ratio. Moreover, the galaxies in our sample cover a range in age of about 3 – 4 Gyrs, with more massive galaxies being on average older than low-mass galaxies. While at high masses early-type galaxies have the same mean age (and a small scatter in metallicity), at lower masses there is an increasing spread toward younger ages. This age spread dominates the scatter about the observed relations at low masses, in the sense that younger galaxies deviate toward bluer colours and lower  $Mg_2$  index strengths than older galaxies of the same mass. These results are consistent with the conclusions from previous studies based on smaller samples of early-type galaxies (Kodama & Arimoto 1997; Colless et al. 1999; Vazdekis 2001; Worthey & Collobert 2003). In addition, we find that the scatter in metallicity at fixed stellar mass contributes significantly to the scatter about the two observational scaling relations, in particular at high masses.

We have checked that our main conclusions are not affected by possible dust effects and that they are robust against sample selection. In particular, the possible contamination of our sample by bulge-dominated star-forming galaxies, which could amount to  $\sim 10$  percent, does not substantially affect our results.

For a small subsample of 1765 galaxies we used information on environmental density available from Kauffmann et al. (2004) to explore the dependence of the observed scaling relations and the stellar physical parameters on environment. We have found a small but detectable difference in the zero-point of the two relations, in the sense that early-type galaxies in dense environments tend to have redder colours and stronger  $Mg_2$  absorption indices than galaxies in low-density regions, at fixed luminosity or velocity dispersion. We also find a systematic increase in the scatter about both relations from high to low densities. These variations appear to be induced by small differences in the light-weighted age and metallicity of galaxies located in different environments. While galaxies with similar mass have the same element abundance ratio regardless of environment, there is an increasing spread toward younger ages and lower metallicities in low-density environments. At fixed stellar mass, early-type galaxies in dense regions are on average 0.02 dex older and more metal-rich than early-type galaxies in low-density regions. We note that these trends are very small and it will be worth re-examining them when a better statistics is available. If confirmed, these results are in agreement with previous studies indicating that early-type galaxies in clusters started to form stars

### 3 Physical origin of the colour-magnitude and the $\text{Mg}_2\text{-}\sigma_V$ relations for early-type galaxies

earlier than, but on the same timescale as early-type galaxies in the field (e.g. Thomas et al. 2005; Bernardi et al. 2006; Clemens et al. 2006).

We have also studied the dependence of the stellar mass on the dynamical mass estimated within the  $r$ -band Petrosian half-light radius of a galaxy. The relation is well described by a power law of exponent  $0.783 \pm 0.019$  (equation 3.3), implying a decrease in the stellar-to-dynamical mass ratio from low- to high-mass galaxies. The correlations of physical parameters with the dynamical mass estimated in this way suggests that metallicity and element abundance ratios in early-type galaxies are more fundamentally related to dynamical mass than to stellar mass.

The increase in total metallicity with dynamical mass favours the classical interpretation of the colour-magnitude and  $\text{Mg}_2\text{-}\sigma_V$  relations in terms of supernova-driven winds (e.g. Trager et al. 2000a; Thomas et al. 2005). To account for the simultaneous increase in total metallicity and  $\alpha/\text{Fe}$  ratio with mass, galactic winds should occur at early times, i.e. prior to the onset of Type Ia supernovae (on a timescale of a few Gyr), which are the main contributors to Fe-peak elements. The winds will be more effective in removing  $\alpha$  elements (produced by Type II supernovae on a time scale of  $\sim 10^8$  yr) from low-mass galaxies with shallow potential wells, while they should not reduce significantly the fraction of primordial gas and hence star formation (Mac Low & Ferrara 1999). Much observational evidence has been accumulated for the importance of galactic outflows in galaxies with masses up to at least  $10^{10} M_\odot$  (Lehnert & Heckman 1996; Heckman et al. 2000; Pettini et al. 2000). Our results, if interpreted in terms of galactic winds, indicate that even more massive galaxies (with masses up to  $\sim 10^{11} M_\odot$  in stars) have been affected by the ejection of metals through galactic winds.

The above scenario, however, cannot account alone for the observed values of  $\alpha/\text{Fe}$  in early-type galaxies. In a galactic-wind scenario, massive galaxies are predicted to have solar  $\alpha/\text{Fe}$  abundance ratios, while low-mass galaxies, which lose  $\alpha$  elements at early times, should have lower than solar  $\alpha/\text{Fe}$  ratios. Instead, galaxies with stellar masses less than about  $3 \times 10^{10} M_\odot$  (corresponding to velocity dispersions less than  $\sim 100 \text{ km s}^{-1}$ ) are observed to have nearly solar  $\alpha/\text{Fe}$  ratios, while this ratio increases to super-solar values in more massive galaxies (the quantity  $\Delta(\text{Mgb}/\langle\text{Fe}\rangle)$  reaching values around 0.3 in galaxies with stellar masses near  $3 \times 10^{11} M_\odot$ ; see Fig. 3.17).

The super-solar  $\alpha/\text{Fe}$  abundance ratios of massive early-type galaxies suggest that these formed on a relatively short timescale and/or have/have had an IMF skewed towards high-mass stars. An IMF enriched in massive stars will produce a larger ratio of Type II to Type Ia supernovae, and hence a larger  $\alpha/\text{Fe}$  ratio. Nagashima et al. (2005) have shown that a top-heavy IMF during the burst ignited by the major merger that formed an elliptical galaxy

can reproduce the observed range in  $\alpha/\text{Fe}$  ratios. However, none of the models they explore yields the observed correlation of  $\alpha/\text{Fe}$  with velocity dispersion (a model in which thermal conduction prevents the gas from cooling at the centres of massive halos is able to produce an increase in the  $\alpha$ -element abundance, but not the  $\alpha/\text{Fe}$  ratio, with mass).

An interpretation of the  $\alpha/\text{Fe}$  ratio in terms of the star formation timescale is supported by the correlation we find between  $\Delta(\text{Mgb}/\langle\text{Fe}\rangle)$  and light-weighted age, independent of mass (Fig. 3.18). This suggests that galaxies with longer star formation timescales (and thus with more recently formed stellar populations) have lower  $\alpha/\text{Fe}$  ratio than galaxies formed on shorter timescales, because they had time to recycle the Fe-peak elements ejected by Type Ia supernovae. We also find that light-weighted age increases with stellar mass with negligible scatter at masses above  $10^{11} M_{\odot}$  (Fig. 3.17d). Early-type galaxies less massive than about  $\sim 10^{11} M_{\odot}$  display an extended tail toward younger ages, the mean age declining markedly with decreasing mass. This suggests either that low-mass galaxies formed more recently than high-mass galaxies, or that they have a more extended star formation history (consistent with their solar  $\alpha/\text{Fe}$  ratios).

Our results represent further evidence for a shift in stellar growth toward less massive galaxies in recent epochs (Cowie et al. 1996; De Lucia et al. 2004; Kodama & et al. 2004; Yi et al. 2005; Treu et al. 2005). This ‘downsizing’ scenario may appear at odds with the expectations of original hierarchical models of galaxy formation. However, observations and the hierarchical paradigm can be reconciled if detailed physics of feedback from supernovae, active galactic nuclei or thermal conduction is introduced (e.g. Benson et al. 2003; Granato et al. 2004; Nagashima et al. 2005). These sources of feedback could inhibit star formation on timescales short enough for the bulk of the star formation to be completed before Type Ia supernovae can substantially increase the iron abundance in massive galaxies. Springel et al. (2005) have shown that, in major mergers of spiral galaxies hosting supermassive black holes, AGN feedback provides a mechanism that can quench star formation on short timescales. This mechanism is more efficient in the most massive early-type galaxies and leaves dwarf spheroids almost unaffected. We also note that the short star formation timescales (i.e. high formation redshifts) of massive early-type galaxies do not preclude longer assembly timescales (De Lucia et al. 2006): massive early-type galaxies could appear old even if they assembled relatively recently. In this context, the new constraints derived here on the physical origin of the colour-magnitude and  $\text{Mg}_2-\sigma_V$  relations for early-type galaxies represent a valuable reference for future models.

## Acknowledgments

We thank Mariangela Bernardi for helpful discussion on sample selection and the anonymous referee for valuable suggestions that have improved our analysis. A.G. and S.C. thank the Alexander von Humboldt Foundation, the Federal Ministry of Education and Research, and the Programme for Investment in the Future (ZIP) of the German Government for funding through a Sofja Kovalevskaja award. A.G. thanks the European Association for Research in Astronomy training site (EARA) and the European Community for a Marie Curie EST fellowship (MEST-CT-2004-504604). J.B. acknowledges the receipt of FCT fellowship BPD/14398/2003.

Funding for the creation and distribution of the SDSS Archive has been provided by the Alfred P. Sloan Foundation, the Participating Institutions, the National Aeronautics and Space Administration, the National Science Foundation, the US Department of Energy, the Japanese Monbukagakusho, and the Max Planck Society. The SDSS Web site is <http://www.sdss.org/>. The Participating Institutions are the University of Chicago, Fermilab, the Institute for Advanced Study, the Japan Participation Group, the Johns Hopkins University, the Max Planck Institute for Astronomy (MPIA), the Max Planck Institute for Astrophysics (MPA), New Mexico State University, Princeton University, the United States Naval Observatory, and the University of Wash-

## Bibliography

- Abazajian K., et al. 2004, AJ, 128, 502
- Abraham R. G., Smecker-Hane T. A., Hutchings J. B., Carlberg R. G., Yee H. K. C., Ellingson E., Morris S., Oke J. B., Rigler M., 1996, ApJ, 471, 694
- Arimoto N., Yoshii Y., 1987, A&A, 173, 23
- Baldry I. K., Glazebrook K., Brinkmann J., Ivezić Ž., Lupton R. H., Nichol R. C., Szalay A. S., 2004, ApJ, 600, 681
- Baldwin A., Phillips M. M., Terlevich R., 1981, PASP, 93, 817
- Baum W. A., 1959, PASP, 71, 106
- Bender R., Burstein D., Faber S. M., 1992, ApJ, 399, 462
- Bender R., Burstein D., Faber S. M., 1993, ApJ, 411, 153
- Benson A. J., Bower R. G., Frenk C. S., Lacey C. G., Baugh C. M., Cole S., 2003, ApJ, 599, 38
- Bernardi M., Renzini A., da Costa L. N., Wegner G., Alonso M. V., Pellegrini P. S., Rit e C., Willmer C. N. A., 1998, ApJ, 508, L143
- Bernardi M., et al. 2003a, AJ, 125, 1817
- Bernardi M., et al. 2003b, AJ, 125, 1849
- Bernardi M., et al. 2003c, AJ, 125, 1866
- Bernardi M., et al. 2003d, AJ, 125, 1882
- Bernardi M., Sheth R. K., Nichol R. C., Schneider D. P., Brinkmann J., 2005, AJ, 129, 61
- Bernardi M., Nichol R. C., Sheth R. K., Miller C. J., Brinkmann J., 2006, AJ, 131, 1288

## Bibliography

---

- Blakeslee J. P., et al. 2003, ApJ, 596, L143
- Bower R. G., Lucey J. R., Ellis R. S., 1992, MNRAS, 254, 589
- Boylan-Kolchin M., Ma C-P., Quataert E., 2005, MNRAS, 362, 184
- Bressan A., Chiosi C., Fagotto F., 1994, ApJS, 94, 63
- Brinchmann J., Charlot S., White S. D. M., Tremonti C., Kauffmann G., Heckman T., Brinkmann J., 2004, MNRAS, 351, 1151
- Bruzual G., Charlot S., 2003, MNRAS, 344, 1000
- Burstein D., Davies R. L., Dressler A., Faber S. M., Lynden-Bell D., Terlevich R., Wegner G., 1988, in IAU Symp. 130: Large Scale Structures of the Universe Spiral Galaxies, Elliptical Galaxies and the Large-Scale Velocity Field Within 3500 Km/s of the Local Group. pp 177–+
- Caldwell N., Rose J. A., 1998, AJ, 115, 1423
- Caldwell N., Rose J. A., Concannon K. D., 2003, AJ, 125, 2891
- Cappellari M., et al. 2006, MNRAS, 366, 1126
- Chabrier G., 2003, PASP, 115, 763
- Clemens M. S., Bressan A., Nikolic B., Alexander P., Annibali F., Rampazzo, R., 2006, astro-ph/0603714
- Cole S., Aragon-Salamanca A., Frenk C. S., Navarro J. F., Zepf S. E., 1994, MNRAS, 271, 781
- Colless M., Burstein D., Davies R. L., McMahan R. K., Saglia R. P., Wegner G., 1999, MNRAS, 303, 813
- Cowie L. L., Songaila A., Hu E. M., Cohen J. G., 1996, AJ, 112, 839
- Croton D. J., Springel V., White S. D. M., De Lucia G., Frenk C. S., Gao L., Jenkins A., Kauffmann G., Navarro J. F., Yoshida N., 2006, MNRAS, 365, 11
- De Lucia G., Kauffmann G., White S. D. M., 2004, MNRAS, 349, 1101
- De Lucia G., Poggianti B. M., Aragón-Salamanca A., Clowe D., Halliday C., Jablonka P., Milvang-Jensen B., Pelló R., Poirier S., Rudnick G., Saglia R., Simard L., White S. D. M., 2004, ApJ, 610, L77

- De Lucia G., Springel V., White S. D. M., Croton D., Kauffmann G., 2006, MNRAS, 366, 499
- Denicoló G., Terlevich R., Terlevich E., Forbes D. A., Terlevich A., 2005, MNRAS, 358, 813
- de Vaucouleurs G., 1961, ApJS, 5, 233
- Djorgovski S., Davis M., 1987, ApJ, 313, 59
- Faber S. M., 1973, ApJ, 179, 731
- Faber S. M., Jackson R. E., 1976, ApJ, 204, 668
- Ferreras I., Charlot S., Silk J., 1999, ApJ, 521, 81
- Forbes D. A., Ponman T. J., 1999, MNRAS, 309, 623
- Gallazzi A., Charlot S., Brinchmann J., White S. D. M., Tremonti C. A., 2005, MNRAS, 362, 41
- Gonzalez J. J., Faber S. M., Worthey G., 1993, Bulletin of the American Astronomical Society, 25, 1355
- Granato G. L., De Zotti G., Silva L., Bressan A., Danese L., 2004, ApJ, 600, 580
- Granato G. L., Silva L., Monaco P., Panuzzo P., Salucci P., De Zotti G., Danese L., 2001, MNRAS, 324, 757
- Greggio L., 1997, MNRAS, 285, 151
- Guzman R., Lucey J. R., Carter D., Terlevich R. J., 1992, MNRAS, 257, 187
- Heckman T. M., Lehnert M. D., Strickland D. K., Armus L., 2000, ApJS, 129, 493
- Hogg D. W., et al. 2004, ApJ, 601, L29
- Humphrey P. J., Buote D. A., Gastaldello F., Zappacosta L., Bullock J. S., Brighenti F., Mathews W. G., 2005, astro-ph/0510819
- Jørgensen I., 1999, MNRAS, 306, 607
- Jørgensen I., Franx M., Kjaergaard P., 1996, MNRAS, 280, 167
- Kauffmann G., 1996, MNRAS, 281, 487

## Bibliography

---

- Kauffmann G., Charlot S., 1998, MNRAS, 294, 705
- Kauffmann G., et al. 2003, MNRAS, 341, 54
- Kauffmann G., White S. D. M., Heckman T. M., Ménard B., Brinchmann J., Charlot S., Tremonti C., Brinkmann J., 2004, MNRAS, 353, 713
- Kauffmann G., White S. D. M., Guiderdoni B., 1993, MNRAS, 264, 201
- Kaviraj S., Devriendt J. E. G., Ferreras I., Yi S. K., 2005, MNRAS, 360, 60
- Kennicutt R. C., 1998, ApJ, 498, 541
- Kodama T., Arimoto N., 1997, A&A, 320, 41
- Kodama T., Arimoto N., Barger A. J., Arag'on-Salamanca A., 1998, A&A, 334, 99
- Kodama T., Bower R. G., Bell E. F., 1999, MNRAS, 306, 561
- Kodama T., et al. ., 2004, MNRAS, 350, 1005
- Kormendy J., 1977, ApJ, 218, 333
- Korn A. J., Maraston C., Thomas D., 2005, A&A, 438, 685
- Kuntschner H., Lucey J. R., Smith R. J., Hudson M. J., Davies R. L., 2001, MNRAS, 323, 615
- Kuntschner H., Smith R. J., Colless M., Davies R. L., Kaldare R., Vazdekis A., 2002, MNRAS, 337, 172
- Larson R. B., 1974, MNRAS, 166, 585
- Larson R. B., Tinsley B. M., Caldwell C. N., 1980, ApJ, 237, 692
- Lehnert M. D., Heckman T. M., 1996, ApJ, 462, 651
- Mac Low M., Ferrara A., 1999, ApJ, 513, 142
- Mehlert D., Thomas D., Saglia R. P., Bender R., Wegner G., 2003, A&A, 407, 423
- Nagashima M., Lacey C. G., Baugh C. M., Frenk C. S., Cole S., 2005, MNRAS, 358, 1247
- Nagashima M., Lacey C. G., Okamoto T., Baugh C. M., Frenk C. S., Cole S., 2005, MNRAS, 363L, 31

- Nelan J. E., Smith R. J., Hudson M. J., Wegner G. A., Lucey J. R., Moore S. A. W., Quinney S. J., Suntzeff N. B., 2005, *ApJ*, 632, 137
- Padmanabhan N., et al. 2004, *New Astronomy*, 9, 329
- Pettini M., Steidel C. C., Adelberger K. L., Dickinson M., Giavalisco M., 2000, *ApJ*, 528, 96
- Pierini D., Gavazzi G., Franzetti P., Scodreggio M., Boselli A., 2002, *MNRAS*, 332, 422
- Pimblet K. A., Smail I., Kodama T., Couch W. J., Edge A. C., Zabludoff A. I., O'Hely E., 2002, *MNRAS*, 331, 333
- Poggianti B. M., Bridges T. J., Carter D., Mobasher B., Doi M., Iye M., Kashikawa N., Komiyama Y., Okamura S., Sekiguchi M., Shimasaku K., Yagi M., Yasuda N., 2001, *ApJ*, 563, 118
- Poggianti B. M., Bridges T. J., Mobasher B., Carter D., Doi M., Iye M., Kashikawa N., Komiyama Y., Okamura S., Sekiguchi M., Shimasaku K., Yagi M., Yasuda N., 2001, *ApJ*, 562, 689
- Renzini A., 2006, *astro-ph/0603479*
- Salpeter E. E., 1955, *ApJ*, 121, 161
- Schmidt M., 1959, *ApJ*, 129, 243
- Schweizer F., Seitzer P., 1992, *AJ*, 104, 1039
- Shimasaku K., et al. 2001, *AJ*, 122, 1238
- Springel V., Di Matteo T., Hernquist L., 2005, *MNRAS*, 361, 776
- Stanford S. A., Eisenhardt P. R., Dickinson M., 1998, *ApJ*, 492, 461
- Strateva I., et al. 2001, *AJ*, 122, 1861
- Tantalo R., Chiosi C., Bressan A., Fagotto F., 1996, *A&A*, 311, 361
- Terlevich A. I., Forbes D. A., 2002, *MNRAS*, 330, 547
- Terlevich A. I., Kuntschner H., Bower R. G., Caldwell N., Sharples R. M., 1999, *MNRAS*, 310, 445
- Thomas D., 1999, *MNRAS*, 306, 655
- Thomas D., Maraston C., Bender R., 2003, *MNRAS*, 339, 897

## Bibliography

---

- Thomas D., Maraston C., Bender R., de Oliveira C. M., 2005, *ApJ*, 621, 673
- Thomas D., Maraston C., Korn A., 2004, *MNRAS*, 351, L19
- Trager S. C., Faber S. M., Worthey G., González J. J., 2000a, *AJ*, 120, 165
- Trager S. C., Faber S. M., Worthey G., González J. J., 2000b, *AJ*, 119, 1645
- Tremonti C. A., et al. 2004, *ApJ*, 613, 898
- Treu T., Ellis R. S., Liao T. X., van Dokkum P. G., 2005, *ApJ*, 622, L5
- van Dokkum P. G., Ellis R. S., 2003, *ApJ*, 592, L53
- Vazdekis A., 2001, *Ap&SS*, 276, 921
- Vazdekis A., Kuntschner H., Davies R. L., Arimoto N., Nakamura O., Peletier R., 2001, *ApJ*, 551, L127
- Visvanathan N., Sandage A., 1977, *ApJ*, 216, 214
- White S. D. M., 1980, *MNRAS*, 191, 1P
- Worthey G., 1994, *ApJS*, 95, 107
- Worthey G., Collobert M., 2003, *ApJ*, 586, 17
- Worthey G., Faber S. M., Gonzalez J. J., 1992, *ApJ*, 398, 69
- Yi S. K., et al. 2005, *ApJ*, 619, L111
- York D. G., et al. 2000, *AJ*, 120, 1579
- Zibetti S., Gavazzi G., Scodreggio M., Franzetti P., Boselli A., 2002, *ApJ*, 579, 261

*Qué sed  
de saber cuánto!  
Qué hambre  
de saber  
cuántas  
estrellas tiene el cielo!*

Pablo Neruda, Oda a los numeros

# 4

## The stellar metallicity distribution in the local Universe

### Abstract

We combine stellar metallicity and stellar mass estimates for a large sample of galaxies drawn from the Sloan Digital Sky Survey Data Release Two (SDSS DR2) spanning wide ranges in physical properties, in order to derive an inventory of the total mass of metals locked up in stars in the local Universe. For galaxies with a high-signal-to-noise (S/N) spectrum we use the physical parameters estimates already derived and studied in the previous chapters. The accuracy of the stellar metallicity estimates is severely limited in galaxies with a low-S/N spectrum. To circumvent this problem, we generate a sample of high-S/N spectra by stacking the individual spectra of galaxies with similar velocity dispersions, absolute  $r$ -band magnitudes and 4000Å-break values. This allows us to accurately estimate stellar metallicity and stellar mass also for this class of galaxies, and thus to derive a fair estimate of the total amount of metals locked up in stars today. We estimate the density of metals  $\rho_Z$  and of baryons  $\rho_*$  in stars and, from these two quantities, we obtain an average stellar metallicity of  $\langle Z_* \rangle = 1.028 \pm 0.002_{-0.489}^{+0.152} Z_\odot$ , i.e. consistent with solar. Note that the large systematic uncertainty is dominated by the aperture bias, that can lead to overestimate the average stellar metallicity by almost a factor of two. We also study how metals are distributed in galaxies according to different properties, such as mass, morphology and light-weighted age, and we then compare such distributions with the corresponding distributions of stellar mass. We find that the bulk of the total amount of metals locked up in stars in the

## 4 The stellar metallicity distribution in the local Universe

---

local Universe resides in massive, bulge-dominated galaxies, with high 4000Å-break values corresponding to old stellar populations. Galaxies with stellar masses greater than  $10^{11} M_{\odot}$  and light concentration parameters characteristic of early-type galaxies contribute half of the total stellar metallicity, while hosting roughly 40 percent of the total mass in stars. Lower-mass galaxies ( $\lesssim 5 \times 10^{10} M_{\odot}$ ) with concentration parameters typical of late-type galaxies contribute only 25 percent of the total stellar metallicity, while hosting 35 percent of the total stellar mass.

### 4.1 Introduction

Constraining the star formation and chemical evolution histories of galaxies is one of the fundamental goals in observational cosmology. The importance of the cosmic chemical evolution of galaxies lies in the fact that it provides a link, through the cosmic star formation history (SFH), between the chemical, stellar and gaseous components of galaxies. The most direct way to constrain the star formation and chemical evolution history over cosmic times is to trace back galaxy properties (star formation rate, metallicity, stellar mass) through observations at different redshifts.

Several studies on high-redshift galaxies, selected with the ‘drop-out’ technique, have measured the evolution of the rest-frame UV emission density of galaxies and converted it into star formation or metal ejection rates. All these studies have converged into a picture in which the maximum of galaxy star formation activity occurs over the redshift range  $1 \lesssim z \lesssim 2$  (Connolly et al. 1997) and declines sharply from  $z = 1$  towards  $z = 0$  according to a law  $(1 + z)^{\alpha}$  with exponent  $\alpha$  that can range from 4 (Lilly et al. 1996) to 1.5 (as found by Cowie et al. 1999, implying that star formation continues smoothly till the present and occurs mainly in low-mass systems). More uncertain is the behaviour of the cosmic star formation rate at redshift higher than 2. Early studies by Madau et al. (1996) suggested a significant decrease in star formation rate density with redshift for  $z > 2$ , but these results suffer from the effect of dust on the star formation rates derived from the UV Spectral Energy Distribution (SED) of high-redshift galaxies. When dust corrections are included, the increase in star formation rate density from  $z \sim 4$  to  $z \sim 1 - 2$  is much more modest (e.g. Steidel et al. 1999; Ivison et al. 2002).

These observations can be reproduced by several models of chemical evolution history which include a self-consistent treatment of dust, linking the production of dust with the production of heavy elements (Pei & Fall 1995; Edmunds & Phillipps 1997; Pei et al. 1999). These models predict a broad peak of high star formation over the redshift range  $z \sim 1 - 2$  and then a rapid decline toward the present as also suggested by semianalytic models of galaxy

formation (e.g. Baugh et al. 1998).

An alternative approach to study the chemical and star formation history over cosmic times is through the so-called ‘fossil cosmology’, i.e. determining the past history of the Universe from its present contents. This approach has received new inputs from large spectroscopic surveys in the local Universe, such as the 2dF Galaxy Redshift Survey (2dFGRS, Colless et al. 2001) and the Sloan Digital Sky Survey (SDSS, York et al. 2000), which provide detailed spectral information for hundred thousands of galaxies. Baldry et al. (2002) and Glazebrook et al. (2003) looked at the ensemble of all galaxies and derived the ‘cosmic optical spectrum’ of the local Universe. This represents the average emission from all the objects in a representative volume of the Universe and has the advantage of being fitted by simpler models of star formation histories than those needed for individual objects. By parametrising the cosmic SFH with a power law  $(1+z)^\alpha$  in the redshift range  $0 < z < 1$  and  $(1+z)^\beta$  in the range  $1 \leq z < 5$ , they constrain the low-redshift slope to be  $2 < \alpha < 3$  and they find a shallower high-redshift slope in the range  $0 < \beta < 1$ .

Additional insight into the star formation rate and chemical evolution histories of galaxies can be gained studying other galaxy parameters such as stellar mass. Studying the evolution with redshift of the star formation rate as a function of galaxy stellar mass can give information about the contribution from different types of galaxies to the star formation rate density at different epochs. Heavens et al. (2004) and Jimenez et al. (2005) have applied a data compression algorithm (MOPED, Heavens et al. 2000) to extract from the optical spectrum of  $\sim 100,000$  SDSS DR1 galaxies the relative contribution of stellar populations of different ages to the total stellar mass of a galaxy. This is equivalent to trace the SFH of a galaxy. This allowed them to derive the cosmic SFH as a function of the present-day stellar mass of galaxies. Taking advantage of the near-infrared selection of the Gemini Deep Deep Survey (GDDS, Abraham et al. 2004), Juneau et al. (2005) studied the dependence of the cosmic star formation history directly on the stellar mass at the epoch of observation over the redshift range  $0.8 < z < 2$ . The results of both studies are consistent with those previously found by Brinchmann & Ellis (2000) for  $0 < z < 1$ , indicating that the most massive galaxies were dominated by star formation at high redshift and should have completed the bulk of their star formation by  $z \sim 1$ . While high- and intermediate-mass galaxies have transitioned to a quiescent phase of star formation by  $z \sim 1$ , less massive systems dominate the star formation rate density till the present epoch.

Another advantage of using the stellar mass is that it provides the coupling between the large-scale cosmological physics (structure growth through collapse and mergers) and the small-scale physics of star formation that govern the evolution of baryonic matter. Measuring the cosmic stellar mass history of

## 4 The stellar metallicity distribution in the local Universe

---

galaxies rather than the cosmic SFH represents a complementary approach in constraining the assembly history of galaxies (but equivalent in that it should correspond to the integral of the cosmic SFH over time). This approach has been adopted by Dickinson et al. (2003) who determined the stellar masses of galaxies in the Hubble Deep Field North and studied the evolution with redshift of the global stellar mass density out to  $z = 3$ . They find a rapid rise in the global stellar mass density from  $z = 2.7$  to  $z = 1$  and then a small change to the present day. These measurements, in agreement with previous estimates of the global SFH, suggest that the redshift range  $1 < z < 2.5$  is a critical epoch when galaxies are growing rapidly attaining their final stellar mass.

An important consistency check for all these studies comes from the comparison of the density of stellar mass and of metals at different epochs expected from the cosmic SFH and chemical enrichment history (i.e. the integral of these histories), with those directly measured. For this reason, much effort has been put in measuring the chemical composition and stellar mass of galaxies at different redshift. Direct measures of the chemical content of high-redshift galaxies is mostly limited to  $z < 1$  where optical nebular emission lines can be used (e.g. Kobulnicky & Zaritsky 1999; Lilly et al. 2003; Kobulnicky & Kewley 2004; Ellison et al. 2005). At higher redshift (up to  $z \sim 3$ ) systematic studies of the chemical composition of galaxies have been carried out on Lyman-break galaxies and UV-selected star-forming galaxies (e.g. Pettini et al. 2001; Steidel et al. 2004; Shapley et al. 2004; Erb et al. 2006). An alternative way to measure the metallicity of galaxies at arbitrarily high redshift is represented by studies on quasar absorption-line systems, in particular Damped Ly- $\alpha$  Absorbers (DLA), which provide the metallicity of gas-rich galaxies weighted by their cross-sectional area (e.g. Pettini et al. 1994; Lanzetta et al. 1995; Pettini et al. 1997). Similarly, several methods have been adopted to estimate the stellar masses of large samples of nearby galaxies from optical spectroscopy (e.g. Kauffmann et al. 2003; Gallazzi et al. 2005) or combining optical and near-IR photometry both for local galaxies (e.g. Cole et al. 2001; Bell et al. 2003) and for galaxies at redshift up to 1 (e.g. Brinchmann & Ellis 2000; Cohen 2002; Drory et al. 2004).

In this work we join information about the stellar mass and chemical properties of present-day galaxies, supported by the large statistics provided by the SDSS, in order to constrain the local values of the mass density of baryons and of metals locked up in stars in present-day galaxies. We can do this by exploiting new estimates of physical parameters, such as stellar metallicity and stellar mass, that we previously derived (Gallazzi et al. 2005, see Chapter 2) for a large sample of nearly  $2 \times 10^5$  galaxies drawn from the Sloan Digital Sky Survey Data Release Two (SDSS DR2). For each galaxy, we compared the

strengths of five spectral absorption features with negligible dependence on the  $\alpha/\text{Fe}$  ratio to a comprehensive library of star formation histories, based on a medium-high resolution population synthesis code (Bruzual & Charlot 2003). The higher resolution and the full temperature coverage of the models allowed us to interpret in this way the spectra of galaxies with different star formation histories, from quiescent early-type to actively star-forming galaxies. In the previous chapters we focused only on galaxies with high signal-to-noise (S/N) spectra, because of the poor constraints that can be obtained on stellar metallicity from low-S/N spectra. We circumvent this problem here by stacking individual spectra of low-S/N galaxies with similar properties in order to obtain (average) high-S/N spectra.

The final sample analysed span large ranges in physical, spectral and morphological properties, and constitute in this sense a representative sample of the local Universe. This allows us not only to quantify the total amount of metals locked up in stars in the present-day Universe, but also to study how metals and baryons are distributed among galaxies with different properties. In particular, we want to understand which are the properties, such as total stellar mass, morphology and light-weighted age, of the galaxies that contain the bulk of the mass and of the metals today.

The sample analysed is described in Section 4.2, along with the stacking technique adopted in order to include galaxies with low-S/N spectra. The results are discussed in Section 4.3 where we derive the mass density of baryons and of metals locked up in stars, expressed also in terms of the average stellar metallicity of the local Universe (Section 4.3.1). Section 4.3.2 provides an inventory of the stellar metallicity and stellar mass today. We finally summarise and conclude in Section 4.4. Throughout the chapter we adopt a flat cosmology with  $\Omega_m = 0.3$ ,  $\Omega_\Lambda = 0.7$  and  $H_0 = 70 \text{ km s}^{-1} \text{ Mpc}^{-1}$ .

## 4.2 The approach

In this section we give a brief description of the sample analysed and the method applied to derive estimates of physical parameters, such as stellar metallicity, light-weighted age and stellar mass, already discussed in Chapter 2 (Section 4.2.1). We then describe the stacking technique adopted to include low-S/N galaxies, in order to derive a fair estimate of the total metal budget of the local Universe (Section 4.2.2).

### 4.2.1 The sample

To derive an estimate of the total amount of metals locked up in stars today and to study their distribution as a function of various galaxy properties

## 4 The stellar metallicity distribution in the local Universe

---

we exploit the largest sample available to date, for which stellar metallicities, as well as other physical parameters, have been estimated. The sample analysed here is drawn from the main spectroscopic sample of the SDSS DR2 (Abazajian et al. 2004) and is based on 164,746 unique spectra of galaxies with Petrosian  $r$ -band magnitudes in the range  $14.5 \leq r \leq 17.77$  (after correction for Galactic extinction using the extinction maps of Schlegel et al. 1998), and with redshift<sup>1</sup> between 0.005 and 0.22. The sample includes all galaxy types, from star-forming late-type to quiescent early-type galaxies.

Bayesian-likelihood estimates of the stellar metallicities,  $r$ -band light-weighted ages and stellar masses of the galaxies in the sample have been obtained in our previous work, by comparing the spectrum of each galaxy to a library of Bruzual & Charlot (2003) models, covering the full range of physically plausible star formation histories. The comparison is based on five spectral absorption features, namely D4000,  $H\beta$  and  $H\delta_A + H\gamma_A$  as age-sensitive indices, and  $[Mg_2Fe]$  and  $[MgFe]'$  as metal-sensitive indices, all of which have at most a weak dependence on element abundance ratios. After constructing the probability density function of age, metallicity and stellar mass for every galaxy, the median of each likelihood distribution represents our estimate of the corresponding parameter, while half of the 16 – 84 percent interpercentile range gives the associated  $\pm 1\sigma$  uncertainty.

The analysis presented in Chapters 2 and 3 has been focused only on spectra with median S/N per pixel of at least 20. As explained there, this is the minimum S/N required in order to obtain reliable estimates of stellar metallicity. The quality of the spectrum influences directly the uncertainties in the derived physical parameters, stellar metallicity being the most affected one: the average error on stellar metallicity decreases from 0.21 dex to 0.12 dex when high-S/N galaxies only are considered. Our cut in S/N excludes roughly 75 percent of the galaxies and biases the sample towards high-surface brightness, high-concentration, low-redshift galaxies. Low-concentration galaxies are the most affected by the S/N cut: only 10 percent of the galaxies with concentration parameter  $C \leq 2.4$  satisfies this requirement. Excluding galaxies with  $S/N < 20$  we would therefore preferentially miss diffuse systems with potentially subsolar metallicity. In order to derive a fair estimate of the total metal budget in the local Universe we need instead to include all galaxies down to the magnitude limit of the survey, therefore low-S/N galaxies need to be considered as well.

---

<sup>1</sup>As explained in Chapter 2, we choose to limit the analysis in this redshift range, in order to avoid redshifts for which deviations from the Hubble flow can be substantial and to include galaxies in the stellar mass range  $10^8 - 10^{11} M_\odot$  with a signal-to-noise per pixel of at least 20.

### 4.2.2 The stacking technique

In order to include low-S/N galaxies, in addition to the subsample with  $S/N \geq 20$ , we divide galaxies in bins of velocity dispersion,  $r$ -band absolute magnitude and 4000Å-break and we create composite high-S/N spectra by coadding the spectra of all the galaxies falling into each bin. We first divide galaxies into bins of velocity dispersion  $\log \sigma_V$  of width  $\Delta \log \sigma_V = 0.05$  and bins of  $r$ -band absolute magnitude  $M_r$  of width  $\Delta M_r = 0.5$ . In each of such bins, galaxies are then ordered with increasing D4000 strength, and their spectra are stacked until a minimum S/N of 40 is reached. Each spectrum is weighted by  $1/V_{\max}$ , where  $V_{\max}$  is the maximum visibility volume given by the bright and faint magnitude limits of the survey, and by our requirement that the galaxy redshift be included between 0.005 and 0.22. The true number density of galaxies in the Universe should be estimated by accounting for galaxies that are missed due to, e.g., fibre collisions and spectroscopic failures. To correct for this, we have compared the  $r$ -band luminosity function obtained with our  $V_{\max}$  estimates with the luminosity function of Blanton et al. (2003) and derived a normalisation factor for our  $V_{\max}$  estimates. At the end we obtain 14,694 coadded spectra from 122,643 spectra of low-S/N galaxies in the redshift interval  $0.005 < z \leq 0.22$ .

Fig. 4.1a,b show the distribution in velocity dispersion and  $r$ -band absolute magnitude for the coadded spectra (solid line), compared to the distribution for the low-S/N galaxies (dot-dashed line). For each stacked spectrum we estimate the absolute magnitude  $M_j$  in a band  $j$  as the weighted sum of the luminosities  $L_{i,j}$  of the low-S/N galaxies contributing to the coadded spectrum, according to:

$$M_j = -2.5 \log \left( \frac{\sum_i (L_{i,j} w_i)}{\sum_i w_i} \right) + const. \quad (4.1)$$

where  $w_i$  is the weight  $1/V_{\max}$  of the individual galaxies. The distribution in these two quantities as obtained from the stacked spectra agrees very well with the original distribution for the low-S/N galaxies, as expected since galaxies have been binned in velocity dispersion and absolute magnitude. It is interesting to look how well the distribution in other morphological and photometric properties, into which galaxies are not explicitly binned, is reproduced. Fig. 4.1c,d show the distribution in the concentration parameter  $C = R_{90}/R_{50}$ , where  $R_{90}$  and  $R_{50}$  are the  $r$ -band Petrosian radii, and in rest-frame  $g - r$  colour. The colour of each stacked spectrum is estimated as the difference between magnitudes defined according to equation 4.1, while the concentration parameter assigned to each stacked spectrum is given by the weighted-average concentration parameter of the galaxies that contribute

## 4 The stellar metallicity distribution in the local Universe

---

to the stacked spectrum<sup>2</sup>. The distributions for the stacked spectra and the low-S/N galaxies agree reasonably well, due to the correlation between colour and velocity dispersion or magnitude, and the small scatter in concentration parameter at given  $\log\sigma_V$ ,  $M_r$  and D4000 (the mean absolute deviation in each such bin is typically 0.18). The dotted line in each panel of Fig. 4.1 shows for comparison the distribution for the high-S/N galaxies. This clearly shows that by excluding low-S/N galaxies we would miss a substantial fraction of small, low-concentration, blue galaxies, i.e. preferentially young, metal-poor, star forming galaxies.

We note that the distribution in concentration parameter obtained from the coadded spectra is clearly bimodal and narrower than the distribution of the original low-S/N sample. This is likely due to the definition of average concentration adopted for the coadded spectra. For a coadded spectrum with a concentration parameter close to the lower end of the possible range in  $C$ , the distribution in  $C$  of the galaxies that contribute to that coadded spectrum is skewed toward higher values of  $C$ . The average concentration (i.e. that assigned to the coadded spectrum) will be therefore shifted to higher values. Conversely, for a coadded spectrum with concentration close to the higher end of the  $C$  range, the distribution in  $C$  of the galaxies that contribute to that coadded spectrum is skewed toward lower values of  $C$ . In this case the average concentration will be shifted to lower values. The distributions in  $C$  for those coadded spectra which fall in the middle of the range in concentration parameter are instead symmetric and there is no systematic offset between the average and the mode of the distributions. This creates an artificial accumulation of points at the edges of the final distribution in concentration parameter of the coadded spectra (Fig 4.1c).

From each stacked spectrum, we also measure D4000, the high-order Balmer lines and the other spectral absorption indices defined in the Lick system, in the same way as they are measured from the spectrum of individual galaxies (see also section 2.2.2 of Chapter 2). They represent the  $1/V_{\max}$ -weighted average of the absorption indices of the galaxies that contribute to each coadded spectrum<sup>3</sup>. In Fig. 4.2 the distribution in the five spectral absorption features used to constrain stellar metallicity, age and stellar mass estimates as measured from the stacked spectra (solid line) is compared to the distribution for the original sample of 122,677 low-S/N galaxies (dotted line). The distributions for the stacked spectra appear in very good agreement with the

---

<sup>2</sup>Very similar results are obtained if we assign to each stacked spectrum a concentration parameter given by the ratio between the weighted-average Petrosian radii.

<sup>3</sup>More properly, the fluxes in the ‘pseudo-continuum’ and central bandpasses measured from the coadded spectrum are the  $1/V_{\max}$ -weighted average of the fluxes measured from individual galaxy spectra.

### 4.3 The distribution of metals in the local Universe

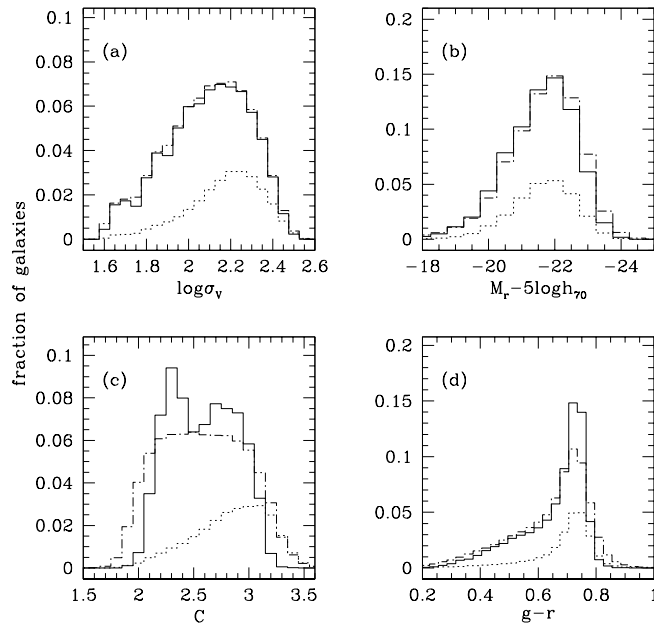


**Figure 4.1:** Distribution in velocity dispersion (a),  $r$ -band absolute magnitude (b), concentration parameter (c), and ( $k$ -corrected)  $g-r$  colour (d). The solid line in each panel shows the distribution for the sample of 14,694 stacked spectra. This can be compared to the distribution of the low-S/N galaxies, shown by the dot-dashed line. The dotted line in each panel represents instead the distribution of the high-S/N galaxies.

distributions for the original low-S/N galaxies. This is particularly true for D4000, as expected, since the spectral coaddition is performed on galaxies with similar D4000. The comparison for the other indices shows that the increased signal-to-noise ratio in the stacked spectra removes the tails of outliers present in the distributions for the original low-S/N galaxies.

### 4.3 The distribution of metals in the local Universe

In this section we derive an estimate of the total amount of baryons and metals locked up in stars in the local Universe, by combining the contribution of individual high-S/N galaxies and the low-S/N galaxies included in the coadded high-S/N spectra (Section 4.3.1). We then study how metals are distributed according to different galaxy properties (Section 4.3.2).

## 4 The stellar metallicity distribution in the local Universe

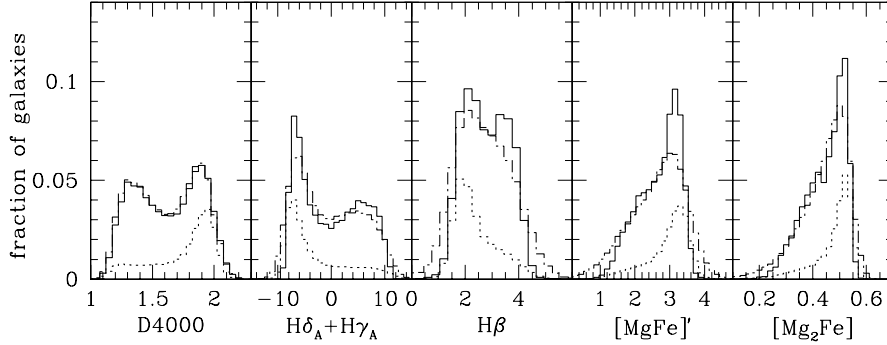


**Figure 4.2:** Distribution in the five spectral absorption features adopted to derive estimates of stellar metallicity, light-weighted age and stellar mass for the sample of 14,694 high-S/N stacked spectra (solid line), corresponding to 122,643 low-S/N galaxies. The absorption indices are measured off the stacked spectra in the same way as they are measured off the spectrum of individual galaxies and they represent the  $1/V_{\max}$ -weighted average index of all the galaxies that enter each stacked spectrum. The distribution in spectral indices as measured from the low-S/N spectra is shown for comparison by the dot-dashed line in each panel. Dotted lines represent the distribution for the 42,103 high-S/N galaxies.

### 4.3.1 The total stellar metallicity in the local Universe

Estimates of stellar metallicity, light-weighted age and stellar mass are derived from the coadded spectra in the same way as they are derived from individual galaxy spectra, as summarised in section 4.2.1 and more extensively described in Chapter 2. These physical parameters, in particular light-weighted age, are derived by fitting the galaxy spectra as observed and so they refer to the galaxies at the time of observation. In Section 4.3.2 we will study the distribution of metals as a function of stellar age. In order to define a characteristic age and interpret it as a characteristic redshift of metal production, we correct the measured light-weighted ages by adding the look-back time to the redshift at which the galaxy is observed. The age obtained in this way represents the effective (light-weighted) epoch when stars formed. For the stacked spectra we assume an average redshift of all the galaxies that contribute to each spectrum. The spread in redshift is on average 30 percent for redshift up to 0.1 and slightly less (20 percent) for  $z > 0.1$ .

The distribution in the derived parameters for the whole sample of 164,746

### 4.3 The distribution of metals in the local Universe

galaxies is shown in the left-hand panels of Fig. 4.3 (thick solid line). The distribution in stellar mass is well represented by a gaussian curve centred at  $\log(M_*/M_\odot) = 10.87$  of width 0.46 dex (i.e. the scatter in  $\log M_*$ ). By contrast, the distributions in age and metallicity are highly skewed, with a primary peak around 9 Gyr and  $1.4 \times Z_\odot$  respectively, and an extended tail towards younger ages and lower metallicities. In particular, light-weighted age shows a roughly bimodal distribution with a secondary bump around 4 Gyr.

The right-hand panels show the distribution in the errors on metallicity, age and mass, given by half of the 16 – 84 percent percentile range of the corresponding likelihood distribution. The dotted line shows the distribution for the high-S/N galaxies, while the dot-dashed line shows the distribution for the errors on the parameters of low-S/N galaxies as derived from the coadded spectra. This can be compared to the errors on the parameters of low-S/N galaxies as derived from their individual spectra (grey-shaded histogram). This makes clear the importance of a good spectral S/N in the determination of the physical parameters (in particular stellar metallicity, see also Chapter 2) and the advantage of the stacking technique: it allows us to retrieve the physical parameters of galaxies with low-S/N spectra with a much better accuracy than what we could do from their individual spectra.

The physical parameters derived from the stacked spectra can be interpreted as the  $(1/V_{\max})$ -weighted average stellar metallicity, age and stellar mass of the galaxies that contribute to each coadded spectrum. To test how well we can recover the physical parameters of individual galaxies with our stacking technique, we have generated a control sample of stacked spectra by coadding the spectra of individual high-S/N galaxies, for which reliable estimates of metallicity, age and mass can be derived, in the same way as described in Section 4.2.2 for the low-S/N galaxies. We then compare the physical parameters estimated from the coadded spectra with the  $(1/V_{\max})$ -weighted average parameters of the galaxies that contribute to each coadded spectrum. This is shown in Fig. 4.4 for stellar metallicity (left panel), stellar mass (middle panel) and light-weighted age (right panel). The histogram of the difference between the derived (‘stack’) and expected (‘wavg’) parameters is compared to gaussian distributions of width given by the average error on the derived parameter (dashed line) and by the average scatter in the physical parameter of the galaxies that contribute to each stacked spectrum (dot-dashed line). For all the three parameters we can recover the expected value within the typical error on each parameter. We note however that there is a small but systematic offset (dotted vertical line) of about  $-0.02$  dex in stellar mass and  $-0.03$  dex in light-weighted age. This offset likely originates from the fact that the stacked spectra tend to be dominated by younger, brighter stellar populations and therefore the derived light-weighted ages and mass-to-light ratio

## 4 The stellar metallicity distribution in the local Universe

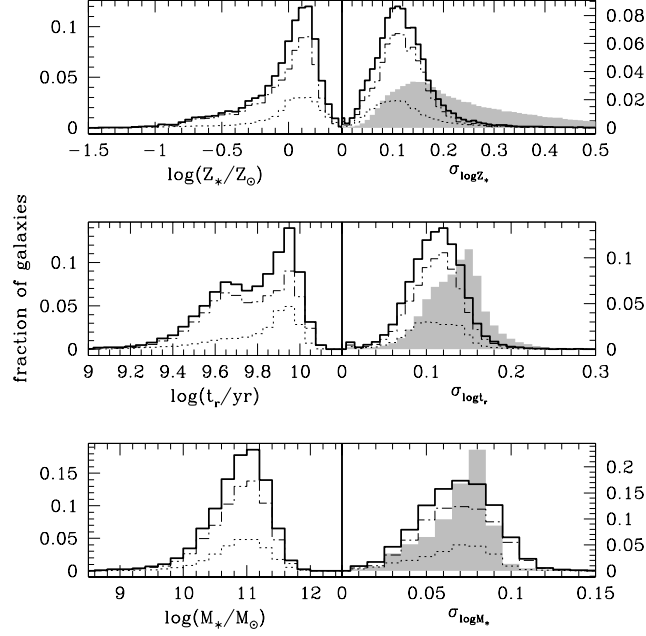


**Figure 4.3:** Distribution in stellar metallicity, light-weighted age and stellar mass (from top to bottom, left panels) for the final sample obtained by combining high-S/N galaxies and the low-S/N galaxies included in the coadded spectra (thick solid line). The dotted lines show the contribution by high-S/N galaxies only, while the dot-dashed lines represent the distribution in the parameters of the low-S/N galaxies, as derived from the stacked spectra. The right-hand panels show the distribution in the corresponding errors, given by half of the 16 – 84 percent percentile range of the likelihood distribution. The grey-shaded histograms in the right-hand panels give for comparison the distribution in the errors on the physical parameters of low-S/N galaxies as derived from their individual spectrum.

tend to be biased low. We take this into account as a systematic uncertainty.

Given our estimates of stellar metallicity and mass, we can now combine the contribution of both high-S/N galaxies and coadded spectra, to derive the density of metals in stars,  $\rho_Z$ , and the stellar mass density,  $\rho_*$ , at redshift 0, as follows:

$$\rho_Z = \sum_i (Z_i M_{*,i} w_i) + \sum_i (Z_i^{st} M_{*,i}^{st} W_i^{st}) \quad (4.2)$$

### 4.3 The distribution of metals in the local Universe

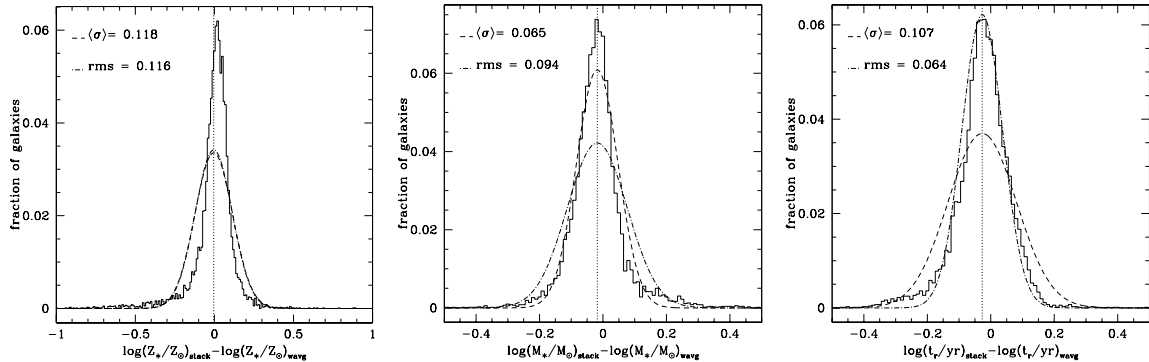


**Figure 4.4:** Distribution of the difference between the stellar metallicity (left), stellar mass (middle) and light-weighted age (right) estimated from the stacked spectra and the  $(1/V_{\text{max}})$ -weighted average parameter (indicated with 'wavg') of the galaxies that contribute to each stacked spectrum. Each histogram is compared to gaussian distributions of width given by the average error ( $\langle\sigma\rangle$ ) on the corresponding parameter (dashed line) and by the average rms scatter (rms) in the physical parameters of the galaxies that enter each stacked spectrum (dot-dashed line). For this test we used a control sample of stacked spectra obtained by coadding the spectra of individual high-S/N galaxies, for which reliable estimates of metallicity, mass and age can be obtained.

$$\rho_* = \sum_i (M_{*,i} w_i) + \sum_i (M_{*,i}^{st} W_i^{st}) \quad (4.3)$$

where  $Z_i$  and  $M_{*,i}$  are the median-likelihood estimates of the stellar metallicity and stellar mass of each high-S/N galaxy, and  $w_i$  are the weights  $1/V_{\text{max}}$ . The symbols  $Z_i^{st}$  and  $M_{*,i}^{st}$  refer to the stellar metallicity and mass estimated from the coadded spectra. These have to be weighted by  $W_i^{st} = \sum_j w_j$ , i.e. the sum of all the weights  $w_j$  of the low-S/N galaxies contributing to each stacked spectrum. The statistical error on  $\rho_Z$  and  $\rho_*$  can be estimated by standard error propagation from the uncertainties on metallicity and mass. The statistical error estimated in this way is very small and represents only the 0.2 percent of the value of  $\rho_Z$  that we derive and 0.1 percent of the value of  $\rho_*$ .

It is of course important to estimate the systematic error on these quantities, which is the dominant source of error. A possible systematic uncertainty comes from our stacking technique. We have shown above the comparison between the parameters derived from the coadded spectra and the  $(1/V_{\text{max}})$ -

## 4 The stellar metallicity distribution in the local Universe

---

weighted average parameter of the galaxies that contribute to each coadded spectrum. While we do not find any systematic offset in the stellar metallicity estimates, the stellar mass is systematically underestimated by 0.02dex. We take this as a source of systematic error on the mass estimates. Other possible sources of systematic uncertainty have been discussed in Chapter 2.

The largest systematic error that can affect our stellar metallicity estimates is the aperture bias, due to the fact that the SDSS spectra sample only a limited inner region of the galaxy. The light collected by the fibre is on average 30 percent of the total flux, but this fraction depends on the stellar mass, morphology and redshift of the galaxy. Due to the presence of metallicity gradients, the metallicities derived from the SDSS spectra are not representative of the galaxy as a whole but only of the bulge or central regions, which are generally more metal-rich than the outskirts. To estimate how much the derived metallicities can be overestimated we looked at the variation of the median metallicity from one edge of the survey to the other, for galaxies of different type and mass (see section 2.3.4 of Chapter 2). While disk-dominated galaxies show weak trends in metallicity with  $z/z_{\max}$  (where  $z_{\max}$  is the redshift at which the galaxy reaches the survey faint-magnitude limit), for bulge-dominated galaxies the largest change in median metallicity is about 0.2 dex. This is consistent with the typical metallicity gradients reported in the literature. A correction for this would require an accurate knowledge of metallicity gradients as a function of galaxy type and mass, and is not feasible here. This is clearly a concern in this work, where we want to estimate the *total* amount of metals in stars today. We express this bias as a systematic error of +0.2 dex, which is the largest bias identified in our sample.

Another possible source of systematic error comes from the choice of prior according to which our model library populates the parameter space, in particular the mixture of bursty and continuous star formation histories. By changing the fraction of bursts in the last 2 Gyr from 10 percent (our standard prior) to 50 percent, the derived stellar metallicities are higher by 0.04 dex on average and the stellar masses are lower by 0.04 dex. Finally, our stellar metallicity estimates may be biased due to the fact that the models used do not take into account the dependence on the  $\alpha/\text{Fe}$  abundance ratio. We expect our stellar metallicity estimates to be overestimated by at most 0.05 dex. To summarise, we estimate the total systematic error on stellar mass to be  $^{0.02}_{-0.04}$  dex (note that the upper error refers only to the stellar masses derived from the stacked spectra) and the total systematic error on stellar metallicity to be  $^{0.04}_{-0.25}$  dex. Finally, the stellar metallicities and stellar masses that enter in Equation 4.2 and 4.3 are the median of the corresponding likelihood distributions. We estimate the error that we make by taking the median instead of the mode of the likelihood distribution recalculating  $\rho_Z$  and  $\rho_*$  using the

### 4.3 The distribution of metals in the local Universe

mode as our metallicity and mass estimates.

Taking all this into account, our final estimates of  $\rho_Z$  and  $\rho_*$  are:

$$\rho_Z = 8.254 \pm 0.019_{-4.659}^{+1.957} \times 10^6 h_{70} M_\odot \text{ Mpc}^{-3} \quad (4.4)$$

$$\rho_* = 4.013 \pm 0.005_{-0.35}^{+0.353} \times 10^8 h_{70} M_\odot \text{ Mpc}^{-3} \quad (4.5)$$

As can be seen from Table 4.1, these values are consistent, within the large uncertainties, with other estimates of the density of metals and of baryons in stars in the local Universe derived from various sources in the literature.

We can now combine Equation 4.2 and 4.3 to estimate the (mass-weighted) average metallicity in stars in the nearby Universe, obtaining:

$$\begin{aligned} \langle Z_* \rangle &= \frac{\sum_i (Z_i M_{*,i} w_i) + \sum_i (Z_i^{st} M_{*,i}^{st} W_i^{st})}{\sum_i (M_{*,i} w_i) + \sum_i (M_{*,i}^{st} W_i^{st})} \\ &= 1.028 \pm 0.002_{-0.489}^{+0.152} Z_\odot \end{aligned} \quad (4.6)$$

The random error has been estimated from standard propagation of the errors on metallicity and mass, and the systematic uncertainty has been estimated taking into account the various sources of bias described above. We note that, when considered separately, high-S/N galaxies give a total metallicity of  $1.120Z_\odot$  while low-S/N galaxies give, as expected, a lower metallicity of  $0.995Z_\odot$ . The conclusion from this calculation is that the average metallicity of stars in the present-day Universe is consistent with solar. As discussed in Edmunds & Phillipps (1997) this result may be expected on the basis of the definition of yield, which is the amount of metals produced for each unit of mass of interstellar medium that is locked up in long-lived stars. If then the majority of baryons today have been locked up into stars, the overall abundance should be approaching the yield, which is basically the solar abundance.

#### 4.3.2 An inventory of the stellar metallicity and stellar mass

In addition to quantify the total metal budget in stars of the local Universe, it is of interest to investigate how much galaxies with different properties contribute to the total metallicity today and how they differ from the galaxies that contain the bulk of the stellar mass in the local Universe. In order to answer these questions we plot in Fig. 4.5 the fraction of the total mass of metals in stars<sup>4</sup> as a function of various galaxy properties, such as the

<sup>4</sup>Obtained by multiplying the stellar metallicity of each galaxy by its mass and by weighting each galaxy by  $1/V_{\text{max}}$ .

## 4 The stellar metallicity distribution in the local Universe

**Table 4.1:** Mass density of metals and baryons in stars at  $z = 0$  derived from this work and from the literature. All values have been adjusted to a flat cosmology with  $H_0 = 70 \text{ km s}^{-1} \text{ Mpc}^{-1}$ , assuming  $\rho_{crit} = 1.36 \times 10^{11} h_{70}^2 \text{ M}_{\odot} \text{ Mpc}^{-3}$ .

Stellar metallicity density		
$\rho_Z (h_{70} \text{ M}_{\odot} \text{ Mpc}^{-3})$	$\Omega_Z h_{70}$	Reference
$8.254 \times 10^6$	$6.06 \times 10^{-5}$	This work
$(2.47 - 6.90) \times 10^6$	$(1.82 - 5.07) \times 10^{-5}$	1
$(3.13 - 6.26) \times 10^6$	$(2.3 - 4.6) \times 10^{-5}$	2,3,4
$1.08 \times 10^7$	$7.92 \times 10^{-5}$	5
$2.74 \times 10^7$	$2.02 \times 10^{-4}$	6
$7.56 \times 10^6$	$1.5 \times 10^{-4}$	7
Stellar mass density		
$\rho_* (h_{70} \text{ M}_{\odot} \text{ Mpc}^{-3})$	$\Omega_* h_{70}$	Reference
$4.013 \times 10^8$	$2.9 \times 10^{-3}$	This work
$3.5 - 7.6 \times 10^8$	$2.6 - 5.6 \times 10^{-3}$	8
$3.9 \times 10^8$	$2.9 \times 10^{-3}$	9
$(1.56 - 2.76) \times 10^8$	$(1.12 - 2.03) \times 10^{-3}$	10
$4.6 \times 10^8$	$3.4 \times 10^{-3}$	11
$5.18 \times 10^8$	$3.2 \times 10^{-3}$	12
$4.79 \times 10^8$	$3.5 \times 10^{-3}$	13

1) Calura & Matteucci (2004), 2) Finoguenov et al. (2003), 3) Balogh et al. (2001), 4) Huang et al. (2003), 5) Pagel (2002), 6) Mushotzky & Loewenstein (1997), 7) Madau et al. (1996), 8) Glazebrook et al. (2003), 9) Bell et al. (2003), 10) Cole et al. (2001), 11) Kochanek et al. (2001), 12) Madau et al. (1998), 13) Fukugita et al. (1998)

velocity dispersion (a), the absolute  $r$ -band magnitude (b), the stellar mass (c), the concentration parameter (d), the  $4000\text{\AA}$ -break strength (e) and the light-weighted age (f). The thick black line gives the distribution for the sample as a whole, while the dotted and the dot-dashed lines represent the contribution from the high-S/N galaxies only and from the low-S/N galaxies only (as derived from the stacked spectra, respectively). It is evident that, neglecting low-S/N galaxies we would have missed a substantial fraction of the total metallicity in the local Universe, in particular at low velocity dispersions, low concentrations, low D4000 values and young ages (while there is no strong segregation in stellar mass and luminosity).

The red line in each panel traces for comparison the fraction of the total stellar mass as a function of the different parameters. The mass density dis-

### 4.3 The distribution of metals in the local Universe

---

tribution for SDSS galaxies has been studied as a function of spectral and photometric properties of galaxies, of their size and morphology, stellar mass and surface mass density by Kauffmann et al. (2003) (see also Brinchmann et al. 2004). Our distributions agree with those previously derived, although some differences may be expected due to the different sample definition. In particular, notice that the stellar mass distribution as a function of the concentration parameter is strongly double-peaked, whereas the distribution shown by Kauffmann et al. (2003) and Brinchmann et al. (2004) does not peak at any particular value. This is likely an artifact in our distribution caused by the definition of average concentration for the stacked spectra (see Fig. 4.1c). In addition to the parameters already studied we are able to show here the distribution of stellar mass directly as a function of age and not only of D4000.

Thanks to the large statistics provided by the SDSS DR2 we can give accurate description of the distributions shown in Fig. 4.5. For the velocity dispersion  $\log \sigma_V$  and the absolute  $r$ -band magnitude we are limited by the size of the bins in which low-S/N galaxies are grouped to obtain high-S/N coadded spectra (0.05 dex and 0.5 mag respectively). In Table 4.2 we give the mode of each distribution, which indicates the characteristic velocity dispersion, luminosity, stellar mass, age, concentration and D4000 of the galaxies that contribute the bulk of the metal budget in the local Universe (last column). The 5, 10, 25, 50, 75, 90, 95 percentiles of each distribution are listed as well. The same quantities are given also for the distribution in stellar mass density. In the last row of Table 4.2 we indicate the fraction of the total stellar mass contained in galaxies that contribute different fractions of the total metal content.

From Fig. 4.5 and Table 4.2 it appears that the distribution of the metals locked up in stars does not differ substantially from the distribution of the stellar mass. In other words, the galaxies that contribute a significant fraction of the total amount of metals locked up in stars today are also those that contain most of the total stellar mass. The greatest difference is evident in galaxies with low concentrations, low velocity dispersions and young ages: they contain a non-negligible fraction of the total stellar mass (almost comparable to that contained in high-concentration galaxies), because they are more numerous (see e.g. Brinchmann et al. 2004), but their stars contain a much smaller fraction of metals.

More quantitatively we can say the following:

- (i) The typical galaxy contributing most of the total mass of metals in the present-day Universe is a massive, bulge-dominated galaxy. It has a velocity dispersion of  $\sim 180 \text{ km s}^{-1}$ , an absolute magnitude almost 2 mag

## 4 The stellar metallicity distribution in the local Universe

---

brighter than  $M_r^* = -20.28$  in  $r$ -band<sup>5</sup>, a concentration parameter of 2.8 (i.e. roughly the threshold separating early-type from late-type galaxies), D4000 of 1.9 corresponding to a fairly old stellar age of  $\sim 8.7$  Gyr, and a typical mass of  $1.2 \times 10^{11} M_\odot$ . We find a similar value ( $10^{11} M_\odot$ ) for the characteristic stellar mass of the galaxies that contain the bulk of the total mass today. This is slightly higher than the characteristic mass of  $6 \times 10^{10} M_\odot$  found by Kauffmann et al. (2003). This likely arises from the systematic offset between our stellar mass determinations and those of Kauffmann, due to the inclusion of metal-sensitive spectral features and the use of different prior in our analysis (see section 2.2.4.3 of Chapter 2).

- (ii) Half of all the metals locked up in stars today are contained in galaxies more massive than  $9.5 \times 10^{10} M_\odot$  or with velocity dispersion higher than  $140 \text{ km s}^{-1}$ , which contain roughly 40 percent of the total stellar mass. Galaxies with masses below  $5 \times 10^{10} M_\odot$  or  $\sigma_V \lesssim 100 \text{ km s}^{-1}$  contain only 25 percent of the total metal budget and about 35 percent of the total stellar mass.
- (iii) The peak of the distribution of metals is at a concentration parameter of 2.8 (therefore it is contributed by galaxies that should be predominantly early-type). The fraction of metals drops quickly in galaxies with concentration parameter below the median value of 2.7 and late-type galaxies, characterised by a concentration parameter lower than 2.4, contribute less than 25 percent of the total mass of metals. The stellar mass distribution shows instead a significant contribution also from galaxies with  $C \leq 2.4$ . An equal fraction of stellar mass is contained in galaxies with  $C$  below and above 2.6, the threshold adopted by Strateva et al. (2001) to separate late- and early-type galaxies. This is consistent with what already found by Kauffmann et al. (2003).
- (iv) The distribution of stellar metallicity as a function of D4000 deviates from the distribution of stellar mass in the range of D4000 occupied by late-type, star-forming galaxies. Both distributions show a strong peak at D4000=1.9: galaxies with D4000 above this value contain roughly 25 percent of the metals and 25 percent of the mass in stars today. The distribution in mass is clearly bimodal<sup>6</sup> and has a secondary peak at D4000  $\sim 1.4$ . Galaxies with D4000  $\leq 1.4$  contribute another 25 percent

---

<sup>5</sup>From Blanton et al. (2003), corrected to  $z = 0$ .

<sup>6</sup>This bimodality reflects a true bimodality in D4000 (see Fig. 4.2), while the double peak in the distribution as a function of concentration is an artifact induced by our definition of  $C$  for the stacked spectra.

to the total stellar mass. On the contrary, the distribution of metals declines steadily, and only 10 percent of metals is contained in galaxies with  $D4000 < 1.4$ .

- (v) The differences in the stellar metallicity and stellar mass distributions with respect to  $D4000$  are reflected in the light-weighted age. Galaxies older than 8.5 Gyr contribute the same fraction (25 percent) of the total stellar mass and the total stellar metallicity in the local Universe, and only 5 percent comes from galaxies older than 10 Gyr. The distribution in stellar metallicity declines rapidly at ages younger than 6.3 Gyr ( $\log(t_r/yr) \sim 9.8$ ), where half of the total stellar mass comes from, but less than 30 percent of the total amount of metals. If we translate the peak in the stellar metallicity distribution at the light-weighted age of  $\log(t_r/yr) = 9.94$  ( $\sim 8.7$  Gyr) into a redshift, it would correspond to a formation redshift of  $z = 1.29$ , which falls in the redshift range over which the cosmic metal ejection rate (and analogously the cosmic star formation rate) starts to decline (e.g. Lilly et al. 1996; Madau et al. 1996, 1998).

Our analysis shows that the bulk of the total metals locked up in stars in the local Universe resides in massive galaxies, with morphology and spectral properties characteristic of early-type galaxies with fairly old stellar populations. Given the shape of the mass density distribution, these results are in agreement with the correlations between stellar metallicity, age and stellar mass studied in Chapter 2. Late-type, star forming galaxies are not expected to be major contributors to the total metal budget. Nonetheless, galaxies with  $D4000 < 1.5$ ,  $C < 2.4$  and stellar masses below  $5 \times 10^{10} M_\odot$  contribute about 25 percent of the total stellar metallicity density and a slightly higher fraction of the total stellar mass density (35 percent). At intermediate  $D4000$ , between 1.5 and 1.8, a significant fraction of metals is likely to be in galaxies with signs of AGN activity. These galaxies would also contribute to the peak at high concentrations.

## 4.4 Summary and conclusions

In this work we have exploited recent estimates of physical parameters, such as stellar metallicity and stellar mass, for a comprehensive sample of more than  $10^5$  nearby galaxies to derive the total mass density of metals and baryons locked up in stars in the local Universe, also expressed in terms of the mass-weighted average metallicity in stars today. Moreover, it has been possible to quantify the contribution to the total amount of metals by galaxies with dif-

## 4 The stellar metallicity distribution in the local Universe

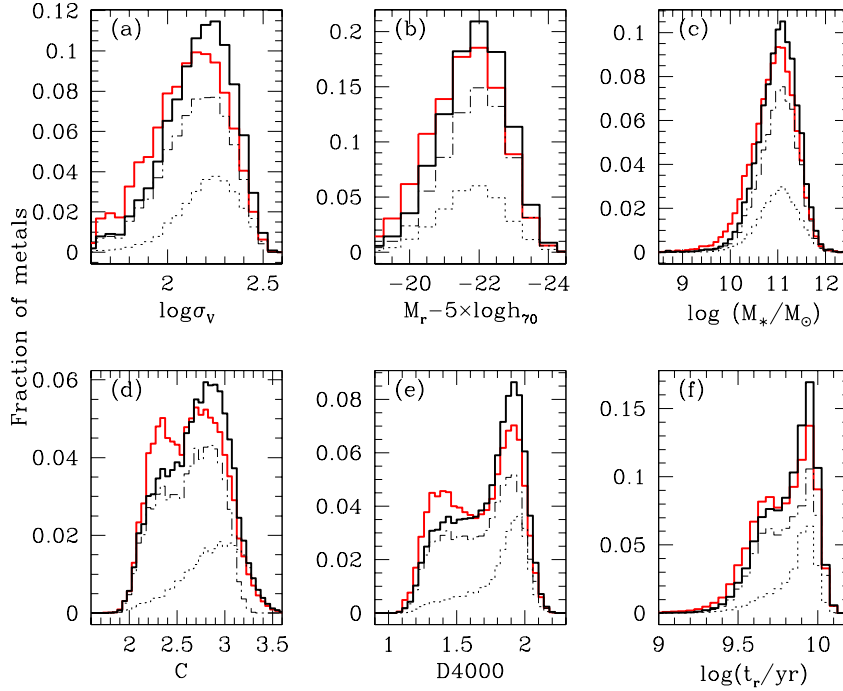


**Figure 4.5:** The fraction of the total mass of metals locked up in stars in the local Universe is shown as a function of various parameters: (a) the stellar velocity dispersion, (b) the absolute  $r$ -band magnitude, (c) the stellar mass, (d) the concentration parameter, (e) the  $4000\text{\AA}$ -break index strength and (f) the light-weighted age. The dotted line shows the contribution from high-S/N galaxies, while the dash-dotted line shows the contribution from low-S/N galaxies (obtained from high-S/N stacked spectra, see text for details). The continuous black line shows the distribution obtained when both contributions are taken into account. The distribution of stellar mass as a function of the various parameters is described by the red histogram in each panel. Note that the resolution in the distribution versus velocity dispersion and absolute magnitude is limited by the width of the bins in which low-S/N galaxies are grouped to obtain the co-added spectra (0.05 dex and 0.5 mag respectively).

ferent morphological and spectral properties, and to compare the distribution of the stellar metallicity density with that of the stellar mass density.

The sample used is drawn from the SDSS DR2 and it includes galaxies spanning a wide range of star formation activities, from quiescent early-type

## 4.4 Summary and conclusions

**Table 4.2:** For each parameter  $X$ , the percentiles of the distribution of stellar mass and of metals as a function of  $X$  are given. In the last column we indicate the mode of each distribution. The last row quotes the fraction of the total stellar mass in the local Universe contained in galaxies that contribute different fractions of the metal content.

Stellar mass distribution								
Parameter	5%	10%	25%	50%	75%	90%	95%	mode
$\log \sigma_V$	1.72	1.81	1.94	2.10	2.22	2.32	2.37	2.20
$M_r - 5 \times \log h_{70}$	-23.43	-23.15	-22.59	-21.89	-21.1	-20.38	-19.94	-22
$\log(M_*/M_\odot)$	10	10.23	10.56	10.89	11.17	11.39	11.52	11.00
$C$	2.11	2.18	2.34	2.62	2.86	3.04	3.14	2.70
D4000	1.24	1.29	1.43	1.69	1.88	1.97	2.01	1.90
$\log(t_r/yr)$	9.46	9.53	9.64	9.80	9.92	9.98	10.01	9.94
Stellar metallicity distribution								
$\log \sigma_V$	1.81	1.89	2.02	2.15	2.27	2.35	2.39	2.25
$M_r - 5 \times \log h_{70}$	-20.4	-20.77	-21.46	-22.14	-22.77	-23.29	-23.53	-22
$\log(M_*/M_\odot)$	10.23	10.41	10.70	10.98	11.23	11.44	11.56	11.10
$C$	2.12	2.21	2.42	2.70	2.92	3.08	3.17	2.80
D4000	1.27	1.34	1.52	1.77	1.91	1.98	2.02	1.90
$\log(t_r/yr)$	9.52	9.58	9.69	9.84	9.93	9.98	10.01	9.94
Fraction of the total stellar mass contributed								
	0.103	0.173	0.342	0.583	0.800	0.922	0.961	

to actively star-forming galaxies. The stellar metallicities, light-weighted ages and stellar masses of these galaxies were previously derived (Chapter 2) by comparing an optimally selected set of spectral absorption features to a comprehensive Monte Carlo library of model star formation histories (SFH), based on the high-resolution Bruzual & Charlot (2003) population synthesis code. We have shown in Chapter 2 that the uncertainties on the derived physical parameters directly depend on the mean spectral signal-to-noise ratio (S/N). Because of this, in previous works we have analysed only galaxies with S/N greater than 20, biasing our sample towards more concentrated, higher surface brightness and higher velocity dispersion galaxies.

We need to include here also galaxies at lower S/N in order to derive a fair estimate of the total metallicity of stars in the local Universe. We do this by coadding (weighting by  $1/V_{\max}$ ) the spectra of low-S/N galaxies with similar  $r$ -band absolute magnitude, velocity dispersion and D4000 until a minimum S/N requirement is satisfied. This allows us to derive estimates of the ( $1/V_{\max}$ -weighted average) stellar metallicity of low-S/N galaxies with an uncertainty not greater than 0.2 dex, i.e. comparable to the accuracy with which

## 4 The stellar metallicity distribution in the local Universe

---

stellar metallicity is derived from individual high-S/N spectra. A similar improvement is obtained for light-weighted age and stellar mass, although these parameters are less affected than stellar metallicity by the quality of the spectrum.

By combining the contribution of the individual high-S/N galaxies and the low-S/N galaxies, as derived from the coadded spectra, we estimated the total mass density of baryons and of metals locked up in stars in the local Universe. We find, respectively,  $\rho_* = 4.013 \pm 0.005^{+0.353}_{-0.35} \times 10^8 h_{70} M_\odot \text{Mpc}^{-3}$  and  $\rho_Z = 8.254 \pm 0.019^{+1.957}_{-4.659} \times 10^6 h_{70} M_\odot \text{Mpc}^{-3}$ , in agreement with other measures from the literature or predictions of chemical evolution models. By combining these two quantities we can estimate the average stellar metallicity today to be consistent with solar (Equation 4.3.1).

The large statistics available from the SDSS allows us to provide a compendium of the distribution of the stellar metallicity density as a function of global galaxy properties, such as velocity dispersion, luminosity and stellar mass, as a function of morphology as approximated by the concentration parameter, and as a function of physical properties of the stellar populations, such as the 4000Å-break strength and the light-weighted age. We have compared such distributions with the corresponding distributions of stellar mass density. Our analysis has shown that the stellar metallicity and the stellar mass distributions do not differ significantly, in particular at the high-mass end. In other words, the galaxies that contribute most of the total amount of metals in stars have properties similar to those containing the bulk of the total mass in stars.

The typical galaxy containing the bulk of the total stellar mass and of the total metals in stars is a massive galaxy ( $10^{11} M_\odot$ ), with concentration parameter characteristic of early-type galaxies ( $\sim 2.8$ ) and  $D4000 = 1.9$ , corresponding to a fairly old stellar age of  $\gtrsim 8.7$  Gyr. Note that the characteristic mass found here is above the stellar mass range  $3 \times 10^9 - 3 \times 10^{10} M_\odot$  over which the transition from low-mass, metal-poor, disc-dominated galaxies to high-mass, metal-rich, bulge-dominated galaxies occurs. Galaxies with masses greater than  $3 \times 10^{10} M_\odot$ , where the mass-metallicity relation starts to flatten (Tremonti et al. 2004; Gallazzi et al. 2005), contain more than 80 percent of the total stellar metallicity and stellar mass.

The stellar metallicity and stellar mass distributions differ most significantly with respect to concentration and stellar age, in particular at low concentrations and low D4000 values (or young ages). The distribution in stellar mass density is double-peaked and galaxies with  $C < 2.5$  or  $D4000 < 1.5$  contain a fraction (roughly 30 percent) of the total stellar mass which is almost comparable to that of galaxies with  $C > 2.8$  or  $D4000 > 1.8$ . On the contrary the

fraction of metals in stars continues to decrease with decreasing concentration or stellar age. To quantify this, we can distinguish early-type from late-type galaxies on the basis of the concentration parameter, defining as early-types those galaxies with  $C \geq 2.8$  and as late-types those galaxies with  $C \leq 2.4$ . While the two classes of galaxies contain a similar fraction of the total stellar mass (31.5 and 30 percent respectively), the fraction of metals locked up in early-type galaxies is 39 percent and only 23 percent in late-type galaxies. These results are all consistent with the stellar mass-stellar metallicity relation and the shape of the mass density distribution.

It is tempting to translate the characteristic age of the stellar populations contributing most of the metals and of the mass into a redshift of formation. Given that our ages are light-weighted ages and are thus very sensitive to the galaxy star formation history, it is reasonable to do so for systems with a star formation history that can be at first order approximated by a burst of star formation, i.e. elliptical galaxies. Considering only early-type galaxies ( $C \geq 2.8$ ) half of the metals (and half of the stellar mass) are contained in galaxies older than 8.2 Gyr, which would correspond to a formation redshift of 1.14. This redshift is consistent with the redshift range  $1 < z < 2$  at which the cosmic star formation rate density starts to decline (Lilly et al. 1996; Madau et al. 1998). Only 10 percent of the metals reside in galaxies older than 9.93 Gyr, i.e. with a formation redshift larger than 1.8, and only 5 percent of metals and of baryons are locked up in stars formed at redshift greater than 2.

Our study provides a new determination of the total amount of metals locked up in stars today and allows for the first time to derive a quantitative and accurate description of the properties of the galaxies hosting different fractions of the metals and of the mass in the local Universe. Such distributions represent important constraints on models of the cosmic star formation and chemical enrichment histories. The detailed knowledge of the distribution of metals, coupled to the stellar mass distribution, will allow a more direct comparison with predictions from semianalytic models of galaxy formation and evolution. Ongoing large redshift surveys, like VVDS (Le Fèvre et al. 2004), GOODS (Dickinson et al. 2003; Vanzella et al. 2005), DEEP2 (Davis et al. 2003; Madgwick et al. 2003), COSMOS (Schinnerer et al. 2004), will make it possible to extend this kind of studies to redshifts as high as  $z \sim 1$  and thus, not only to build a more consistent picture of the cosmic star formation history, but also to understand which are the galaxies that most strongly contributed to its evolution since  $z = 1$ .

#### 4 The stellar metallicity distribution in the local Universe

---

## Bibliography

- Abazajian K., et al. 2004, AJ, 128, 502
- Abraham R. G., et al 2004, AJ, 127, 2455
- Baldry I. K., et al 2002, ApJ, 569, 582
- Balogh M. L., Pearce F. R., Bower R. G., Kay S. T., 2001, MNRAS, 326, 1228
- Baugh C. M., Cole S., Frenk C. S., Lacey C. G., 1998, ApJ, 498, 504
- Bell E. F., McIntosh D. H., Katz N., Weinberg M. D., 2003, ApJS, 149, 289
- Blanton M. R., et al. 2003, ApJ, 592, 819
- Brinchmann J., Charlot S., White S. D. M., Tremonti C., Kauffmann G., Heckman T., Brinkmann J., 2004, MNRAS, 351, 1151
- Brinchmann J., Ellis R. S., 2000, ApJ, 536, L77
- Bruzual G., Charlot S., 2003, MNRAS, 344, 1000
- Calura F., Matteucci F., 2004, MNRAS, 350, 351
- Cohen J. G., 2002, ApJ, 567, 672
- Cole S., et al. 2001, MNRAS, 326, 255
- Colless M., et al 2001, MNRAS, 328, 1039
- Connolly A. J., Szalay A. S., Dickinson M., Subbarao M. U., Brunner R. J., 1997, ApJ, 486, L11+
- Cowie L. L., Songaila A., Barger A. J., 1999, AJ, 118, 603
- Davis M., et al. 2003, in Discoveries and Research Prospects from 6- to 10-Meter-Class Telescopes II. Edited by Guhathakurta, Puragra. Proceedings of the SPIE, Volume 4834, pp. 161-172 (2003). Science Objectives and Early Results of the DEEP2 Redshift Survey. pp 161–172

## Bibliography

---

- Dickinson M., Giavalisco M., The Goods Team 2003, in Bender R., Renzini A., eds, *The Mass of Galaxies at Low and High Redshift The Great Observatories Origins Deep Survey*. pp 324–+
- Dickinson M., Papovich C., Ferguson H. C., Budavári T., 2003, *ApJ*, 587, 25
- Drory N., Bender R., Feulner G., Hopp U., Maraston C., Snigula J., Hill G. J., 2004, *ApJ*, 608, 742
- Edmunds M. G., Phillipps S., 1997, *MNRAS*, 292, 733
- Ellison S. L., Kewley L. J., Mallén-Ornelas G., 2005, *MNRAS*, 357, 354
- Erb D. K., Shapley A. E., Pettini M., Steidel C. C., Reddy N. A., Adelberger K. L., 2006, *ArXiv Astrophysics e-prints*
- Finoguenov A., Burkert A., Böhringer H., 2003, *ApJ*, 594, 136
- Fukugita M., Hogan C. J., Peebles P. J. E., 1998, *ApJ*, 503, 518
- Gallazzi A., Charlot S., Brinchmann J., White S. D. M., Tremonti C. A., 2005, *MNRAS*, 362, 41
- Glazebrook K., et al. 2003, *ApJ*, 587, 55
- Heavens A., Panter B., Jimenez R., Dunlop J., 2004, *Nature*, 428, 625
- Heavens A. F., Jimenez R., Lahav O., 2000, *MNRAS*, 317, 965
- Huang J.-S., Glazebrook K., Cowie L. L., Tinney C., 2003, *ApJ*, 584, 203
- Iverson R. J., et al 2002, *MNRAS*, 337, 1
- Jimenez R., Panter B., Heavens A. F., Verde L., 2005, *MNRAS*, 356, 495
- Juneau S., Glazebrook K., Crampton D., McCarthy P. J., Savaglio S., Abraham R., Carlberg R. G., Chen H.-W., Le Borgne D., Marzke R. O., Roth K., Jørgensen I., Hook I., Murowinski R., 2005, *ApJ*, 619, L135
- Kauffmann G., et al. 2003, *MNRAS*, 341, 33
- Kobulnicky H. A., Kewley L. J., 2004, *ApJ*, 617, 240
- Kobulnicky H. A., Zaritsky D., 1999, *ApJ*, 511, 118
- Kochanek C. S., Pahre M. A., Falco E. E., Huchra J. P., Mader J., Jarrett T. H., Chester T., Cutri R., Schneider S. E., 2001, *ApJ*, 560, 566

- Lanzetta K. M., Wolfe A. M., Turnshek D. A., 1995, *ApJ*, 440, 435
- Le Fèvre O., et al 2004, *A&A*, 428, 1043
- Lilly S. J., Carollo C. M., Stockton A. N., 2003, *ApJ*, 597, 730
- Lilly S. J., Le Fevre O., Hammer F., Crampton D., 1996, *ApJ*, 460, L1+
- Madau P., Ferguson H. C., Dickinson M. E., Giavalisco M., Steidel C. C., Fruchter A., 1996, *MNRAS*, 283, 1388
- Madau P., Pozzetti L., Dickinson M., 1998, *ApJ*, 498, 106
- Madgwick D. S., et al 2003, *ApJ*, 599, 997
- Mushotzky R. F., Loewenstein M., 1997, *ApJ*, 481, L63+
- Pagel B. E. J., 2002, in *ASP Conf. Ser. 253: Chemical Enrichment of Intracluster and Intergalactic Medium Metals in the Universe and Diffuse Background Radiation. (I)*. pp 489+
- Pei Y. C., Fall S. M., 1995, *ApJ*, 454, 69
- Pei Y. C., Fall S. M., Hauser M. G., 1999, *ApJ*, 522, 604
- Pettini M., Shapley A. E., Steidel C. C., Cuby J.-G., Dickinson M., Moorwood A. F. M., Adelberger K. L., Giavalisco M., 2001, *ApJ*, 554, 981
- Pettini M., Smith L. J., Hunstead R. W., King D. L., 1994, *ApJ*, 426, 79
- Pettini M., Smith L. J., King D. L., Hunstead R. W., 1997, *ApJ*, 486, 665
- Schinnerer E., et al 2004, *AJ*, 128, 1974
- Schlegel D. J., Finkbeiner D. P., Davis M., 1998, *ApJ*, 500, 525
- Shapley A. E., Erb D. K., Pettini M., Steidel C. C., Adelberger K. L., 2004, *ApJ*, 612, 108
- Steidel C. C., Adelberger K. L., Giavalisco M., Dickinson M., Pettini M., 1999, *ApJ*, 519, 1
- Steidel C. C., Shapley A. E., Pettini M., Adelberger K. L., Erb D. K., Reddy N. A., Hunt M. P., 2004, *ApJ*, 604, 534
- Strateva I., et al. 2001, *AJ*, 122, 1861
- Tremonti C. A., et al. 2004, *ApJ*, 613, 898

## Bibliography

---

Vanzella E., et al 2005, A&A, 434, 53

York D. G., et al. 2000, AJ, 120, 1579

*Qu'on ne dise pas que je n'ai rien dit de nouveau :  
la disposition des matières est nouvelle ; quand on  
joue à la paume, c'est une même balle dont joue  
l'un et l'autre, mais l'un la place mieux.*

Blaise Pascal, Les Pensées

# 5

## Conclusions and outlook

### Abstract

In this chapter I summarize the main achievements of this thesis and the methodology adopted to reach them. The main objective of this thesis was to constrain the physical parameters of the stellar populations of present-day galaxies from their optical spectra in order to gather new insight into the processes that were important in the formation and evolution of the galaxies we see today. The importance of this work relies in the unprecedented statistics offered by modern large spectroscopic surveys and the new methodology applied, that allowed more stringent constraints on stellar physical parameters.

I exploited these new constraints to explore in detail and with great statistical significance the mean relations between stellar metallicity, age and stellar mass (Chapter 2), to re-address the physical origin of observed scaling relations obeyed by early-type galaxies (Chapter 3), and to quantify the total amount of metals and baryons locked up in stars in the present-day Universe (Chapter 4).

### 5.1 Motivations

The integrated spectra of galaxies contain valuable clues about the ages and metallicities of the stars producing the optical light. These parameters are direct tracers of the star formation and chemical enrichment histories of the Universe. They can be constrained by comparing observed galaxy spectra with predictions from population synthesis models. Broadband colours are however

## 5 Conclusions and outlook

---

of limited use in this sense because they tend to be reddened in a similar way by age, metallicity and dust. To try and solve these degeneracies, refined spectral diagnostics have been used that involve single spectral absorption features which show distinct sensitivities to age and metallicity, and are less affected by dust attenuation because defined on narrower wavelength ranges. However, this approach has been applied so far only to relatively small samples of early-type galaxies, while the interpretation of younger stellar populations has been hampered so far by the lack of hot stars in the stellar libraries at the basis of population synthesis models.

This work improves on previous studies in that new, high-resolution models including stars in the full temperature range are adopted to interpret large samples of nearby galaxies, spanning a wide range in star formation activity. The sample analysed in this work includes almost  $2 \times 10^5$  galaxies drawn from the Sloan Digital Sky Survey Data Release Two (SDSS DR2), going from quiescent early-type to actively star-forming galaxies. Their spectra are interpreted with the use of the recent Bruzual & Charlot (2003) population synthesis models. They have a resolution of  $3\text{\AA}$  over the wavelength range from 3200 to 9500 $\text{\AA}$ , which perfectly matches the resolution of the SDSS spectra. This allowed to measure stellar absorption features in the same way in model and observed spectra, avoiding any loss of information from the observed spectra. The higher resolution of the new models is also crucial in order to measure absorption features from the spectra of star-forming galaxies, where it is necessary to first remove emission lines with high accuracy.

A median-likelihood estimates approach ('Bayesian statistics') has been adopted to derive simultaneous estimates of stellar metallicity, light-weighted age and stellar mass, by simultaneously constraining the strengths of a set of optimally selected optical absorption features. These have been chosen to have different sensitivities to age and metallicity and to show negligible dependence on element abundance ratios. The last requirement is necessary because the models used do not take into account the dependence of index strengths on variations of  $\alpha$ -elements-to-Fe abundance ratio. Each observed spectrum is compared to a comprehensive library of Monte Carlo models spanning the full range of possible star formation histories. By weighting each model by its goodness of fit, the entire probability density function (PDF) of stellar metallicity, age and stellar mass is derived. The novelty of this method is that it allows not only to define the (median-likelihood) estimates of physical parameters, but also to assess their accuracy, given by the width of the corresponding likelihood distribution.

## 5.2 Main results

I have shown in Chapter 2.2.3 and 2.2.4 that this method allows to derive from a limited number of observational constraints the stellar masses of large samples of galaxies with an accuracy better than  $\pm 0.1$  dex. The stellar metallicities and light-weighted ages can be constrained to within  $\pm 0.15$  dex for the majority of the galaxies in the sample. It is important to note that to simultaneously constrain age and metallicity with this accuracy it is necessary to use simultaneously both age-sensitive and metal-sensitive indices. Moreover, while the uncertainties on stellar mass are almost independent of galaxy type, the random error on age and, especially, metallicity depends on the strengths of the absorption lines and, hence, on the galaxy star formation history: it is smallest for the galaxies with the strongest absorption features, that have a smooth, continuous star formation history. I have also shown that the observed spectral signal-to-noise (S/N) ratio directly influences the accuracy of the metallicity estimates (but has a smaller effect on the age and stellar mass estimates). A median S/N per pixel of at least 20 is required to reliably constrain stellar metallicity. For this reason, most of the analysis presented has been limited to galaxies with S/N greater than 20. This cut affects almost 75 percent of the original sample, excluding preferentially galaxies at higher redshift ( $z \gtrsim 0.15$ ) with low surface brightness, low concentration and hence potentially subsolar metallicity. While this bias does not affect the general results discussed in Chapter 2 and 3, low-S/N galaxies need to be included in order to estimate the total amount of metals locked up in stars in the local Universe (Chapter 4).

Before reviewing the main results of this thesis, it is worthwhile mentioning that, in addition to the random error on the physical parameters, reflected in the width of the corresponding PDF, there are possible sources of systematic errors that come from limitations in both model and observed spectra. The models used do not include the effects of variations in heavy-element abundance ratios. For this reason special care has been taken to select only those spectral features with negligible dependence on element abundance ratios. However, there might be a residual overestimate of the metallicities and an underestimate of the ages of massive elliptical galaxies, which are overabundant in  $\alpha$ -elements with respect to Fe. From the observational side, the biggest concern comes from the fixed 3-arcsec diameter of the fibre with which SDSS spectra are taken. The fraction of light collected by the fibre is on average 30 percent (and no more than 60 percent) of the total galaxy light and it depends on the redshift and the surface brightness profile of the galaxy. Therefore the derived metallicities and ages are representative of a limited inner region of the galaxies and cannot be easily extrapolated to their total values

## 5 Conclusions and outlook

---

without accurate information on radial gradients. On average, the metallicities of both bulge-dominated and disk-dominated galaxies are overestimated by about 0.2 dex. While no significant gradient in the light-weighted ages of bulge-dominated galaxies is expected, the ages of massive disk-dominated galaxies can be underestimated by up to 0.2 dex. I have checked that the aperture bias does not affect the relations between metallicity, age and stellar mass (but it can affect the zero-point of such relations) discussed in Chapter 2 and 3, however it is the biggest source of systematic uncertainty on the estimate of the total stellar metallicity density derived in Chapter 4. Finally, it is worth mentioning the extent to which the ‘age-metallicity degeneracy’ (i.e. the confusion between young, metal-rich and old, metal-poor populations) persist in the physical parameters derived in this work. I could re-calibrate the relation between the two physical parameters for both early-type and late-type galaxies, by means of the joint likelihood distributions of metallicity and age for individual galaxies. The age-metallicity degeneracy varies systematically as a function of galaxy type and mass. It is stronger for massive elliptical galaxies.

The new estimates of stellar metallicity, age and stellar mass and the unprecedented statistics offered by the SDSS allowed me to give a detailed description of the mean relations between these parameters and their dependence on other galaxy properties, such as morphology. I have shown that both metallicity and age increase with increasing stellar mass, with a rapid transition from young, metal-poor to old, metal-rich galaxies over the stellar mass range  $3 \times 10^9 \lesssim M_*/M_\odot \lesssim 3 \times 10^{10}$ . This range corresponds to the transition range of several observed bimodalities in galaxy properties. The relations between age, metallicity and stellar mass hold for both early-type and late-type galaxies, but the age range of early-type galaxies is less mass dependent than for late-type galaxies.

The relation between stellar metallicity and stellar mass derived for all galaxy types is very similar to the relation between gas-phase metallicity and stellar mass derived for star-forming galaxies only. This suggests a similar origin for the two relations in terms of galactic winds, which are more efficient in removing metals from low-mass galaxies, which have shallower potential wells. This interpretation is supported by the fact that stellar metallicity decreases with mass also for galaxies which have completed their star formation: if no gas and metals outflows occur (i.e. in a ‘closed-box’ system) the final stellar metallicity should be independent of stellar mass (and reach the stellar yield). Moreover there is a large scatter in the age-mass and metallicity-mass relations, only in part explained by the errors on the derived parameters. This scatter is highest at intermediate masses and persists even when bulge-dominated and disk-dominated galaxies are considered separately. This

further indicates that stellar mass is not the unique parameter determining the galaxy star formation histories (and hence their physical parameters), but additional variations induced by, e.g., gas inflows or outflows are required to explain these parameters.

I then explored the implications of the above relations between metallicity, age and stellar mass to re-assess the physical origin of the colour-magnitude relation and the relation between the  $Mg_2$  index strength and velocity dispersion for early-type galaxies only. These two scaling relations connect the luminous and dynamical mass of elliptical galaxies to the properties of their stellar populations. I could demonstrate unambiguously that both relations are primarily a sequence in stellar mass and that stellar metallicity, age and element abundance ratio all increase with mass along the two relations. The scatter about the two relations is contributed by a similar amount by both age and metallicity. The small intrinsic scatter in the mass-metallicity relation contributes at all masses. The scatter in age at fixed stellar mass is negligible for massive ellipticals. However, at lower stellar masses there is an increasing spread toward younger ages that significantly correlates with the scatter in colour and index strength at fixed stellar mass.

The decrease in stellar metallicity with decreasing mass (both stellar and dynamical) favours the classical interpretation of the two observational relations in terms of supernova-driven winds. In this context, the results of this work indicates that galaxies as massive as  $10^{11} M_{\odot}$  have been affected by metal ejection through galactic winds. The older mean ages and the higher  $\alpha/Fe$  abundance ratio at higher masses hint at earlier epochs and shorter timescales of star formation in more massive ellipticals. On the contrary, the larger spread toward younger ages and the solar abundance ratios of low-mass galaxies indicates that low-mass ellipticals either formed stars more recently or have more extended star formation histories. These results represent further evidence for a shift in stellar growth toward less massive galaxies in recent epochs. To reconcile these results with predictions from hierarchical models of galaxy formation a feedback mechanism that is more efficient in quenching star formation on short timescales in more massive galaxies is required. Such source of feedback may be provided by active galactic nuclei. Moreover, it is important to note that the short star formation timescales are not in conflict with longer assembly timescales: massive ellipticals may have old stellar populations even if they finish their assembly relatively late.

Finally, I have compared the stellar mass of early-type galaxies with the dynamical mass estimated within the optical galaxy radius. I could show that the ratio of stellar over dynamical mass (i.e. the baryonic fraction) decreases from the least massive to the most massive ellipticals. The implied shallower

## 5 Conclusions and outlook

---

gradient in the dynamical mass-to-light ratio of massive ellipticals could result from a more efficient mixing of stars and dark matter within the optical radius of massive galaxies with respect to low-mass galaxies. This could be produced if the most massive ellipticals assembled through multiple dissipationless mergers.

Thanks to the large ranges in observational and physical properties covered by SDSS galaxies, I could further exploit the estimates of stellar metallicity and mass to quantify the total mass density of metals and of baryons locked up in stars in the present-day Universe. These quantities represent the fundamental constraint at  $z = 0$  of the cosmic star formation and chemical enrichment histories. As mentioned before, it is crucial here to include also galaxies with low-S/N spectra. To derive reliable constraints on the stellar metallicities of such galaxies, a stacking technique has been adopted to generate a sample of co-added high-S/N spectra. These have been obtained by co-adding the spectra of individual low-S/N galaxies with similar properties, such as velocity dispersion, absolute magnitude and  $4000\text{\AA}$ -break strength, so that small scatter in physical properties is expected within each bin. This method allowed to derive the (average) physical parameters of low-S/N galaxies with an accuracy comparable to that obtained for individual high-S/N galaxies.

The mass density of baryons and of metals derived in this work agree well with previous determinations, based on smaller samples and different methods to derive metallicities and masses, and with the values expected by integrating observationally- and model-derived cosmic star formation and metal enrichment histories. Combined together, these estimates give a mass-average total stellar metallicity of the local Universe consistent with solar. A major concern in this result comes from the aperture bias, due to the fact that the fibre with which SDSS spectra are collected samples only a small fraction of the total galaxy light. The derived stellar metallicities represent more properly the metallicity of the bulges or inner regions of the galaxies. This can lead to overestimate the total stellar metallicity of the Universe by up to a factor of two.

I have also shown how metals and stellar mass are distributed as a function of various galaxy properties, such as their mass, morphology and mean stellar age. The large statistics allows to derive accurate functional forms for the distributions of stellar metallicity and stellar mass density. I have shown that the galaxies that contain the bulk of the total stellar mass in the local Universe are also those that contribute the largest fraction of metals locked up in stars, as expected from the mass-metallicity relation. In particular, the typical galaxy contributing most of the metals and of baryons in stars today is a massive ( $M_* \sim 10^{11}M_\odot$ ), bulge-dominated galaxy, with old stellar pop-

ulations. Above  $3 \times 10^{10} M_{\odot}$ , where the transition from young, metal-poor to old, metal-rich galaxies occurs and the mass-metallicity relation starts to flatten, galaxies contain about 80 percent of the total mass of metals and of baryons in stars. I have been able to quantify the different contribution by bulge-dominated and disk-dominated galaxies (without considering intermediate systems). While these two classes of galaxies contain a similar fraction of the total stellar mass (30 percent), bulge-dominated galaxies contain a larger fraction (39 percent) of metals with respect to disk-dominated galaxies (23 percent). Finally, the distribution of metals as a function of mean stellar age for early-type galaxies only indicates that half of the metals and of the baryons are in galaxies older than 8.2 Gyr, which corresponds to an effective formation redshift of  $z = 1.14$ . This redshift falls in the range  $1 < z < 2$  where the cosmic star formation rate density starts to decline to its present value.

The method developed and adopted in this work revealed to be very powerful in deriving, for the first time, accurate quantitative constraints on physical parameters, such as stellar metallicity, light-weighted age and stellar mass, for very large samples of galaxies. While the uncertainties on individual galaxies can be significant and dependent on various factors, this method and the unprecedented statistics provided by modern large spectroscopic surveys allow to constrain robustly the mean relations between physical parameters. Moreover, it allowed to give an accurate description of the entire distribution in physical parameters space and to study its dependence on various galaxy properties. A complete census of the physical parameters of galaxies out to  $z \sim 0.1$ , such that derived in this work, is essential for constraining models of galaxy evolution. Moreover the more detailed description of the physical origin of well-known observational relations and of the distribution of metals, coupled to the distribution of stellar mass, represent a valuable reference for future models and will allow a more direct comparison with their predictions.

Finally, this work represents an important calibration at redshift zero, which is essential in order to extend the application of such technique on large samples of galaxies at higher redshift. Large surveys over the entire wavelength range, from the ultra-violet (*GALEX*), to the optical (VVDS, DEEP2) and infrared (*Spitzer*), are collecting such high-redshift samples. A similar analysis, as the one developed in this work, applied to these galaxy samples will allow to study how the distribution in physical parameters observed at  $z \sim 0.1$  evolves with lookback times. It will also lead to a more consistent picture of the cosmic chemical enrichment and star formation history, and to quantify the contribution of different galaxies to its evolution since  $z = 1$  and above.

### 5.3 Outlook

Future developments of the present work will be focused on one side to refine the tools for the interpretation of the spectro-photometric properties of nearby galaxies, exploiting recent or future advances in population synthesis models, and on another side to extend these tools to a broader wavelength range for application to high-redshift galaxies.

From the modelling side there are mainly two limitations that affect the derived parameters of nearby galaxies and hamper the interpretation of high-redshift galaxies. First of all it will be extremely important to include the effect of variations in element abundance ratios in population synthesis models. Performing the analysis presented in this work with such models will allow to assess the accuracy of the previously derived physical parameters and their dependence on element abundance ratio. Moreover, deriving estimates of  $\alpha$ -elements-to-Fe abundance ratio is important in itself because it provides information about the timescales of star formation in nearby galaxies. Studying the dependence of  $\alpha$ /Fe ratio on various galaxy properties can also be useful to derive galaxy formation epochs and reconstruct the cosmic star formation history from its ‘fossil records’.

Another crucial aspect is the understanding and modelling of attenuation by dust. An important development of this work will be the implementation of novel and more realistic physical prescriptions concerning dust attenuation and polycyclic aromatic hydrocarbons emissions in the mid-IR wavelength range. Including a proper treatment of dust attenuation will help to break physical parameter degeneracies, in particular for star-forming galaxies (the most affected by dust), both in studies of broad-band colours and of spectral absorption features, for which the common assumption of weak dust sensitivity needs to be validated.

Studying and modelling the effect of dust attenuation on the multi-wavelength emission of galaxies is of the greatest relevance in order to calibrate diagnostics of star formation rates on low-redshift galaxy samples and to interpret the spectral information available from high-redshift galaxy surveys. In particular, a great effort will be put in studying how attenuation by dust relates to various physical properties of nearby galaxies, in order to derive the minimum set of observables needed to derive corrections for dust and hence to constrain star formation rates. This can be done on large samples of nearby galaxies with information over the entire spectral energy distribution. Such samples are becoming available now by combining the best spectroscopic data in the optical from the SDSS with far- and near-UV observations collected by *GALEX*, near-IR imaging from 2MASS, and IR observations from the IRAS catalog. A median-likelihood estimate approach, as the one adopted in this

work, can be applied to simultaneously constrain UV, optical and IR spectra of observed galaxies with large libraries of Monte Carlo star formation histories and dust parameters. This will allow to assess the accuracy with which dust attenuation and star formation rates can be constrained based on different combinations of UV, optical and IR emission.

The calibration on nearby galaxies is essential for studying large samples of high-redshift galaxies for which more limited spectral information is available. Moreover, bridging studies of the star formation rates and physical parameters of high-redshift galaxies based on their UV or IR emission will allow to derive a more consistent picture of the cosmic star formation history.

This thesis has provided the zero-point measurement of the stellar population properties of present-day galaxies, which is of fundamental relevance in order to study the evolution of such properties, and hence the processes of galaxy formation and evolution. The methodology adopted here also represents a modern and powerful tool for the detailed interpretation of present and forthcoming large databases of multi-wavelength observations at higher redshift, which will allow to directly trace back in time the evolutionary history of galaxies.

## 5 Conclusions and outlook

---

## Acknowledgements

At the end of my thesis I realize that there are many people to thank for having pushed me on my way here, and many people to thank for having made these three years a challenging and extremely rich experience.

A special thank goes to my advisor Stéphane Charlot. It is hard to tell what a unique experience is to work with him, without living it. I had the chance to take the best and the hardest of working side by side with you. Thank you for your constant support since the beginning of my thesis, for involving me in several activities and for the opportunity to spend a period at IAP with an EARA fellowship. I am not ironic when I thank you for being so peaky in the tiny details of my work and, especially, my writing, and for putting me under pressure, more than what I do by myself. Of course it has not been always easy, but if I could face your critiques it is because you have also constantly and enthusiastically encouraged and trusted me.

I sincerely thank my supervisor Simon White for his deep, straight and critic insight into my science. Discussions with him always resulted in significant improvement and refinement of my work. I wish to thank him also for his support and his efficient point of view about the organization of the work, which helped me a lot in many phases of my thesis.

I warmly thank Jarle Brinchmann for his extremely precious help, fundamental for me especially during the first period of my thesis. Much of this work could not have been done (at least not so well and quickly) without his prompt replies to all my technical questions and requests. I also thank him for offering me a different point of view and his support also in the hardest periods of my thesis.

I wish to thank other people with whom I had the opportunity to work and interact at different levels during my thesis. First of all Guinevere Kauffmann for involving me in many scientific activities, in particular in the MAGPOP network; Tim Heckman and Charles Hoopes for their help in my visit at JHU which, although very short, opened me to new perspectives for my work; David Elbaz for his precious effort and suggestions in the preparation of a Marie Curie proposal.

During these three years I have met many people who contributed in different ways to make me enjoy much better this period. Among them I want to

## Acknowledgements

---

mention Kate for helping me in finding home when I arrived here, Maria and Gabi for their kindness, smiles, and help in different things, Cornelia for her patience and comprehension all the times I was hopelessly looking for Simon. I want to thank Chantal, my helping hand at IAP: I was impressed by her kindness, strength and joy of living.

All my days at work would not have been so nice without all the friends I have met at MPA. First of all my thanks go to the very special 'extended Italian community': Luigi and Giovanna, Gabriella, Maurilio, Veronica, Larry, Andrea, Alessia, Kalliopi, Daniele, Alessandro 'le parisien', Klaus. Thank you all for all the lunches, coffees, dinners and evenings together. Among them I especially thank my office-mate Debora, for making our 'second home' such a lively and pleasant environment. Thanks for all the laughs (with which we often entertained our neighbours..), the complaints, the satisfactions, the secrets we shared. Briefly, thanks for being such a good friend. Together with her I cannot but mention Manfred and the delightful 'cake-breaks' to which, unfortunately, I only passively participate. I thank him also for his excellent translation of my summary (it was so excellent that you might be asked to do others..).

My thought goes also to Roberto 'Rb' for his humour and sensibility; Hans-Jakob, Samir and Matteo with whom I shared the office for some periods; Ben, Brent, Jeremy, Paula, Vivienne, Dimitri, Jakob for their nice company during the MAGPOP meetings or during their visit at IAP while I was there.

I also want to mention few people who made my three months in Paris such an unforgettable period: my office-mate Tatiana, Elisabetta, Sara, Elisabete, Rodney, Jaime, Chiara, Anthony...mais surtout merci a Jean-Christophe, avec son 'petit bonhomme', pour l'aide, les sourires, les gateaux aux chocolats, et beaucoup de petites et grandes choses qu'on ne peut pas expliquer.

My deep thank goes to those who have followed my three years of thesis from faraway, but making me feel constantly their support, friendship and esteem. Thanks to my special friends Alberto, Andrea, Fabrizio, Luca, Paolo, Susanna. Thanks to Elisa, Luca, Silvia, Ilaria for your sincere friendship in all these years. Special thanks to Gabriele for keeping alive such a unique relationship and trusting me always, no matter what I do.

Finally I want to thank few people for just being part of my life. Cara mamma, Stefano e Nicola, thanks for your love, for your support, trust and encouragement, for your patience, for being always with me even if we are apart, for making me feel the most welcome and important princess in the world when I come back home. Thanks papà because, wherever you are, you are next to me. Last but not least, thanks Stefano for helping me so much and so patiently since the beginning, for your support and love for which these words are not enough.

# Curriculum vitae

## PERSONAL DATA

---

Anna Gallazzi

Born 16 November 1978 in Busto Arsizio (Varese), Italy, italian citizen

Current address: c/o Max-Planck-Institut für Astrophysik, Karl-Schwarzschild-Str. 1, 85748, Garching bei München, Germany

Tel.: +49 089 30000 2019

e-mail: gallazzi@mpa-garching.mpg.de

Permanent address: Via Carnia, 5, 21052 Busto Arsizio (Varese), Italy

## EDUCATION AND TRAINING

---

- |                       |  |
|-----------------------|--|
| 1992-1997             | high school at “Liceo Classico Statale D.Crespi” in Busto Arsizio; experimental courses in physics   |
| July 1997             | high school diploma (“Maturità Classica”) at “Liceo Classico Statale D.Crespi” in Busto Arsizio, reporting the degree of 60/60   |
| 1997-2002             | Physics at Università degli Studi di Milano Bicocca. Overall average score is 27.8/30.   |
| September 27, 2002    | Laurea in Fisica reporting the final score of 110/110 at Università degli Studi di Milano Bicocca. The thesis “La formazione stellare attuale nelle galassie di tipo avanzato. Influenza dell’ambiente” (a study on the environmental dependence of the star formation rate in nearby late-type galaxies) was supervised by Prof. Giuseppe Gavazzi (Università degli Studi di Milano Bicocca) and Prof. Monica Colpi (Università degli Studi di Milano Bicocca). |
| February 2003-present | “International Max-Planck Research School on Astrophysics” PhD fellowship at Max-Planck-Institut für Astrophysik, Garching. Thesis project on the interpretation of galaxy spectra by means of the most recent population synthesis models supervised by Dr. Stephane Charlot and Prof. Dr. Simon White. The school program includes the attendance of one introductory course and three advanced courses covering all the aspects of modern astrophysics.       |

## Curriculum vitae

---

### SCHOLARSHIPS AND HONOURS

---

- November 27, 2002 8<sup>th</sup> rank position (60 participants) in “Concorso di Dottorato di Ricerca in Fisica ed Astronomia”. Admitted to the Italian PhD program (selected for PhD at the Università di Milano-Bicocca/Insubria).
- December 2002 3-year PhD fellowship from the “International Max-Planck Research School on Astrophysics” at Ludwig-Maximilians-Universität, München.
- September 12 - December 11, 2005 3-month EARA-EST fellowship at Institut d’Astrophysique de Paris.

### SCIENTIFIC INTERESTS

---

Galaxy formation and evolution  
Stellar populations of nearby galaxies  
Galaxy physical parameters and star formation history and their environmental dependence  
Scaling relations of early-type galaxies

### FOREIGN LANGUAGES

---

- English very good  
German basic knowledge of written and spoken language  
French basic knowledge of written and spoken language

### PUBLICATIONS

---

- In refereed journals
- The ages and metallicities of galaxies in the local universe*, **Gallazzi A.**, Charlot S., Brinchmann J., White S.D.M., Tremonti C.A., 2005, MNRAS, 362, 41.
- The colours of elliptical galaxies*, Chang R., **Gallazzi A.**, Kauffmann G., Charlot S., Ivezić Ž., Brinchmann J., Heckman T.M., 2006, MNRAS, 366, 717
- H $\alpha$  surface photometry of galaxies in nearby clusters. V: The survey completion*, Gavazzi G., Boselli A., Cortese L., Arosio I., **Gallazzi A.**, Pedotti P., Carrasco L., 2006, A&A, 446, 839
- H $\alpha$  surface photometry of galaxies in the Virgo cluster. I: Observations with the San Pedro Martir 2.1 m telescope.*, Gavazzi G., Boselli A., Pedotti P., **Gallazzi A.**, Carrasco L., 2002, A&A, 386, 114.
- H $\alpha$  surface photometry of galaxies in the Virgo cluster IV: the current star formation in nearby clusters of galaxies.*, Gavazzi G., Boselli A., Pedotti P., **Gallazzi A.**, Carrasco L., 2002, A&A, 396, 449.

